NASA CONTRACTOR REPORT

NASA CR-2832

FLIGHT EVALUATION OF AN ADVANCED TECHNOLOGY LIGHT TWIN-ENGINE AIRPLANE (ATLIT)

Bruce J. Holmes

Prepared by
UNIVERSITY OF KANSAS
Lawrence, Kans. 66045
for Langley Research Center

NATIONAL AERONAUTICS AND SPACE ADMINISTRATION • WASHINGTON, D. C. • JULY 1977

1. Report No.	2. Government Accession No.	3. Recipient's Catalog No.
NASA CR-2832		

4. Title and Subtitle	5. Report Date
FLIGHT EVALUATION OF AN ADVANCED TECHNOLOGY LIGHT TWIN-ENGINE AIRPLANE (ATLIT)	July 1977
	6. Performing Organization Code
7. Author(s)	8. Performing Organization Report No.
Bruce J. Holmes	
9. Performing Organization Name and Address	10. Work Unit No.
The University of Kansas Lawrence, Kansas 66045	505-10-11-03
	11. Contract or Grant No.
	NGR 17-002-072
12. Sponsoring Agency Name and Address	13. Type of Report and Period Covered
National Aeronautics and Space Administration Washington, DC 20546	Contractor Report
	14. Sponsoring Agency Code

15. Supplementary Notes

Topical report.
Langley Technical Monitor: Harold L. Crane

16. Abstract

The project organization and execution, the airplane description and performance predictions, and the results of the flight evaluation of an advanced technology light twin-engine airplane (ATLIT) are presented. The ATLIT is a Piper PA-34-200 Seneca I modified by the installation of new wings incorporating the GA(W)-1 (Whitcomb) airfoil, reduced wing area, roll-control spoilers, and full-span Fowler flaps. The conclusions for the ATLIT evaluation are based on complete stall and roll flight-test results and partial performance test results. Stalling and the rolling characteristics met design expectations. The cruise and climb performance did not meet the predictions. Climb performance was penalized by extensive flow separation in the region of the wing-body juncture. Cruise performance was found to be penalized by a large value of zero-lift drag. Calculations showed that, with proper attention to construction details, the improvements in span efficiency and zero-lift drag would permit the realization of the predicted increases in cruising and maximum rate-of-climb performance. Plans for future tests include the following topics: climb performance will be documented with the flow separation at the wing-body juncture cleaned up; the noise and performance characteristics of a set of supercritical propellers will be measured; testing is planned for ATLIT in the NASA-LaRC full-scale (30- by 60-foot) wind tunnel in the fall of 1976; and, after the wind-tunnel tests, ATLIT will return to flight status for evaluation of the final wind-tunnel optimized configuration

17. Key Words (Suggested by Author(s))	18. Distribution Statement
Advanced technology light twin; GA(W)-1 airfoil; LS-1 0417 airfoil; spoilers; full-span Fowler flaps; airspeed calibration; aerodynamic parameter extraction; airplane performance measurements	Unclassified - Unlimited Subject Category 02

19. Security Classif. (of this report)	20. Security Classif. (of this page)	21. No. of Pages	22. Price*
Unclassified	Unclassified	287	$9.25

*For sale by the National Technical Information Service, Springfield, Virginia 22161

LIST OF ACRONYMS

ACD:	Analysis and Computation Division (at LaRC)
ADTRAN:	Analog to Digital Translation
ATLIT:	Advanced Technology Light Twin
cg:	Center of Gravity
CRINC:	(KU) Center for Research, Inc.
DOC:	Direct Operating Cost
FM:	Frequency Modulated
FRD:	Flight Research Division (at LaRC)
FRL:	Flight Research Laboratory (at KU)
GA(W):	General Aviation (Whitcomb) (airfoil)
ILS:	Instrument Landing System
KU:	University of Kansas
LaRC:	(NASA)-Langley Research Center
LS-1:	Low Speed (family of airfoils)
mac:	Mean Aerodynamic chord
NACA:	National Advisory Committee on Aeronautics (became NASA in 1957)
NASA:	National Aeronautics and Space Administration
NCSU:	North Carolina State University
PAM:	Pulse Amplitude Modulated
QA:	Quality Assurance Office (LaRC)
RMS:	Root Mean Square

SOPB:	Safety and Operating Problems Branch (in FRD)
V/STOL:	Vertical/Short Takeoff and Landing
W.S.:	Wing Station
WSU:	Wichita State University

TABLE OF CONTENTS

LIST OF FIGURES

LIST OF TABLES

LIST OF SYMBOLS

Symbol	Definition	Dimension
A	Aspect ratio, $\frac{b^2}{S}$	
a_x	Acceleration along airplane longitudinal axis	g
b	Wing span	m (ft)
c	Wing chord	m (ft)
C	Constant	
c	Specific fuel consumption	$\frac{N}{\text{Watt-hr}}$ $\left(\frac{\text{lb}}{\text{HP-hr}}\right)$
c_{d_o}	Two-dimensional zero-lift drag coefficient	
C_{D_o}	Three-dimensional zero-lift drag coefficient	
C_H	Hinge moment coefficient $\frac{H}{q_c S \cdot c}$	
c_ℓ	Two-dimensional lift coefficient	
C_L	Three-dimensional lift coefficient	
c_{ℓ_α}	Two-dimensional lift-curve slope, $\frac{\partial C_\ell}{\partial \alpha}$	rad^{-1} (deg^{-1})
C_{L_α}	Three dimensional lift curve slope, $\frac{\partial C_L}{\partial \alpha}$	rad^{-1} (deg^{-1})
$C_{\ell'}$	Airplane rolling moment coefficient, $\frac{L'}{q_c S b}$	

Symbol	Definition	Dimension
$C_{\ell_{\delta_s}}$	Variation of rolling moment coefficient with spoiler deflection, $\frac{\partial C_\ell}{\partial \delta_s}$	rad^{-1} (deg^{-1})
C_{ℓ_p}	Airplane roll damping, $\frac{\partial C_\ell}{\partial\left(\frac{pb}{2v}\right)}$	rad^{-1} (deg^{-1})
c_{m_o}	Two-dimensional zero-lift pitching moment coefficient	
C_r	Wing root chord	m (ft)
C_t	Wing tip chord	m (ft)
d	Lateral distance between fuselage centerline and nacelle centerline	m (ft)
D	Drag	N (lb)
e	Airplane (Oswald's) efficiency factor	
g	Acceleration of gravity	m/sec^2 (ft/sec^2)
h	Altitude	m (ft)
$\frac{\Delta h}{c}$	Spoiler projection height	
H	Hinge moment	N-m (ft-lb)
k	Constant	
k_x	Distance behind airplane in terms of wing spans ($k_x = x/b$)	
k_z	Distance below airplane in terms of wing spans ($k_z = z/b$)	
L	Lift	N (lbf)
L'	Airplane rolling moment	N-m (ft-lbf)

Symbol	Definition	Dimension
ℓ_1	Airplane horizontal tail length (elevator hinge line to airplane center of gravity)	m (ft)
ℓ/d	Two-dimensional lift to drag ratio	
L/D	Three-dimensional lift to drag ratio	
M	Mach number, $\frac{V}{V_a}$	
mac	Mean aerodynamic chord	m (ft)
n	Load factor	
n_α	Gust load factor, $\frac{\partial n}{\partial \alpha}$	g/rad
P	Roll rate, $\frac{d\phi}{dt}$	deg/sec
p	Static pressure	pa (psf)
P_t	Total pressure	pa (psf)
P	Airplane power	watts (HP)
P	Coefficients in polynomial expression of power available	
pb/2V	Roll helix angle	rad
q	Dynamic pressure, $1/2\,\rho V^2$	pa (psf)
Q	Pitch rate, $\frac{d\theta}{dt}$	deg/sec
RN	Reynolds number	
R	Gas constant for air	
R	Yaw rate, $\frac{d\psi}{dt}$	deg/sec
S	Reference wing area	m^2 (ft^2)
S_n	Nacelle planform area	m^2 (ft^2)

Symbol	Definition	Dimension
S	Error term	
T	Temperature	^{o}K, ^{o}C, (^{o}R, ^{o}F)
t	Time	sec
T	Thrust	N (lb)
$\frac{t}{c}$	Wing thickness ratio	%
u	Component of velocity along airplane longitudinal axis	m/sec (ft/sec)
V	True airspeed	knots (mph)
V_a	Local speed of sound	m/sec (ft/sec)
V_c	Calibrated airspeed	knots (mph)
V_i	Indicated airspeed (= V_c')	knots (mph)
V_{NE}	Never exceed airspeed	knots (mph)
V_{S_o}	Airplane power-off stall speed in landing configuration	knots (mph)
W	Airplane weight	N (lb)
w	Component of velocity along airplane vertical axis	m/sec (ft/sec)
x	Distance between accelerometer location and airplane center of gravity (longitudinal)	m (ft)
x/D	Ratio of distance along airplane longitudinal axis to maximum fuselage diameter	
z	Distance between accelerometer location and airplane center of gravity (vertical)	m (ft)

GREEK SYMBOLS

α	True (geometric) angle of attack (referenced from fuselage centerline)	deg
α'	Measured (indicated) angle of attack (referenced from fuselage centerline)	deg

Symbol	Definition	Dimension
β	Sideslip angle	deg
β'	Measured sideslip angle	deg
Δ	Difference or increment	
δ	Deflection	deg
δ^*	Boundary layer displacement thickness	cm (in)
Γ	Circulation $\frac{L}{\rho V b}$	m^2/sec (ft^2/sec)
γ	Flight path angle	deg
γ	Ratio of specific heats for air	
λ	Taper ratio, $\frac{C_t}{C_r}$	
η	Efficiency	
ϕ	Bank angle	deg
ψ	Yaw angle	deg
ρ	Air density	N/m^3 ($slugs/ft^3$)
θ	Pitch attitude	deg
θ	Airplane pitch attitude	deg
σ	Density ratio, $\frac{\rho}{\rho_o}$	
τ	Time constant	sec
SUBSCRIPTS		
a	Airplane	
A	ATLIT	
A	Airplane	
ac	Aerodynamic center	
b	Barograph	
c	Calibrated	

Symbol	Definition
c	Corrected
c/4	Quarter chord
f	Flap
fus	Fuselage
g	Gross
i	Indicated
in	Installed
ind	Indicated
m	Measured
max	Maximum
min	Minimum
n	Nacelle
s	Spoiler
o	Zero lift value
o	Sea level value
o	Starting or reference value
p	Propeller
ref	Reference
s	Stagnation
s	Static
S	Seneca
s	Spoiler
t	Trim
t	Total

Symbol	Definition
t	(Horizontal) tail
te	Trailing edge
te,o	Trailing edge at zero wing incidence
t_v	(Vertical) tail
w	(Control) wheel
w	Wing

SUPERSCRIPTS

·	Dotted symbols represent time derivatives (e.g., $\dot{V} = \frac{dV}{dt}$)
'	Primed symbols represent measured or indicated values, with position error

CHAPTER 1

INTRODUCTION

This report presents the project organization and execution, the airplane design description, the airplane performance predictions, and the results of the flight evaluation of an advanced technology light twin-engine airplane (ATLIT). The results cover the period from the ATLIT first flight in October 1974, to June 1976. Some pre-ATLIT historical notes are also included.

The flight-test results include stall characteristics, spoiler roll performance, cruise and single/multi-engine climb performance, and pilot comments on stability and handling qualities. Planned tests which are not in the scope of this report include takeoff and landing performance evaluation, stability derivative determination, supercritical propeller evaluation, and full-scale (30- by 60-foot) wind-tunnel tests.

The ATLIT is the second airplane designed and constructed as part of a general aviation research program at the University of Kansas (KU) Flight Research Laboratory (FRL), sponsored by grants (NGR 17-002-072) from the National Aeronautics and Space Administration (NASA), Langley Research Center (LaRC). The airplane which preceded ATLIT in development is the Redhawk, a modified Cessna Cardinal (references 1, 2, and 3). The object of the research under these grants has been to apply existing jet-transport wing technology and advanced airfoil technology to general aviation airplanes for the purpose of improving safety, efficiency, and utility.

The ATLIT is a Piper PA-34-200 Seneca I with the following modifications:

1. Wing planform modified for cruise efficiency with taper, reduced area, and increased aspect ratio.
2. Full-span Fowler trailing edge flaps.
3. Spoilers for roll control.
4. GA(W)-1, general aviation (Whitcomb) 17-percent thick airfoil.
5. Ground-adjustable wing incidence.
6. Advanced-technology propellers incorporating a supercritical airfoil.

The airplane appears in figure 1.1.

The ATLIT project is a multi-purpose program. Performance improvements throughout the flight envelope are sought, with emphasis on the enhancement of the safety of light, twin-engine airplanes by increasing the single-engine climb performance through aerodynamic changes. Preliminary design estimates (reference 4 and unpublished data[1]) indicate that the airplane modifications mentioned above would result in improvements to both the single-engine rate of climb and the cruise performance. The ATLIT wing was designed to take advantage of the low profile drag characteristics (at climb conditions) of the GA(W)-1 airfoil (reference 5), and of the lower induced and profile drag characteristics (at both climb and cruise conditions) of the modified wing planform. The cruise-optimized planform logically led to the use of full-span Fowler flaps for acceptable landing speeds with roll control

1. Conceptual Design of an Advanced Technology Light Twin Aircraft, Phase I Report: Prepared by Robertson Aircraft Corporation, and the University of Kansas Center for Research, Inc., for NASA Langley Research Center under NASA Grant NGR 17-002-072, 1972.

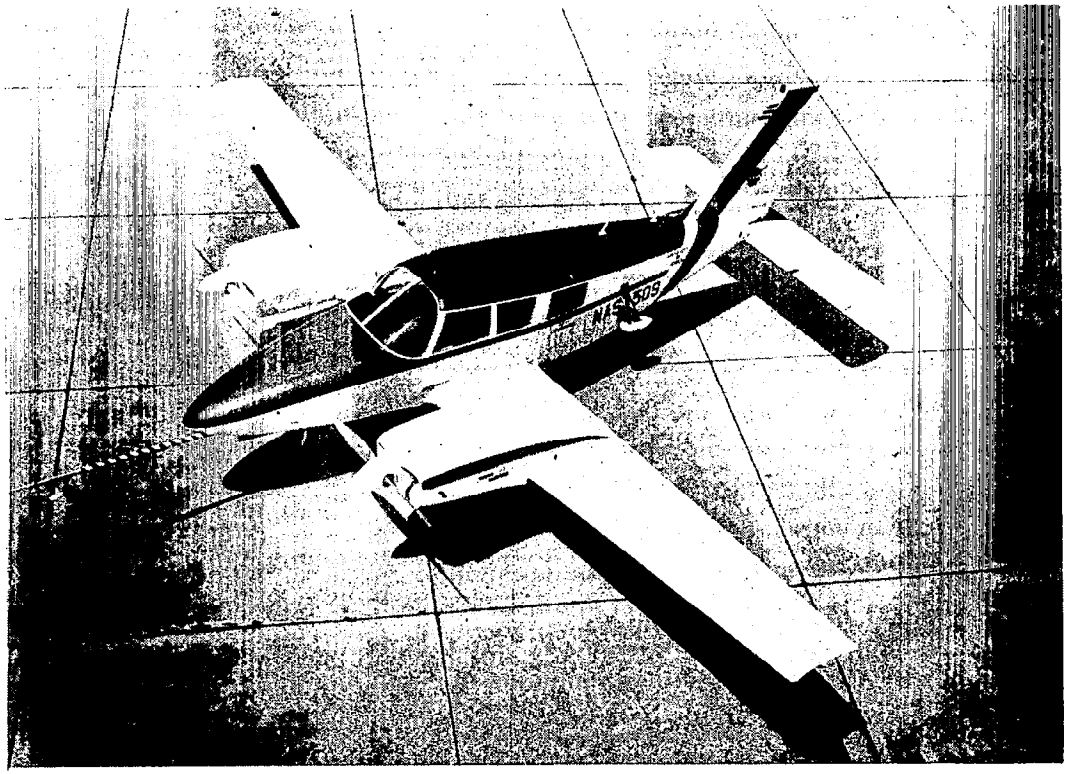

Figure 1.1.- The advanced technology light twin-engine airplane (ATLIT)

provided by spoilers. Along with predicted performance improvements, the wing modifications would result in improved ride quality (due to higher wing loading) and would permit lighter structural wing weight (due to thicker wing sections and reduced wing area).

Stimulated by the ATLIT project, and in fulfilling its role to provide technology to aircraft manufacturers, NASA has undertaken the development of a new family of low-speed airfoils for use on general aviation aircraft. This new airfoil family is a product of the development of computational methods for designing optimized airfoil shapes (reference 6). Application of the GA(W)-1 section to the ATLIT wing represents the first effort to verify the characteristics of a computer-designed airfoil in flight. This flight verification closes the loop in the computer/wind-tunnel/flight hardware design process. In addition to documenting the new airfoil characteristics, ATLIT provides data on the use of full-span Fowler flaps combined with roll-control spoilers on the GA(W)-1 wing. Although the performance characteristics of these roll-control and high-lift devices have been documented in the literature, there currently exist little practical experience and data (spoiler hinge-moments and flap effectiveness with the new GA(W)-1 airfoils, for instance,) concerning their application to modern general aviation aircraft. The complete documentation of the ATLIT airplane characteristics will make such information available to the U.S. industry.

The interest shown by the general aviation industry in the aerodynamic devices used on the two KU-modified airplanes can be illustrated by table 1.1. The ten airplanes listed in the table have flown with or are being designed utilizing some combination of the devices discussed.

TABLE 1.1.- INDUSTRY UTILIZATION OF ADVANCED GENERAL AVIATION TECHNOLOGY

AIRPLANE	GA(W) AIRFOIL	ROLL CONTROL SPOILERS	FOWLER FLAPS
BEECHCRAFT PD-285	X		
ROBERTSON/SENECA		X	X
BEDE 5 (JET)	X		
BEDE 5 (PROP)	X		
AMERICAN JET "HUSTLER"	X	X	X
ROBERTSON/CESSNA 400-SERIES			X
ROBERTSON/BONANZA		X	X
PIPER TRAINER	X		
RUTAN/VARI-EZE	X		
CESSNA 441			X

The ATLIT flight-test program is being conducted at NASA Langley Research Center, in Hampton, Virginia. Many individuals support the project directly or indirectly. Those directly contributing to the preparation of this project report are acknowledged below:

Mr. Harold L. Crane, NASA LaRC (Project Technical Monitor): Flight data analysis on spoiler roll characteristics (Chapter 5.3).

Mr. Joseph H. Judd, NASA LaRC: Flight data analysis on cruise and single/multi-engine climb performance (Chapter 5.4).

Mr. Robert A. Champine and Mr. Philip W. Brown, NASA LaRC (research pilots): Pilot comments on ATLIT stability and handling qualities (Chapter 5.5).

Mr. Robert T. Taylor, NASA LaRC: Performance predictions (Chapter 5.4).

Mr. Laurence K. Loftin, Jr., NASA LaRC: Performance predictions (Chapter 5.4).

Dr. Frederick O. Smetana, North Carolina State University: Lift, drag, performance, and stability predictions (Chapter 5.4), and drag/power parameter extraction method (Appendix A).

Mr. Bradley J. Vincent, Embry-Riddle Aeronautical University: Roll damping derivative predictions (Appendix C).

Flight testing of ATLIT will continue from the date of this report until early fall 1976, when the airplane will enter the full-scale (30- by 60-foot) wind tunnel at LaRC. Flight-test results for this period will be presented in NASA and technical society publications.

Commercial products and/or names of manufacturers are used in this report documenting the flight evaluation results of ATLIT. These commercial products and/or names of manufacturers do not constitute official endorsement, expressed or implied, of such products or manufacturers by the National Aeronautics and Space Administration.

CHAPTER 2

PROJECT CHRONOLOGY AND MANAGEMENT

This chapter contains a chronological history of the project, an outline of the organizations and individuals involved in the project, the project budget, and the project schedule.

2.1 Project History

The ATLIT airplane represents the culmination of a long-term general aviation research program embarked on by KU-FRL in 1967. The broad goals of this program were to improve safety, performance, and handling qualities, as well as to advance the technology of the general aviation industry products. It has been argued that the basic control systems and aerodynamic designs of general aviation airplanes have changed very little in as long as thirty years. Furthermore, the advanced technology which resulted in marked performance improvements in commercial (jet transport) and military aircraft had not been applied to any significant extent in general aviation. In addressing the goals of the research program, efforts were to be made to apply both existing and advanced technology to light airplane designs.

Under NASA grants to FRL, the general aviation work has evolved in two major phases, beginning with the modified Cessna Cardinal "Redhawk" project (Phase I) and continuing to the present ATLIT project (Phase II).

Phase I, the development and testing of the Redhawk, began with the awarding of NASA Grant NGR 17-002-072 in 1969. The planform modifications to the Cessna C-177 Cardinal are illustrated in Figure 2.1. The changes

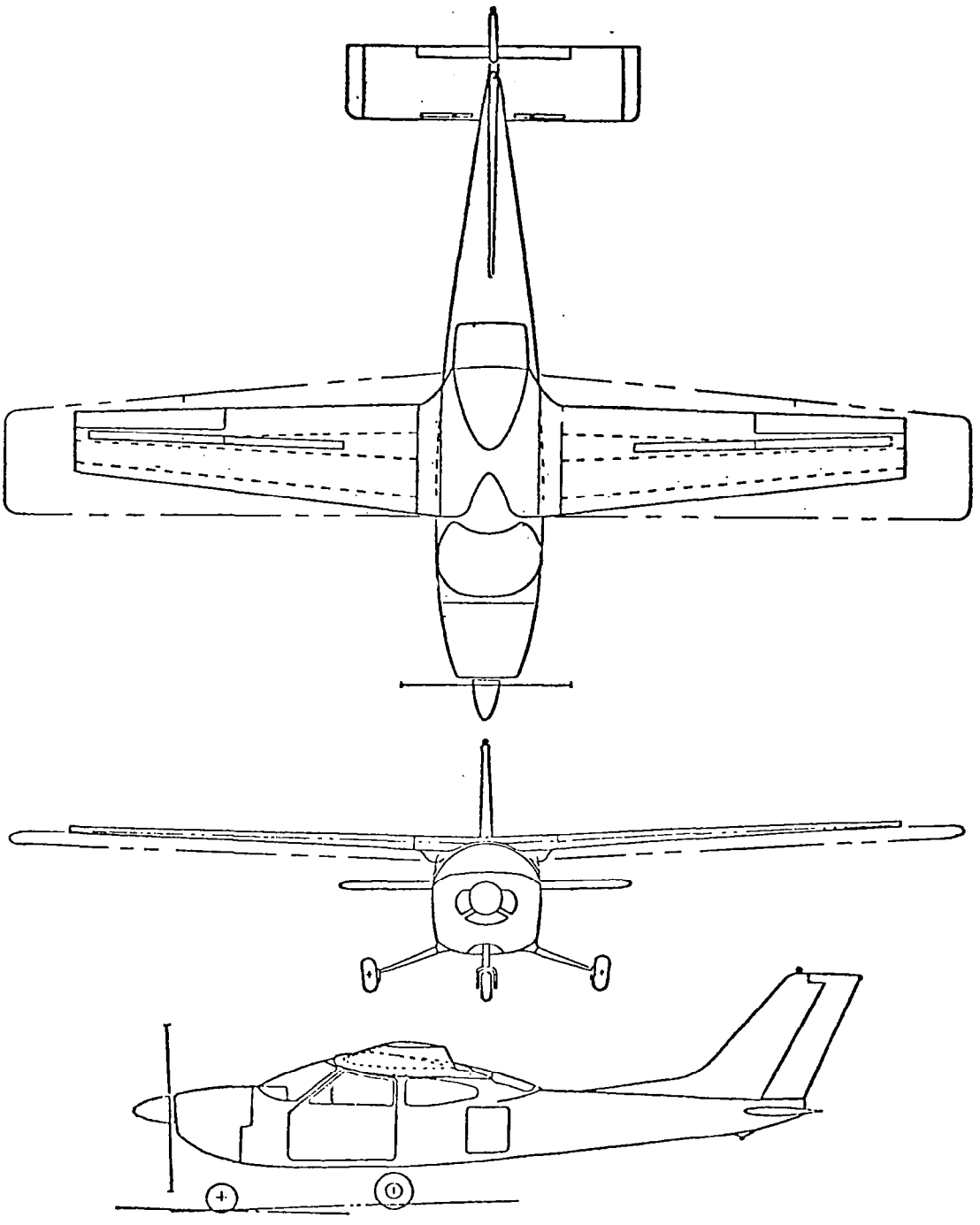

Figure 2.1.- Three-view of Redhawk compared to original Cessna Model 177 Cardinal

made to the airplane are quantified in table 2.1. The major goal in applying jet-transport wing technology to the Redhawk was to design a wing optimized for cruise efficiency with taper, increased aspect ratio, reduced area, and reduced thickness. The reduced wing area led to the use of high-lift devices to maintain takeoff and landing performance comparable to the unmodified airplane. The development of the Fowler and Kruger flaps for the Redhawk made use of two-dimensional KU wind-tunnel test data (reference 7). The use of spoilers rather than ailerons for roll control was investigated to permit the use of full-span flaps and to provide flightpath control by direct-lift control. The Redhawk spoiler design also made use of KU wind-tunnel test data (references 8 and 9).

First flight of the Redhawk took place in 1972. The results of the Redhawk performance evaluation (reference 3) show increased cruise speed (decreased $C_{D_o} \cdot S$), increased maximum lift coefficient, and smoother ride in turbulence as a by-product of reduced wing area (increased wing loading). The Redhawk spoilers provide adequate roll control with neither deadband nor nonlinearity in roll response. The lack of any significant net yawing moments during rolls with these spoilers makes it possible to make coordinated turns with no rudder deflections. The Redhawk lateral control forces, due to friction, are high in the all-mechanical system. This results, in part, from the use of cams, allowing individual movement of the spoilers for roll control as well as allowing symmetric spoiler displacements for direct-lift control. However, there is positive wheel centering in all flight conditions.

Analysis of the Redhawk climb performance (reference 3) shows reduced maximum rate of climb in comparison with the unmodified Cardinal, as predicted by preliminary design analysis (reference 10). This

TABLE 2.1

COMPARISON OF REDHAWK AND CESSNA CARDINAL DESIGN SPECIFICATIONS

(FROM REFERENCE 3)

	Cardinal	Redhawk
Gross Weight, N, (lb)	11,120, (2500)	11,120, (2500)
Wing Area, m^2, (sq ft)	16.23, (175)	10.21, (110)
Wing Loading, N/m^2, (lb/sq ft)	648, (14.3)	1089, (22.7)
Span, m, (ft)	10.82, (35.5)	9.58, (31.4)
Aspect Ratio	7.4	9.0
Taper Ratio	0.7	0.5
Twist, deg	3.0	3.0
Dihedral, deg	1.5	3.0
Airfoil Section		
Inboard	NACA 64A215	NACA 2412
Outboard	NACA 64A212	NACA 2409
Trailing-edge Flap		
Type	Single Slot	Fowler
Span, percent	53	47
Area (both), m^2, (sq ft)	2.74, (29.5)	2.93, (31.5)
Leading-edge Flap	-	Kruger
Span, percent	-	83
Deflection	-	135°
Aileron		
Type	Frise	Round Nose
Chord, percent	41	24
Span, percent	33	36
Spoiler		
Type	-	Modified Mitsubishi
Span		
Inboard	-	28.5
Outboard	-	32
Maximum Deflection	-	53°

results directly from the effect of the reduced Redhawk span (increasing span loading) in increasing induced drag. Calculations of reference 3 show climb performance improvements which would have accrued due to construction of the Redhawk wing with the original Cardinal wing span.

The Redhawk is presently active at the University of Kansas in a flight-test program to evaluate the direct-lift control spoilers as flightpath control devices on ILS approaches.

Phase II of the general aviation research program, the development and testing of ATLIT, began in 1972. Much of the work done on the Redhawk had direct or indirect applications on ATLIT. The same type of parametric analysis that was performed during the design of the Redhawk indicated that an ATLIT wing with increased aspect ratio, reduced area, and using the GA(W)-1 airfoil would improve single- and multi-engine climb performance and cruise performance. As on the smaller Redhawk wing, the ATLIT wing required some form of a high-lift device. With the confidence in roll-control spoilers gained on Redhawk, the application of these devices on ATLIT freed the full span of the wing trailing edge for use of the Fowler flap.

The maiden flight of ATLIT took place on October 12, 1974, at the Piper Aircraft Corporation Facility in Lakeland, Florida. Mr. W. P. Kelly of Piper was the test pilot. Following a period of debugging, final construction, and about 10 hours of acceptance testing, the airplane was delivered by Piper to NASA-Langley Research Center on November 26, 1974. At LRC, the airplane was grounded until April 1975, for inspection by LRC Quality Assurance Office and for installation of the flight-test instrumentation system and recording package. Instrumented test flights began May 28, 1975.

Figure 2.2 presents some of the milestones during the Redhawk and ATLIT research projects.

2.2 Project Support Organization

The groups and organizations involved in the various aspects of the ATLIT research program are indicated in Figure 2.3. A description of the extent of each organization's contribution and related literature published is presented here.

The Safety and Operating Problems Branch (SOPB) in the Flight Research Division (FRD) at NASA-LRC has had responsibility in funding the general aviation work done under NASA Grant NGR 17-00-072. Mr. Harold L. Crane (LRC) has been the project technical monitor of this grant and other grants related to the ATLIT project at Wichita State University, North Carolina State University, and Princeton University. He was also the LRC project engineer for the ATLIT flight-test program.

The University of Kansas has been responsibile for overall ATLIT program management.

Much of the associated project work was performed under subcontract from KU. Dr. David L. Kohlman (KU) is the principal investigator for the project. Mr. Bruce J. Holmes (KU-Doctor of Engineering Degree Candidate) was the KU project engineer for the ATLIT flight-test program at LRC. The design of an advanced technology light twin-engine type of airplane was first suggested in reference 4. Development of a cruise-optimized planform was performed with the aid of KU computer programs. References 1, 11, 12, 13 and unpublished data[2] resulted largely from work done by KU personnel on the ATLIT project.

Under subcontract from KU, Wichita State University (WSU) did the wind tunnel development on the Fowler flap and roll-control spoiler systems

2. Ibid.

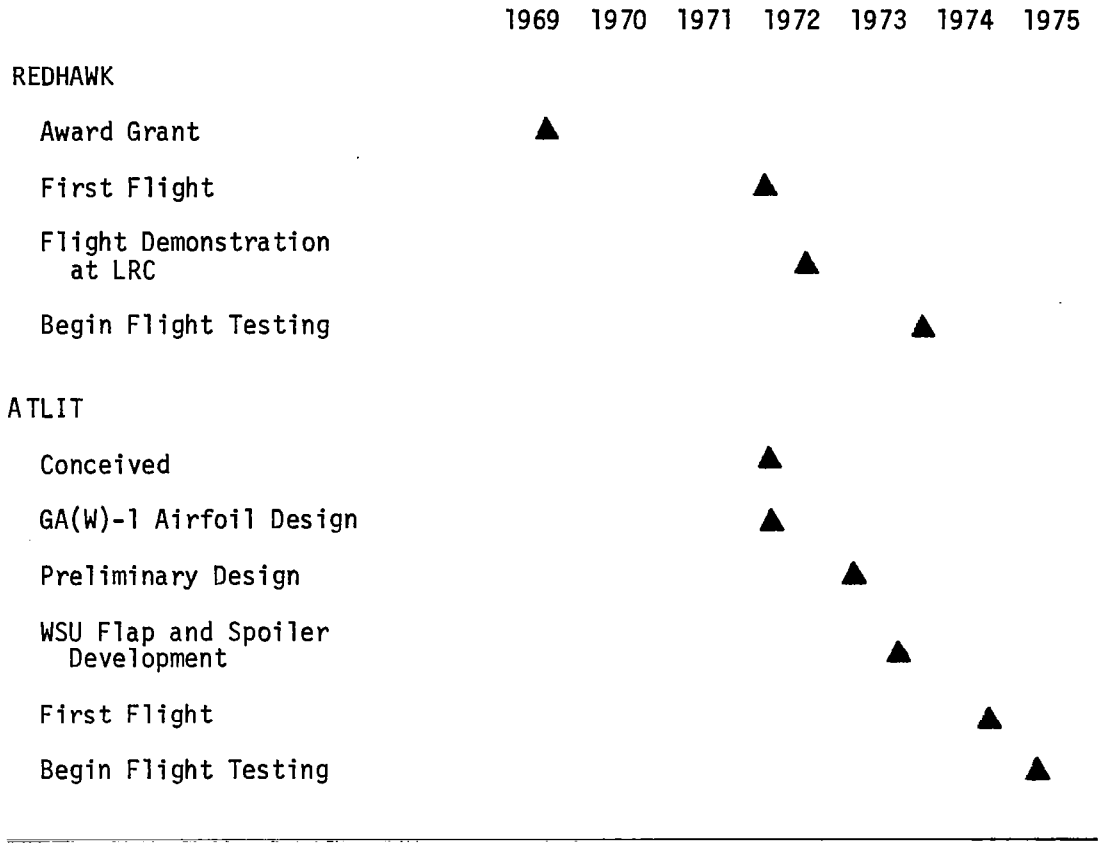

Figure 2.2 Milestones in General Aviation NASA Grant Research at the University of Kansas.

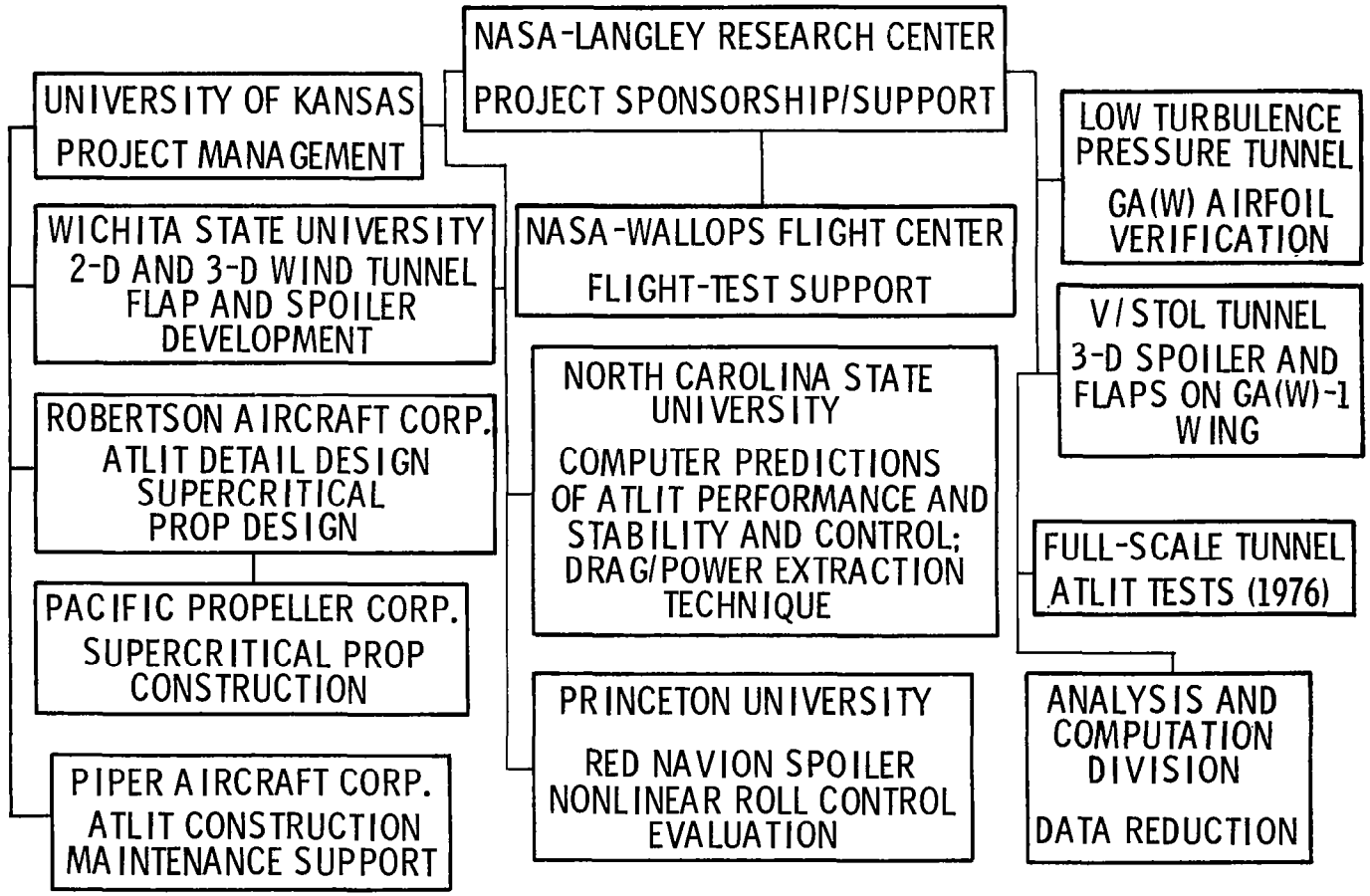

Figure 2.3.- ATLIT project support organization.

for the ATLIT wing. Dr. William H. Wentz, Jr. (WSU) had responsibility for this development work. In addition to the 2-D wind tunnel work on the airfoil-flap-spoiler configuration, WSU ran reflection plane wind-tunnel tests directly under an NASA-LRC grant. The purpose of these tests was to document the ATLIT airfoil-flap-spoiler configuration in three dimensions. This testing included documentation of wing forces, spoiler hinge moments, and tufted stall patterns. References 14, 15, 16 and 17 are products of this work.

Robertson Aircraft Corporation, Renton, Washington, under Piper Aircraft Corporation and KU subcontracts did a majority of the ATLIT detail design. They also designed a set of propellers incorporating a supercritical airfoil for testing on ATLIT. The ATLIT design drawings and design loads analysis were prepared by Robertson. The early preliminary design work on ATLIT was done by Mr. James D. Raisbeck of Robertson. After Mr. Raisbeck's departure from the company, Mr. John T. Calhoun had primary responsibility for completing the ATLIT detail design. Unpublished reports[3,4] contain data from the Robertson Corporation work on ATLIT. In addition, the engineering design drawings for ATLIT listed in Table 3.2, Chapter 3, were prepared.

Construction of the Robertson-designed supercritical propellers was done by Pacific Propeller Corporation, Kent, Washington, under subcontract from Robertson.

Construction of the ATLIT wing was done under a KU subcontract to Piper Aircraft Corporation, Lakeland, Florida. Mr. H. Raymond Bazo (Piper) was the project engineer in charge of this construction. Approximately

3. Ibid.
4. Budish, Nathan N.: ATLIT Design Loads, Robertson Aircraft Corp. report TR-ATLIT-1. Prepared for the University of Kansas Center for Research, Inc., under NASA Grant NGR-17-002-072, June 1973.

20 hours of acceptance testing was done by Piper prior to delivery of the airplane to LRC. Piper also did approximately 5 hours of flight evaluation of the supercritical propellers installed on a standard PA-34 Seneca. Piper provides maintenance support when required for ATLIT during flight testing. The title to the airplane remains in Piper's name with a lease arrangement to KU-FRL for the purpose of flight testing at LRC. Piper work related to ATLIT was documented in unpublished reports.[5,6]

The NASA - Wallops Flight Center, Wallops Island, Virginia, provides an isolated environment for flight testing. Wallops has extensive capabilities in flight tracking, data reduction, and ground support. These facilities are used for such ATLIT tests as airspeed calibrations, takeoff and landing performance, single-engine climb performance, and noise measurement.

Under a grant from LRC, North Carolina State University did analytical work in the areas of predicting ATLIT performance and stability and control characteristics. Dr. Frederick O. Smetana (NCSU) is the principle investigator for the grant. The purpose of the computer predictions of airplane characteristics, in addition to evaluating the ATLIT design, was to provide data for correlation with flight-measured characteristics and thus attempt to build confidence in the computer-predictive techniques. In additon to this work, a computer method is under development for extracting drag and power data from continuous, dynamic flight-maneuver data. The technique is presented in detail as Appendix A. Reference 18 is a product of NCSU work related to ATLIT.

5. Kimberlin, Ralph D.: Flight Test Evaluation of the NASA/University of Kansas Advanced Technology Light Twin, Parts I and II. Piper Aircraft Corporation In-House Reports, 1975.
6. Kimberlin, Ralph D.: Comparative Evaluation of the NASA/University of Kansas Supercritical Propellers with Standard Propellers on the PA-34-200 Seneca I. Piper Aircraft Corporation In-House Report, 1974.

Under a grant from LRC, the Princeton University Flight Research Laboratory conducted an in-flight simulation to explore the effects on handling qualities of wind-tunnel predicted spoiler-type roll-control nonlinearities. This work consisted of programing a variable stability airplane for several different cases of nonlinearity and deadband combinations. Flight evaluations by LRC research pilots developed confidence that certain degrees of nonlinearity would be tolerable. The flight experience prepared the pilots for the possible cases of nonlinearity for the ATLIT first flight. Mr. David R. Ellis was the principal investigator, and reference 19 is a product of this grant work.

A few months after ATLIT was conceived, the characteristics of one of the first computer designed airfoils, the GA(W)-1, were being documented in the Low-Turbulence Pressure Tunnel at LRC. Mr. Robert J. McGhee (LRC), working with Dr. Richard T. Whitcomb (LRC), completed development of the airfoil by early 1973. The airfoil, a spinoff of Dr. Whitcomb's supercritical airfoil work, showed promise for general aviation applications and was incorporated into the ATLIT design. Reference 5 is a product of this wind-tunnel work.

Mr. John W. Paulson, Jr. (LRC) conducted 3-D wind-tunnel investigations in the LRC V/STOL Wind Tunnel on a wing with a GA(W)-1 section. The tests included evaluation of Fowler flaps with roll-control spoilers, and plain and slotted flaps with roll-control ailerons. These tests generated wing-force data with the three types of flap systems and data on roll-control characteristics with either ailerons or spoilers. References 20 and 21 are products of these wind-tunnel tests.

In the fall of 1976, ATLIT will be tested in the LRC Full-Scale (30- by 60-Foot) Wind Tunnel.

The Analysis and Computation Division (ACD) at LRC has supported the project in data-reduction tasks. A sample of the work this division performs is illustrated in figure 2.4. The process illustrated in the figure traces the reduction of flight-test data from analog flight data on magnetic tape to the final engineering units time histories. The ATLIT project will continue to receive support from other organizations at LRC. Planned testing will involve personnel outside the Flight Research Division for propeller noise tests and stability derivative extraction tests.

2.3 Project Budget

The total funding for the ATLIT project is outlined below. Funding was obtained from the National Aeronautics and Space Administration, Langley Research Center, Hampton, Virginia, and the University of Kansas on a cost sharing basis. All income and outflow of project funds were handled through the business office of the Center for Research, Inc. (CRINC), by the principal investigator for the project. Table 2.2 outlines the project budget in terms of grant (cost-shared) funding and costs incurred by LRC in directly supporting the ATLIT flight-test program. The amounts of cost shared funding provided by KU are excluded from the table. These amounts generally consisted of small matching funds from the University for the principal investigator's salary during the academic year. The Langley direct funding does not include overhead charges for the operation of the airplane at Langley.

Each item in the breakdown of funding in table 2.2 is underlined and explained below.

The funding for ATLIT development includes conceptual design of the wing, stability and control analysis, handling qualities analysis, airfoil

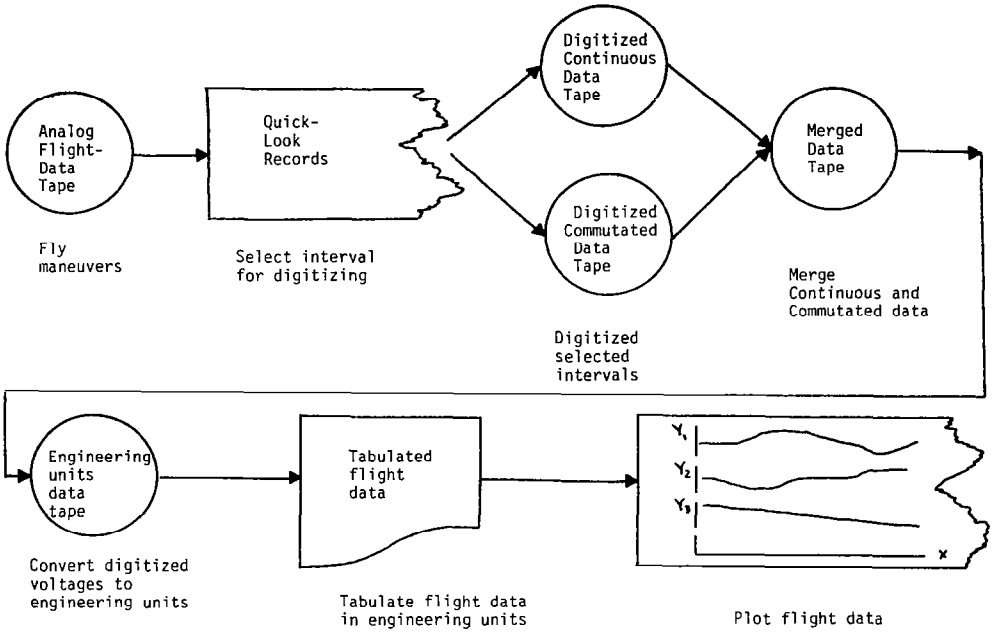

Figure 2.4.- Data reduction work-flow diagram.

TABLE 2.2

TOTAL ATLIT PROJECT BUDGET

Grant Funding (during four year period 3/72 to 6/76)	
ATLIT Development	$ 245,519.00
Wing Construction	359,000.00
Supercritical Propeller Design and Construction	22,000.00
Flight Test Program Support (two years)	62,498.00
Hull and Liability Insurance	9,500.00
(1) Total Grant Funding	$ 698,517.00
Langley Direct Funding (during two year period, 6/74 to 6/76)	
Salaries and Wages	
Engineering, Pilots, and Maintenance	$ 123,000.00
Instrumentation Support	130,000.00
Wallops Flight Center Support	1,500.00
Langley Chase Aircraft Support	2,500.00
Standard Seneca Rental	350.00
Airplane Direct Operating Costs (for 85 flight hours)	1,100.00
Computer Time	6,000.00
Travel	4,500.00
Miscellaneous Equipment, Parts, and Supplies	4,500.00
Grants (other than K U)	80,000.00
(2) Total Langley Direct Funding	$ 353,450.00
Total Program Costs (1) + (2)	$1,051,967.00

development studies (at WSU) and selection, two- and three-dimensional wind-tunnel development work of the Fowler flap and spoiler roll-control systems, and detailed engineering design.

The funds for wing construction were paid under a subcontract from KU to Piper Aircraft Corporation.

Under a subcontract from KU, funds for the supercritical propeller design and construction were paid to Pacific Propeller, Inc., under contract from Robertson.

The flight-test program support funding was awarded primarily to pay for the services of one KU graduate student at LRC to serve as KU project engineer during the flight testing of ATLIT.

Under the $1 per year airplane lease arrangement between CRINC and Piper Aircraft Corporation, hull and liability insurance was required for ATLIT. Funds were provided through the grant for coverage against any possible claim not covered under the Federal Tort Claims Act. Any claims involving negligence on the part of the Federal Government (NASA) would be covered by this act.

Under funding for salaries and wages, the amount for engineering, pilots, and maintenance covers one full-time engineer (2 years), two one-quarter-time research pilots (1 year), one full-time mechanic (2 years), and a one-third-time maintenance supervisor (2 years). The instrumentation support is contracted and includes salaries, wages, and company overhead for one engineer and one technician.

Funds for the Wallops Flight Center support paid for about 95 man-hours of services during two tower-flyby airspeed-calibration flights and two

single-engine climb test flights. The services included radar tracking with recorded time histories and meteorological data recording.

The Langley chase aircraft support consisted of approximately 25 hours of flight time in various aircraft. These flights were made to observe and/or photograph ATLIT during trailing anemometer airspeed calibration tests and tuft studies. Chase aircraft used included fixed-wing single- and multi-engine airplanes and helicopters. The cost for operating these chase aircraft was estimated to average $100 per flight hour, including ground and flight crew costs.

Approximately 5 hours of flying was done in an unmodified PA-34 with the funds indicated under standard Seneca rental. These flights were made to document performance characteristics of the standard Seneca and to do tuft studies.

Airplane direct operating costs are based on fuel, oil, filters, tires, and miscellaneous expendable parts used during approximately 85 hours of research flying (from April 1975, to May 1976). This direct operating cost averaged about $12/flight hour. No account has been made in this analysis for avionics repair costs.

The funds for digital computer time represent computer costs for work by both ATLIT project personnel and Analysis and Computation Division support personnel.

Travel funds include all ATLIT-related travel by LRC employees with the exception of trips to technical society meetings.

The amount for miscellaneous equipment, parts, and supplies, includes purchases of a digital fuel monitor for accurate weight control during

flight testing and a programmable pocket calculator for flight test data reduction. Also included is the cost of magnetic tape for the flight data recorder.

The funds for grants (other than KU) include work by North Carolina State University on predictions of ATLIT lift, drag, moments, performance, and stability and control characteristics (Chapter 5) as well as work on a method for extracting drag and power data from dynamic maneuvering flight data (Appendix A). Also included is an in-flight simulator experiment to evaluate the influence of spoiler-type roll-control nonlinearities on lateral handling qualities. This work was performed by Princeton University.

Table 2.3 presents the project costs which may be charged to the operation of the airplane during the flight test program involving about 85 research flight hours. The result of this analysis suggests that the cost to Langley Research Center in operating a flight test program with the scope and duration of the ATLIT project is about $4,000 per flight hour or about $170,000 per flight-program year. No account is made in this analysis for LRC overhead costs. The salaries and wages figured into this average cost account for approximately six months of start-up time for the flight-test phase of the project, one year of active flying, and about six months of data analysis and report preparation. The flight hours and man-years used are representative of those required to document airplane characteristics including airspeed and angle-of-attack calibrations, extensive tuft studies, lateral handling qualities, stall characteristics, and cruise and climb performance.

TABLE 2.3

TOTAL FLIGHT PROGRAM OPERATING COSTS FOR 85 HOURS OF RESEARCH FLYING

Grant Funding	
Flight Test Program Support (two years)	$ 62,498.00
Hull and Liability Insurance	9,500.00
Langley Direct Funding	
Salaries and Wages	$253,000.00
Wallops Flight Center Support	1,500.00
Langley Chase Aircraft Support	2,500.00
Standard Seneca Rental	350.00
Airplane Direct Operating Costs (85 flight hours)	1,100.00
Computer Time	6,000.00
Miscellaneous Equipment, Parts, and Supplies	3,200.00
Total Flight Program Operating Costs	$339,648.00
Approximate cost per flight hour (for 85 research flight hours)	$4,000/HR.
Approximate cost per flight-program-year	$170,000/YR.

2.4- Project Schedule

Since ATLIT first flew on October 12, 1975, about 130 hours of flight time in approximately 60 flights have been logged. Of the total flight time, about 85 hours have involved research work, with the remaining hours consisting of ferry time. Figure 2.5 presents the overall ATLIT project timetable.

Following the first flight, the LRC Quality Assurance (QA) Office sent a representative to the Piper plant in Lakeland, Florida, for an inspection of the airplane prior to its delivery to NASA. These QA inspections were addressed solely to matters of mechanical safety of flight. Matters concerning operational safety of flight (handling qualities and the like) were taken up in NASA-LRC safety committee meetings. The outcomes of the QA inspections and safety committee meetings included several recommendations which were to be implemented prior to beginning ATLIT flight operations from Langley Field.

Most of the recommendations of the two investigating groups were implemented before final adjustments to the airplane at the Piper plant. The decision was made at Langley to have the airplane delivered (on November 26, 1975) with a small amount of work remaining to be finished on the airplane. This would allow completion of final preflight test-airplane modifications at Langley with the QA inspection personnel readily available. In addition, installation of the instrumentation system and data recording package could begin immediately upon arrival of the airplane.

The original planning for the flight-test program called for research flights to begin in early 1975, and continue to late 1975, with documentation of the flight-test results planned for the first 6 months of 1976.

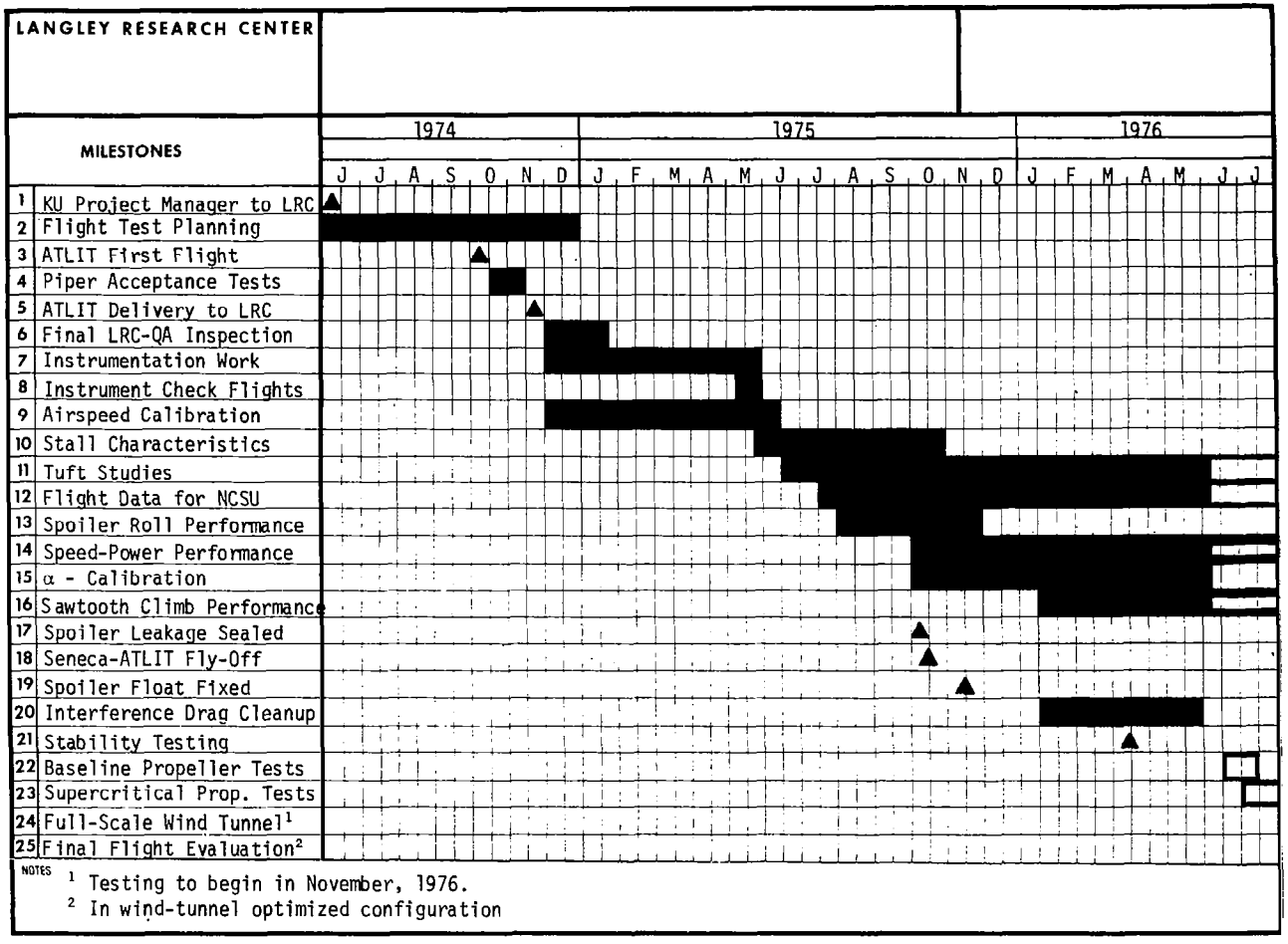

Figure 2.5.- ATLIT flight-test program timetable.

After arrival of the airplane at LRC, the work required to meet QA office standards combined with instrumentation difficulties to delay the first instrumented test flight until May 19, 1975. Further setbacks to the planned flight program were encountered upon the discovery of (and research to cure) a region of wing/body interference-induced flow separation at climb speeds. An estimated four months was spent investigating this flow problem. An estimated three months was invested in attempts to refine the accuracies of the flight data instrumentation system. One month of time was lost due to defective recording tape for the flight data recording system. These developments necessitated a twelve month extension (May 15, 1976 to May 15, 1977) of the grant for the purpose of fully documenting the airplane cruise and climb performance, and to document the characteristics of the supercritical propellers. The lease arrangement for the airplane has also been extended. The extension will also allow for the planned Full-Scale (30- by 60-Foot) Wind-Tunnel tests.

CHAPTER 3

AIRPLANE MODIFICATIONS

This chapter presents a detailed description and the design approach for the ATLIT wing and supercritical propellers. In presenting the airplane details, comparisons are made with the unmodified Piper PA-34-200 Seneca I wing and standard propellers.

3.1 General Seneca/ATLIT Description and Comparison

The PA-34 Seneca I is representative of general aviation light twin-engine airplanes which are used extensively by third-level air carrier, air taxi, corporate, and private operators. It is a low-wing airplane with retractable landing gear and a maximum range of 745 n.m. at a 75-percent power cruise speed of 162 knots. With a gross weight of 1.87 kN (4200 lb), the airplane seats up to seven occupants. The power plants are normally aspirated, reciprocating engines with constant-speed propellers.

The selection of the Seneca I for the project modifications followed a major goal in the ATLIT design, that of improving single-engine climb performance. General aviation airplanes in the light (less than 26.69 kN (6000 lb)), propeller-driven, twin-engine (normally aspirated), four- to eight-passenger class are virtually all very limited in single-engine climb performance at gross weight. For ten airplanes of this class on the market in 1975-1976, single-engine rates-of-climb at sea-level average 96 m/min (320 fpm) and single-engine service ceilings average 2000 m (6600 ft).

The Seneca I, with a single-engine rate-of-climb (at sea level and gross weight) of 57 m/min (190 fpm) and a single-engine service ceiling of 110 m (3650 ft), is a typical example. Reference 22 includes comments that, short of significant reduction in payload or range, no technology has been developed to improve climb performance. Increases in horsepower are economically unacceptable. Even turbo/supercharging, while, on the average, doubling the single-engine service ceilings, does not improve the sea-level rates-of-climb.

The conceptual studies which led to the ATLIT design revealed the potential of these approaches to improving engine-out climb:

1. Planform changes for lower induced drag with high-lift, large span flaps and roll-control spoilers.
2. GA(W)-1 airfoil for higher L/D, especially at climb, and for higher $C_{L_{max}}$.
3. Supercritical propellers designed for increased propulsive efficiency.

Figure 3.1 compares the planform, flap, and lateral control modifications of ATLIT with the unmodified Seneca. Pertinent dimensions for both airplanes are presented in table 3.1.

3.2 ATLIT Design Description

To supplement the following detailed description of ATLIT, a three-view is presented as figure 3.2 and a list of all engineering design drawings for ATLIT is given in table 3.2.

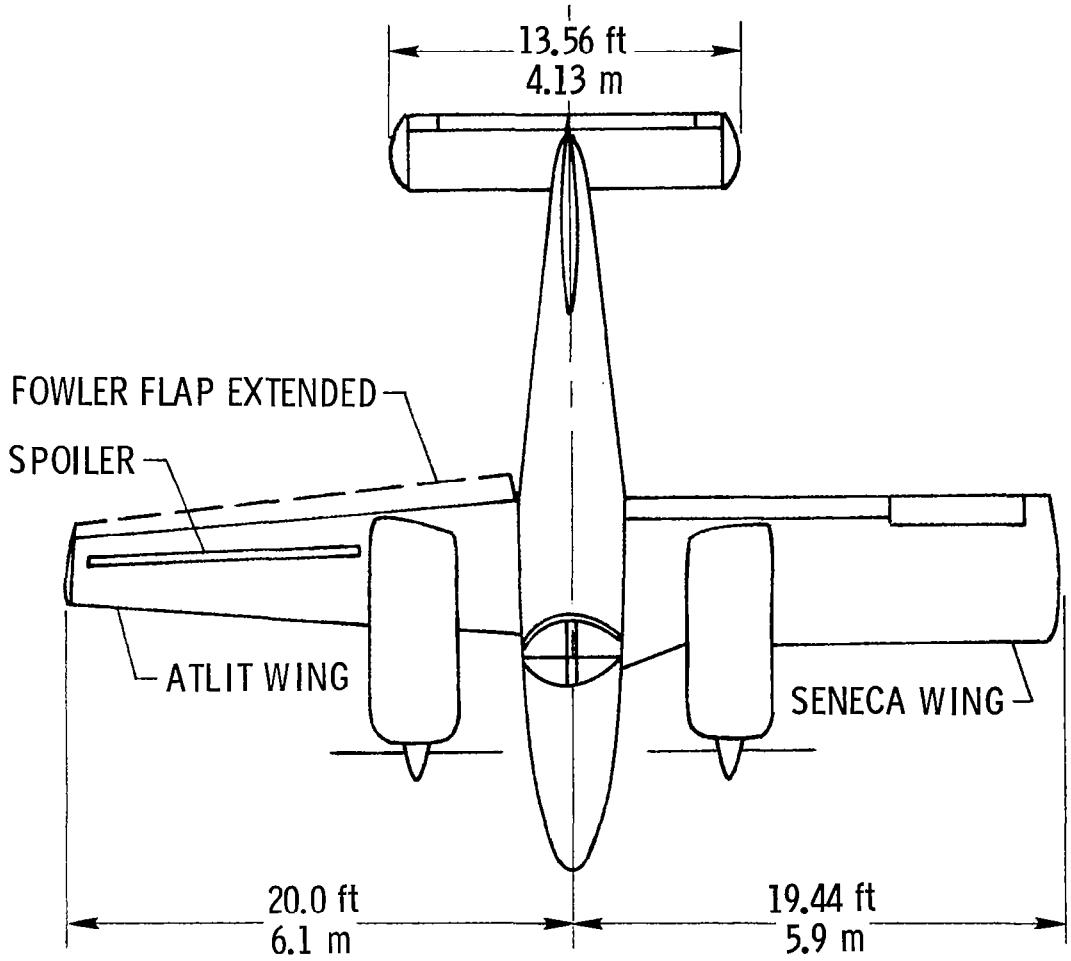

Figure 3.1.- Planview comparison of the ATLIT and the unmodified Piper PA-34-200 Seneca I.

TABLE 3.1 - COMPARISON OF ATLIT AND PIPER PA-34-200 SENECA I DESIGN SPECIFICATIONS

ITEM	ATLIT	PA-34
GROSS WEIGHT, N (lb)	18700 (4200)	18700 (4200)
WING AREA, M^2 (sq ft)	14.4 (155.0)	19.4 (208.7)
TAPER RATIO	0.5	1.0
ASPECT RATIO	10.32	7.25
SPAN, M (ft)	12.19 (40.0)	11.85 (38.88)
SPAN LOADING, N/M (lb/ft)	1536 (105)	1581 (108.2)
WING LOADING, N/M (lb/sq ft)	1298 (27.1)	964 (20.12)
FLAP TYPE	FOWLER	PLAIN
SPAN, PERCENT OF b	88	50
CHORD, PERCENT OF c	30	20
SPOILER TYPE	TRIANGULAR CROSS-SECTION	-
SPAN, PERCENT OF b/2	49.6	-
CHORD, M (inches)	0.089 (3.5)	-
AIRFOIL	GA(W)-1 (17% t/c)	65_2-415

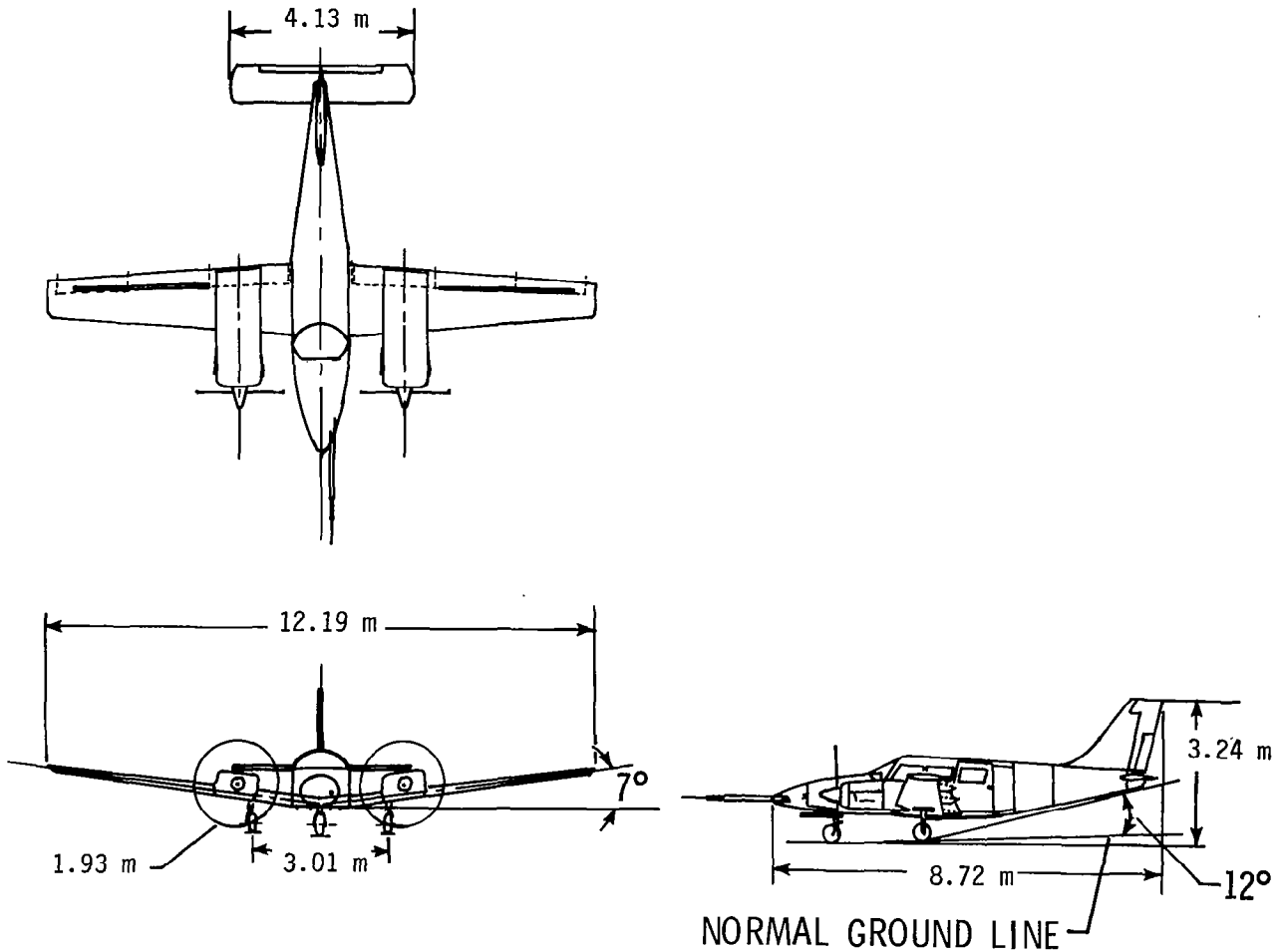

Figure 3.2.- ATLIT three-view.

TABLE 3.2- ATLIT ENGINEERING DESIGN DRAWINGS

DRAWING NO.	TITLE
90-000140	Lines - Nacelle
90-000145	Lines - Wing Tip
90-010010	Master Diagram - Wing
90-010011	ATLIT Wing General Dimensional Info.
90-020000	ATLIT Three View Drawing
90-100000	Wing Installation
90-110000	Wing Assy Complete
90-110001	Wing Assy Outboard
90-110002	Wing Assy Inboard
90-110100	Spar Assy - Wing Main
90-110101	Cap - Wing Main Spar Lower
90-110102	Cap - Wing Main Spar Upper
90-110106	Doubler Instl. Brake Clearance
90-110107	Side Brace Supt Instl. - Landing Gear
90-110108	Fitting - Side Brace - Landing Gear
90-110200	Spar Assy - Wing Rear (64%) Outbd
90-110210	Cap 64% Spar - Outbd
90-110211	Tee 64% Spar - Outbd
90-110212	Angle 64% Spar Splice
90-110250	Spar Assy - Wing (64%) Inbd
90-110255	Cap - 64% Spar - Inbd
90-110300	Sub Spar Assy - 24% - Wing
90-110301	Cap - 24% Spar - Details
90-110302	Angle - 24% Spar Splice
90-110400	Spar Assy - Center Section, Wing
90-110401	Cap - Lower, Center Section, Wing
90-110402	Cap - Upper, Center Section, Wing
90-110403	Tie - Lower, Center Section, Wing
90-110404	Tie - Upper, Center Section, Wing
90-110500	Stringer - Wing
90-110550	Stringer Assy - 24%
90-110555	Angle - Stringer Splice
90-110600	Door - Wing Access
90-110700	T. E. Instl.
90-110701	Flap Track Instl. - Sta. 28.00
90-110702	Flap Track Instl. - Sta. 100.00
90-110703	Flap Track Instl. - Sta. 171.00
90-110704	Flap Track Instl. - Sta. 231.00
90-110710	Track - Wing Flap
90-110711	Rib Instl - Sta. 45.50 Wing T. E.
90-110712	Rib Instl - Sta. 64 Wing T. E.
90-110713	Rib Instl - Sta. 79.50 Wing T. E.
90-110714	Rib Instl - Sta. 114.00 Wing T. E.
90-110715	Rib Instl - Sta. 126.00 Wing T. E.
90-110716	Rib Instl - Sta. 142.50 Wing T. E.
90-110717	Rib Instl - Sta. 151.50 Wing T. E.
90-110718	Rib Instl - Sta. 186.00 Wing T. E.
90-110719	Rib Instl - Sta. 201.00 Wing T. E.
90-110270	Rib Instl - Sta. 215.00 Wing T. E.
90-110721	Beam Wing T. E.
90-110722	Angles - Wing T. E.
90-110723	Angle - T. E.
90-110724	Plate - Wing T. E.
90-110728	Zee Section - T. E. Rib 142.50
90-110729	Doubler - T. E. Rib 142.50
90-110730	Clip - T. E. Rib
90-110731	Angle - W. S. 114.00
90-110732	Zee Section - T. E. Rib W. S. 114.00
90-110733	Channel - W. S. 114.50
90-110734	Angle - W. S. 126.00
90-110735	Zee Section - T. E. Rib 126.00
90-110736	Channel - T. E. Rib 126.00
90-110737	Zee Section - T. E. Rib 186.00
90-110738	Channel - T. E. Rib 186.00
90-110743	Angle - T. E. Rib 151.50
90-110744	Zee Section - T. E. Rib 151.50
90-110745	Channel - T. E. Rib 151.50
90-110748	Angle - T. E. Rib 215.00
90-110749	Channel - T. E. Rib 215.00
90-110750	Zee Section - T. E. Rib 215.00
90-110751	Angle - T. E. Rib 201.00
90-110752	Zee Section - T. E. Rib 201.00
90-110753	Channel - T. E. Rib 201.00
90-110754	Angle - Wing R. E.
90-110756	Angle - Track W. S. 28.00
90-111001	Rib Instl - Wing Cant. - Sta. 28
90-111002	Rib Instl - Wing - Sta. 41
90-111003	Rib Instl - Wing - Sta. 54
90-111004	Rib Instl - Wing - Sta. 64
90-111005	Rib Instl - Wing - Sta. 86.00
90-111006	Rib Instl - Wing - Sta. 100
90-111007	Rib Instl - Wing - Sta. 111.00
90-111008	Rib Assy - Wing - Sta. 126
90-111009	Rib Assy - Wing - Sta. 141
90-111010	Rib Assy - Wing - Sta. 156
90-111011	Rib Assy - Wing - Sta. 171
90-111012	Rib Assy - Wing - Sta. 186
90-111013	Rib Assy - Wing - Sta. 201
90-111014	Rib Assy - Wing - Sta. 216
90-111015	Rib Assy - Wing - Sta. 231
90-111020	Rib - Wing Cant - Sta. 28
90-111021	Fitting - Wing Mount, Fwd
90-111022	Fitting - Wing Mount, Aft
90-111023	Tee - Rib, Cant. - Sta. 28
90-111024	Angle - Rib, Cant. - Sta. 28

TABLE 3.2- Continued

DRAWING NO.	TITLE
90-111025	Frame Assy - Leading Edge, Inbd Wing
90-111026	Frame Instl. - Canted, Inbd Wing
90-111027	Frame - Leading Edge, Inbd Wing
90-111028	Angle - Leading Edge, Inbd Wing
90-120000	Flap Instl.
90-120100	Flap Assy - Inbd
90-120101	Carriage Assy, W. S. 28.00
90-120102	Rib Assy - Flap W. S. 42.40
90-120103	Rib Assy - Flap W. S. 56.80
90-120104	Rib Assy - Flap W. S. 71.20
90-120105	Rib Assy - Flap W. S. 85.60
90-120106	Rib Assy - Flap W. S. 28.00
90-120107	Carriage - Flap W. S. 28.00
90-120108	Gusset - Inbd Flap
90-120109	Gusset - Inbd Flap
90-120111	Spar Assy - Flap Inbd
90-120114	Clip - Inbd Flap
90-120115	Clip - Inbd Flap
90-120116	Clip - Inbd Flap
90-120117	Clip - Inbd Flap
90-120200	Flap - Assembly Center
90-120201	Carriage - Flap W. S. 100.00
90-120202	Rib Assy - Flap W. S. 100.00
90-120203	Carriage Assy - W. S. 100.00
90-120204	Rib - Flap W. S. 114.20
90-120205	Rib - Flap W. S. 128.40
90-120206	Rib - Flap W. S. 142.60
90-120207	Rib - Flap W. S. 156.80
90-120208	Gusset - Flap Drive W. S. 166.00
90-120209	Spar Assy - Flap Ctr.
90-120210	Angle - Center Flap
90-120300	Flap Assembly - Outboard
90-120301	Carriage - Flap W. S. 231.00
90-120302	Rib Assy W. S. 230.34
90-120303	Carriage Assy W. S. 231.00
90-120304	Rib - Flap W. S. 186.00
90-120305	Rib - Flap W. S. 201.00
90-120306	Rib - Flap W. S. 216.00
90-120307	Carriage - Flap W. S. 171.00
90-120308	Rib Assy - Flap W. S. 171.00
90-120309	Carriage Assy W. S. 171.00
90-120310	Spar Assy Outbd Flap
90-120311	Gusset - Flap Drive - 227
90-120315	Angle - Clip Flap Spar
90-120400	Pushrod Assy - Wing Flap
90-120532	Bracket - Flap Lever
90-120600	Support Bracket - Flap B/C
90-120700	Lever Assy - Flap

DRAWING NO.	TITLE
90-120800	Link Assy - Flap Drive
90-120801	Universal - Flap Drive
90-120802	Bracket
90-120803	Bracket - Inbd Flap
90-120804	Bracket - Inbd Flap
90-120805	Bracket - Weld Assy
90-120806	Bracket - Weld Assy, 227.0
90-120900	Angles - Flap Bracket Attachment
90-130000	Spoiler Instl.
90-130100	Spoiler Assy
90-130200	Spoiler Assy Center
90-130300	Spoiler Assy - Outbd
90-130401	Pushrod - Spoiler
90-130402	Link Assy - Spoiler
90-130403	Lever Assy - Spoiler
90-130404	Sector Assy - Spoiler Drive
90-130405	Bracket Assy - Spoiler
90-130406	Hinge Assy - Spoiler
90-130407	Hinge Half Assy - Spoiler
90-130408	Hinge Half - Spoiler
90-130409	Fitting - Link Attachment
90-130410	Bracket Details - Spoiler
90-130411	Rod End - Spoiler Drive
90-130501	Bracket Assy - Spoiler Pulley
90-130503	Spring - Spoiler
90-130504	Bracket Assy - Spoiler
90-130505	Bracket - Details - Spoiler
90-130506	Bracket Assy - Spoiler
90-130507	Bracket Details - Spoiler
90-130508	Cable Assy - Spoiler
90-140000	Nacelle Instl.
90-140001	Rib Instl. - Nacelle - Wing Sta. 64.00
90-140002	Rib Instl. - Nacelle - Wing Sta. 86.00
90-140003	Frame Instl. - Nacelle - Wing Sta. 82.26
90-140004	Frame Instl. - Nacelle - Wing Sta. 94.26
90-140005	Frame - Nacelle - Wing Sta. 82.26
90-140006	Frame Instl. - Nacelle 64%
90-140007	Bracket - Nacelle
90-140008	Angle - Nacelle - Rib
90-140009	Angle - Nacelle - Rib
90-140011	Frame - Nacelle - Sta. 94.26
90-140012	Frame - Nacelle - Sta. 94.26
90-140013	Frame - Nacelle - Sta. 94.26
90-140014	Fitting - Upper, Nacelle
90-140015	Fitting - Lower, Nacelle
90-140016	Tee - Nacelle Rib
90-140017	Angle - Nacelle Rib

TABLE 3.2- Concluded

DRAWING NO.	TITLE
90-400100	Fuselage Structure Assy
90-400101	Frame Instl. - F. S. 73.04
90-400102	Frame Instl. - Sta. 106.628
90-400103	Fitting - Fwd Fuselage Wing Attach
90-400104	Fitting - Wing Mount, Aft, Fuselage
90-400105	Gusset - Lower Fuselage - Sta. 73.04
90-400106	Gusset - Lower Fuselage - Sta. 73.04
90-400107	Side Frame - Sta. 73.04
90-400108	Channel - F. S. 73.04
90-400109	Channel - Sta. 74.105
90-400110	Frame - F. S. 73.04
90-400111	Channel - Lower Fuselage, Sta. 73.04
90-400112	Clip - Lower Fuselage, Sta. 73.04
90-400113	Bracket - Lower Fuselage, Sta. 73.04
90-400114	Web - Upper Cockpit - Left Side
90-400115	Web - Upper Cockpit - Right Side
90-400116	Dblr - Cockpit - Fwd - Lwr
90-400117	Channel - Cockpit - Fwd - Lwr
90-400118	Support Fittings BHD 106.628
90-400119	Dblr - Cockpit - Lwr - Aft
90-400120	Angle - Lower Fuselage - Sta. 128.737
90-400121	Clip - Lower Fuselage - Sta. 128.737
90-400122	Support Fittings BHD 106.628
90-400123	Channel - Spar Box - Left Forward
90-400124	Channel - Lwr Fuselage - Sta. 104
90-400125	Bracket - Lwr Fuselage - Sta. 106.628
90-400126	Bracket - Lwr Fuselage - Sta. 106.628
90-400127	Channel - Lwr Fuselage - Sta. 106.628
90-400128	Strap - Lwr Fuselage - Sta. 106.628
90-400129	Web - Sta. 72.105
90-400130	Channel - Lwr Fuselage - Sta. 97
90-400131	Plate - Lwr Fuselage - Sta. 97
90-500000	Wing Elec. Harness Instl.
90-600000	Hydraulic Systems Instl.
90-700100	Sender Instl. - Fuel
90-800100	Landing Gear Instl. - Main
90-800101	Gear Assy - Main
90-800110	Fitting Assy Gear Attach, Aft
90-800111	Fitting Assy Gear Attach, Fwd
90-800211	Over Center Assy
90-800212	Link Assy - Over Center
90-800213	Lever Assy - Over Center
90-800214	Side Brace Assy
90-800215	Bolt Over Center Adjust
90-800216	Bracket Assy - Over Center - Spring
90-800217	Spring - Over Center - Gear
90-800218	Bracket Assy Cylinder Support

DRAWING NO.	TITLE
90-800300	Trunnion Assy
90-800310	Cylinder - Main Landing Gear
90-800311	Beam - Trunnion
90-800312	Brace - Trunnion
90-800353	Orifice Weld Assy
90-800354	Orifice Tube Assy
90-800382	Plate Assy - Orifice
90-800400	Bearing - Landing Gear
90-800500	Stop Instl. - Landing Gear
90-800501	Stop Assy - Landing Gear
90-800502	Up Limit Switch Instl. - Main Landing Gear
90-800600	Door Instl. - Main Landing Gear
90-900000	Fuel System Instl.
90-920000	Controls Instl. - Engine
90-920500	Lines and Tachometer Instl - Engine Instruments
90-930000	Pitot Boom Instl.

3.2.1 ATLIT Planform Changes

The ATLIT planform has an aspect ratio of 10.32, taper ratio of 0.5, and a wing span of 12.1 m (40 ft). These planform changes should produce performance and ride-quality improvements for the following reasons:

1. The induced-drag term of the airplane wing may be written as

$$D_i = \left(\frac{W}{b}\right)^2 \frac{1}{\pi e q_c} \quad . \tag{3.1}$$

It follows that (for a fixed weight and velocity) the induced drag is

$$D_i \sim \frac{1}{b^2 \cdot e} \tag{3.2}$$

or the equivalent expression

$$D_i \sim \frac{1}{S \cdot A \cdot e} \quad . \tag{3.3}$$

On ATLIT, the increase in aspect ratio offsets the decrease in wing area so that the product, S·A, is increased about 5 percent. As relation (3.3) indicates, an increase in S·A will reduce the induced drag by about 5 percent for ATLIT. In simpler terms, the same induced-drag change may be explained by noting the effect in relation (3.2) of the slight increase in the ATLIT span over the Seneca span. In this case, increasing aspect ratio (alone) does not reduce induced drag; but, increasing span does.

The effect of the 5-percent reduction in D_i for ATLIT, on total airplane drag is small. Induced drag on ATLIT is 10 percent of total drag at cruise and 50 percent of total drag at climb. These contributions of the ATLIT planform changes to reducing total airplane drag become less than 1 percent at cruise and less than 3 percent at climb.

2. With the 25-percent smaller wing area, the profile drag of the airplane will be reduced. As shown below, this reduction occurs in spite of the higher $C_{d_{o,\,min}}$ of the 17-percent thick airfoil on ATLIT because

the product, $C_{d_o} \cdot S$, decreases compared to the standard wing. The magnitude of this change is estimated, using section data, as follows:

Airplane	Airfoil	$C_{d_{o,\,min}}$ (fixed transition, RN = 6×10^6)	S	$C_{d_{o,\,min}} \cdot S$	Wing profile drag Δ%
ATLIT	17%t/c, GA(W)-1	0.0106	14.4 m^2	0.15	-25%
PA-34	65_2 415	0.0101	19.4 m^2	0.20	

Assuming that wing-profile drag is about 35 percent of total airplane drag at cruise and about 20 percent of total airplane drag at climb, the 28-percent change in wing-profile drag reduces airplane drag by the following amounts:

	change in wing-profile drag for smaller wing	X	wing-profile drag / total airplane drag	=	change in total airplane drag
at cruise	28%	X	35%	=	9.8%
at climb	28%	X	20%	=	5.6%

3. The tapered ATLIT wing contributes to increasing the wing-span efficiency factor (e) by 3.4 percent (reference 23). However, it is difficult to translate this into an effect on total airplane drag without knowledge of the interference effects of the modified wing on the standard fuselage. Interference-induced separation drag, varying with C_L^2, will appear as reduced span efficiency. It is also difficult to account for the effect on span efficiency of reducing the wing area with no change in fuselage or engine nacelles. With the fuselage and nacelle wetted areas

becoming proportionately larger in relation to wing area, the effect of these bodies on span loading may also become proportionately larger. The result could be reduced span efficiency.

Assuming no detrimental interference effects, the contribution of taper to increased span factor could reduce both climb and cruise drag by about 4 percent.*

4. The 25-percent reduction in wing area on ATLIT will reduce the airplane cruise gust response by about 20 percent.** The improvement in ride quality (sorely needed in general aviation airplanes) would add to the attraction of designing light airplanes with higher wing loadings.

The wings for both the basic Seneca and ATLIT have 3 degrees of twist for desirable stall characteristics.

---

* At cruise, $D_i = \frac{C_L^2 \, q_c \, S}{\pi e A}$ = 10 percent of total airplane drag. Assume e increases from 0.75 to 0.783, then for V = 170 knots and S = 14.4 m^2, cruise D_i decreases from 250 N (56 lb) to 239 N (54 lb). For climb, V = 90 knots, D_i decreases from 779 N (175 lb) to 745 N (167 lb).

** $n_\alpha = C_{L_\alpha} \, q_c \, S$

at cruise

for ATLIT: $n_{\alpha,A} = (0.100 \text{ deg}^{-1}) \times (4.26 \text{ kPa}) \times (14.4 \text{ m}^2)$

for PA-34: $n_{\alpha,S} = (0.080 \text{ deg}^{-1}) \times (4.26 \text{ kPa}) \times (19.4 \text{ m}^2)$

$$\frac{n_{\alpha,S} - n_{\alpha,A}}{n_{\alpha,S}} \times 100 \simeq 20\%$$

Summarizing, the net effect of the ATLIT wing-planform changes are given below:

1. Increased span for lower induced drag.
2. Tapered wing for increased span efficiency.
3. Reduced wing area for lower wing profile drag.

3.2.2 Roll Control Spoilers

The decision to provide roll control on ATLIT by means of spoilers freed the entire trailing edge of the wing for a high-lift device. The requirement for a large-span, high-lift flap follows the decision to design the planform with high wing loading.

The spoilers on ATLIT can be described as vented, gapped, upper-surface, roll-control spoilers. Figure 3.3 illustrates the geometry of this spoiler in cross section. In the literature (references 24 and 25), this type of spoiler has been referred to as a "slot-lip aileron." In order to make the difference between spoilers and ailerons distinct, any reference in this report to roll-control spoilers will imply an aerodynamic device which creates airplane rolling motion by the mechanism of separated flow on only one wing at a time. An aileron roll-control system, on the other hand, creates airplane rolling motion by changing lift on both wings simultaneously (by deflecting the wake due to a change in camber).

The design details of the spoilers on ATLIT are presented here.

Spoiler Vent-Path

In the past, typical defects of roll-control spoilers have included nonlinear rolling moment variations with control-wheel deflections, control reversal for small deflections, and reduced effectiveness at

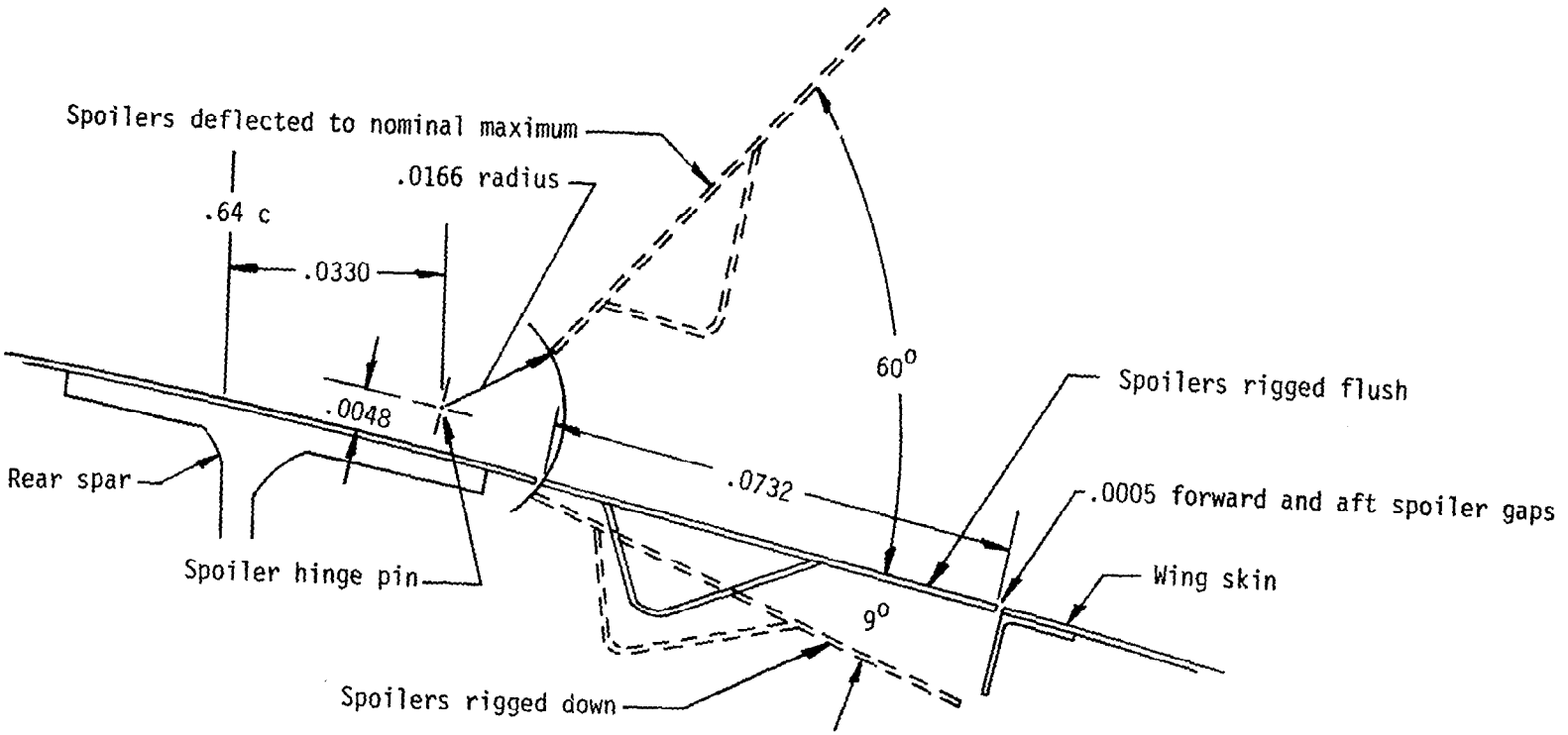

Figure 3.3.- Spoiler installation detail.

high angle of attack. Wind-tunnel spoiler-development tests (references 15, 16, and 17) confirmed these defects for an unvented spoiler in the flap-deflected configurations. In general, roll-control spoilers will not exhibit these characteristics in a flaps-nested configuration.

The three undesirable traits of spoilers noted above are created by flow conditions at the spoiler. With a Fowler flap deflected, flow through the flap slot is accelerated, generating additional accelerated flow by a "jet effect" in the region by the spoilers. Under these conditions, a small spoiler deflection will create flow separation; but, because of the higher local dynamic pressure, this separated flow behind the spoiler is prone to reattach itself to the wing upper surface before reaching the trailing edge. The net effect of this small spoiler deflection, then, is an increase in effective camber. The increased camber creates lift and results in a control reversal. With flaps up, however, flow conditions at the spoiler location have relatively lower dynamic pressure. Under these conditions, flow separation caused by small spoiler deflections tend to remain separated into the wake, thus creating a proper rolling moment.

The preceding wind-tunnel development work was done, in part, to optimize the vent-path or spoiler-cavity geometry (see figure 3.3) to provide some relief from the objectionable spoiler traits. The vent path on ATLIT eliminates control reversal and reduces the nonlinearity in roll response. The shape of the spoiler cavity also influences the hysteresis characteristics in rolling moments due to spoiler deflections (reference 16).

Spoiler Leading Edge Gap

An important development in the application of roll-control spoilers to airplanes was the addition of a leading edge gap to the device (see figure 3.3). This feature improved the linearity of hinge moments, improved roll-control effectiveness of small spoiler deflections, and reduced the lag in roll acceleration (reference 13). The first spoiler design of note to fly incorporating leading edge gap was the Mitusbishi MU-2 of the early 1960's.

Spoiler Cross-Sectional Shape

Wind-tunnel studies (reference 17) indicate that spoiler hinge moments are apparently influenced by the combination of the underside contour of the spoiler and the leading edge gap. The cross-sectional shape of the spoiler apparently has only a slight effect on rolling moment charactistics.

The triangular cross section for the ATLIT spoilers was chosen for its light weight and simple construction. Hinge-moment characteristics for this spoiler were documented in 3-D wind-tunnel tests (reference 17).

Design for Lateral-Control Feel*

During the mechanical design of the ATLIT lateral-control system, there were virtually no data available on spoiler-hinge moments. The mechanical system was designed using available split-flap data to estimate hinge-moment characteristics of the spoilers. Figure 3.4 presents a comparison of the estimated and wind-tunnel measured spoiler-hinge moments.

---

*Mr. John T. Calhoun of Robertson Aircraft Corporation should be credited with the design of the ATLIT spoiler roll-control system.

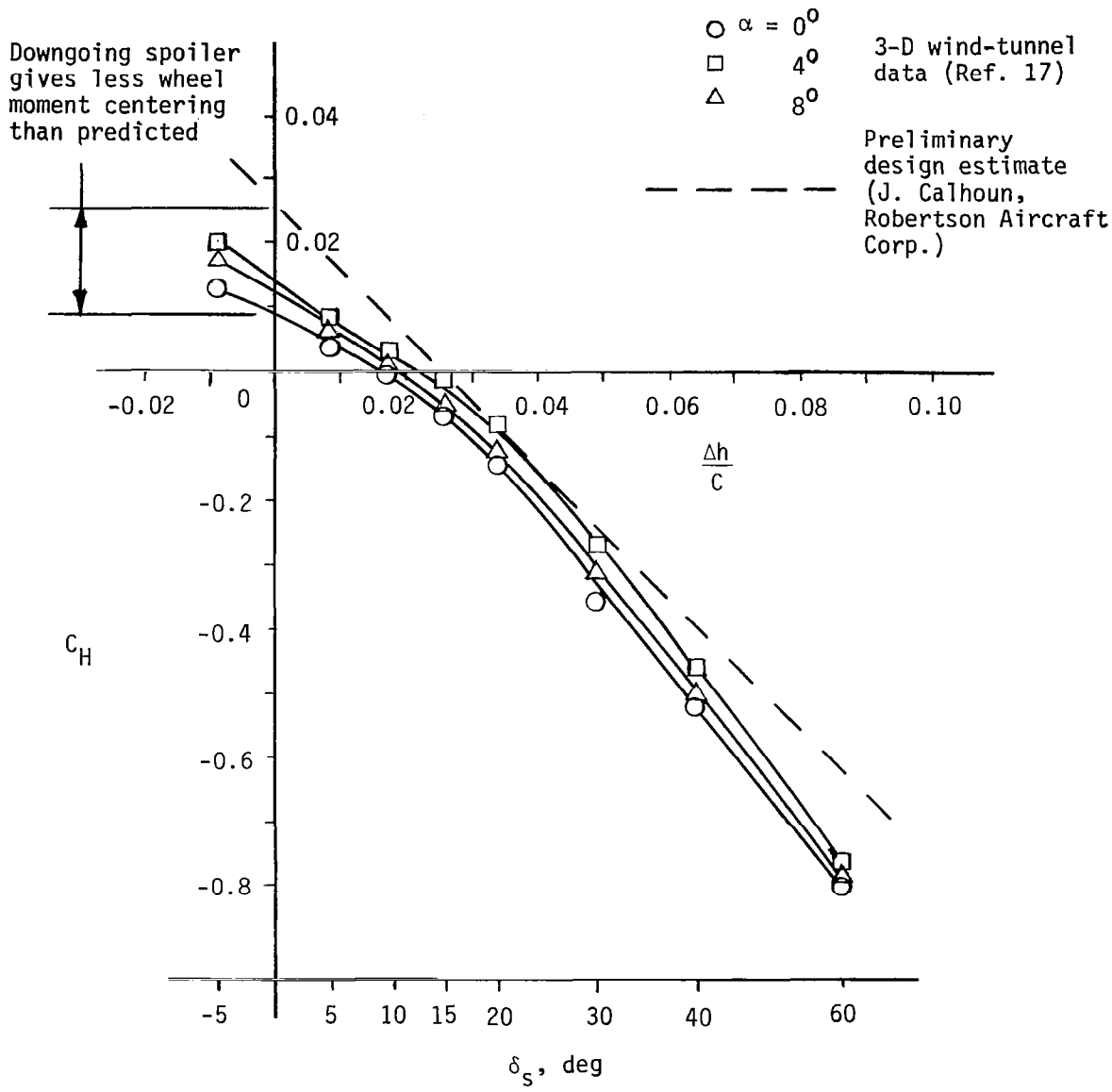

a) Flaps nested

Figure 3.4.- Comparison of predicted and wind-tunnel measured (Ref. 17) spoiler hinge moments for ATLIT

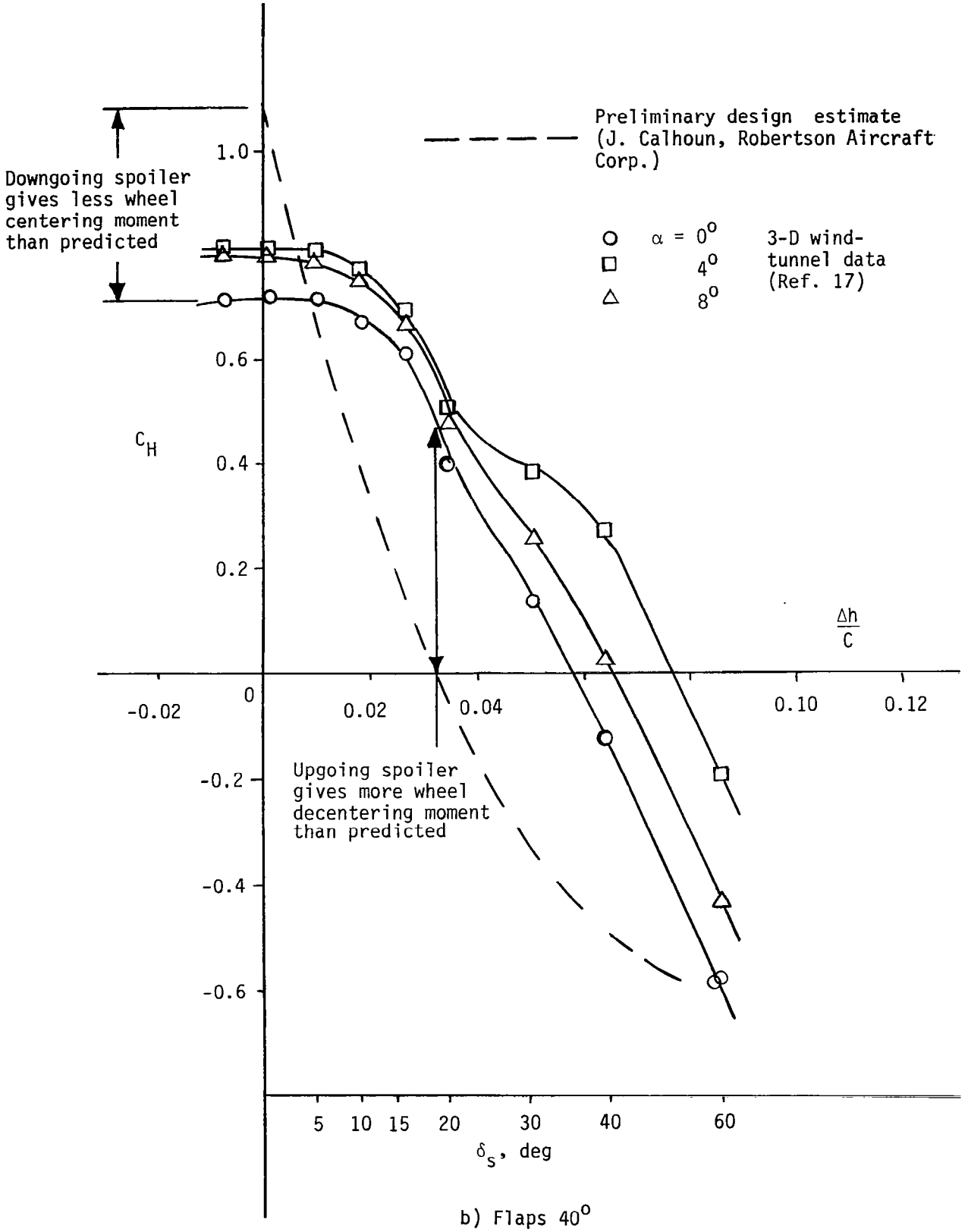

b) Flaps 40°

Figure 3.4.- Concluded.

Wheel forces in a lateral-control system are tailored to provide wheel centering without excessive force for maximum wheel travel. Meeting this requirement with spoilers presents a problem, because the hinge moments are in the wrong direction during the first 20^{o} to 30^{o} of deflection.

Vented spoilers in the neutral position are subject to positive or opening hinge moments. As the spoiler is deflected up to some intermediate position, the hinge moment will go to zero, change sign, and the spoiler will experience a closing moment. The ATLIT spoiler-control linkages are designed to provide a wheel centering force during the initial spoiler deflections where the aerodynamic forces tend to open the spoiler and decenter the wheel.

The source of the wheel centering force on ATLIT and on several other mechanical spoiler designs is the aerodynamically inactive spoiler. On ATLIT, the left and right spoilers are connected by a high-differential solid linkage (no cams). Figure 3.5 illustrates the gearing of the spoiler motion with varying wheel position. The figure shows that when one spoiler goes up, the other moves down, then back up slightly as the wheel reaches full travel. The system is designed to allow the hinge moments of the downgoing spoiler to oppose the wheel decentering hinge moments of the upgoing one (see figure 3.6).

A comparison of estimated and measured hinge moments in figure 3.4 indicated that ATLIT would have undesirable lateral-feel characteristics. In the flap-nested case, the wind-tunnel measured opening hinge moment

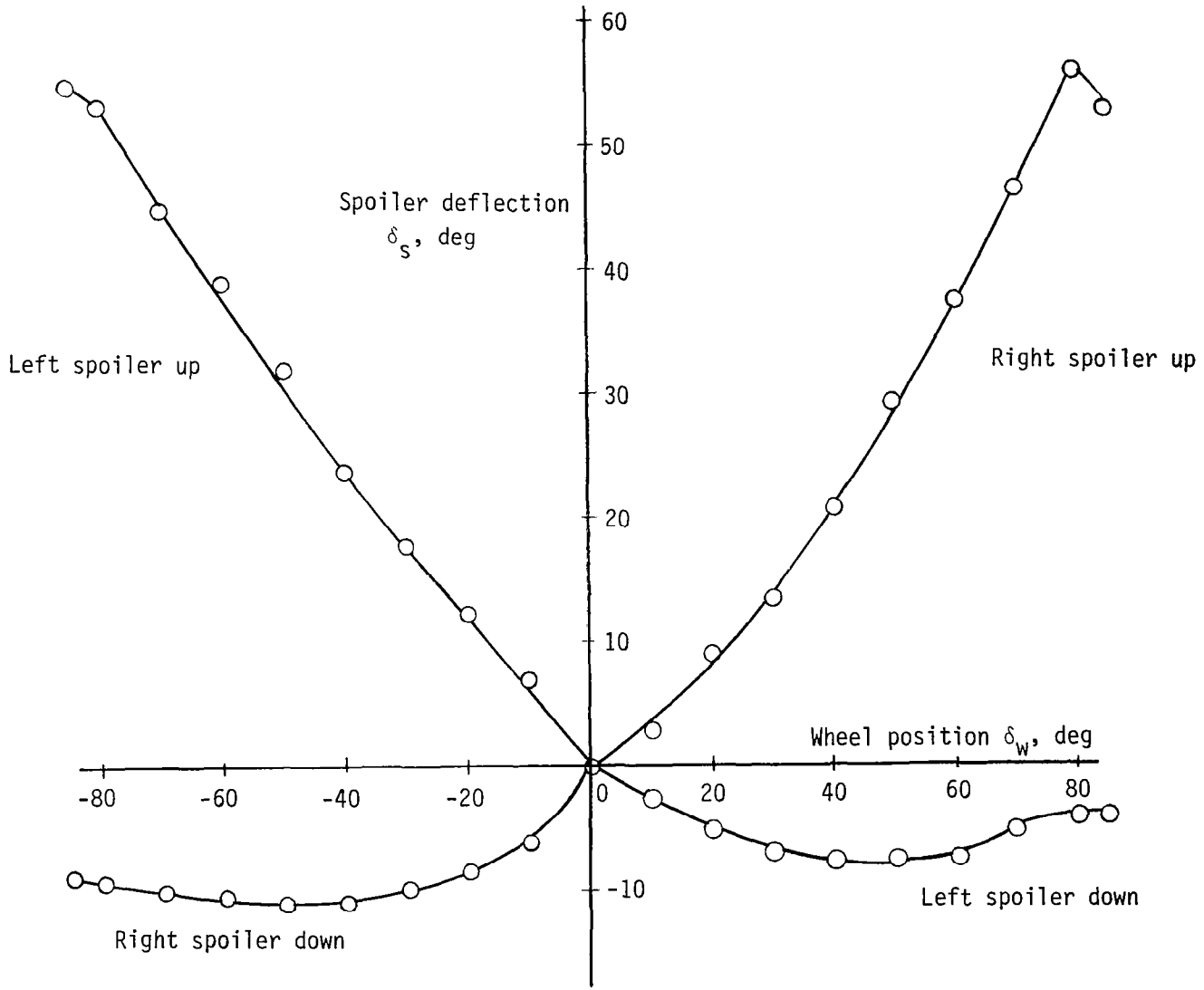

Figure 3.5.- Gearing between spoiler deflection and control-wheel position.

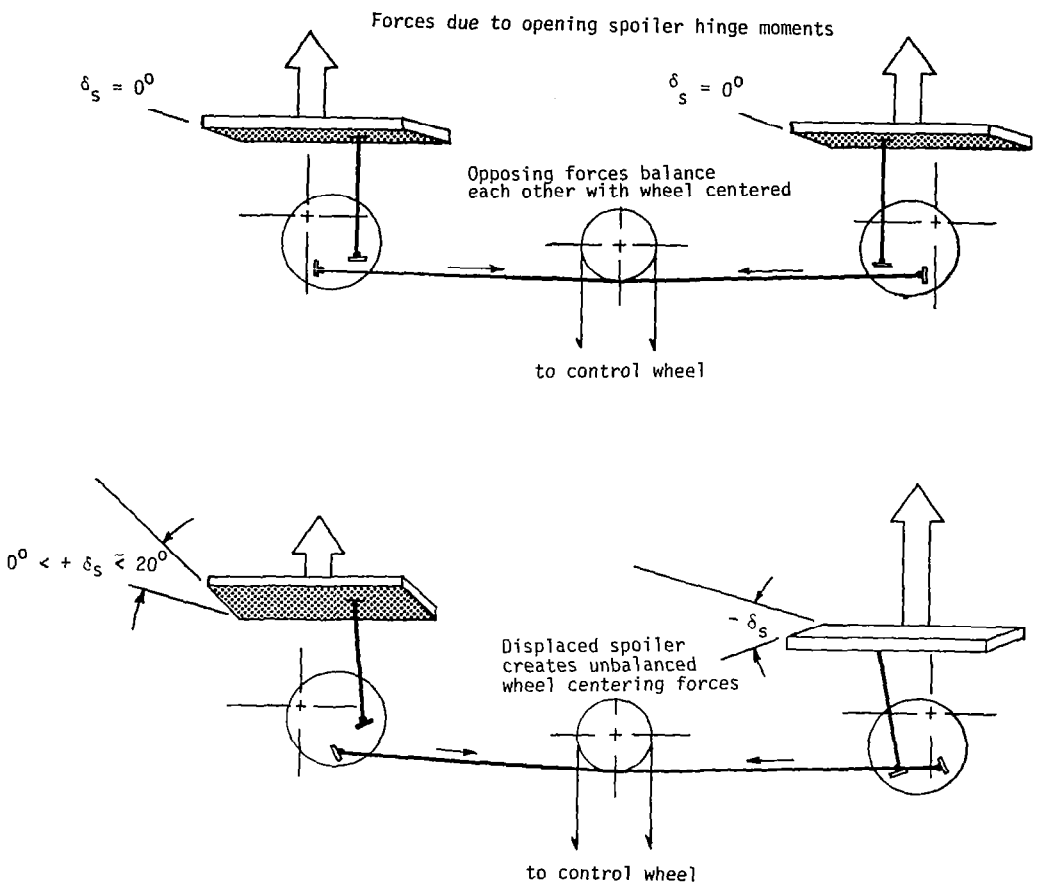

Figure 3.6.- The effect of opening (positive) spoiler hinge moments on wheel forces.

of a downgoing spoiler is about one-half of the design estimate. The flaps-up wheel centering force was reduced accordingly. This means that the opening hinge moment of the upgoing spoiler dominates, resulting in net wheel decentering forces. The same holds true for the flaps-down case, except that the difference and forces involved are larger.

The amount of friction in the ATIT lateral-control system is large. This friction, by itself objectionable, partially masks the aerodynamic wheel decentering forces for small or large control inputs.

A conclusion which may be drawn from this analysis is that accurate hinge-moment data are prerequisite to the design of mechanically-actuated roll-control spoilers with tolerable lateral control wheel-force characteristics. This requirement necessitates strong justification for putting a spoiler system on an airplane (e.g., a need for full-span flaps or direct-lift control). When a strong case can not be made for spoilers, the relative simplicity and lower cost of an aileron roll-control system will sway the decision to ailerons.

Spoiler Leakpath Seals

As discussed earlier, there is no requirement for lower- to upper-wing surface venting with flaps up. Quite to the contrary, any leakage of pressure through the wing is to be avoided. The ATLIT design did not consider the effect of allowing leakage through the spoilers. Wind-tunnel studies late in the design stages (reference 17) indicated that there would be lift and drag penalties due to leakage. Therefore,

as an operational solution to the leakage effects, a rubber weatherstripping seal was added (see figure 3.7). As shown in the wind tunnel, a beneficial effect of sealing the leakpath is that the flaps-up spoiler hinge moments are eliminated (spoilers neutral).

Spoiler Rigging

With the spoiler leakpath unsealed, the spoilers floated up about 2 or 3 degrees. This floating was eliminated by rigging the spoilers symmetrically down below the wing surface. Thus, with flight airloads, the spoilers would float up no higher than flush with the wing surface. A system with no leakage is doubly advantageous since there will be no spoiler float either with flaps up.

3.2.3 Full-Span Fowler Flaps

Increased flexibility in wing-area design is achieved by the application of high-lift devices. On the ATLIT design, this flexibility is provided by 30% c full-span Fowler flaps.

Two dimensional wind-tunnel development of this Fowler flap (reference 14) defined the slot gap and overlap for maximum lift in the $\delta_f = 40^o$ position (see table 3.3). This 2-D optimized gap and overlap is incorporated in the ATLIT design. Three-dimensional tunnel tests (reference 17), at a reduced Reynold's number using the optimum 2-D gap and overlap, failed to generate the expected maximum lift. A modified gap and overlap were defined which achieved the expected maximum lift on the 3-D model, but it is suspected that this anomaly is a Reynold's number effect rather than a 2-D to 3-D effect.

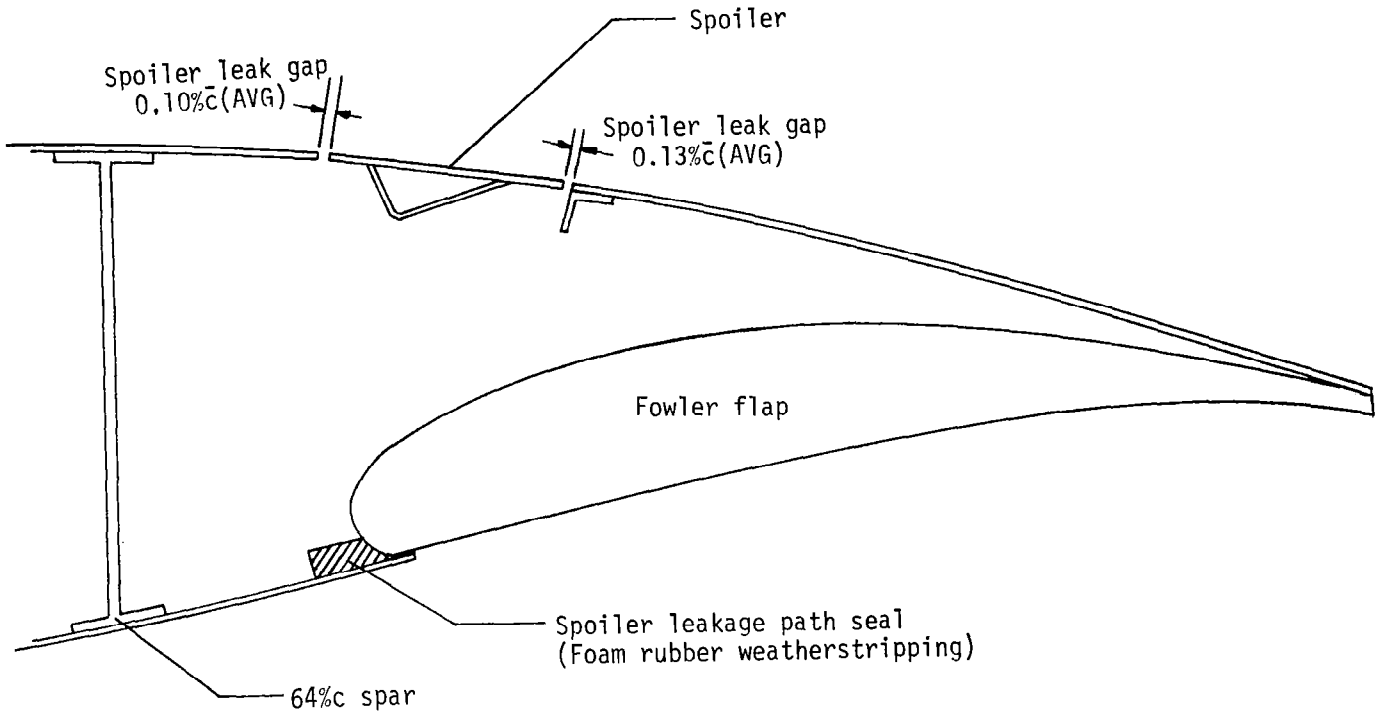

Figure 3.7.- ATLIT spoiler-leakage path with seals.

TABLE 3.3 - FOWLER FLAP SLOT DIMENSIONS FOR WIND TUNNEL AND FLIGHT TESTING

TESTS	GAP	OVERLAP	REYNOLDS NUMBER
2-D, REF. 4, OPTIMUM FOR $\delta_f = 40°$	2.7%c	-0.7%c	2.2×10^6
3-D, REF. 17, OPTIMUM FOR $\delta_f = 40°$	2.2%c	0.8%c	1.0×10^6
ATLIT TESTS, $\delta_{f_{max}} = 37.8°$	$2.8 \pm 0.5\%$	$0.7 \pm 0.4\%$c	2.2×10^6

The actual gap and overlap for the ATLIT has some span-wise variations due to construction tolerances. These are indicated below:

	Gap	Overlap
Average	+2.8% c	+0.7% c
Maximum	+3.3% c	+1.5% c
Minimum	+2.3% c	+0.4% c

The maximum flap deflection on ATLIT of $\delta_{f,\ max} = 37.8^{o}$ resulted from an NASA Langley Research Center, Quality Assurance Office, inspection requirement for certain clearances of the flap rollers in their tracks. The flap positions are illustrated in figure 3.8.

3.2.4 GA(W)-1 Airfoil

The development of the GA(W)-1, general aviation (Whitcomb), airfoil followed an iterative procedure of defining an airfoil shape, then evaluating its characteristics by the method of reference 6. The procedure required about 17 iterations to transform a Whitcomb 17-percent thick supercritical airfoil into one especially suited for a low-speed subsonic airplane (i.e., 200 knots top speed and RN = 6×10^{6}). The computer optimization of the airfoil emphasized low drag for lift coefficients ranging from cruise to climb and high maximum lift with docile stall characteristics. It was convenient, while not necessarily desirable, to retain the 17-percent thickness of the supercritical section. The final airfoil shape was evaluated in the wind tunnel (reference 5).

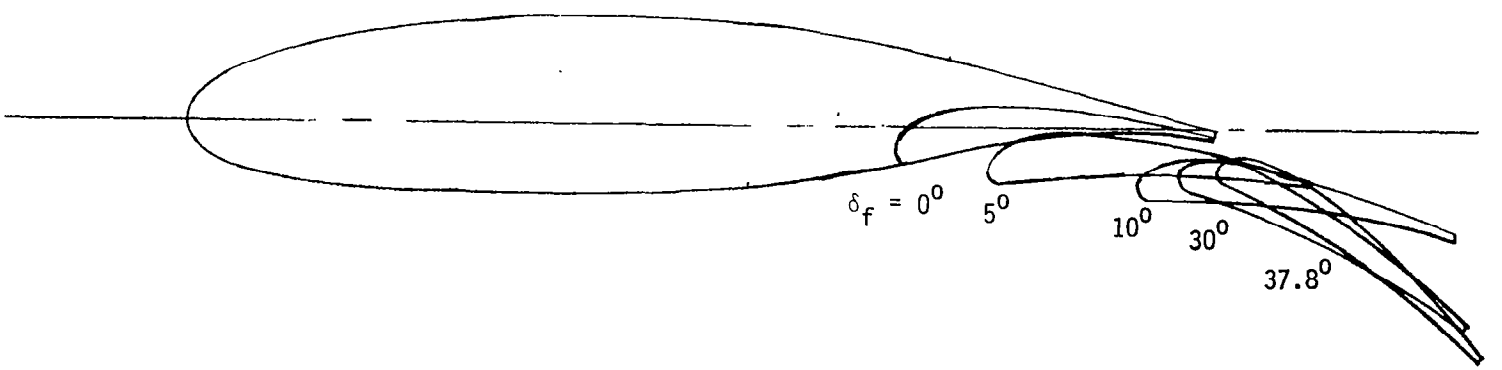

Figure 3.8.- ATLIT airfoil and flap geometry.

The GA(W)-1 17-percent thick airfoil is likely to be redesignated as the NASA-417 airfoil of the LS-1 (low-speed) family. This family, so far, includes airfoils which have design-lift coefficeints ranging from 0.2 to 0.6 and thicknesses from 13 percent to 21 percent. The family is being expanded and several GA(W)-1 airfoils are being modified to have different camber and thickness distributions.

For the ATLIT project, the 17-percent (GA(W)-1 section replaced the thinner airfoil of the standard wing, the 65_2-415 "laminar" section. Although this older 6-series airfoil was designed to have a laminar boundary layer over a large portion of the chord, the maintenance of conditions for laminar flow on a production light airplane is impractical. Thus, a comparison of section characteristics for the 6- and the GA-series airfoils with fixed transition is reasonable.

The essential differences in the two airfoils are apparent in figures 3.9 and 3.10. In particular, for the GA(W)-1 section, $(\frac{l}{d})_{max}$ is about 50-percent higher, $C_{l_{max}}$ is almost 30-percent higher, and, unfortunately, C_{d_o} is about 6-percent higher and C_{m_o} is about 60-percent higher than for the older 6-series airfoil.

The improvement in $\frac{l}{d}$ with the GA(W)-1 section should contribute to improvements in range and in climb performance.

The increase in section maximum lift permits greater flexibility in the design of a wing planform. Smaller wing areas may be designed while keeping the product, $C_{L_{max}} \cdot S$, constant.

A discussion of the effect of the higher C_{d_o} appears in section 3.2.1.

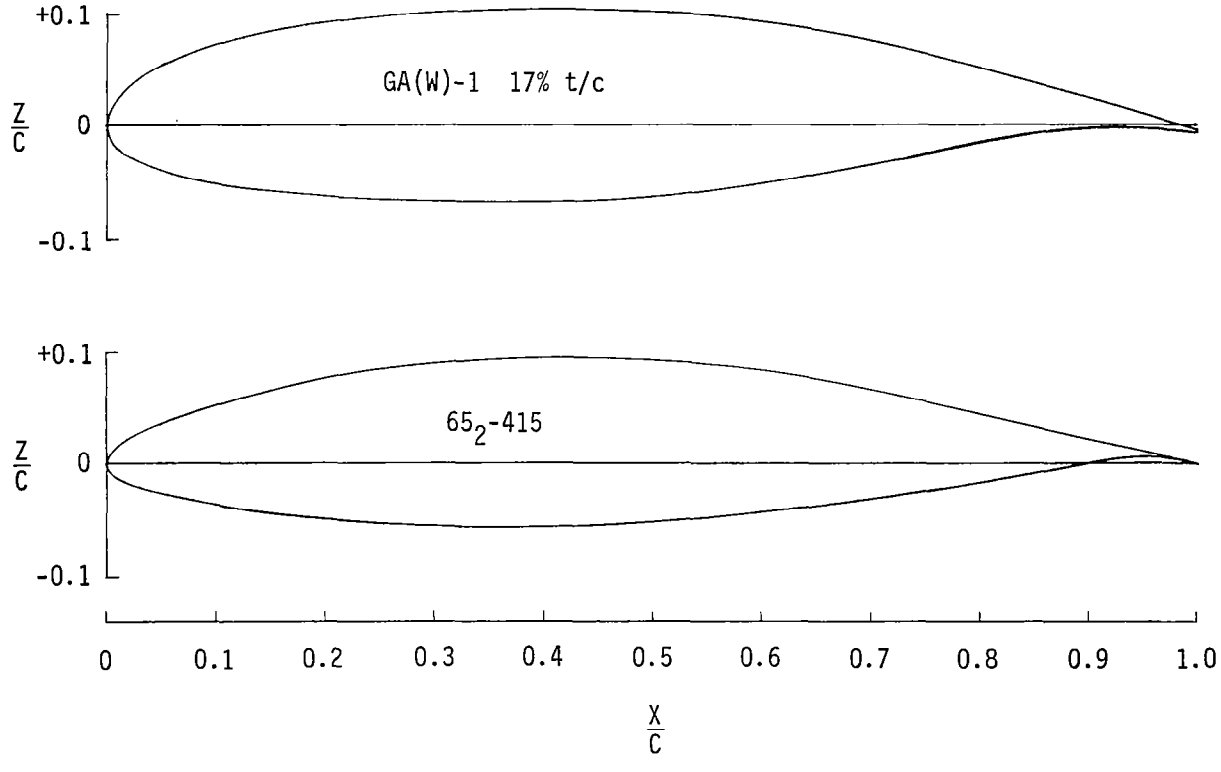

Figure 3.9.- Comparison of the GA(W)-1 and 65_2-415 airfoil shapes.

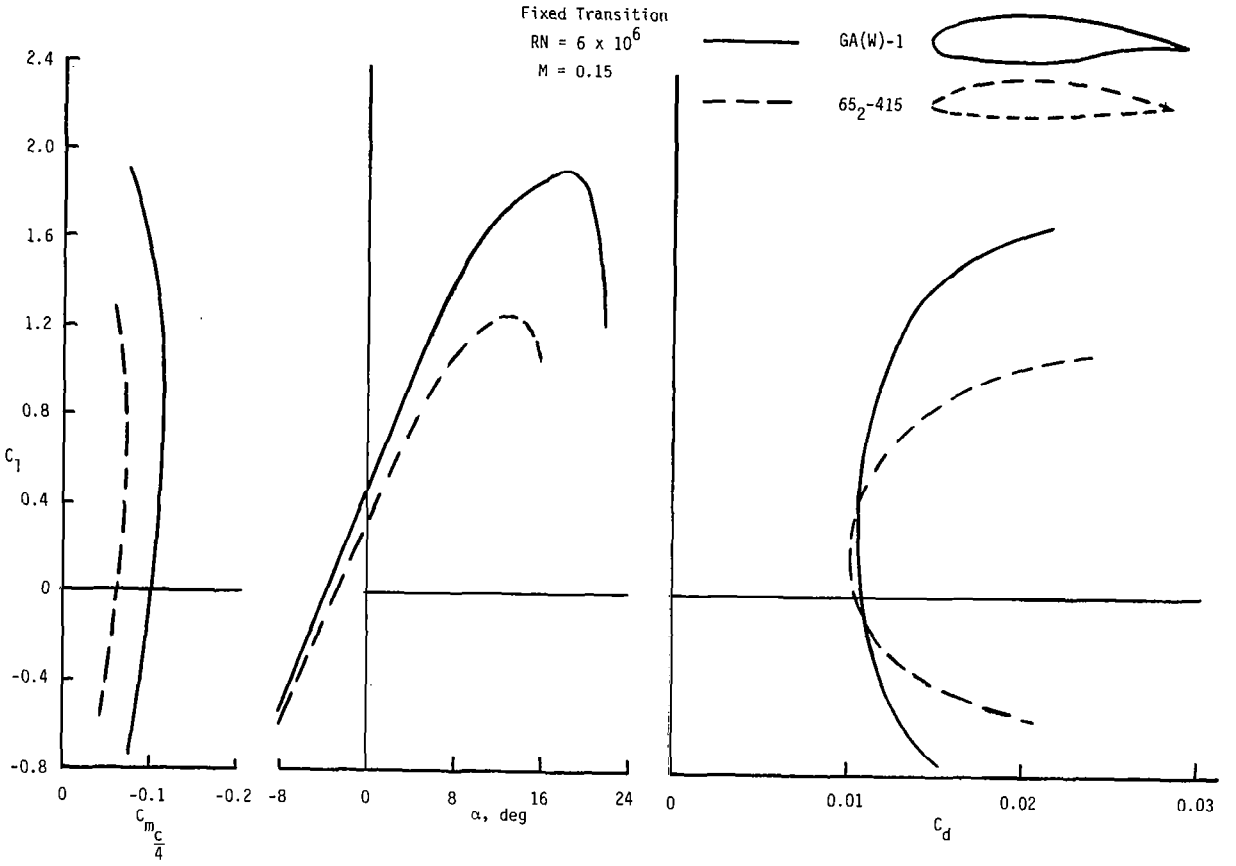

Figure 3.10- Comparison of section characteristics of the GA(W)-1 and 65_2-415 airfoil.

Increasing C_{m_o} was apparently regarded as unimportant, during the GA(W)-1 development. It remains to be seen whether this assumption is valid. Increased GA(W)-1 C_{m_o} will cause increased trim drag. According to reference 23, longitudinal trim drag ranges from 1 percent to 10 percent of total airplane drag. For the cruise condition, trim drag will be in the lower part of this range, and during a climb, in the upper part. Therefore, the increased pitching moment of the GA(W)-1 section is likely to produce an appreciable increase in total airplane drag over the whole operating range of the airplane.

During the conceptual design of ATLIT, it was estimated that the weight of the wing could be reduced about 10 percent. This reduced weight would result from the lower wing root bending moments for the tapered ATLIT wing and from the lower weight of materials for the smaller wing. In practice, this weight savings could be used to provide either increased single-engine rate of climb or increased useful load. On ATLIT, however, this potential was not realized. The design of the prototype-wing structure was done with little regard for weight. The resulting ATLIT wing is about 1.34 kN (300 lb) heavier than the standard wing. The conservative-design wing root bending moment for ATLIT is about 55-percent higher than for the standard Seneca.[7] This moment is also about 60-percent higher than it need be for the design of such a wing to conventional limits.

Early in the flight program, wing templates were made at eight span-wise locations on ATLIT to determine how well the actual wing sections

7. Unpublished data in "Conceptual design of an Advanced Technology Light Twin."

compare to the true GA(W)-1 shape. Figure 3.11 presents this comparison. In general, the ATLIT wing sections are representative of the GA(W)-1 shape; however, the figure shows some discrepancies near the wing trailing edge. On the average, the ATLIT wing trailing edge is twice as thick as it was designed to be. The design trailing edge thickness varies from a maximum of 2.3% c to a minimum of 0.9% c with an average of 1.4% c. The ATLIT trailing edge thickness variations result from the difficulty in matching the position of the Fowler flap trailing edge with the wing trailing edge in the flap-nested configuration. The effect of these thickness variations will be most pronounced on section drag. Lift and pitching moment will be affected very little.

3.3 Supercritical Propellers

An analysis[8] made on a modern light twin-engine airplane suggested that the efficiency of the installed propeller may be as much as 5 percent to 15 percent (at cruise and climb, respectively) less than the efficiencies which larger, transport-category airplanes had been able to approach. A significant recommendation of this reference was that a propeller should be designed so that the twist and planform are optimized for operation in the flow field of the nacelle behind it. Such a propeller would improve climb and cruise performance.

The propeller design was accompanied by a suggested design for modified engine nacelles which would achieve improvements in propulsive efficiency. Data of reference 22 indicate significant improvement in propulsive efficiency due to changes in the nacelle blockage effects behind a propeller. However, the design of modified engine nacelles for ATLIT was never completed.

8. Correspondence from Mr. Howard Piper (Piper Aircraft Corporation) to Mr. John P. Reeder (NASA Langley Research Center). Subject: Advanced Technology Wings, Control Systems, and Propellers for General Aviation Twin Engine Aircraft, April 12. 1972.

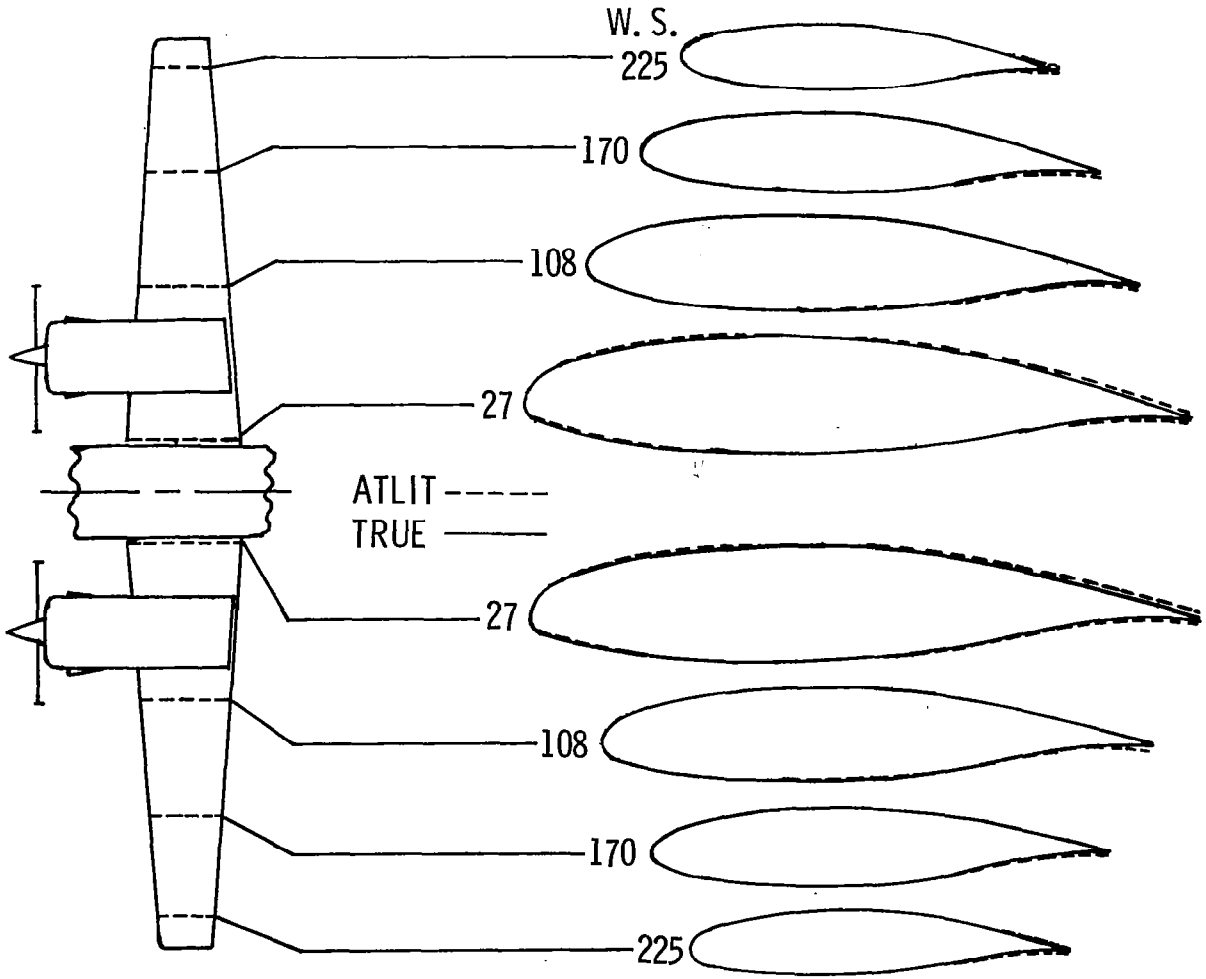

Figure 3.11.- ATLIT wing templates.

Another recommendation[9] was to consider both the older "traditional" sections (e.g., Clark Y, NACA 2412, or NACA 23012) and the newer supercritical sections for application to a new propeller design. The supercritical section was chosen to replace the airfoil of the standard propeller (approximated by the NACA 66-206). This choice was made in an effort to utilize the lift and drag characteristics of the supercritical sections to the best advantage in a propeller design. The design of the propellers was performed to provide an optimum combination of cruise and climb performance.[10] Figure 3.12 illustrates the blade planform and airfoil used on the propeller.

Additional anticipated advantages of the supercritical props include the more blunt blade leading edge and reduced blade weight. The blunt leading edge (in contrast to the sharp leading edge of the original blade section) will be less susceptible to damage from rocks and debris. The weight of the supercritical propellers is 27.8 N (12.5 lb) less per prop than the weight of the original propellers. A supercritical propeller weighs 291 N (65.5 lb) compared to 317 N (71.25 lb) for a standard Hartzell prop.

---

9. Ibid.
10. The propeller design was documented in the unpublished report "Conceptual Design of an Advanced Technology Light Twin".

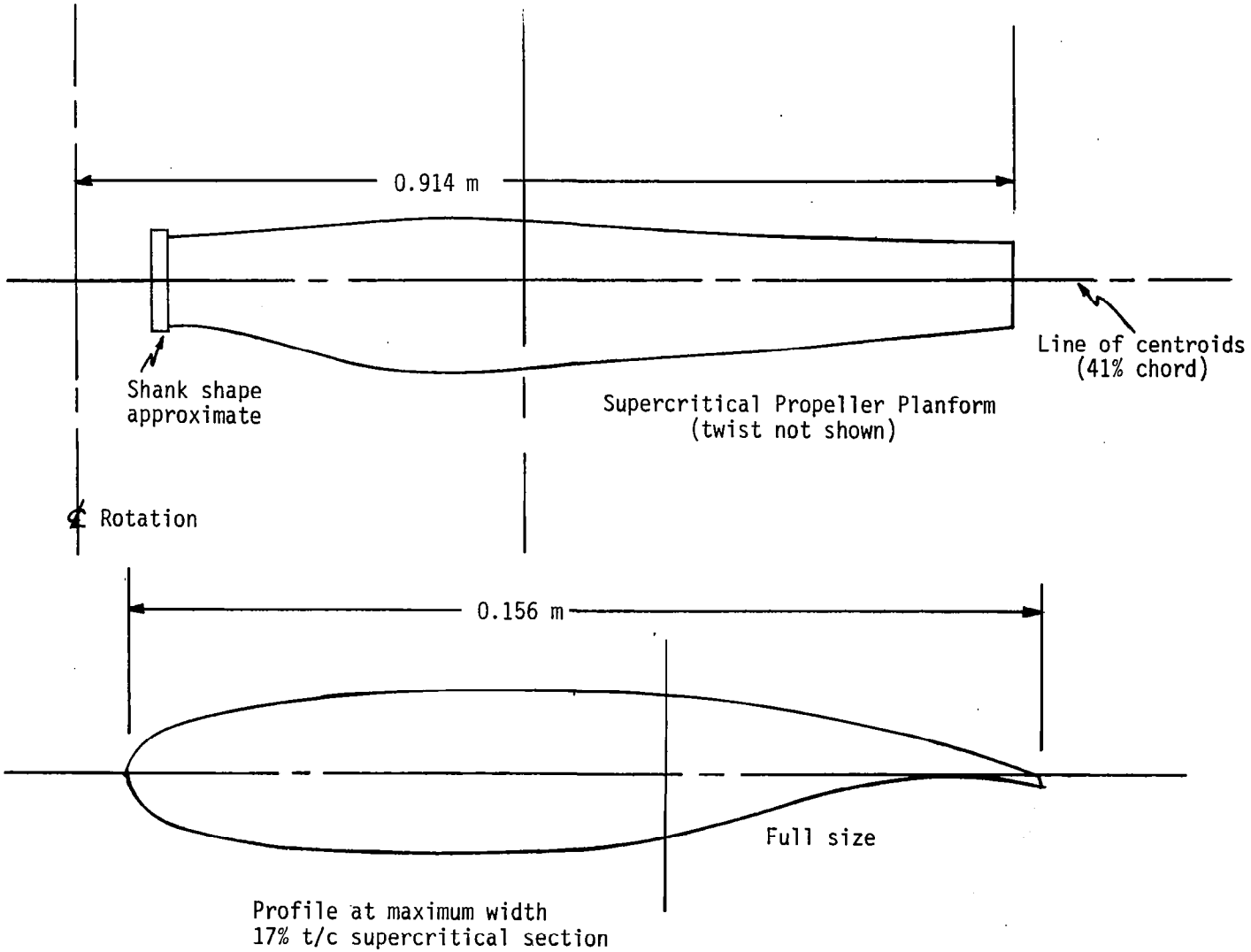

Figure 3.12.- Supercritical propeller planform and cross-section.

CHAPTER 4

FLIGHT-TEST PROGRAM

This chapter presents the objectives and planning of the flight-test program and a description of the instrumentation system and flight envelope for the airplane.

4.1 Program Objectives and Planning

The flight evaluation of ATLIT has the objectives of determining:

1. Stall speeds and characteristics
2. Spoiler roll-control characteristics
3. Cruise and single/multi-engine climb performance
4. Longitudinal and lateral dynamic response characteristics
5. Takeoff and landing distances
6. Noise and performance characteristics of advanced technology propellers incorporating a supercritical airfoil.

Items 1, 2, and 3 above are presented in this report. Items 4, 5, and 6 are in progress at Langley and will be reported in proposed NASA technical publications.

The flight-test program to complete items 1 through 6 above was estimated to require 100-flight hours in 50-calendar weeks. The purpose of the estimate was to provide data for support organizations at Langley to plan for such things as pilot man-hour and fuel requirements. In retrospect, these estimates would have been quite accurate but for the impact of the tuft studies and instrumentation delays

discussed in chapter 2.4. Revised estimates for the complete program increased the times to 150-flight hours in 70-calendar weeks.

An approximate breakdown is given below of the actual flight times required for completed tasks and estimated flight times required for planned tasks. The times listed under productive flight hours generated useful engineering data. The unproductive flight hours resulted in unusable data due to faulty equipment or procedures. About 30 percent of the total flight hours were unproductive.

Task	Total flight hours	Productive flight hours	Unproductive flight hours
1. Airspeed and angle of attack calibrations	15	7	8
2. Documentation of stall speeds and characteristics	6	3	3
3. Spoiler roll-control evaluation	16	10	6
4. Cruise and single-/multi-engine climb performance measurements	26	25	1
5. Tuft studies for wing/body separation cleanup	21	16	5
6. Evaluation of longitudinal and lateral dynamic response characteristics	(10*)	-	-
7. Takeoff and landing distance measurements	(15*)	-	-
8. Measurement of noise and performance characteristics of the supercritical propellers	(35*)	-	-
TOTALS	(144*)	61	23

* estimated

4.2 Flight Test Instrumentation

The basic data recording system is described here. Special instrumentation and equipment required for airspeed calibrations are discussed in Appendix B.

4.2.1 ATLIT Instrument Recording Package

ATLIT was equipped to record on magnetic tape the 36 flight parameters shown in table 4.1. The tape recorder had 14 continuous, FM (frequency modulated) data tracks. One FM track was commutated to record as many as 28 channels of PAM (pulse amplitude modulated) data at a rate of ten samples per second. The approximate accuracies listed on the table are estimates of possible errors incurred between the in-flight measurement of a variable and the documentation of the variable on the ground in engineering units. Several possible sources of error are listed below. In general, the largest errors are caused by noise in the data system. The combined errors amount to about $\pm$ 2% of full scale for each recorded parameter. This estimated maximum error represents three standard deviations. The sources of the errors are as follows:

1. noise anywhere in the system (commutator, tape recorder, power sources).

2. sensor hysteresis, deadband, drift, and calibration accuracy (nonlinearity).

3. intermodulation errors during mixing of frequency signals for tape recording.

TABLE 4.1 - ATLIT INSTRUMENTATION PARAMETERS AND ACCURACIES

	Parameter	Range	Approximate Accuracy	Units
	Time	-	-	Sec
	Total air temperature	-18 to +38 (0 to 100)	±0.6 (±1.0)	^{o}C (^{o}F)
	Glideslope deviation	±0.7	±0.05	Deg
	Localizer	±2.5	±0.05	Deg
Pitot-Static Variables	Pressure altitude	0 to 1524 (0 to 5000)	±30 (±100)	M (Ft)
	Static pressure	0 to 103,421 (0 to 15)	±142 (±0.30)	Pa (PSIA)
	Fine static pressure	95,975 to 103,077 (13.92 to 14.96)	±142 (±0.30)	Pa (PSIA)
	Airspeed	0 to 200	±3.00	Knots
	Fine airspeed	0 to 90	±1.8	Knots
	Vertical speed	±762 (±2500)	±30 (±100)	M/min (FPM)
Motion Variables	Longitudinal acceleration	±0.50	±0.01	G
	Normal acceleration	0 to 4	±0.08	G
	Lateral acceleration	±0.50	±0.01	G
	Roll rate	±100	±2.0	Deg/Sec
	Pitch rate	±30	±0.6	Deg/Sec
	Yaw rate	±30	±0.6	Deg/Sec
	Roll attitude	±180	±3.6	Deg
	Pitch attitude	±35	±0.70	Deg
	Yaw attitude	±30	±0.60	Deg
	Angle of attack	±20	±0.40	Deg
	Angle of sideslip	±20	±0.40	Deg
Control Forces and Deflections	Longitudinal wheel force	±133 (±30)	±5 (±1.2)	N (Lb)
	Lateral wheel force	±445 (±100)	±18 (±4.0)	N (Lb)
	Rudder pedal force	±667 (±150)	±27 (±6.0)	N (Lb)
	Stabilator deflection	-16 to +5	±0.4	Deg
	Stabilator trim tab deflection	±9	±0.4	Deg
	Left spoiler deflection	-10 to 57	±1.2	Deg
	Right spoiler deflection	-10 to 57	±1.2	Deg
	Rudder deflection	±35	±1.4	Deg
	Rudder trim tab deflection	±20	±0.8	Deg
	Flap deflection	0 to 40	±0.8	Deg
Engine-Power Variables	Left engine manifold pressure	0 to 101,592 (0 to 30)	±2031 (±0.6)	Pa (In. Hg)
	Right engine manifold pressure	0 to 101,542 (0 to 30)	±2031 (±0.6)	Pa (In. Hg)
	Left engine RPM	0 to 3000	±60	RPM
	Right engine RPM	0 to 3000	±60	RPM
	Left engine throttle position	0 to 100	±2	Percent

4. excitation voltage error.

5. analog to digital translation (ADTRAN) ground station nonlinearities.

4.2.2 Nose Boom Installation

A four parameter transducer instrument head is mounted on the ATLIT nose boom. The head senses:

1. dynamic pressure (q_c') for both cockpit panel and recorded airspeed data

2. static pressure (p') for both cockpit panel and recorded altitude and vertical speed data.

3. angle of attack (α') for recorded data.

4. angle of sideslip (β') for both a cockpit indicator and recorded data.

The noseboom, which is shown in figure 4.1, places the static pressure ports 1.7m (5.6 ft.) (approximately one maximum fuselage diameter) in front of the airplane nose. Data of references 31 and 32 indicate that locating the static port at least one body diameter in front of the fuselage nose minimizes the position error.

The instrument head used is typical of heads presently in use on NASA and other flight test aircraft. A detailed description of this head is contained in reference 33, and a summary of the pressure measuring characteristics of the head appears as table 4.2. The characteristics in the table apply at M = 0.6 (the minimum speed for which characteristics were

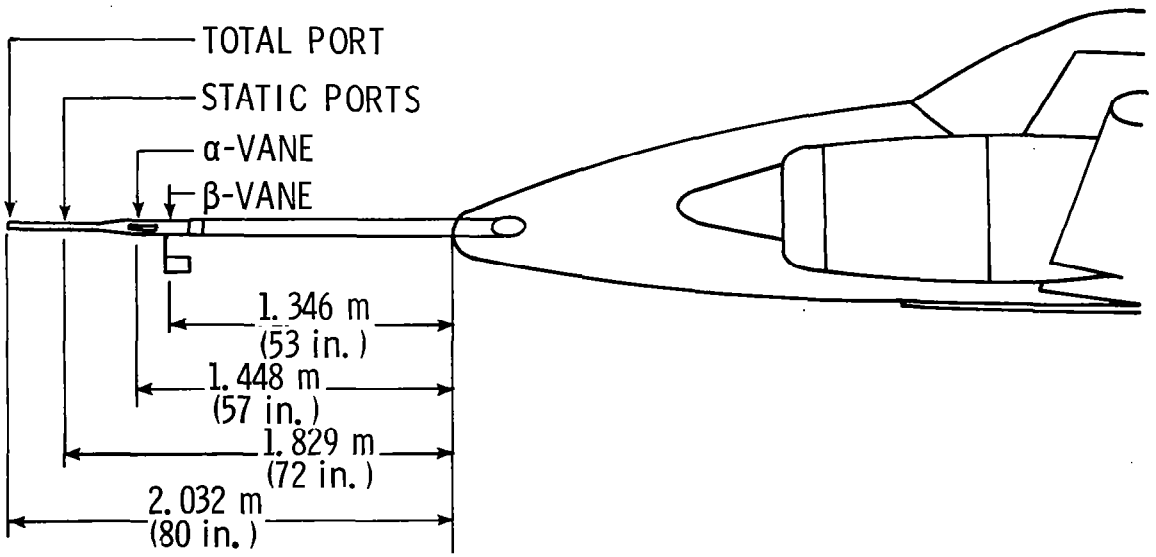

Figure 4.1 ATLIT noseboom detail

Table 4.2 Effects of Flow Angularity on the Pitot-Static Measurements (from ref. 28, M = 0.6)

	STATIC PRESSURE MEASUREMENT ERROR	TOTAL PRESSURE MEASUREMENT ERROR
Variation with angle of attack ($\beta = 0$)	$\pm$ 1.0% for $-15^0 < \alpha < +35^0$	- 0.2% for $-5^0 < \alpha < +20^0$
Variation with angle of sideslip ($\alpha = 0$)	$\pm$ 2.5% for $-10^0 < \beta < +10^0$	- 0.2% for $-10^0 < \beta < 10^0$
$\alpha = 0$, $\beta = 0$	+ 0.5%	0%

documented in the reference); however, for decreasing subsonic Mach numbers, the magnitudes of errors given in the table decrease. The static pressure errors shown are accounted for during the position-error calibration procedure of Appendix B.

The effect of lag in the pitot-static system was measured, ensuring that the time-dependent behavior of the system would not have a significant effect on data recorded during nonsteady airplane maneuvers. The time histories for the pitot and static system responses appear as figures 4.2 and 4.3, respectively. The effect of lag in the pitot system was shown to be small in comparison to that for the static system. Therefore, only the effect of the static system lag is summarized as follows:

Acoustic lag (time for a pressure signal to travel through the static system)	0.033 sec.
Pneumatic lag	0.056 sec.
Static pressure transducer response time constant	0.094 sec.
Total ATLIT static pressure system lag	0.183 sec.

The small amount of lag in this system will result in less than 1.0% static pressure error ($\Delta p/q'_c$) for nonsteady maneuvers in ATLIT which meet the following conditions:

1. rate of change of airspeed less than about one knot per second at constant altitude or,

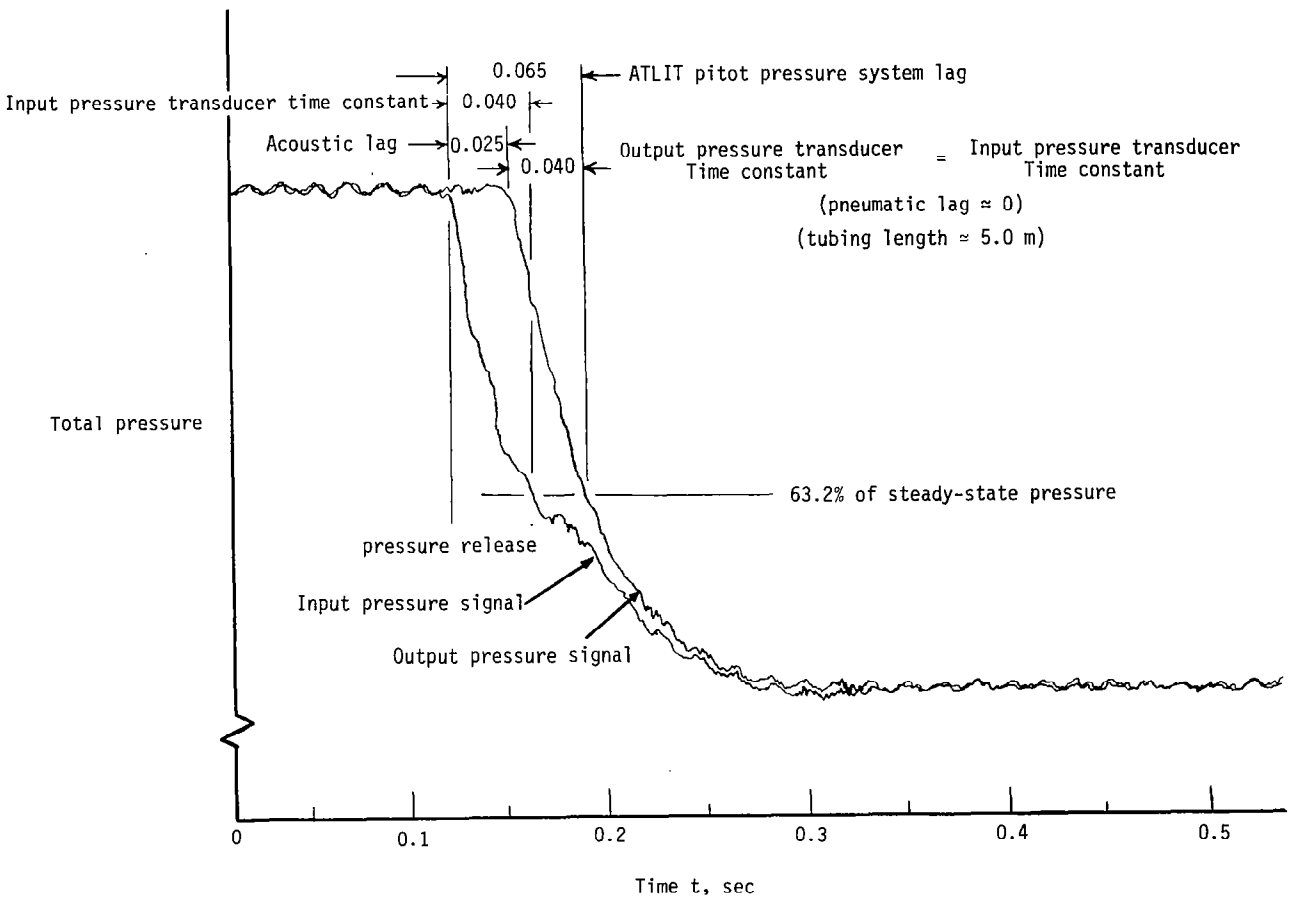

Figure 4.2.- Time-dependent characteristics of the ATLIT pitot pressure measuring systems.

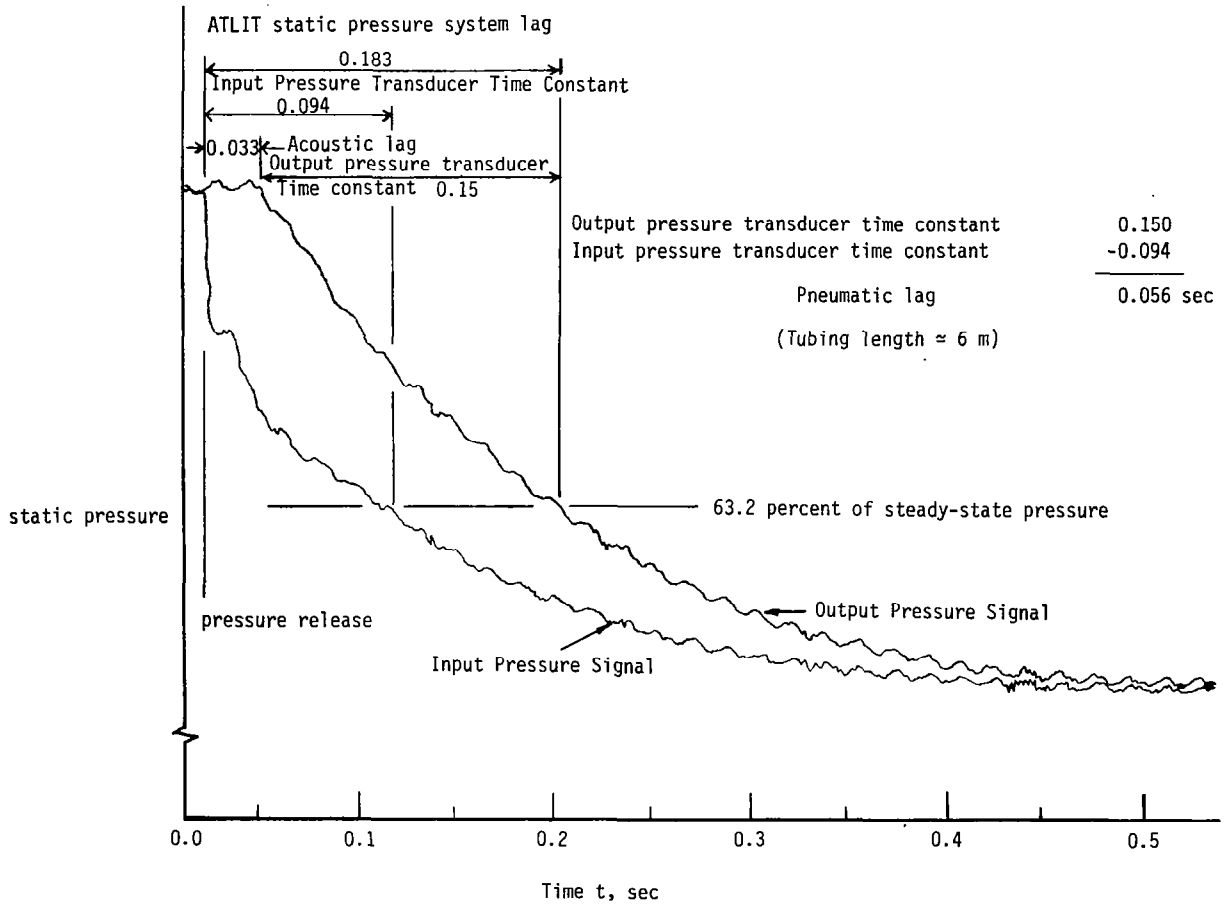

Figure 4.3 Time dependent characteristics of the ATLIT static pressure measuring system.

2. rate of change of altitude less than 122 meters/min (400 FPM) at constant airspeed.

4.3 ATLIT Flight Envelope

The flight envelope for ATLIT is essentially the same as for the standard Seneca. The ATLIT was designed to at least meet FAR Part 23 "normal" category limits. In order to adapt the new wing to the standard Seneca fuselage, it was most convenient for the main-wing bending member to cross through the fuselage at the same location as in the original airplane. For the symmetrically tapered ATLIT wing configuration, a line from root to tip through the carry-through spar contains the 50% chord points for all wing sections. As a result, as seen in figure 4.4, the quarter chord of the mean aerodynamic chord for ATLIT is slightly aft of that for the original airplane.

The CG envelope for both airplanes is shown in figure 4.5. Empty weight for ATLIT is 13.26 kN (2,980 lbs, without instrumentation). This weight reflects an increase in ATLIT wing weight of about 1.33 kN (300 lbs). This increase is explained by the use of easily-designed, heavy, machined components and conservative assumptions in the wing design and construction. The ATLIT CG range in terms of fuselage stations was designed to be the same as for the original airplane. The limits relative to the mac for each airplane appear below (from reference 4):

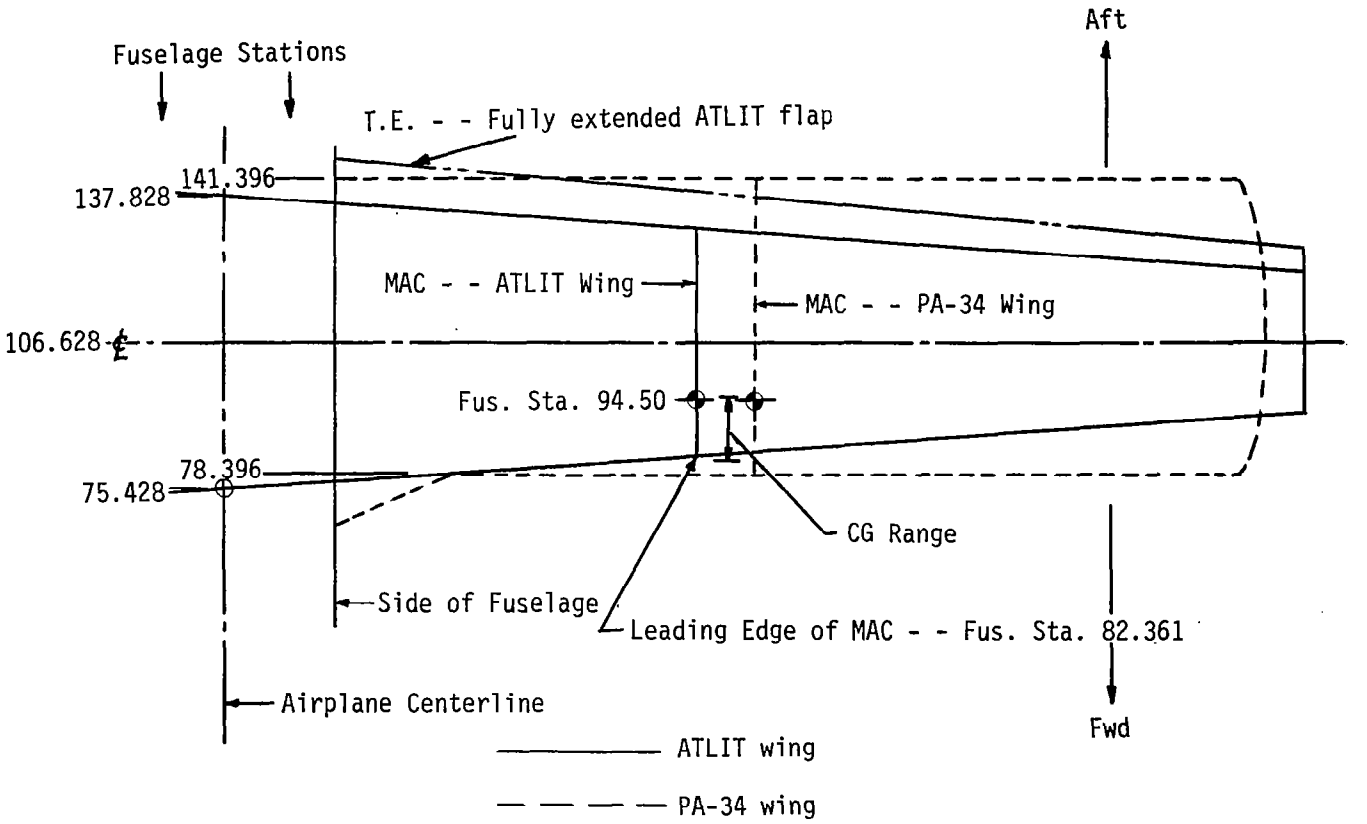

Figure 4.4 Comparison of PA-34 and ATLIT planforms

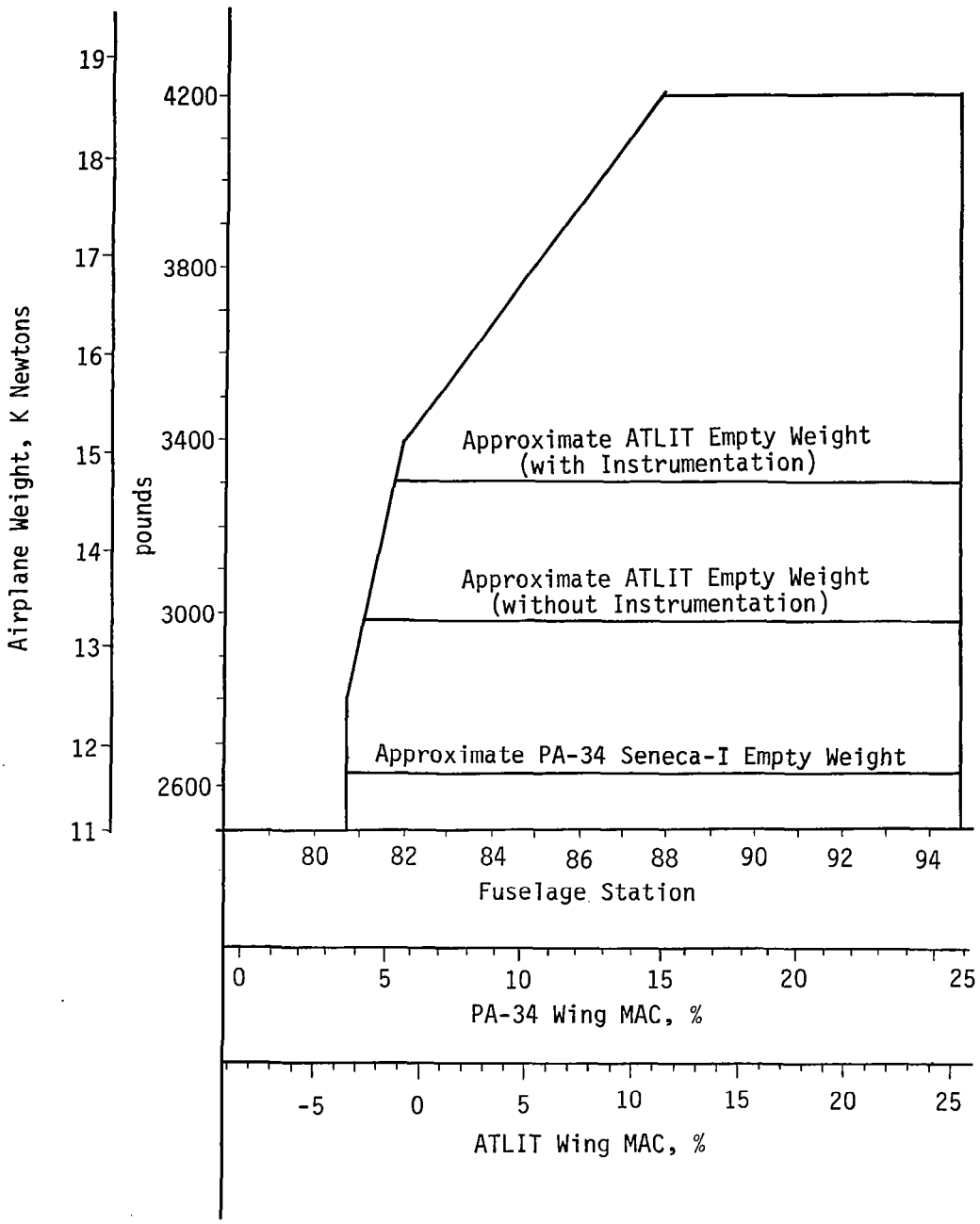

Figure 4.5 Airplane CG Envelope for ATLIT and PA-34 mac's.

	Fuselage Station	% of PA-34 mac	% of ATLIT mac
Forward CG limit 4200 lbs	87.9	15.11	11.41
Aft CG limits (all weights)	94.6	27.75	25.22

The standard Seneca I is placarded for a maximum landing weight of 17.79 kN (4,000 lbs). Therefore, all weight added above 17.79 kN up to the gross weight of 18.68 kN (4,200 lbs) must be fuel. However, no such limitation applies to ATLIT. The fuel capacity of the modified wing is at least 568 l (150 gal) compared to 379 l (100 gal) for the original wing. Unfortunately, because of the large empty weight, the ATLIT full - fuel capacity can only be used with one person onboard.

The permissible speed range for ATLIT was expanded slightly over that for the standard Seneca. For ATLIT, V_{NE} = 211 knots versus 189 knots for the PA-34 and V_{S_0} = 51 knots versus 58 knots for the PA-34. The maximum flaps operating speed for the two airplanes remained the same at 109 knots. The use of full flap deflection (37.8^{o}) on ATLIT for landing has been avoided because of the likelihood of the nose wheel touching down first.

CHAPTER 5

FLIGHT-TEST RESULTS

Flight-test results are presented in this chapter for ATLIT in essentially the configuration in which the airplane was delivered to Langley Research Center. The airplane characteristics reported on here include the following:

1. Static pressure and angle-of-attack position-error calibrations.
2. Stall characteristics.
3. Roll characteristics.
4. Cruise and Climb performance
5. Pilot comments on stability and handling qualities.

After the flight-test program began at Langley Research Center, several modifications were made to the airplane. These modifications are described as follows:

1. Several devices (strakes, fillets, and vortex generators) were tried on the airplane to reattach a region of separated flow which was caused by interference effects at the wing/body juncture (see figure 5.1).
2. Seals were added to the wing to reduce leakage of pressure through the gaps around the spoilers. (A description of the seals contained in chapter 3.2.2).

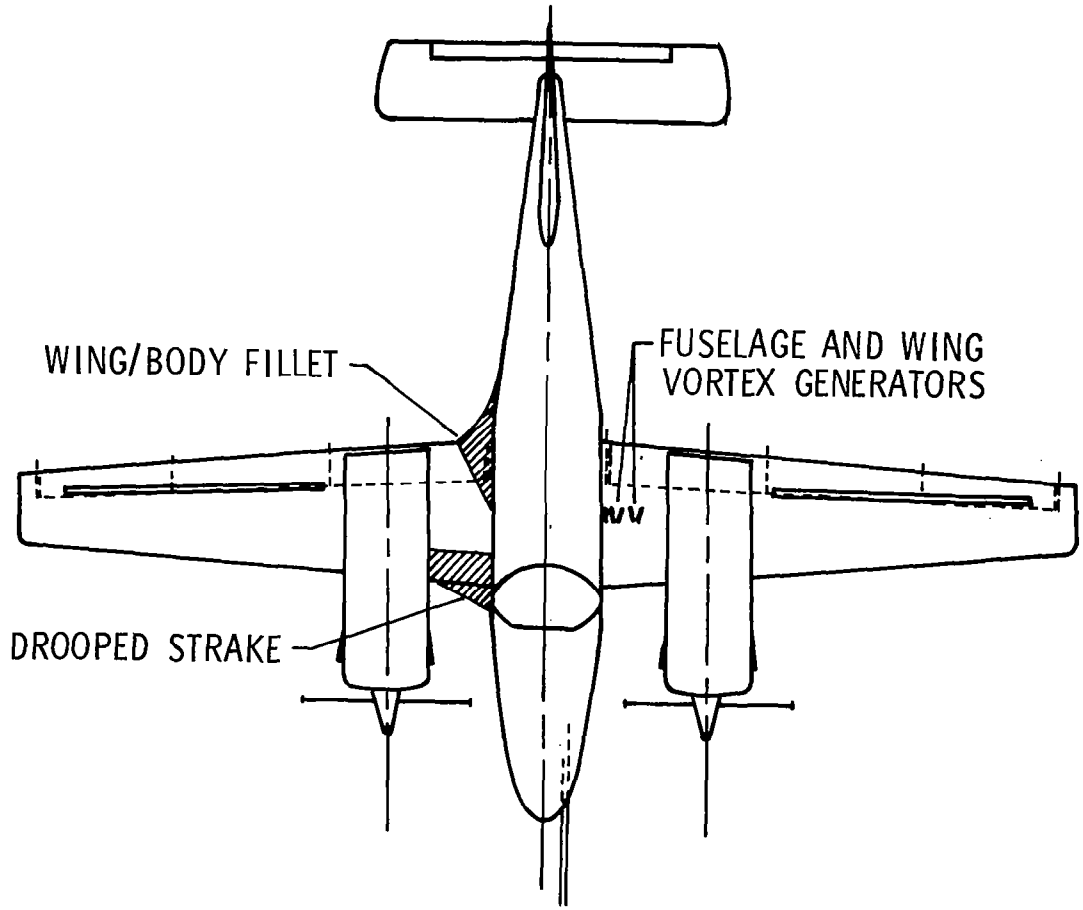

Figure 5.1.- Devices for wing/body flow attachment.

3. The spoilers were rigged symmetrically down below the wing surface to reduce the drag penalty due to spoiler "float." (The rigging of the spoilers is described in chapter 3.2.2.)
4. To reduce drag, the ATLIT wheel wells were fitted with balsawood blocks which formed wells similar in shape to those on the standard PA-34.

Flight data are not presented in this report for an airplane configuration with all of the above modifications. The effect of these modifications on most of the present test results is expected to be small. The possible exception is climb performance. These results will be reported in planned, future publications.

Where appropriate, predictions of ATLIT characteristics are included in this chapter. Performance predictions were computed by three different methods; one rapid sizing procedure[11] and two lifting line theory methods (references 29 and 30). The purpose in presenting the results of these different predictive techniques is to compare them to one another and to flight-test results.

5.1 Position Error Calibrations for Static Pressure and Angle of Attack

The position error calibrations presented here summarize the results of tests which are discussed in Appendix B. These calibration corrections have been made to all pressure and angle-of-attack data appearing in this report.

The effects of both flap deflections and power changes on static pressure and angle-of-attack position errors are appreciable. The displacements of the calibration curves with changing flap position or

11. Unpublished report: Loftin, L. K. (NASA Langley Research Center): Conceptual Design of Subsonic Aircraft, Chapter 6 - Estimation of the Size and Performance of Subsonic Aircraft, Feb. 1976.

power may be explained by the effects of these changes on circulation. According to the Kutta-Joukowski theorem of lift,

$$\frac{L}{b} = \rho V \Gamma \qquad (5.1)$$

or

$$\Gamma \sim \frac{1}{V} \quad ; \qquad (5.2)$$

that is, wing circulation is proportional only to velocity. For a fixed airspeed, then, the position errors of a wing alone (as influenced by circulation) are constant. However, position errors for a three-dimensional airplane are also a function of flap deflection and power setting, as explained below.

Variation of Fowler-flap deflection will affect position error in two ways:

1. As the Fowler flaps are deflected, the location of the lifting line (center of circulation) will move rearward. This effect changes the upwash conditions at the flow-sensor locations either ahead of the wing or ahead of the fuselage nose. The result is a shift in the calibration curve.
2. Span-wise lift distribution is affected by changes in the fuselage and nacelle attitudes due to flap deflections at a given airspeed. These changes in lift distribution will also affect local circulation at the flow-sensor locations, causing a shift in the position-error curves.

The effects of power changes on position errors are explained by the influence of body attitudes and of propeller slipstream on spanwise lift distribution. As in (2) above, the result is a change in local circulation which affects the position-error calibration.

5.1.1 Static Pressure Calibrations

The corrections made to static-pressure measurements are given in figure 5.2 for all flap settings and for power-on and power-off at two flap positions. Little effect of landing gear position was detected during the calibrations; therefore, all calibration data are presented with gear up. Calibrated airspeed can be computed from the data on the figure using the equation

$$V_c = V_c' \sqrt{1 + \frac{\Delta p}{q'_c}} \quad . \tag{5.3}$$

Corrections to altitude (static pressure) data can be computed using the equation

$$p = p' - \left(\frac{\Delta p}{q'_c}\right) \cdot q'_c \tag{5.4}$$

where V'_c and q'_c are flight-measured values and $\frac{\Delta p}{q'_c}$ is from figure 5.2.

5.1.2 Angle-of-Attack Calibrations

The corrections made to indicated angles-of-attack are given by the linear functions presented in table 5.1 and in figure B.10 of Appendix B.

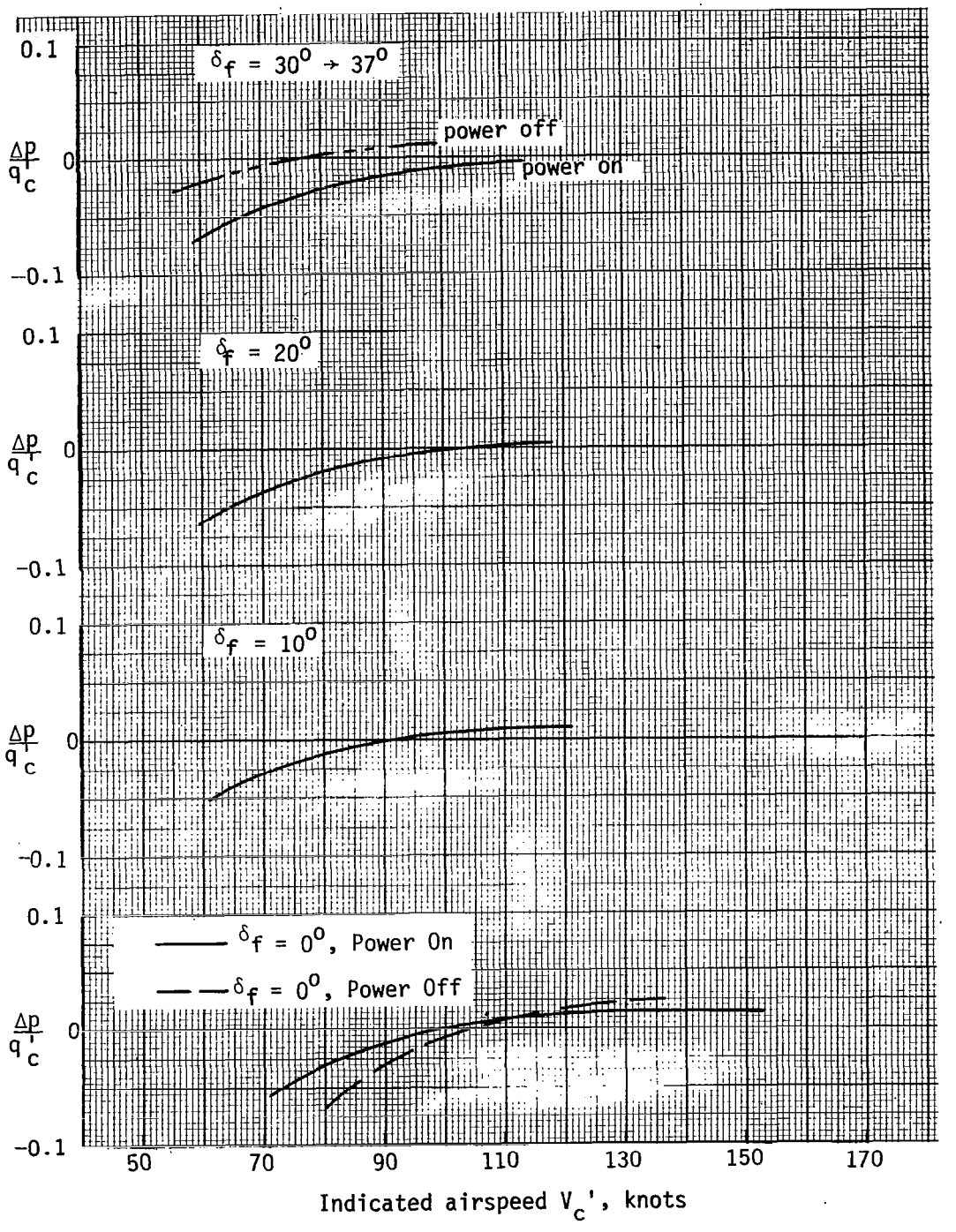

Figure 5.2.- Static pressure position-error calibrations.

TABLE 5.1- ANGLE-OF-ATTACK CALIBRATION EQUATIONS

Flap Position	Angle-of-Attack Correction from Indicated to True	Approximate Limits of Linearity	
		Power Off	Power On
$\delta_f = 0^o$	$\alpha = 0.88\,\alpha' + 0.15$	$\alpha = 11^o$	$\alpha = 15^o$
$\delta_f = 10^o$	$\alpha = 0.80\,\alpha' - 0:02$	$\alpha = 10^o$	$\alpha = 12^o$
$\delta_f = 30^o$	$\alpha = 0.82\,\alpha' - 0.44$	$\alpha = 8^o$	$\alpha = 11^o$

5.2 Stall Speeds and Characteristics

5.2.1 Predictions

The preliminary design estimates[12] for maximum lift were based on section data for the GA(W)-1 airfoil and lift effectiveness data for a 30%c Fowler flap. Flaps up $C_{L_{max}}$ was predicted to be 1.8, and flaps 20^{o} $C_{L_{max}}$ (trimmed to forward cg for gross weight) was predicted to be 2.6. A comparison of these predictions with flight-test measured values, presented below, shows fair agreement.

After the optimum flap configuration for ATLIT was developed in two dimensional tests (reference 14), the final wing-spoiler-flap configuration was evaluated in three-dimensional tunnel tests (reference 17). A summary of flap effectiveness from 2-D and 3-D testing appears as figure 5.3. The figure shows a loss in flap effectiveness in going from 2-D to 3-D configurations. For instance, at $\delta_f = 40^{o}$ (no spoiler leakage), $\Delta C_{L_{max}}$ is reduced by about 0.69 (or 30 percent) from the value for $\Delta C_{l_{max}}$. This loss can be explained by a combination of the following items:

1. The 3-D flap span is less than the airplane wing span. For ATLIT, $b_{flap}/b_{wing} = 0.88$ compared to 1.0 for the 2-D tunnel tests

   Thus, at $\delta_f = 40^{o}$, $\Delta C_{l_{max}}$ is reduced by

   $$\Delta C_{l_{max}} - 0.88 \times \Delta C_{l_{max}} = 2.3 - 0.88 \times 2.3 = 0.28,$$

   or about $\frac{0.28}{0.69} = 40\%$ of the total loss in maximum lift.

---

12. Unpublished data: "Conceptual Design of an Advanced Technology Light Twin Airplane."

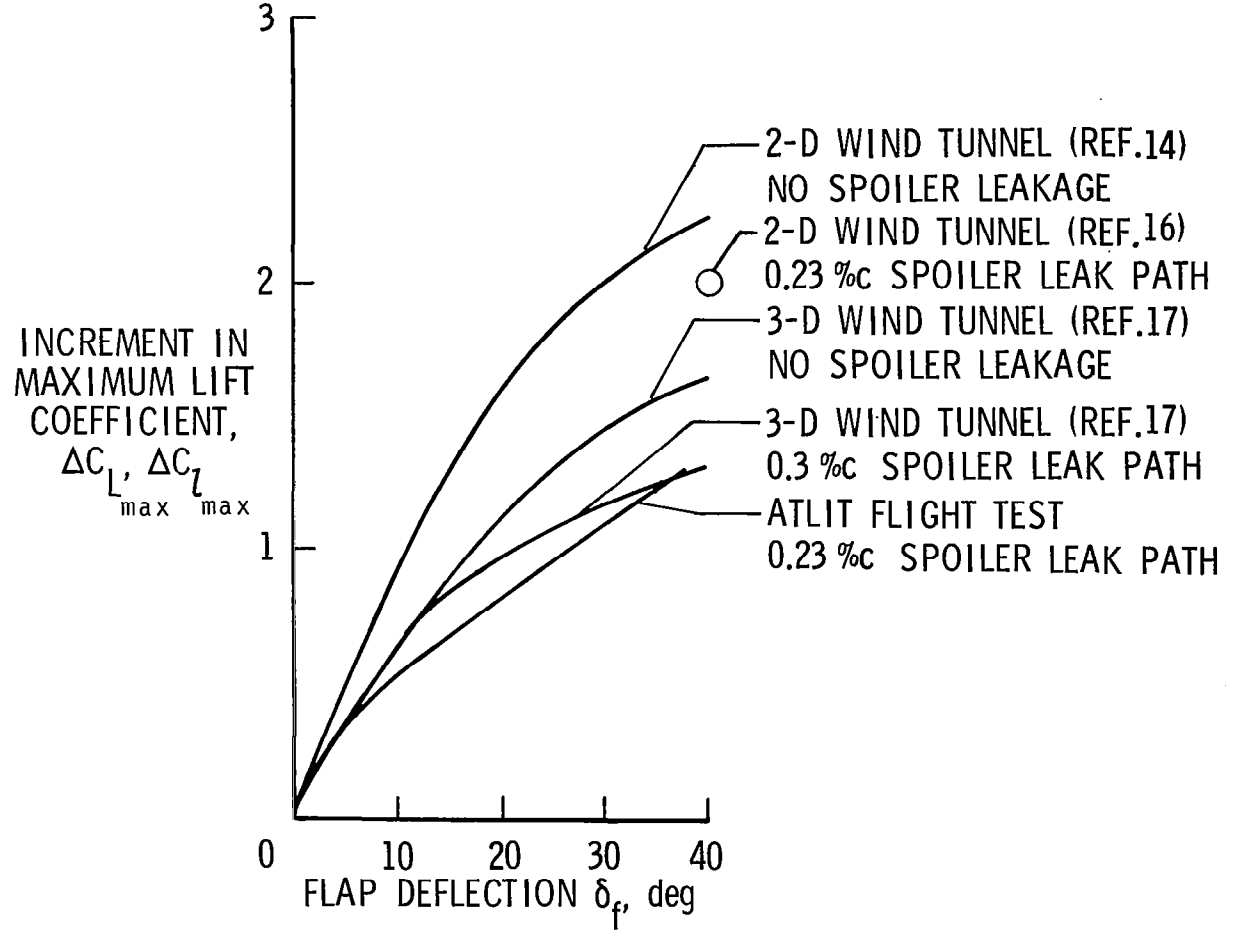

Figure 5.3.- Comparisons of Fowler flap effectiveness from wind tunnel and flight tests.

2. The 3-D wings on the tunnel model and on the airplane had 3 degrees of twist and finite aspect ratio compared to no twist and infinite A for the 2-D tests. Using the method of reference 31 and the theoretical wing span loading for ATLIT (not accounting for the nacelles and fuselage) from unpublished data[13], maximum lift was compared for the two- and three-dimensional cases. By such an analysis, it can be shown that $C_{l_{max}}$ is reduced by about 0.1 compared to the $C_{l_{max}}$ of the section near the mac of the wing. This reduction accounts for about $0.1/0.69 = 15\%$ of the 3-D loss in maximum lift.

3. Adding the fuselage and nacelles to the wing has an effect on maximum lift which is difficult to determine. On the one hand, addition of the bodies can be considered as providing additional (though small) lifting forces, thus increasing maximum lift. On the other hand, the interference effects of the bodies on the wing may reduce maximum lift. A method is given in reference 29 for estimating this lift loss. Treating each engine nacelle and the fuselage independently, the method yields $(C_{L_{max}})_{WB}/(C_{L_{max}})_{W} \simeq 0.95$. This ratio predicts a flaps up lift loss of $0.95 \times 1.7 = 0.09$ or $\frac{0.09}{0.69} = 13\%$ of of the overall 3-D loss in maximum lift.

---

13. Budish.

4. The 3-D flaps were constructed in span-wise segments compared to the one-piece construction for the 2-D tests. At each flap bracket location on the airplane, there is about 3 cm of open space (span wise) between the flap sections. No estimate is given here for the loss in lift due to these gaps.

Although the data in figure 5.3 are presented for several different Reynold's numbers, direct comparison of flap effectiveness curves is still valid. This is true since the effect of Reynold's number and (in the case of flight data) cg location on flap effectiveness is negligible.

5.2.2 Test Methods and Data Reduction

The procedures for conducting stall tests outlined in reference 32 were used as a guide for the ATLIT stall testing. Briefly, the power-off stalls were entered with throttles idled and with a rate of airspeed reduction not greater than 1 knot per second.

In most cases, it was possible to define the stall point from flight records by a simultaneous occurrence of a "g"- and a pitch-break. Figure 5.4 illustrates such a case. Most stalls occurred at $n_z < 1.0$. In order to make a valid comparison between flight- and wind-tunnel lift data, airplane $C_{L_{max}}$ was computed based on the measured value of n_z at the stall break, or

$$C_{L_{max,\ A}} = \frac{n_z \cdot W}{q_c \cdot S} \tag{5.5}$$

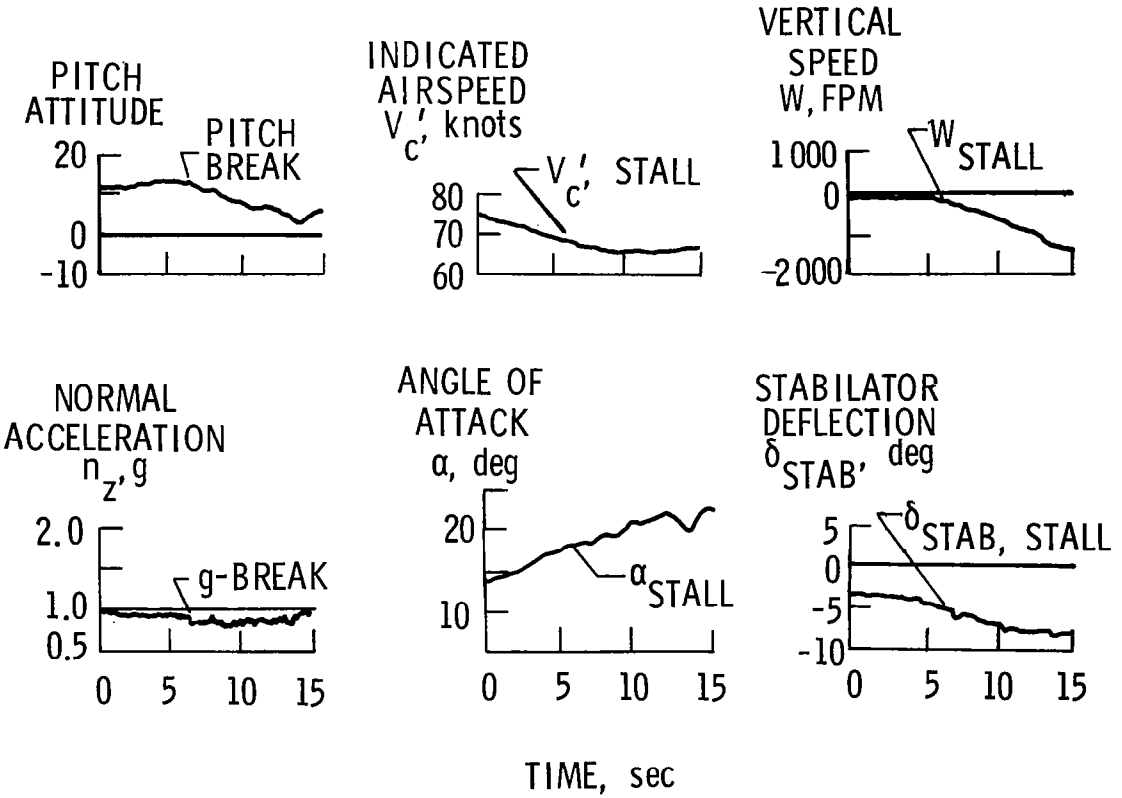

Figure 5.4.- ATLIT stall time history (flaps up, approach power).

The values of $C_{L_{max,\ A}}$ for several stalls in each configuration were averaged. These averaged data appear in table 5.2. The maximum airplane lift data in the table were also corrected to the aft CG (25% mac) for both airplanes. This correction was made to minimize the trim-lift penalty in the data so that a more direct comparison can be made with wind-tunnel results. The correction was made using the following equation from reference 33:

$$(C_{L_{max,\ A}})_2 = (C_{L_{max,\ A}})_1 + \left[\frac{CG_2 - CG_1}{\frac{l_1}{max} - CG_1}\right] (C_{L_{max,\ A}})_1 \qquad (5.6)$$

where the quantities subscripted with a 1 represent flight-test values and those subscripted with a 2 represent the condition to which the data are being standardized.

5.2.3 Results and Discussion

As shown in table 5.2 , the highest lift coefficient attained by ATLIT was $C_{L_{max,\ A}} = 3.03$ with $\delta_f = 37^o$. The corresponding stall speed is $V_{s_o} \doteq 51$ knots, which is 7 knots less than V_{s_o} for the standard Seneca I. With flaps up and spoiler leakage unsealed, $C_{L_{max,\ A}} = 1.73$. The corresponding stall speed is $V_{s_1} = 68$ knots, which is only 4 knots faster than the flaps-up stall speed of the standard Seneca I (which has 35 percent more wing area than the ATLIT). The flaps-up maximum lift coefficient and the $\Delta C_{L_{max}}$ due to flap deflection on ATLIT appear to

TABLE 5.2.- COMPARISON OF ATLIT AND SENECA STALL SPEEDS AND MAXIMUM TRIMMED LIFT COEFFICIENTS.

CONFIGURATION	SENECA I		ATLIT	
	V_S kts. (mph)	$C_{L_{max,A}}$	V_S kts. (mph)	$C_{L_{max,A}}$
FLAPS 0°	64 (74)	1.45	-	-
SPOILER LEAKAGE SEALED	-	-	72 (83)	1.54
SPOILER LEAKAGE UNSEALED	-	-	68 (78)	1.73
FLAPS 10°	-	-	59 (68)	2.28
FLAPS 20°	-	-	56 (65)	2.54
FLAPS 30°	-	-	53 (61)	2.81
FLAPS 35°	-	-	52 (60)	2.87
FLAPS 37°	-	-	51 (59)	3.03
FLAPS 40°	58 (67)	1.76	-	-

ALL DATA PRESENTED FOR c.g. = 25 % M.A.C AND
GROSS WEIGHT = 18 700 N (4200 lb)

be the largest ever generated by an airfoil and a single-element flap of similar geometric configuration. This improved lifting capability of the ATLIT wing bears out the most useful quality of the new GA(W) airfoils, that of increased flexibility in designing smaller wings.

As illustrated in figure 5.3, wind tunnel testing (reference 17) predicted that sealing the spoiler leakage path would increase $C_{L_{max}}$, flaps up or down. However, as shown in table 5.2, the reverse occurred in flight. That is, when the spoiler leakage path was sealed with plastic tape, $C_{L_{max}}$ (flaps up) decreased by about -0.2. These results are based on data averaged for less than a dozen stalls in each configuration, leakpath sealed and unsealed. It has been hypothesized that flow through the spoiler leak gaps provides a beneficial boundary-layer control effect to postpone flow separation in flight. Another possible explanation is from the effect of small spoiler deflections on wing lift. As discussed in the spoiler description of chapter 3.2.2, separated flow behind a small spoiler deflection can reattach before reaching the wing trailing edge. The net effect is increased camber and increased lift. The stall tests discussed here were done with the spoilers floating symmetrically up above the wing surface by about 2 to 3 cm. This small float angle could be responsible for the increase in $C_{L_{max,\ A}}$ with the spoiler leakpath unsealed. This phenomenon will be investigated in planned full-scale wind tunnel testing with ATLIT.

A direct comparison between 3-D wind-tunnel data (reference 17) and flight data on flap effectiveness is made in figure 5.3. The figure shows that the ATLIT flap effectiveness (with a 0.23% c spoiler leak gap) agrees closely with that measured on the reflection plane wind-tunnel model (which had a 0.36% c spoiler leak gap). The figure also shows consistently increasing lift increments with increasing flap deflections.

Qualitative comments on stall characteristics appear in chapter 5.5.

5.3 Spoiler Rolling Characteristics*

5.3.1 Spoiler System Development

The following discussion will cover many of the points discussed in chapter 3.2.2, but with the emphasis on the historical development of the ATLIT roll-control spoiler system.

When construction of the ATLIT wing was started, only the span, chord, and location of the spoilers at the 70-percent chord line had been decided. The wing was therefore under construction with a hole provided behind the 70-percent chord line for the spoilers. The Mitsubishi and Redhawk spoiler configurations were being considered for use on ATLIT. However, at that point, W. H. Wentz, Jr. and H. L. Crane, among others, became concerned about the need to minimize the nonlinear spoiler characteristics which would be induced by the large full-span Fowler flaps. Therefore, a two-dimensional investigation of several proposed spoiler configurations was made in the Wichita State University wind tunnel. Unfortunately, no hinge-moment data were obtained. Design details for the ATLIT spoiler system, such as spoiler cross section, spoiler vent path, and spoiler leading edge gap, were then based largely on the WSU tunnel data. One feature, the leading edge gap, was adapted from the Mitsubishi, MU-2 spoiler design and, therefore, may be covered by the MU-2 patent. The aforementioned two-dimensional WSU data were reported in reference 15.

It should be noted that Wenzinger and Rogallo, in NACA TR 706 (reference 37) examined spoiler configurations similar to the one adopted for ATLIT (except for the absence of leading edge gap).

*The contributions of Mr. Harold L. Crane (NASA-LaRC) in preparing materials for this chapter are gratefully acknowledged.

Conclusion 1. from TR 706 was as follows:

> "Spoilers alone were found to be generally unsuitable for lateral control on wings with full-span split or slotted flaps because of excessive lag and because of ineffectiveness at small spoiler projections. The characteristics were improved as the location of the device was moved toward the trailing edge of the wing. Spoilers alone may give acceptable control for some types of airplane if they are located sufficiently near the wing trailing edge."

Therefore, the LaRC monitors also arranged that before ATLIT flew, Paulson (reference 16) would measure the lateral control characteristics of the ATLIT spoiler configuration on an available rectangular wing with an aspect ratio of 9 and a GA(W)-1 airfoil section. The nonlinearities of flap-down spoiler effectiveness with increasing spoiler deflection measured by Paulson were found to be similar to the Wentz two-dimensional results.

A second NASA contractor report (reference 17) by Wentz, et. al., which presents spoiler characteristics including hinge moments on a one-fourth scale model of the ATLIT wing panel is now being printed. This paper confirmed that, as Calhoun* had estimated, the spoilers would have a positive (i.e., self deflecting) hinge moment over much of the deflection range. This undesirable characteristic persists to larger deflections flaps down than flaps up.

*John T. Calhoun of Robertson Aircraft Corporation, the designer of the ATLIT spoiler roll-control system.

As a further precautionary step, the newer Princeton variable-stability Navion, which was developed using NASA LaRC funds, was configured to evaluate pilot tolerance to various degrees of nonlinear roll control. The results of this in-flight simulation were reported by Ellis, et. al., in reference 19.

In summary, then, the Calhoun design estimates as well as the several wind-tunnel investigations showed that the spoilers would provide powerful lateral control with undesirable variations in the rolling effectiveness derivative $\partial C_l/\partial \delta_s$ between small, medium, and large spoiler deflections. However, the two-dimensional tests at WSU made it possible to select spoiler vent-path geometry to both eliminate reversals of spoiler effectiveness at small deflections, and also to always provide at least some spoiling of lift, which resulted in some pro-roll rolling moment at small deflections. Also, the flight simulation at Princeton University showed that the very experienced NASA research pilots could cope with extreme nonlinearities of lateral control effectiveness during approach and landing in strong, gusty crosswinds. Apparently they were able to concentrate entirely, or solely, on airplane response and almost instinctively move the wheel as required to get the desired lateral response.

In the rest of this chapter, plotted examples of the estimated and measured spoiler stability and control characteristics from the aforementioned sources will be shown and discussed in more detail.

5.3.2 Methods and Data Reduction

All spoiler roll-control data presented here were generated (rudder locked) by abrupt spoiler inputs with an adjustable wheel travel limiting

chain attached to the pilot's control wheel. These abrupt spoiler inputs (in practice) were ramp inputs of about 0.2-second duration. The combinations of configurations and airspeeds tested are given in table 5.3.

Two types of rolling maneuvers were used for the roll tests. At first, rolls were initiated from a bank angle of 30 degress and were allowed to continue to a bank of 30 degrees in the opposite direction. This conventional bank-to-bank type of maneuver proved to be undesirable for gathering spoiler roll data. In the second type of rolling maneuver, the roll was initiated from level flight and was allowed to continue to about 45 degrees of bank. This second type of maneuver was favored over the first for several reasons. With a sample rate of 10 per second on all recorded flight parameters (see chapter 4.2), the pertinent data for analyzing roll performance are gathered during the first second or so of the maneuvers; thus, no real need exists for the long duration of roll rate provided in the bank-to-bank type of maneuver. More important is the fact that spoiler produced rolling moments are sensitive to angle of attack; therefore, angles of attack must be consistent and accurately defined during the maneuver. Beginning the roll from a wings-level attitude simplifies data reduction since it is then not necessary to account for a varying load-factor-induced angle-of-attack (varying as bank angle varies) encountered during the bank-to-bank type of maneuver. In addition to these reasons for favoring the maneuver with a wings-level initial condition, the rolling maneuver from wings level is easier to perform from a piloting standpoint. Establishing a wings-level initial condition for the rolling maneuver requires less

TABLE 5.3- CONFIGURATIONS AND AIRSPEEDS FOR SPOILER ROLL TESTS

Flap setting, deg	Calibrated Airspeeds, V_c, knots
0	79, 100, 123, 148
10	64, 79, 95
20	64, 78, 95
30	59, 69, 76, 95
37	55, 64, 78, 95

Note: The data are largely for rolls to the right with spoiler deflections up to about 55^o, i.e., $\delta_{s_{max}} \geq 50^o$ or $\Delta h/c \geq .05$ (with c referenced from the wing chord at the midspan of the spoilers).

effort and is less time consuming than establishing a banked-initial condition.

In order to present data in the form of rolling moment coefficients, the roll damping coefficient, C_{l_p}, was first required for ATLIT in all configurations of interest. The C_{l_p} estimation procedure and results are presented in appendix C. Then, C_l can be determined simply by

$$C_l = -C_{l_p} \cdot \left(\frac{pb}{2V}\right) \quad . \tag{5.7}$$

The helix angles $\left(\frac{pb}{2V}\right)$ for equation (5.7) are based on flight-derived values for roll rate (p) and true airspeed (V).

5.3.3 Flight-Test Results

Because the wing designers allowed inadequate room for the spoiler and flap systems, the ATLIT spoiler actuating system had to be crowded into a space which was inadequate both chordwise and vertically. Largely as a result of this crowding, there is an excessive breakout force of about 44 N (10 lbf) in the lateral-control system. Therefore, the reader should keep in mind that the ATLIT spoiler roll-control system, although it is very powerful, represents an example of a far-from-optimum spoiler system.

As with any cable-driven system, the amount of stretch in the system (i.e., the reduction in maximum deflection of the control surface) is roughly proportional to the dynamic pressure or to a squared function of the airspeed. Figure 5.5 shows that the maximum stretch was about 30 percent which, because the authority of the spoilers was so great, was considered to be readily acceptable.

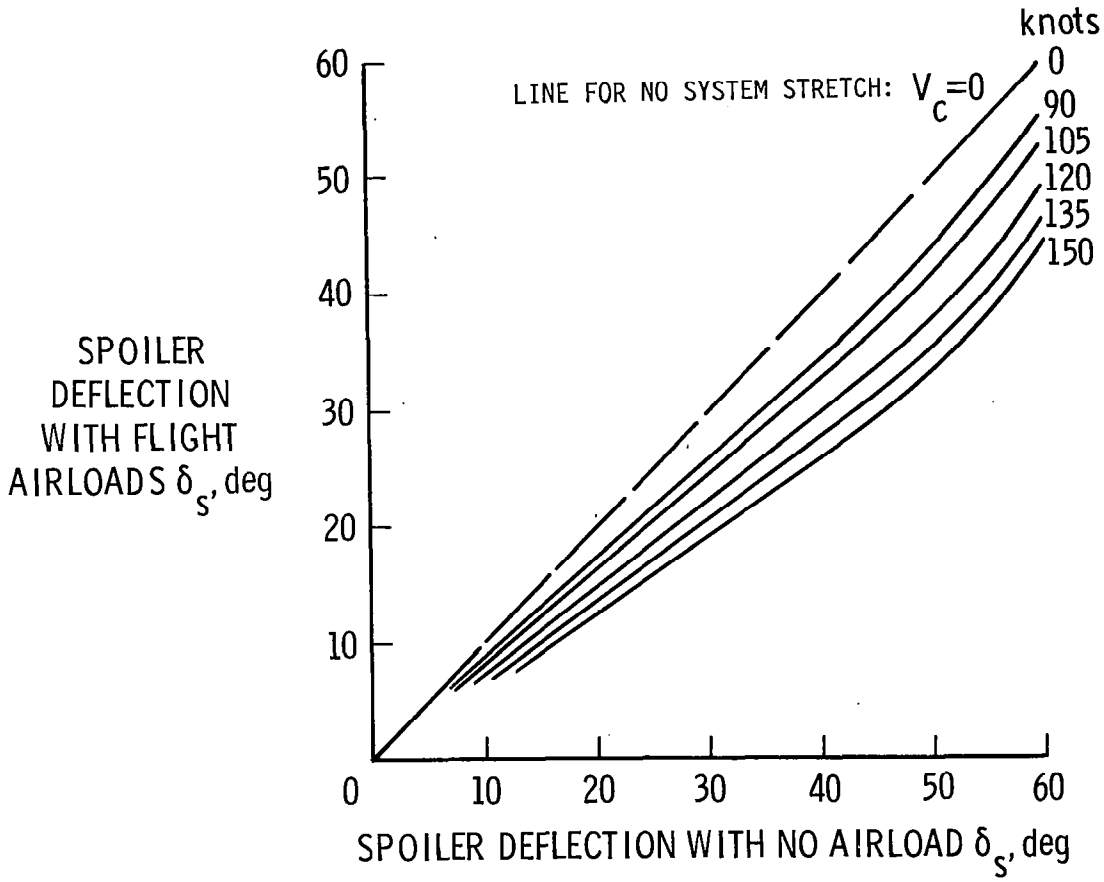

Figure 5.5- Variation of ATLIT spoiler system stretch with airspeed (flaps up, spoiler leakpath sealed)

As of this date, the airplane has been flown with the spoilers rigged several different ways. The characteristics are very strongly influenced by the spoiler rigging. To be on the safe side, the early flights at Piper were made with the spoilers rigged up 8 degrees to be certain that there was no dead band in effectiveness. The pilot comments about the lateral control with the spoilers rigged 8 degrees were very favorable. Piper flew about 20 hours including the ferry flight to Langley Research Center with the spoilers still rigged up 8 degrees; they had to make a crosswind takeoff and landing enroute and did so with no problems. While the airplane was being instrumented at Langley (LaRC), the spoilers were rerigged to be flush with the wheel centered. All the flying done by LaRC pilots was with the spoilers either rigged flush or, to provide a possible drag improvement, with the spoilers rigged symmetrically down 2 degrees. All of the roll-control data presented in this report were obtained with the spoilers rigged flush with the top of the wing with no air loads. However, some of the unfavorable pilot comments given in chapter 5.5 were obtained with the spoilers rigged down slightly for possible drag improvement. This rigging was discussed in chapter 3.2.2.

Figure 5.6 shows two example time histories of the roll response to spoilers of the ATLIT airplane. These rolls were made at 78 knots with the flaps down 30 degrees. The spoiler deflections for the two rolls were about 15 degrees for the small input maneuver and almost 50 degrees for the large deflection roll. It can be seen that it took the pilot about three-tenths of a second to deflect the spoilers. There was a

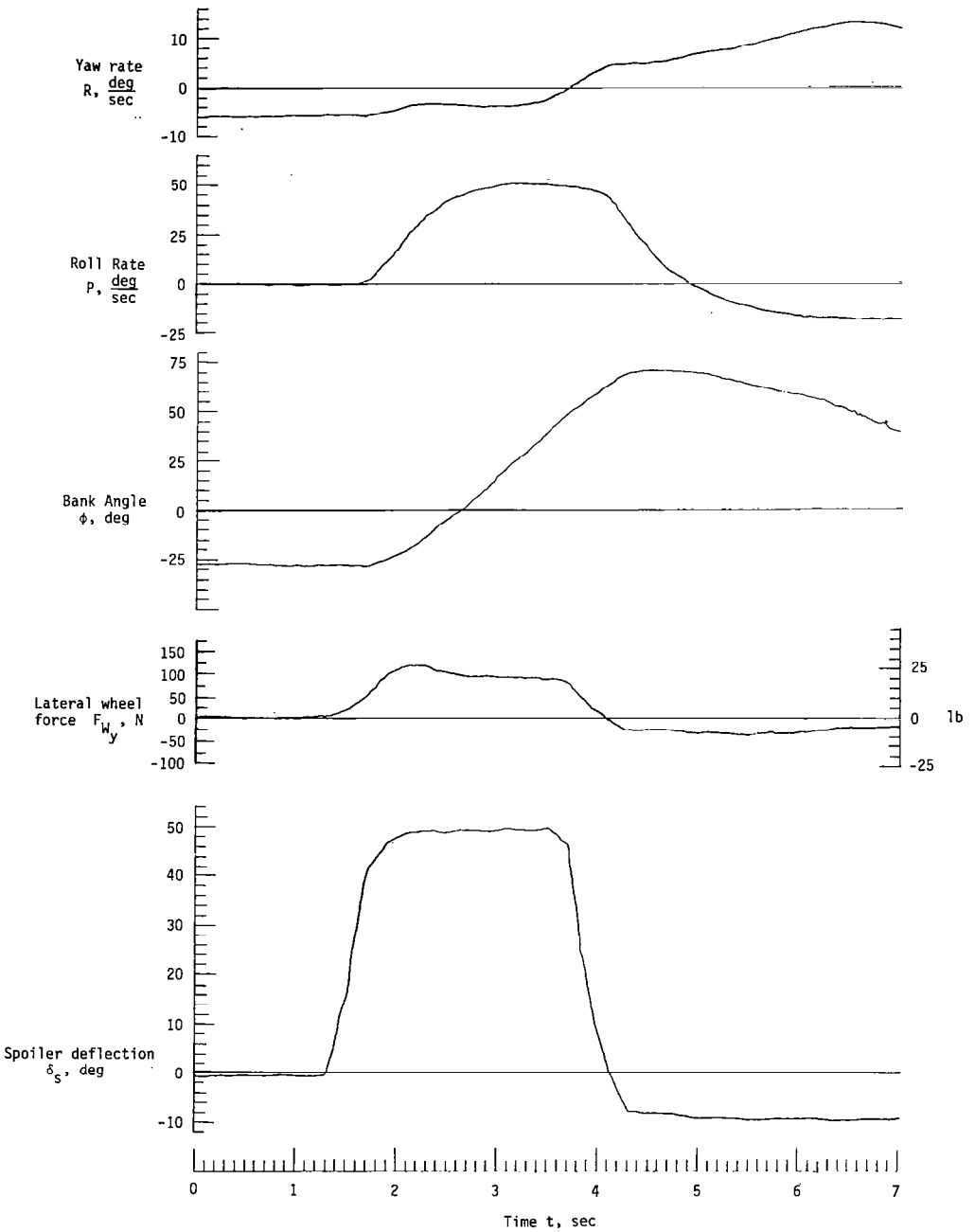

(a) Large spoiler deflection

Figure 5.6 - Roll response time histories

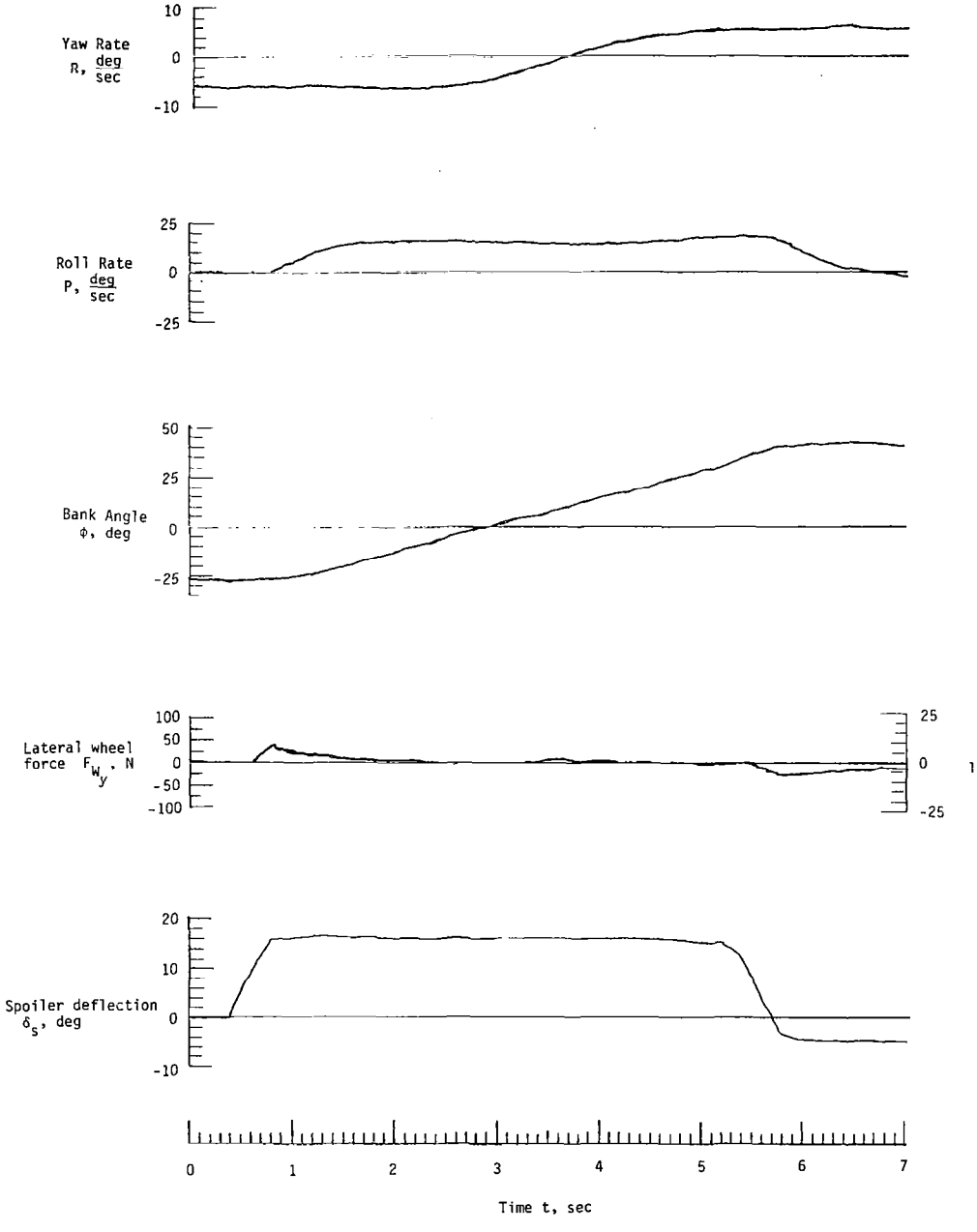

(b) Small spoiler deflection

Figure 5.6- Concluded.

breakout force of about 40 Newtons in each case. For the smaller input maneuver, the roll-control force went to zero in the steady part of the roll. In each case, the bank angle varied smoothly from a left bank to a right bank. These rolls were started from 25-degrees left bank and, in the case with the small spoiler deflection, continued to about a 30-degree bank to the right. The maneuver with the large spoiler input was continued to a right-bank angle of about 70 degrees. In each case, it took about 1 second for the roll rate to reach its maximum value. At the top of the figures, the yaw rate shows no sign of adverse yaw for either roll. As explained elsewhere in the paper, the raw data shown here cannot be used to determine the phasing of the various parameters. Reduction of the data introduces an erroneous phase difference of as much as two-tenths of a second between different parameters. The only undesirable characteristics shown by these time histories appear on the force trace for the smaller deflection roll. A large breakout force of approximately 40 Newtons shows clearly and the time history also shows that the force goes to zero during the steady part of the maneuver. Except for this undesirable characteristic, everything else shown on these two plots indicates characteristics of a satisfactory lateral-control system for rolling maneuvers.

Figure 5.7, a five-part figure on 5 pages, shows the measured maximum rolling velocities as a function of spoiler deflection for flap deflections from 0 to 37 degrees and several airspeeds as were listed in table 5.3. Most of these data are from rolls to the right. However,

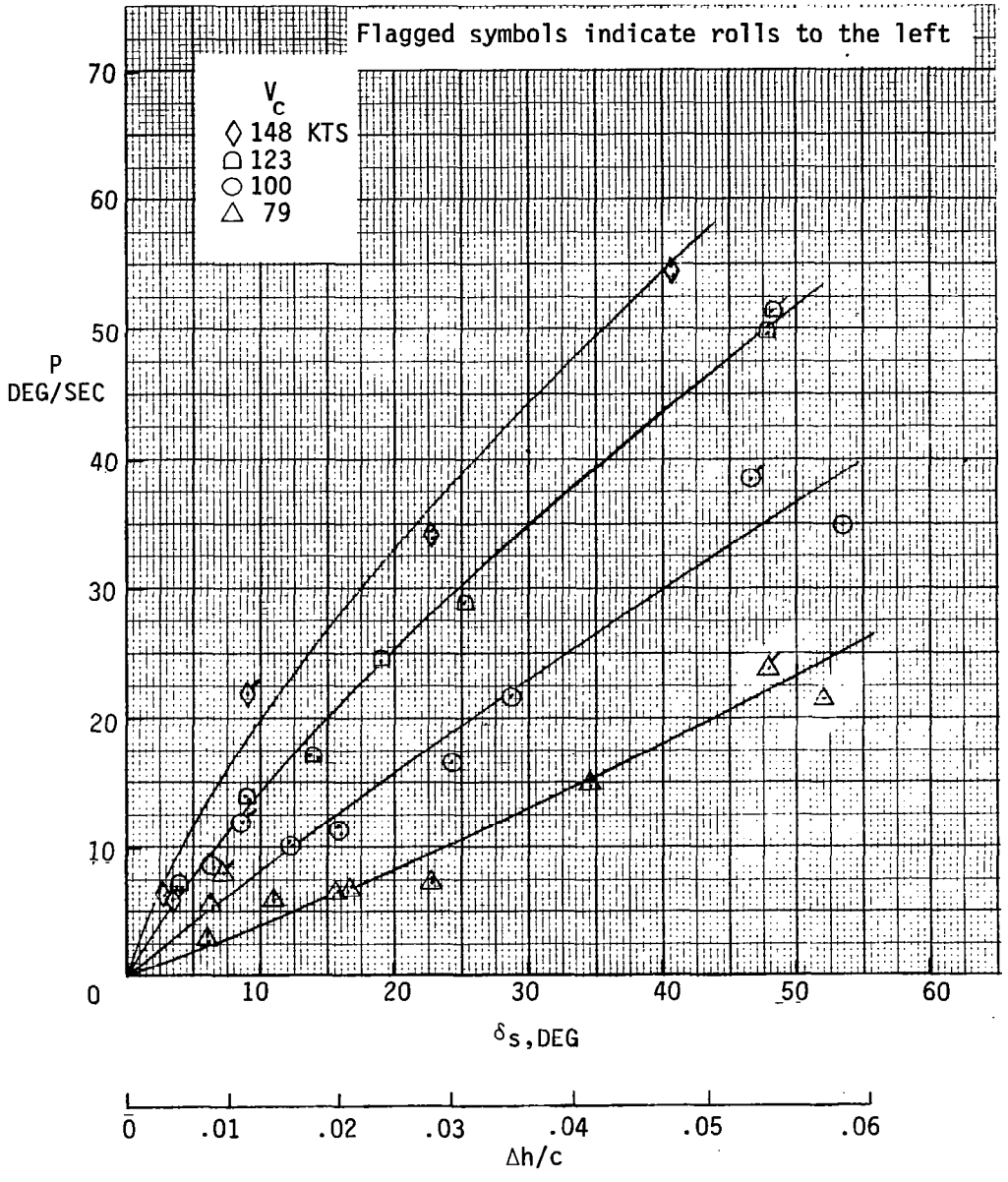

(a) Flaps 0^o

Figure 5.7- Rolling velocities as a function of spoiler deflection

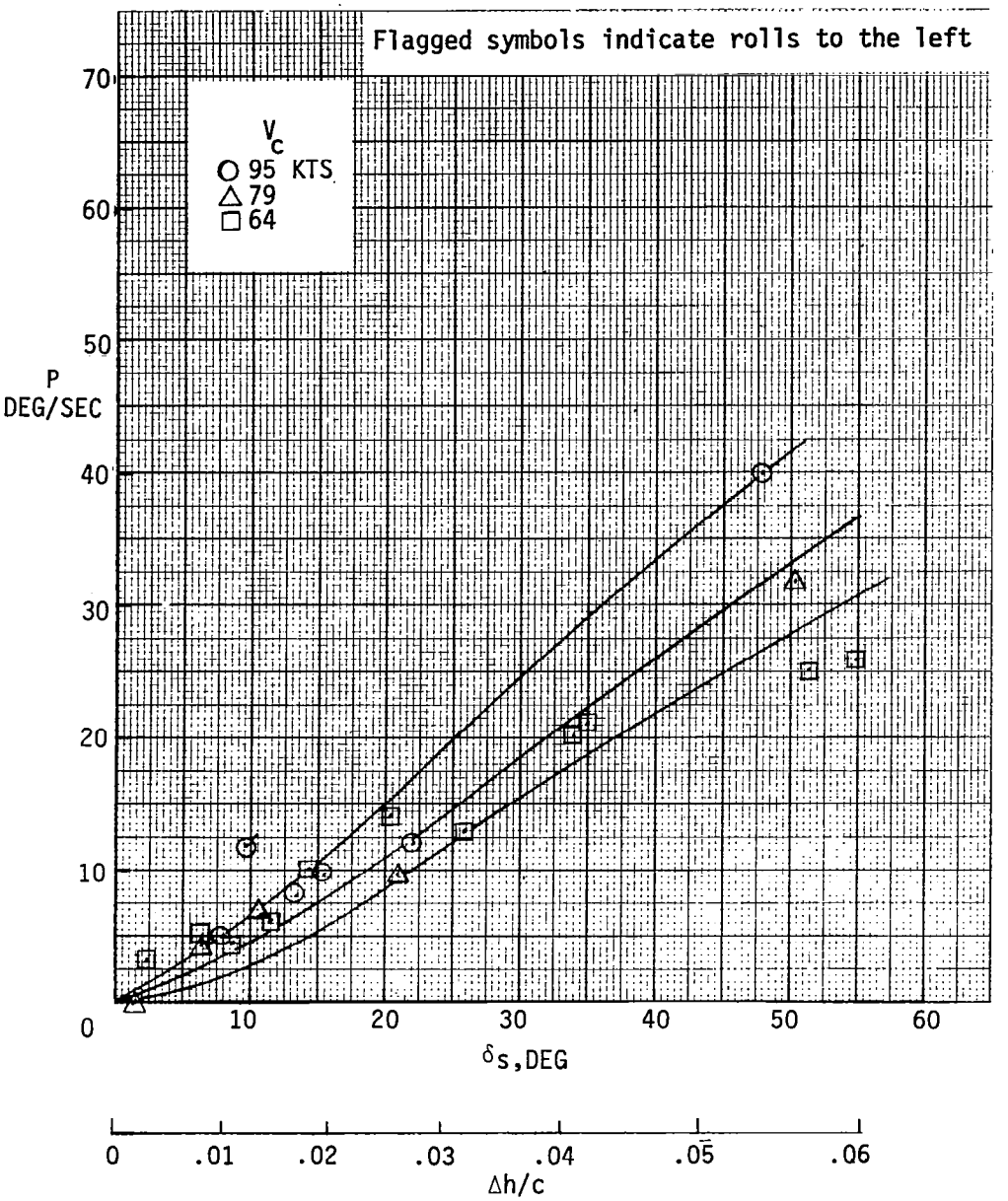

(b) Flaps 10^o

Figure 5.7- Continued.

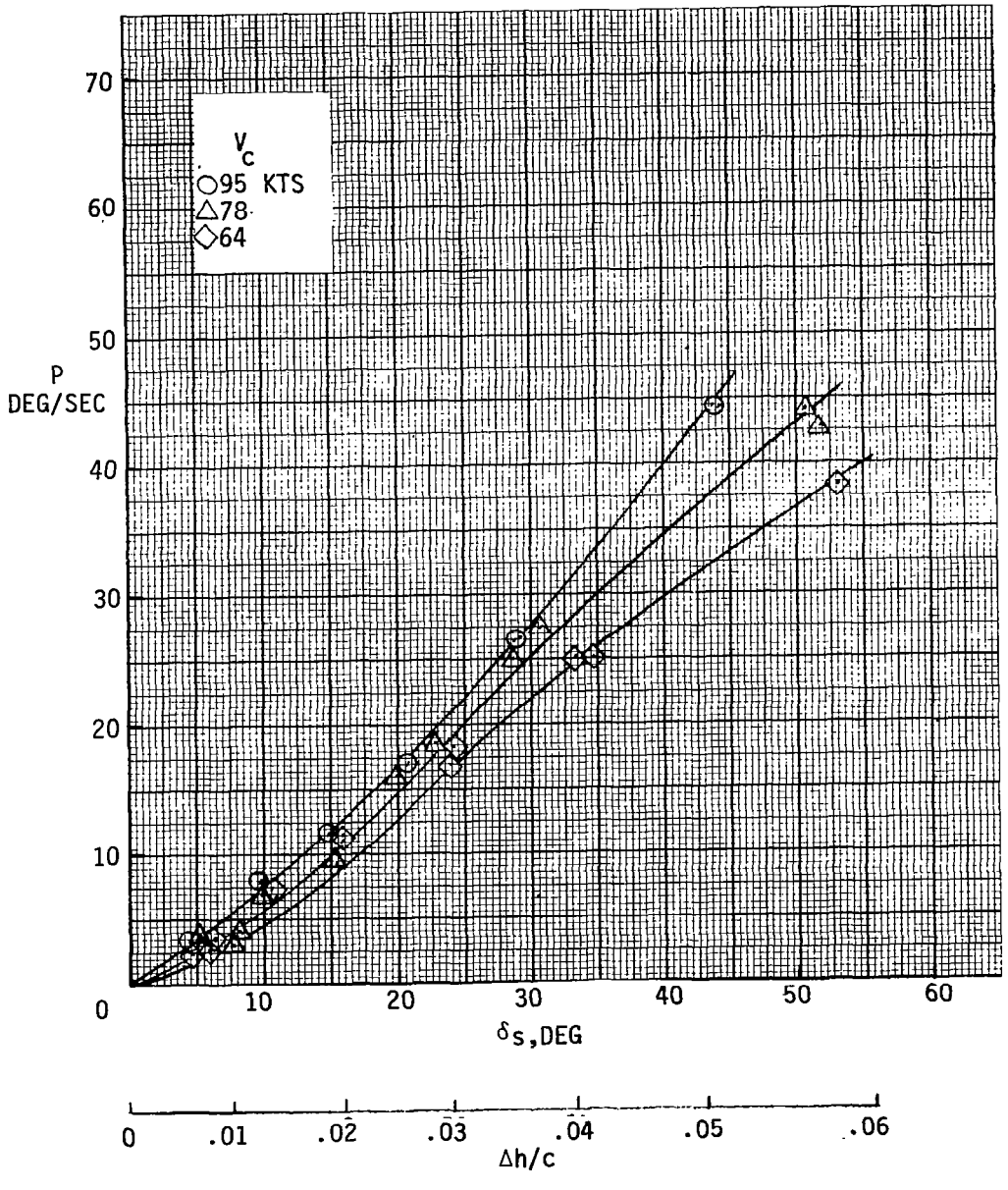

(c) Flaps 20^o

Figure 5.7- continued

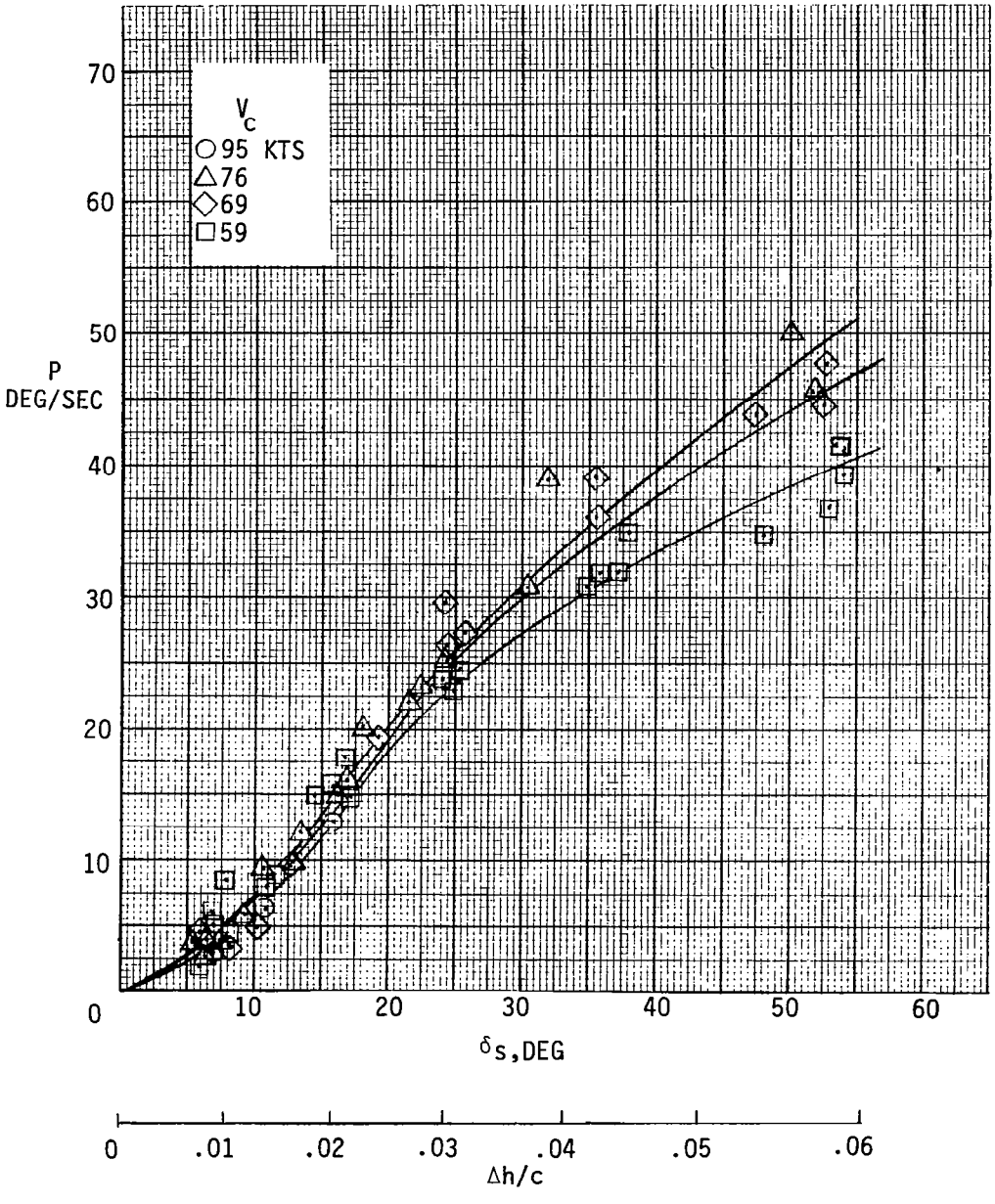

(d) Flaps 30^o

Figure 5.7- continued

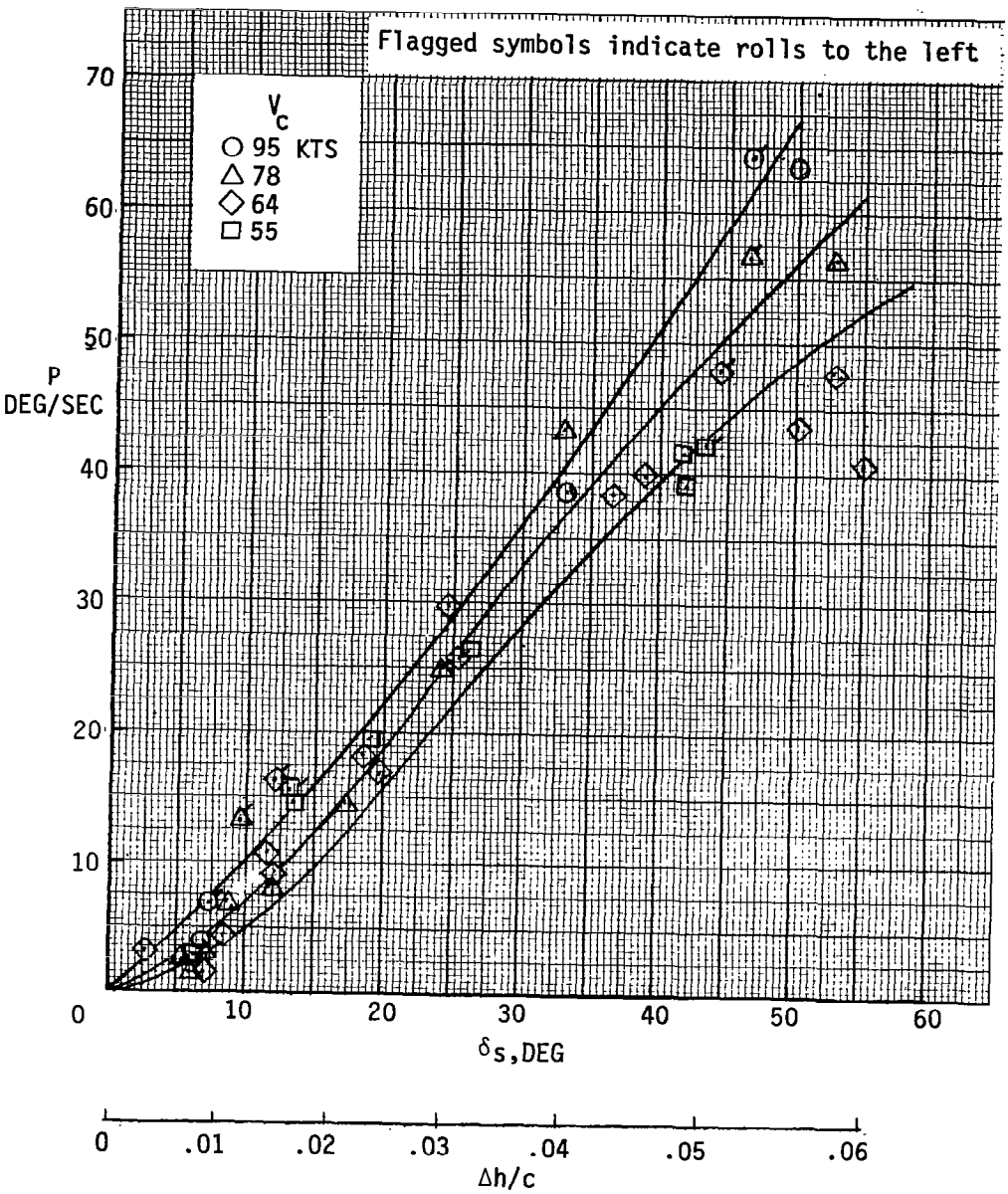

(e) Flaps 37^o

Figure 5.7- Concluded.

data from a few left rolls are shown and can be identified by the flagged symbols. Figure 5.8 shows the same roll data converted to the maximum roll helix angles, $\frac{pb}{2V}$, attainable with the varying spoiler deflections.

The original Gilruth standard of reference 38 was that for acceptable roll-control power $pb/2V$ should be at least 0.07. This standard still remains a good one for most general aviation airplanes. It is apparent from figure 5.8 that the roll authority of the ATLIT spoilers ($\frac{pb}{2V}$ = 0.10 to 0.15) far exceeded the Gilruth standard for large flap deflections. A spoiler will obviously become less effective as the portion of the wing behind the spoiler becomes less heavily loaded. Therefore, it was to be expected that $pb/2V_{max}$ would be lower for a flap deflection of 10 degrees than for larger flap deflections. However, the Gilruth standard was still exceeded with $\frac{pb}{2V} \geq 0.075$ for $\delta_f = 10^o$. With flaps up, the ATLIT $pb/2V_{max}$ response was about 0.08 at cruising speeds, but was slightly below the standard with a $pb/2V_{max}$ of 0.055 at a speed of 80 knots for $\delta_s \simeq 50^o$. However, it should be noted that an actual spoiler deflection of 60 degrees could probably be used to increase the attainable $pb/2V_{max}$ at 80 knots to at least 0.065.

Figure 5.9 presents the roll-control authority of the ATLIT spoiler as a function of airspeed for 40 degrees of spoiler deflection. The figure shows that even though 40 degrees is less than 80 percent of the

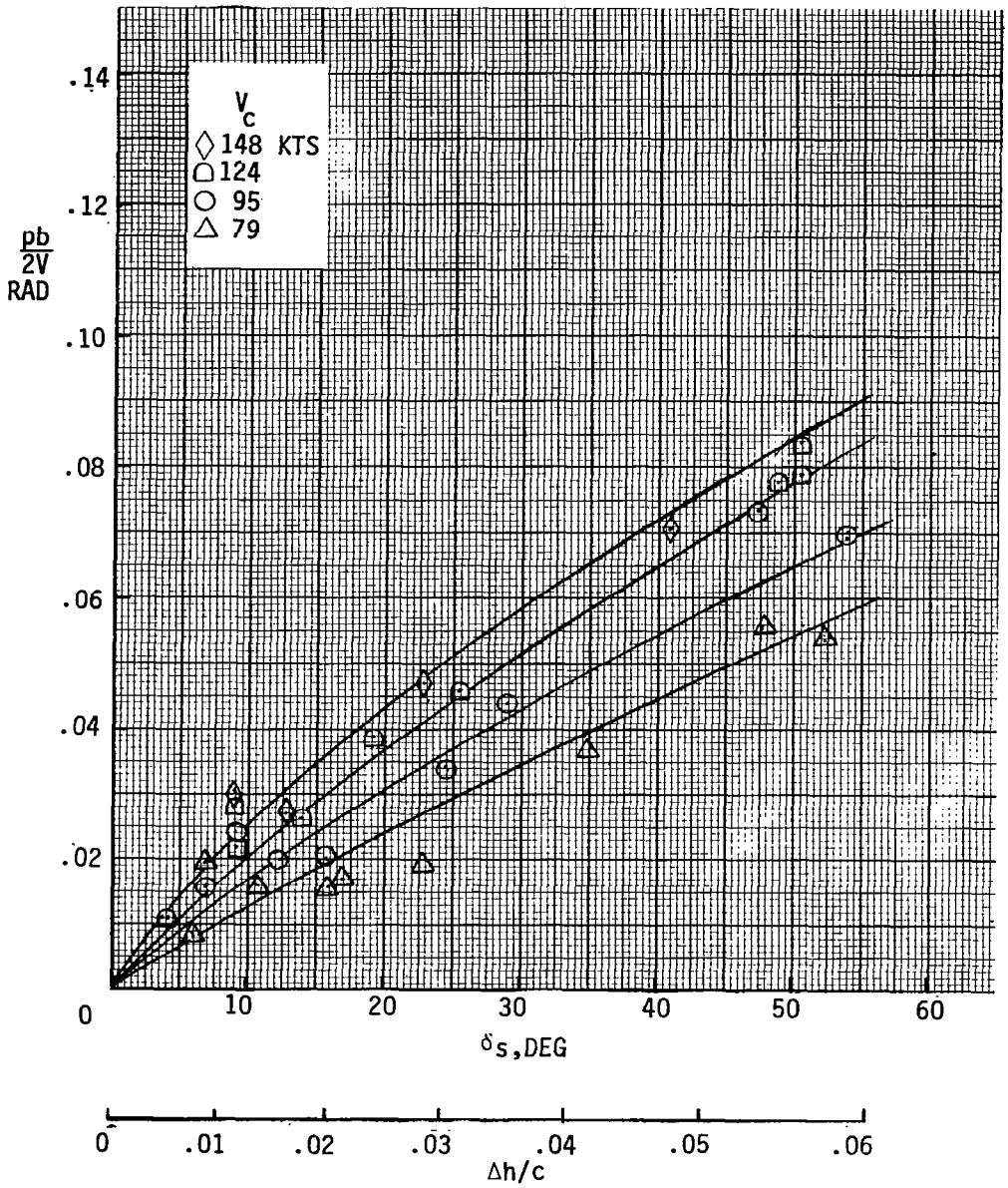

(a) Flaps 0^o

Figure 5.8- Roll helix angles for varying spoiler inputs

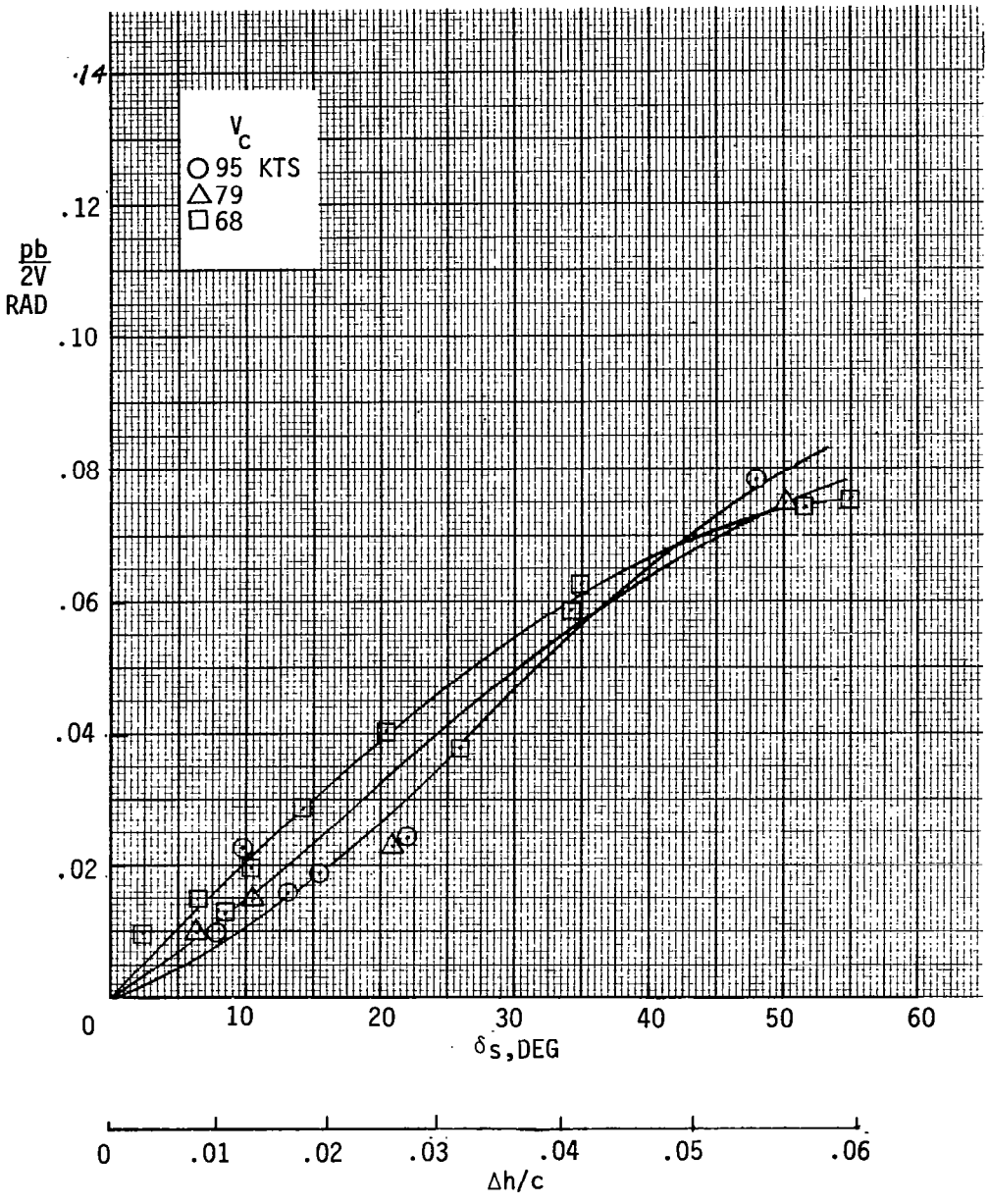

(b) Flaps 10^o

Figure 5.8- continued

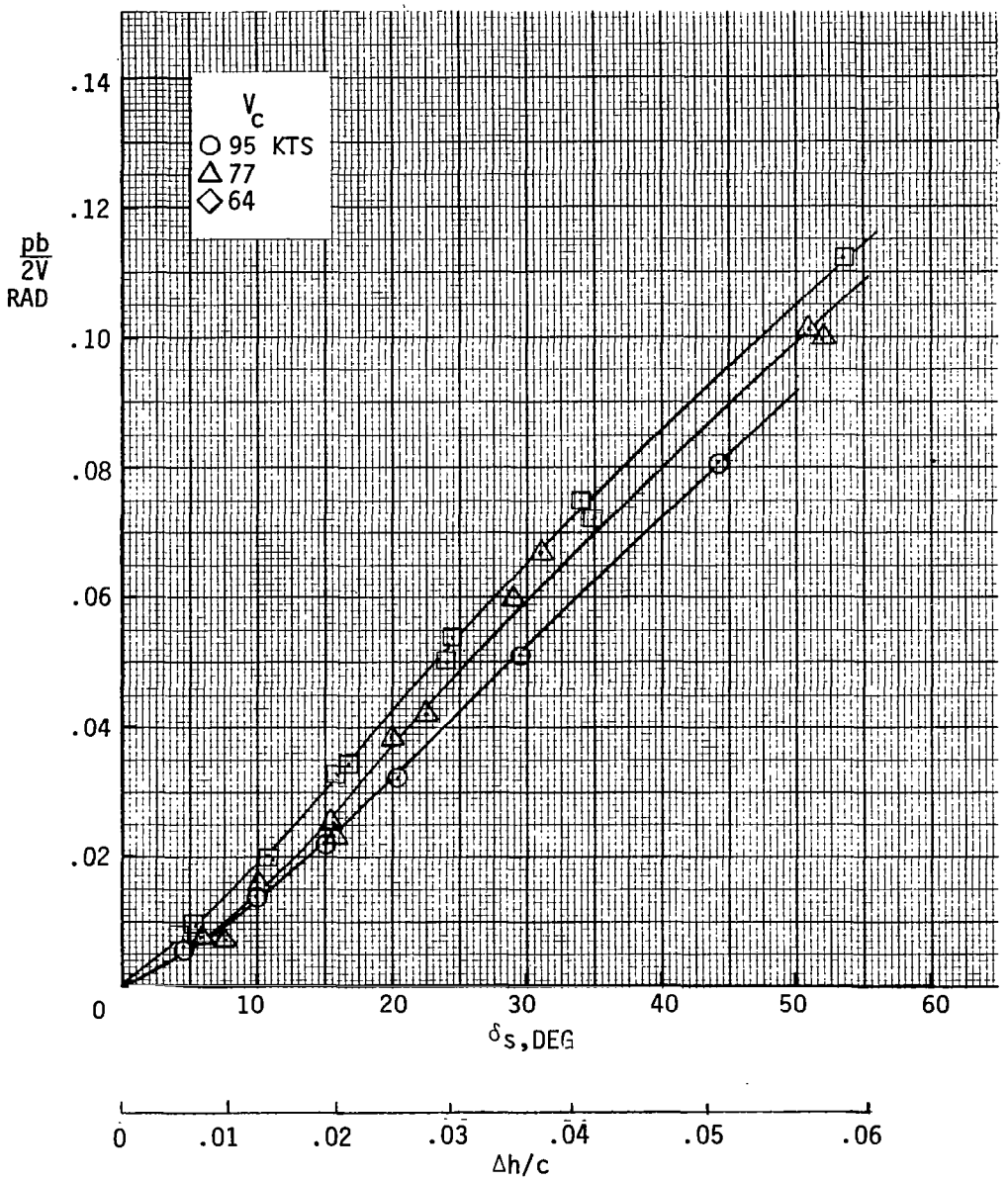

(c) Flaps 20°

Figure 5.8- Continued.

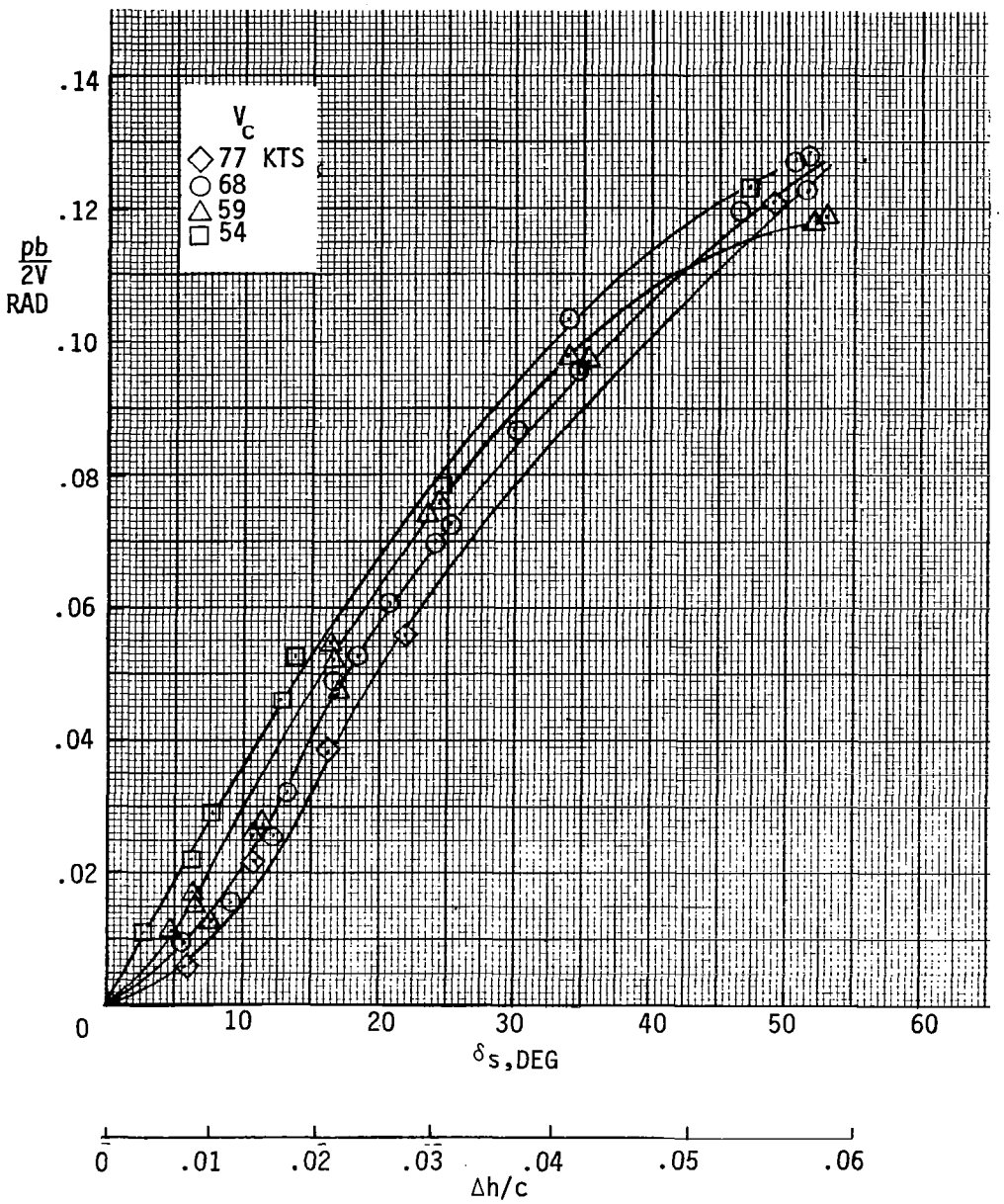

(d) Flaps 30^o

Figure 5.8- continued

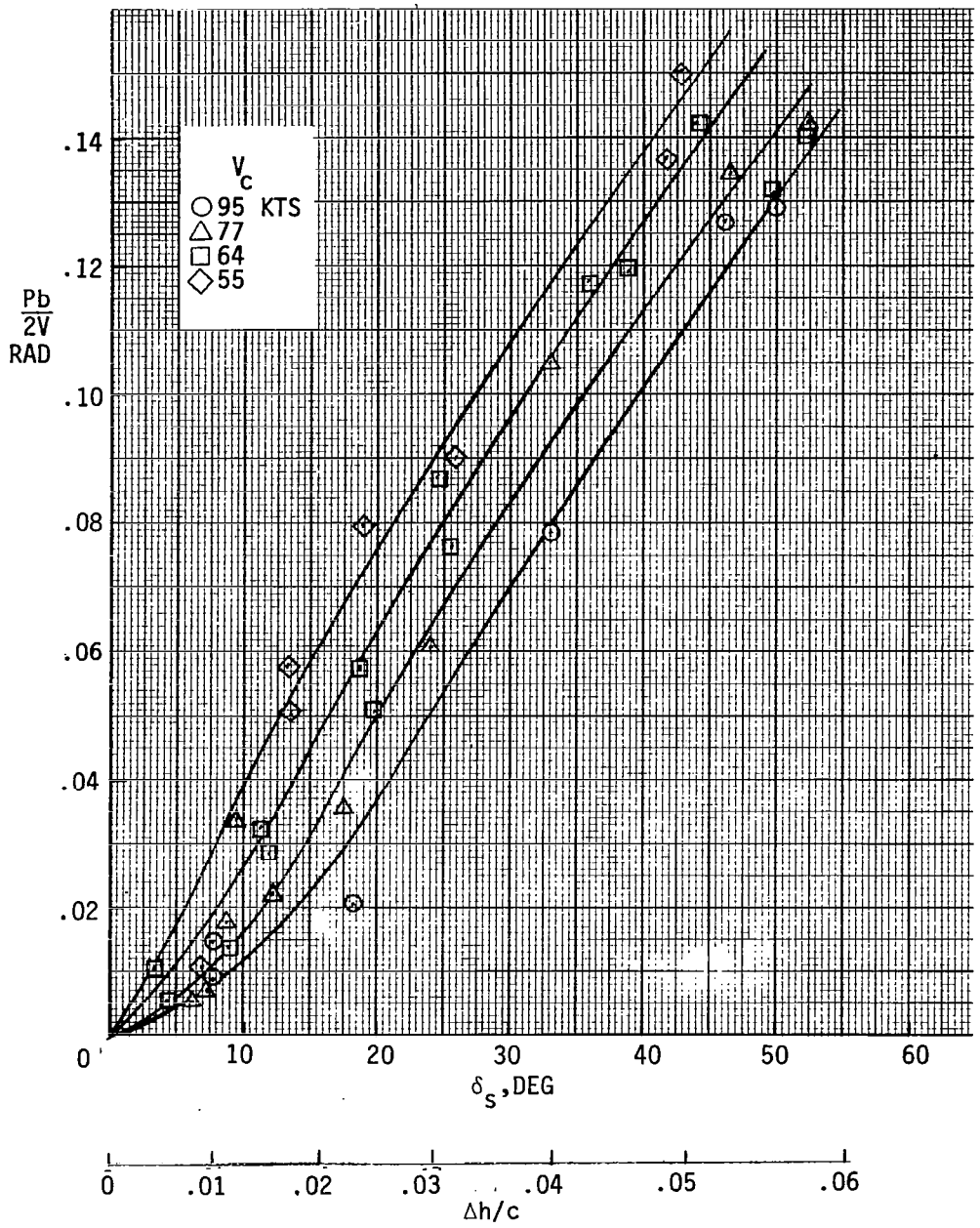

(e) Flaps 37°

Figure 5.8- Concluded.

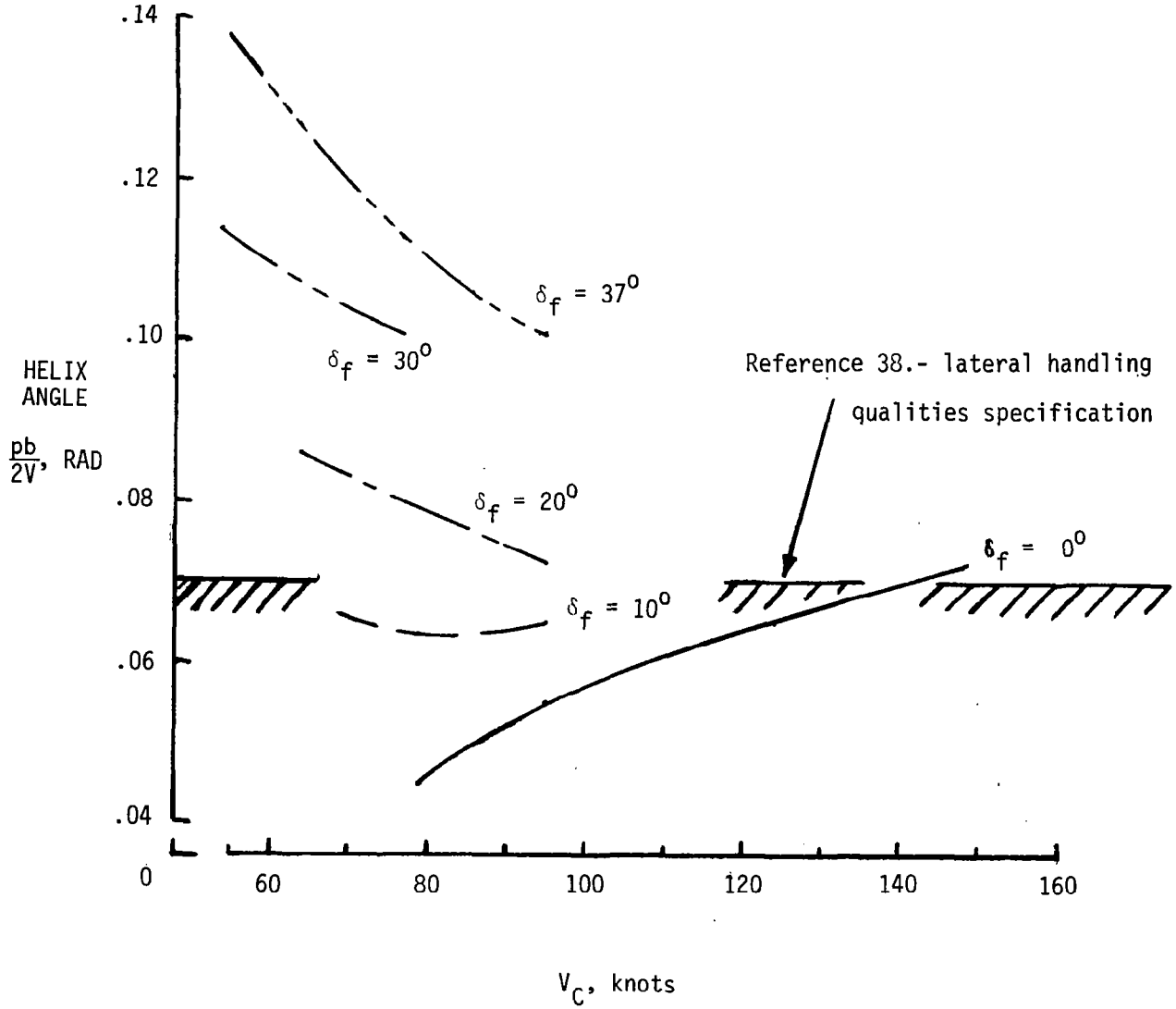

Figure 5.9- The effect of flaps on ATLIT rolling performance for 40^{o} of spoiler deflection ($\delta_f = 0^{o}, 10^{o}, 20^{o}, 30^{o}, 37^{o}$).

net spoiler deflection available on this airplane, after allowing for cable stretch, the rolling performance is generally well above the desired $pb/2V = 0.07$ level. It can be readily determined from this figure that the roll-control authority is strong, or at least adequate, with the exception of the clean configuration near the stalling speed.

In order to be able to determine values of C_l', the rolling moment coefficient, C_{l_p}, the roll damping coefficient (flaps up) was calculated using the methods discussed in appendix C. Values of C_{l_p} for flap-down configurations were estimated based on the projected planform area for each flap position. The aspect ratio and taper ratio were adjusted accordingly for the calculation. The calculated variations of C_{l_p} with C_L for the flaps-up case and for $\delta_f = 10^o$ and 30^o are presented in figure C.3 of appendix C. The ranges of the estimated values of C_{l_p} over the appropriate ranges of C_L were approximately 0.5; + 0.05, with flaps up and approximately 0.6; + 0.04, -0.06 with $\delta_f = 30^o$.

Figure 5.10 shows the variation of C_l' for ATLIT with spoiler deflection for three flap deflections and several speeds. It should be noted that the spoiler deflection is given both in degrees of arc and in terms of exposed height of the spoiler above the wing (using the wing chord at the spoiler mid-span as a reference length). Of these measures, spoiler projection in percent chord is a much more significant indicator of spoiler effectiveness. These data were determined using faired values

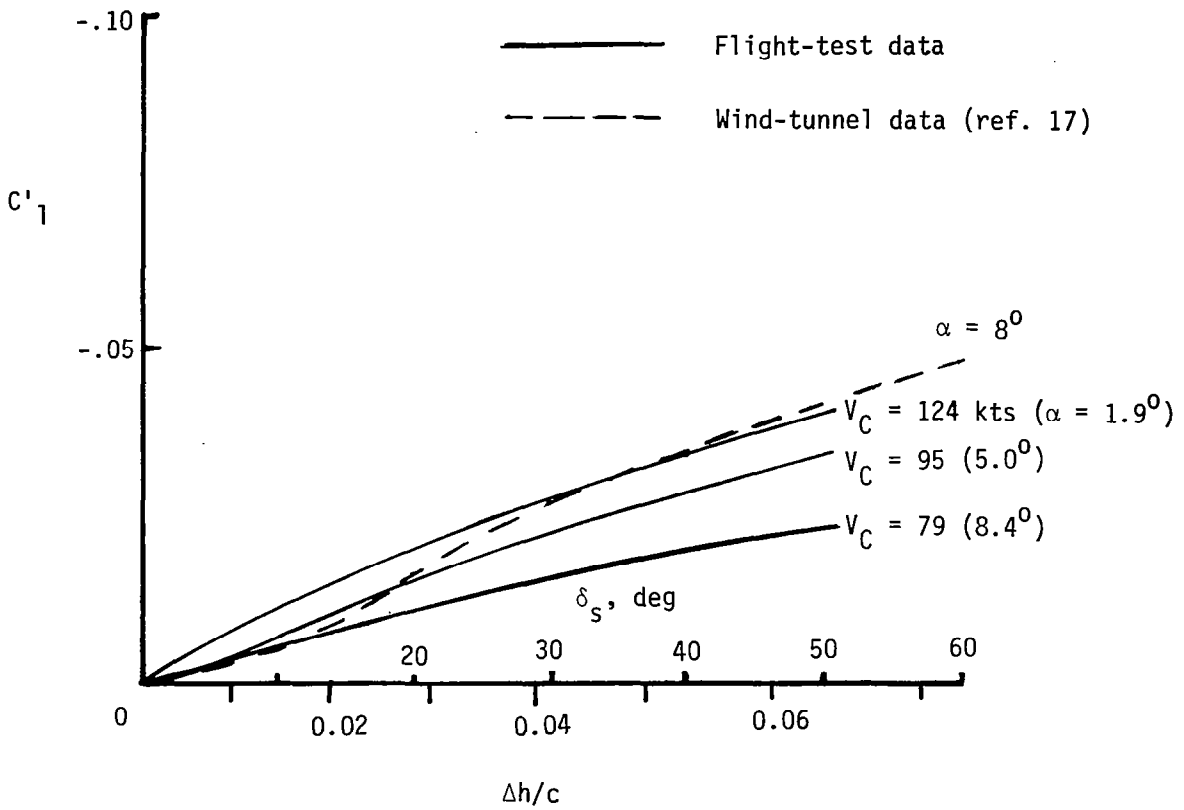

(a) Fowler flaps nested

Figure 5.10 ATLIT spoiler produced rolling moments

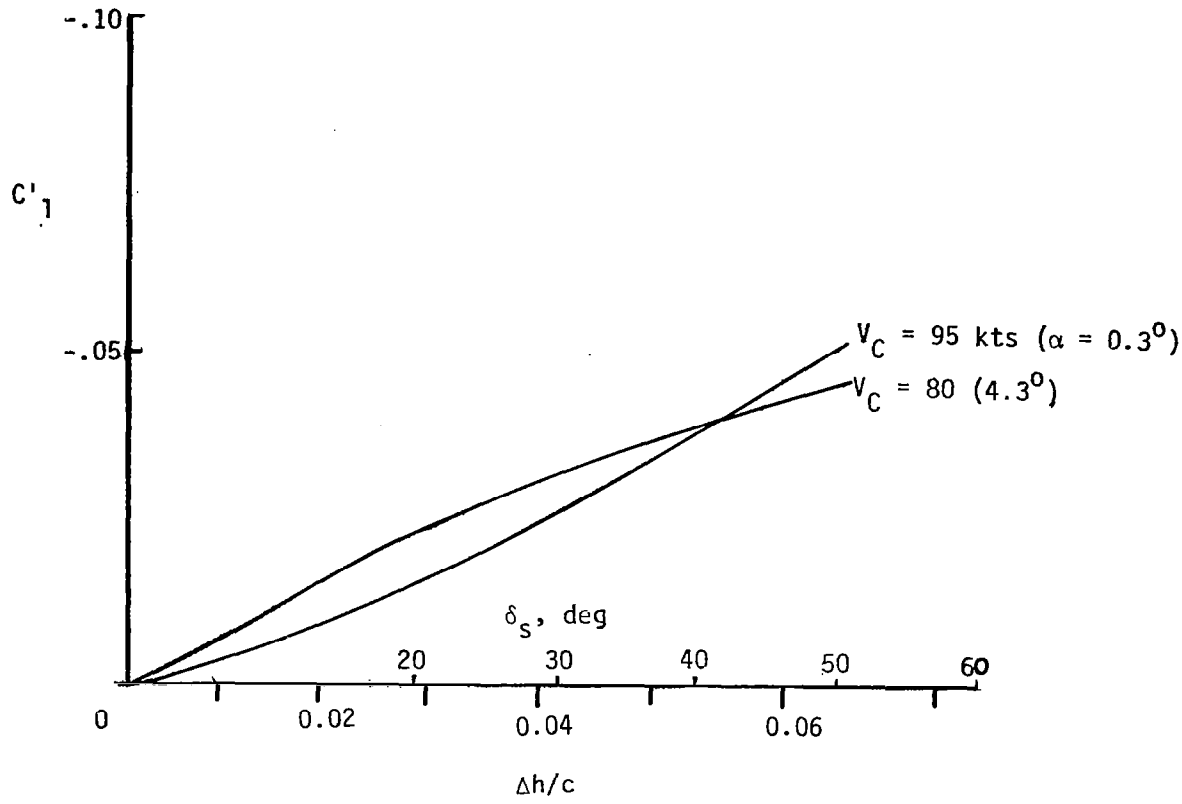

(b) Fowler flaps 10°

Figure 5.10 continued

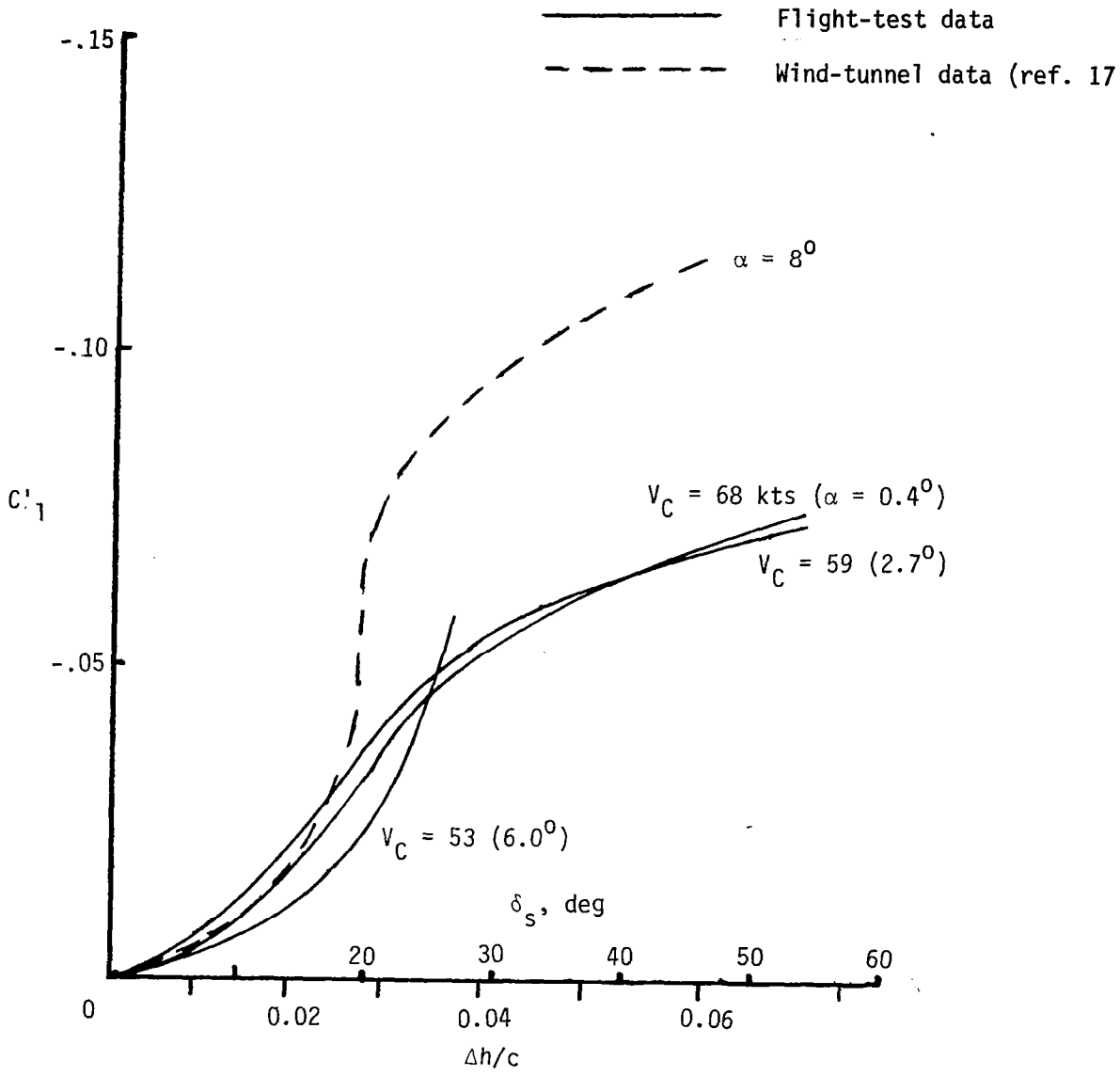

(c) Fowler flaps 30^o

Figure 5.10 Concluded.

of pb/2V. As would be expected, the C_l' curves are quite similar to the roll-rate plots of figure 5.7 or the pb/2V plots of figure 5.8. The designer, who plans to use spoilers, should be on the lookout for unusual trends near the stall such as occurred with $\delta_f = 30^o$ at an airspeed of 53 knots. In that case, the value of $\partial C_l'/\partial \delta_s$ was smaller than usual at small deflections, but it became larger than usual at medium-sized deflections. It should be noted that nonlinearities of the magnitude shown here could cause the pilot to overcontrol. On ATLIT, this tendency is compounded by the existence of a large wheel-breakout force. These ATLIT deficiencies are discussed further by the research pilots in chapter 5.5. Discrepancies between wind-tunnel and flight values of C_l' in figure 5.10 are most likely due to inaccurate estimations of C_{l_p}.

Figure 5.11 summarizes, in terms of numerical pilot ratings, the conclusions from the Princeton in-flight simulation of nonlinear roll-control effectiveness of reference 19. However, it should be noted that the variable stability Navion used for these tests had a very smooth lateral-force characteristic with negligible friction or breakout force.

On the favorable side, it should be noted that for ATLIT the characteristic variation of C_l' with δ_s was never as nonlinear as the one-fourth scale wind-tunnel tests indicated. (Examples of the wind-tunnel data of reference 17 are shown on figure 5.10.)

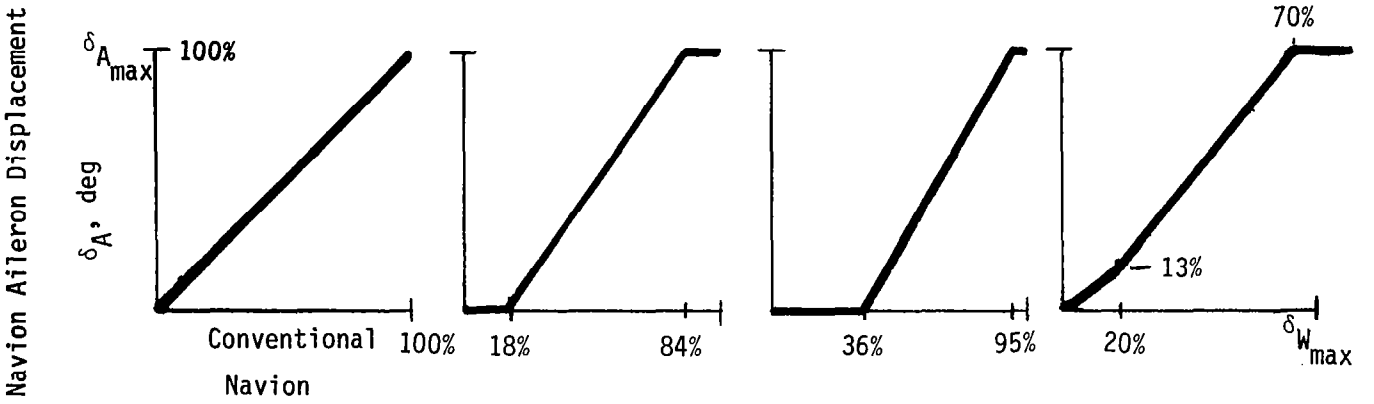

δ_{AW} - NAVION WHEEL DISPLACEMENT (DEG)

Low Inertia Case Pilot Ratings	2	4 - 4½	5½	3½ - 4
High Inertia Case Pilot Ratings	4	6½	8 - 9	5½
Low Inertia High Crosswind Ratings	3	-	-	4½ - 5

Figure 5.11- Pilot rating for nonlinear roll-response variations (reference 19).

5.4 Cruise and Climb Performance

5.4.1.1 Method A: Performance Predictions*

The method used to make these predicitons of airplane performance is a rapid sizing procedure.[14] A brief description of some assumptions and procedures used in the method is presented here.

The procedure makes use of correlations of characteristics for 140 different present and past aircraft. These aircraft were classed into different groups according to aerodynamic sophistication. ATLIT was classed with a group of aircraft having internally braced wings and retractable landing gear. A comparison of ATLIT to other airplanes in this class showed that the ATLIT characteristics (zero lift drag, aspect ratio, and wing loading, in particular) fell near the extremes of the ranges of these characteristics for this airplane class. The effects of this result are not accounted for in the performance predictions which are given in table 5.4.

Maximum level-flight speed can be estimated by rewriting the equation for power required for level flight

$$550P\eta = C_D \frac{\rho}{2} SV^3 \qquad (5.8)$$

as

$$V = 77.3 \sqrt[3]{\frac{W/S}{W/P} \frac{\eta}{\sigma C_D}} \qquad (5.9)$$

---

*The contributions of Mr. Laurence K. Loftin, NASA-LaRC, in the preparation of materials for this chapter are gratefully acknowledged.

---

14. Loftin.

TABLE 5.4- COMPARISON OF PIPER SENECA I PERFORMANCE WITH PREDICTIONS FOR ATLIT.*

Performance Characteristic (Sea-level values unless indicated otherwise.)	(1) Piper Seneca Handbook Values	(2) Method A (Loftin) Using Piper-Seneca Geometry	(3) Method A (Loftin) Using ATLIT Geometry	(4) Method B (Ref. 30) Using Light-Twin Wind-Tunnel Polar (Eqn. 5.17)	(5) Method B (Ref. 30) Using NCSU ATLIT Drag Polar (Eqn. 5.16)	(6) Method C (Ref. 29) Using Seneca Geometry (Fig. 5.16)	(7) Method C (Ref. 29) Using ATLIT Wing Geometry (Fig. 5.16)
Max. level-flight speed, knots, (mph)	170 (195)	182 (210)	200 (230)	178 (205)	177 (204)	164 (189)	173 (199)
Max. rate of climb, m/min (ft/min)	415 (1360)	475 (1560)	487 (1598)	496 (1626)	518 (1701)	470 (1570)	517 (1695)
Single-engine rate of climb, m/min (ft/min)	58 (190)	140 (460)	152 (500)	111** (364)	143** (469)	143 (470)	163 (530)
Best rate of climb speed, knots, (mph)	91 (105)	71 (82)	70 (80)	100 (115)	96 (111)	94 (108)	94 (108)
Best single-engine rate of climb speed, knots (mph)	91 (105)	71 (82)	70 (80)	92** (106)	85** (98)	94 (108)	94 (108)
Best range speed, knots, mph	95 (109)	94 (108)	92 (105)	99 (114)	91 (105)	95 (109)	92 (106)
Service ceiling, m (ft) MSL	5486 (18,000)	6103 (20,025)	6422 (21,070)	5999 (19,681)	6866 (22,525)	- -	- -
Single-engine service ceiling, m (ft) MSL	1113 (3650)	2551 (8370)	2883 (9460)	1714 (5623)	2682 (8800)	- -	- -

*All ATLIT performance predictions were computed assuming that power available = 400 BHP.

**These single-engine characteristics were combined using a $C_D = 1.05\ C_D$ to account for engine-out trim drag and using half of the total assumed power available.

An examination of propeller-driven aircraft shows that for the higher speeds in an airplane performance envelope, the induced drag averages about 10 percent of the total airplane drag. In addition, zero-lift drag coefficients for airplanes of a given class of aerodynamic sophistication were assumed to be of the same order. It was also assumed that propulsion efficiency for a given class of airplanes was approximately the same. With these assumptions, maximum speed of the airplane is then related to the ratio of wing loading to power loading

$$V \sim \sqrt[3]{\frac{W/S}{W/P}\ \frac{1}{\sigma}} \quad . \tag{5.10}$$

To estimate climb performance, the basic performance equation can be written

$$\dot{h} = 33{,}000 \left(\eta \frac{P}{W} - \frac{\sqrt{W/S}}{19 \left(C_L^{3/2}/C_D\right) \sqrt{\sigma}}\right) . \tag{5.11}$$

Equation (5.11) simply states that rate of climb ($\dot{h}$) is proportional to the difference between power available and power required. Approximately, then, maximum rate of climb occurs at the point on the power curve where $\left(C_L^{3/2}/C_D\right)$ is maximum, that is, at the point for minimum power required for a propeller-driven aircraft. In practice, best rate of climb does not occur at the point for $\left[C_L^{3/2}/C_D\right]_{max}$; however, for rapid performance

estimations or for comparative purposes, the assumption is a fair one. Actual maximum rate of climb must be computed taking account of the changes in propulsive efficiency with forward velocity. The maximum rate of climb will then be found where maximum excess power occurs.

For a parabolic drag polar, the maximum value of $C_L^{3/2}/C_D$ and corresponding lift coefficient can be given as

$$(C_L^{3/2}/C_D)_{max} = \frac{1.345\ (Ae)^{0.75}}{(C_{D_o})^{0.25}} \qquad (5.12)$$

and

$$C_{L_C} = \sqrt{3\ C_{D_o}\ \pi\ Ae} \quad . \qquad (5.13)$$

The airspeed for best rate of climb can be estimated using the lift coefficient from equation (5.13).

For estimating range, the values for the maximum lift-to-drag ratio and the corresponding lift coefficient can be given as

$$(L/D)_{max} = 1/2\sqrt{\frac{\pi Ae}{C_{D_o}}} \qquad (5.14)$$

and

$$C_{L_M} = \sqrt{\pi Ae\ C_{D_o}} \qquad (5.15)$$

The airspeed for best L/D can be estimated using the lift coefficient from equation (5.15).

Single- and multi-engine service ceilings were estimated by solving for the density ratio (σ) in equation (5.11). With $\dot{h}$ defined ($\dot{h}$ = 15.2 m/min (50 fpm) for single engine and $\dot{h}$ = 30.5 m/min (100 fpm)

for multi-engine), the altitude for service ceilings was then computed from the resulting value of σ.

Since one of the primary values in this method is for making performance comparisons, estimates were computed using both the standard Seneca geometry and the ATLIT geometry. These comparisons appear in columns (2) and (3) of table 5.4.

It is instructional to evaluate the ATLIT wing modifications using the above equations while varying e and C_{D_o}.

Table 5.5 presents the results of these computations for five cases as follows:

1. Using flight-measured values of e and C_{D_o} for the standard Seneca: $e = 0.78$, $C_{D_o} = 0.026$.

2. Using the values of e and C_{D_o} predicted for the ATLIT design: $e = 0.8$, $C_{D_o} = 0.035$.

3. Using values for e and C_{D_o} which have been determined based on preliminary flight-test results: $e = 0.67$, $C_{D_o} = 0.044$. These values represent the airplane in a configuration with massive wing- body interference-induced separation (which reduces e), and with added drag due to excessive wing trailing edge thickness, instrumentation noseboom, protruding flap and spoiler brackets, square wheel well openings, and ten

inspection covers located along the span protruding into the airstream (all of which increase C_{D_o}).

4. Using values of e and C_{D_o} which assume lift-dependent drag is cleaned up (i.e., that e is increased) and zero-lift drag is unchanged from the value based on flight-test results: $e = 0.80$, $C_{D_o} = 0.044$. This case demonstrates the effect e has on $(C_L^{3/2}/C_D)_{max}$ and $(L/D)_{max}$.

5. Using values of e and C_{D_o} which assume zero-lift drag is reduced and e is unchanged from the value based on flight-test results: $e = 0.67$, $C_{D_o} = 0.035$. This case demonstrates the effect C_{D_o} has on $(C_L^{3/2}/C_D)_{max}$ and $(L/D)_{max}$.

TABLE 5.5- COMPARISONS OF PREDICTED PERFORMANCE PARAMETERS FOR THE STANDARD SENECA AND ATLIT (W = 1.87 kN, σ = 1)

Case	Maximum Climb Performance		Best Cruising Performance	
	$(C_L^{3/2}/C_D)_{max}$ by eqn. (5.12)	Minimum Thrust Power Required* i.e. @$(C_L^{3/2}/C_D)_{max}$	$(L/D)_{max}$ by eqn. (5.14) (C_L for $(L/D)_{max}$**)	Thrust Power Required*** (@ $(L/D)_{max}$)
1. Piper Seneca A = 7.25 S = 19.4 m^2 e = 0.78 C_{D_o} = 0.026	12.3	70 kw (81 hp)	13.1 (0.68)	69 kw (92 hp)
2. ATLIT-best case A = 10.32 S = 14.4 m^2 e = 0.80 C_{D_o} = 0.035	15.2	57 kw (76 hp)	13.6 (0.95)	65 kw (87 hp)
3. ATLIT-worse case A = 10.32 S = 14.4 m^2 e = 0.67 C_{D_o} = 0.044	12.5	69 kw (92 hp)	11.1 (0.98)	78 kw (105 hp)

TABLE 5.5- Concluded.

Case	Maximum Climb Performance		Best Cruising Performance	
	$(C_L^{3/2}/C_D)_{max}$ by eqn. (5.12)	Minimun Thrust Power Required* i.e @$(C_L^{3/2}/C_D)_{max}$	$(L/D)_{max}$ by eqn. (514) (C_L for $(L/D)_{max}$**)	Thrust Power Required*** (@ $(L/D)_{max}$
4. ATLIT-degraded C_{D_o} A = 10.32 S = 14.4 m^2 e = 0.80 C_{D_o} = 0.044	14.3	60 kw (81 hp)	12.1 (1.07)	68 kw (92 hp)
5. ATLIT-degraded e A = 10.32 S = 14.4 m^2 e = 0.67 C_{D_o} = 0.035	13.3	65 kw (87 hp)	12.5 (0.87)	74 kw (99 hp)

*From eqn. (5.11): $\frac{\text{power required (hp)}}{\text{weight (lb)}} = \frac{\sqrt{W/S}}{19\,(C_L^{3/2}/C_D)\,\sqrt{\sigma}}$

for any $(C_L^{3/2}/C_D)$.

**@$(L/D)_{max}$, $C_{L_M} = \sqrt{\pi\, Ae\, C_{D_o}}$

***At $(L/D)_{max}$, $(C_L^{3/2}/C_D) = \frac{C_{L_M}}{C_{D_o} + \frac{1}{\pi Ae} \cdot C_{L_M}^2}$. Then, power required at $(L/D)_{max}$ is computed by the equation above*.

128

An analysis of the results in table 5.5 demonstrates two major points concerning the relative effects of e and C_{D_o} on $(C_L^{3/2}/C_D)_{max}$ (the most important parameter for climb performance) and $(L/D)_{max}$ (the most important parameter for cruise efficiency).

1. Improving e has stronger effect on $(C_L^{3/2}/C_D)_{max}$ than it does on $(L/D)_{max}$. A comparison of case (2) with (5) and case (2) with (4) shows that improving e from 0.67 to a near-optimum value of 0.80 reduces $(C_L^{3/2}/C_D)_{max}$ more than does reducing C_{D_o} from 0.044 to 0.035.

2. Improving C_{D_o} has a stronger effect on $(L/D)_{max}$ than on $(C_L^{3/2}/C_D)$. A comparison of case (2) with (4) and case (2) with (5) shows that reducing C_{D_o} from 0.044 to 0.35 increases $(L/D)_{max}$ more than does increasing e from 0.67 to 0.80.

An important observation can be made using the data in table 5.5 concerning the effect of wing loading on climb performance. Comparing the Piper Seneca (case 1) predictions with the ATLIT best-case (case (2)) predictions, it can be seen that the value of $(C_L^{3/2}/C_D)_{max}$ is increased by about 27 percent for ATLIT. However, as illustrated by comparing the values for climb power required, the large increase in $(C_L^{3/2}/C_D)_{max}$ for ATLIT does not translate into a

proportionately large decrease in power required to climb. Thus, the predicted improvement in climb performance (given in table 5.4) is small (about 12m/min (40 ft/min)). It can be shown that had the aspect ratio been allowed to increase while wing loading remained constant, the improvement in climb performance over case (1) would have been much larger. Cases (3), (4), and (5) demonstrate the potential penalties paid in increased power required to climb due to lack of attention to construction details, allowing e and C_{D_o} to be degraded; that is, not one of these cases for ATLIT predicts improved climb performance.

A final observation which can be made using the data on table 5.5 concerns the effect of C_{D_o} on the predicted best cruise performance. A comparison of the Piper Seneca (case (1)) predictions with the ATLIT-best case (case (2)) predictions shows that $(L/D)_{max}$ is increased and power required at $(L/D)_{max}$ is decreased for ATLIT. Cases (3), (4), and (5) demonstrate the penalties paid in increased best-cruise power required due to degraded e and C_{D_o}; that is, none of these cases predict cruise performance improvements for ATLIT.

5.4.1.2 Method B: Lift, Drag, and Performance Predictions*

These predictions, of lift, drag, and pitching moment to be encountered during cruise flight, were developed using the computer program

*The materials for this section were prepared by Dr. Frederick O. Smetana of North Carolina State University.

described in reference 34 and the vehicle's geometry as obtained from Piper shop drawings. Performance predictions were also made using, in these instances, the programs described in reference 30.

LIFT AND DRAG PREDICTIONS

Wing

The ATLIT airplane employs a straight, tapered wing with a GA(W)-1 airfoil section 17-percent thick. The computational technique distributes 65 regions of constant vorticity on the surface of the airfoil, calculates from this an inviscid flow field and pressure distribution, then determines the boundary layer growth corresponding to this pressure distribution, and recomputes the inviscid flow field of a pseudo airfoil whose ordinates are now the physical airfoil ordinates plus the local values of δ^* with a modification so as to locate the trailing edge stagnation point downstream in the wake. This process goes through four iterations so that the computed pressure distribution obtained after the last potential (inviscid) solution is essentially the same as that used to generate the boundary layer solution which formed the basis for that potential solution. The program gives section lift, drag, and moment. The drag includes both skin friction drag and form drag. However, because of the flow model used, extensive regions of flow separation cannot be treated. For this reason, the data are unreliable above $C_L = 0.8$.

The outputs (lift, drag, and moment vs. α for a given Reynolds number) from the airfoil program are fed into a curve fitting routine which provides polynomial representations of the results for use by the wing program. This program uses lifting line theory to modify the local

angle of attack which the airfoil data "sees" according to spanwise changes in twist, camber, thickness, and chord length. Spanwise variations in Reynolds number are handled by providing as input tip and root data at the correct Reynolds number with the program interpolating to obtain the data for other spanwise stations. Inviscid wing-fuselage interference is treated by transforming the fuselage mathematically into a vertical slit and distributing its effects along the span. The output of the program is the three-dimensional lift, drag, and pitching moment of the wing. Note that the drag includes both profile and induced drags.

The same procedure is employed to find the contributions of the tail surfaces to the overall aircraft lift, drag, and moment. The vertical tail was considered to be half of a symmetric surface unaffected by the presence of the horizontal tail. The horizontal tail was assumed to be unaffected by the presence of the vertical tail, propeller slipstream, or the downwash of the wing.

Fuselage and Nacelles

The program to compute the forces and moments on isolated, quasi-streamlined bodies having a plane of symmetry represents the half surface by 560 flat panels of more or less equal area. On each panel is distributed a uniform source whose strength is such that the flow due to all sources is everywhere parallel to the surface. Then, a streamline which goes through the centroid of a particular panel is traced upstream to its inception point. Along this streamline is calculated the boundary-layer displacement thickness and skin friction by a momentum integral method. This is done for all 560 panels. At the downstream end of the body, the wake is arbitrarily assumed to begin at the upstream end of the

last two sets of panels. The angle of the wake leaving the body is determined by the history of the boundary layer displacement up to that point. This wake is then paneled to a stagnation point downstream in the physical wake and the inviscid pressure distribution on the body plus wake body recomputed. The calculated skin friction is integrated over the body to find the skin friction drag and the recomputed pressure distribution is integrated in the normal and axial directions to find the lift and form drag. The same data are also used in computing the pitching moment.

Because the boundary layer routine used is two-dimensional, it is not valid when the flow is expanding or contracting rapidly, i.e., near the nose or tail of a body, or when there is a significant cross flow, i.e., at angle of attack. For this reason, the aircraft drag computation is reasonable only in the cruise configuration. In the context of an overall drag computation, this is not unduly limiting because the wing-drag calculation fails for high angles of attack as well. Several attempts were made to extend the angle-of-attack range of the computation, at least for axisymmetric bodies, by using an axisymmetric finite difference boundary layer routine in the plane of symmetry in order to locate the lee-side separation point and then applying the Allen-Perkins (reference 35) technique to determine the normal force. However, the computed separation point was not regularly located sufficiently close to physical separation point (as found experimentally) to make this approach viable.

Of course, modeling fuselages and nacelles for the purposes of drag computation as isolated bodies ignores interference effects. While it is

conceivable that the inviscid aspects of interference could be treated adequately (and, in fact, have been in many cases), it will require a general three-dimensional boundary layer solution to treat the viscous aspects adequately. Since such solution techniques will be some time in coming, it continues to be necessary to treat these effects empirically. Because other approximations in the model can be expected to yield uncertainties of the same order of magnitude, no attempt was made to account for these effects.

Protuberances

No accounting for the drag due to protuberances was made in the drag buildup. In general, it is difficult to predict the geometry and location of miscellaneous protuberances during preliminary design. The drag due to these protuberances can be significant.

Trim Drag

The trim drag estimates shown in table 5.6 account only for the drag of the horizontal tail which is flying at the lift coefficient required to trim the wing-body pitching moment. As pointed out by Mr. R. T. Taylor (NASA-LaRC), no account has been made of the additional trim drag due to the fact that, with the additional trim lift of the horizontal tail, the wing must fly at a new (increased) angle of attack. Thus, total airplane longitudinal trim drag includes increased wing drag as well as the horizontal tail drag.

TABLE 5.6

ATLIT DRAG BUILDUP

C.G. @ 26.5% MAC

α_{wing} (deg)	$C_{L_{wing}}$	TRIM $C_{L_t} S_{t/S_w}$	$C_{D_t} S_{t/S_w}$	C_{D_w}	$C_{D_{TOTAL}}$	C_L
-4	-.134569	-.003474	.001879	.007316	.038473	-.138043
-2	.063437	.001638	.001852	.006045	.037175	.065075
0	.259752	.006707	.0019772	.008349	.039604	.266459
2	.454464	.011736	.00200	.014132	.04541	.4662
4	.648280	.016741	.00210	.023051	.054429	.66502
6	.841217	.021724	.002184	.034891	.066353	.86294
8	1.032682	.02666	.002265	.049506	.081049	1.05934
10	1.221700	.031549	.002346	.066789	.098413	1.24324
12	1.405880	.036306	.002424	.086509	.118211	1.442
14	1.582697	.040872	.002618	.108327	.140223	1.6235

$$C_{D_{TOTAL}} = C_{D_w} + C_{D_t} S_{t/S_w} + C_{D_{t_v}} S_{v/S_w} + C_{D_{fus}} + 2\, C_{D_{NACELLE}}$$

$$= C_{D_w} + C_{D_t} S_{t/S_w} + .0018487 + .01299 + 2(.00722)$$

$$= C_{D_w} + C_{D_t} S_{t/S_w} + .0292787$$

$$C_L = C_{L_w} + C_{L_t} S_{t/S_w}$$

Calculated and Estimated Lift-Drag Polar

As shown in table 5.6, summing the results of the previous calculations yields a drag polar represented by the equation

$$C_D = 0.0358 + 0.04056\ C_L^{1.94} \tag{5.16}$$

This polar, as indicated previously, does not include the effects of flow separations at the higher lift coefficients. In an effort to develop a more accurate polar upon which to base performance estimates, full-scale wind-tunnel test data on a similar aircraft (reference 36) were examined and fitted by the equation

$$C_D = 0.035 + 0.051\ C_L^{2} + 0.00138\ C_L^{13.42} \tag{5.17}$$

Plots of these equations are shown in figure 5.12. Note that the two curves differ little for $C_L < 0.8$. Above $C_L = 0.8$ it is to be expected that equation (5.17) will more nearly represent the behavior of the ATLIT than equation (5.16). Despite the fact that equation (5.16) describes the drag of an unpowered airplane and that drag under some conditions of powered flight may exceed the drag in unpowered flight, equations (5.16) and (5.17) were treated as the probable boundaries for the actual ATLIT drag polar. Because of the relatively smaller ATLIT wing area (compared with the aircraft tested in reference 36) it is not expected that the ATLIT drag will rise as rapidly with increasing C_L as it does for the aircraft of reference 36. Thus, even if the ATLIT drag in powered flight is somewhat greater than in unpowered flight, the drag should be below the boundary given by equation (5.17).

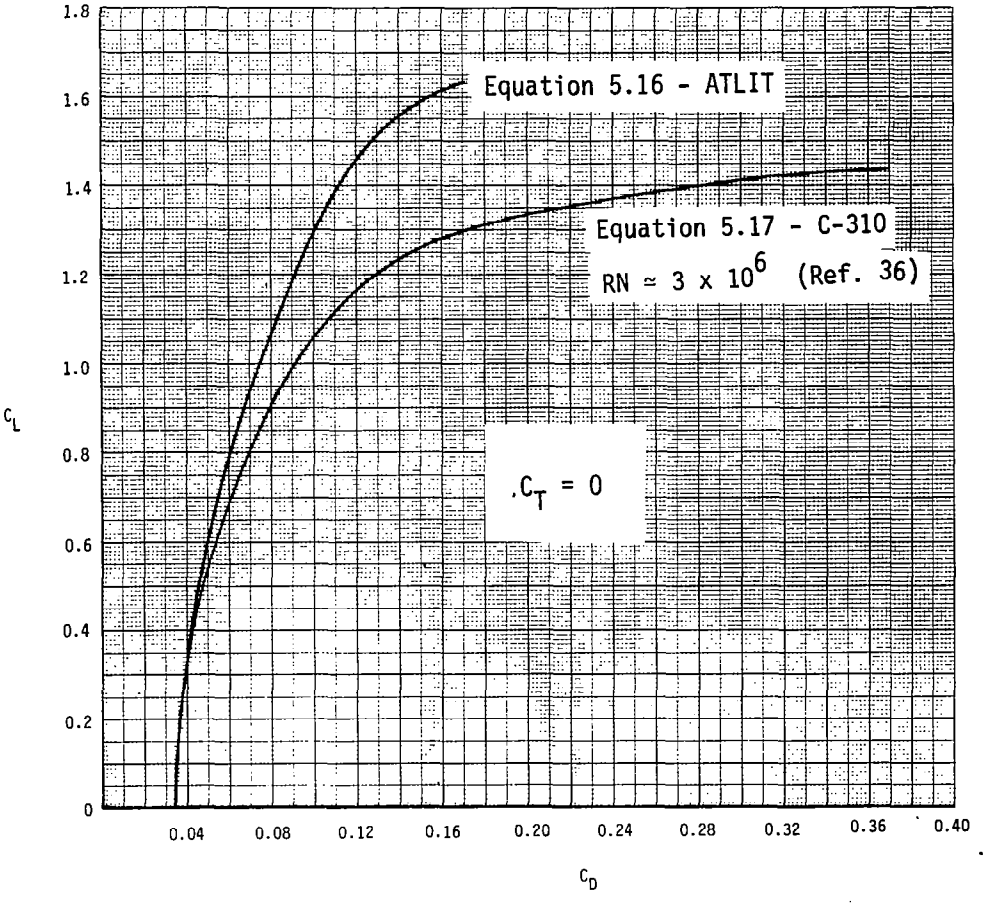

Figure 5.12- Predicted ATLIT drag polar (method B) and wind-tunnel measured light-twin drag polar, (Reference 36).

PERFORMANCE PREDICTIONS

The drag polars given by equations (5.16) and (5.17) were submitted to the point-performance program described in reference 30 along with the thrust horsepower data given in figure 5.13. The latter were derived from engine test-cell data and propeller-performance charts. They do not include any installation-dependent effects. The data given in columns (4) and (5) in table 5.4 represent the output of this program. It will be noted that, compared with the original Seneca, only small improvements in rate-of-climb and cruise speed are expected. This can be explained by the fact that although the airfoil itself offers about a 10-percent improvement in L/D at $C_L = 0.8$ (the nominal C_L for the climb) the wing is responsible for only about 40 percent of the total drag. Overall aircraft drag is, as a result, only about 4 percent lower.

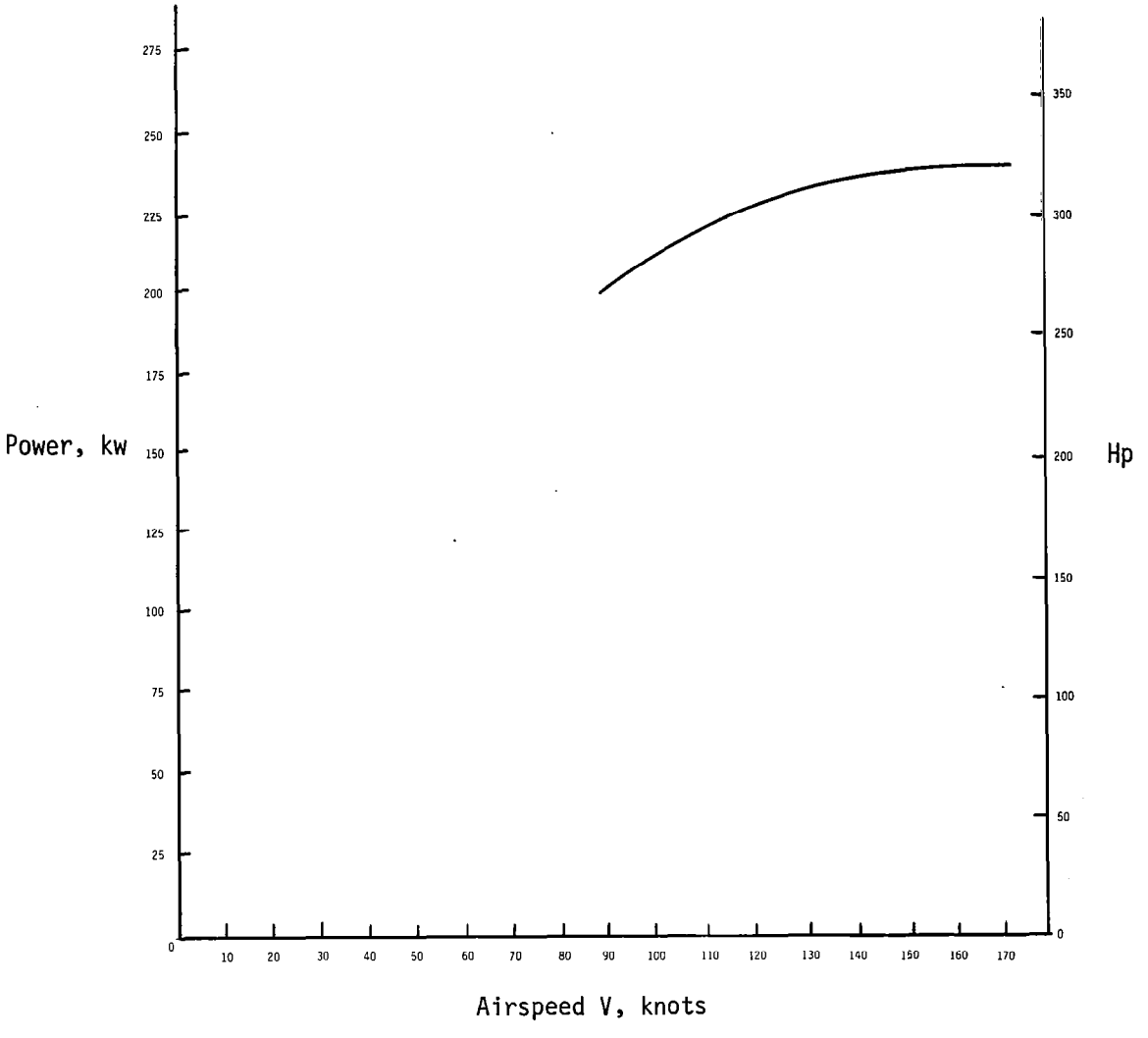

Figure 5.13- Assumed thrust power available for performance prediction by method B.

5.4.1.3 Method C: Lift, Drag, and Performance Predictions*

The airplane lift, drag, and performance predictions presented here are based on the method of reference 29. The drag characteristics of the fuselage, nacelles, and empennage were borrowed from the predictions of Method B. The prediction of airplane lift and drag essentially consists of the following procedure. With a known geometric angle of attack, lift data at the α, RN, and M are obtained from tables of 2-D, section characteristics. The initial spanwise load distribution is then calculated, followed by a determination of the (spanwise) induced angles of attack. With these induced angles of attack, a new spanwise load distribution is computed. With a satisfactory span loading determined, the 3-D aerodynamic coefficients are computed (C_L, C_{D_i}, C_{D_o}).

The section characteristics for the NACA 65_2-415 and the GA(W)-1 airfoils were used to predict wing lift and drag (with nonlinear effects) for the standard Seneca and ATLIT. The airplane lift and drag predictions are given in figures 5.14 and 5.15.

The predictions of airplane performance were made assuming available shaft power = 298 kw (400 BHP). Propulsive efficiency was estimated in Method B. The calculated curves for thrust power required and available appear in figure 5.16.

---

*The contributions of Mr. Robert T. Taylor (NASA-LRC) in preparing materials for this chapter are gratefully acknowledged.

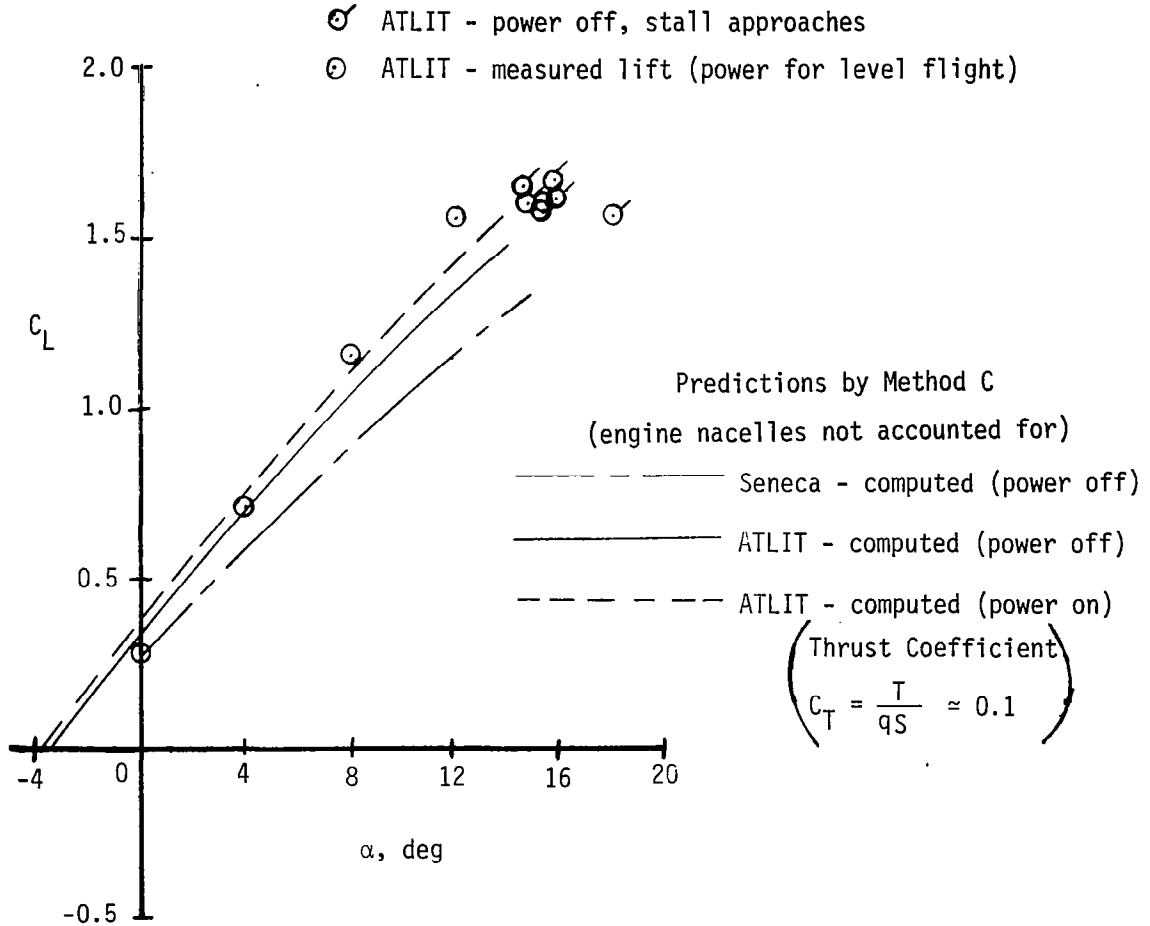

Figure 5.14- Comparison of measured and predicted lift characteristics for ATLIT and the Seneca.

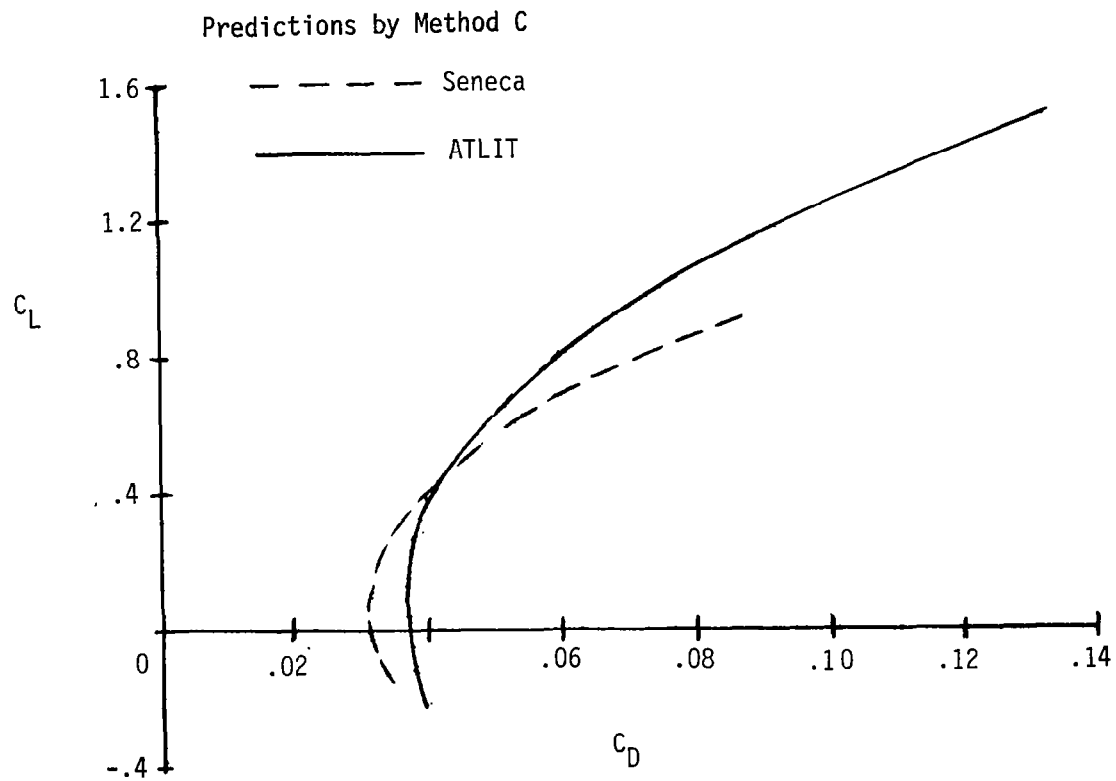

Figure 5.15- ATLIT and Seneca predicted airplane drag-polar comparison (ideal skin friction, 2-D profile drag used with standard roughness).

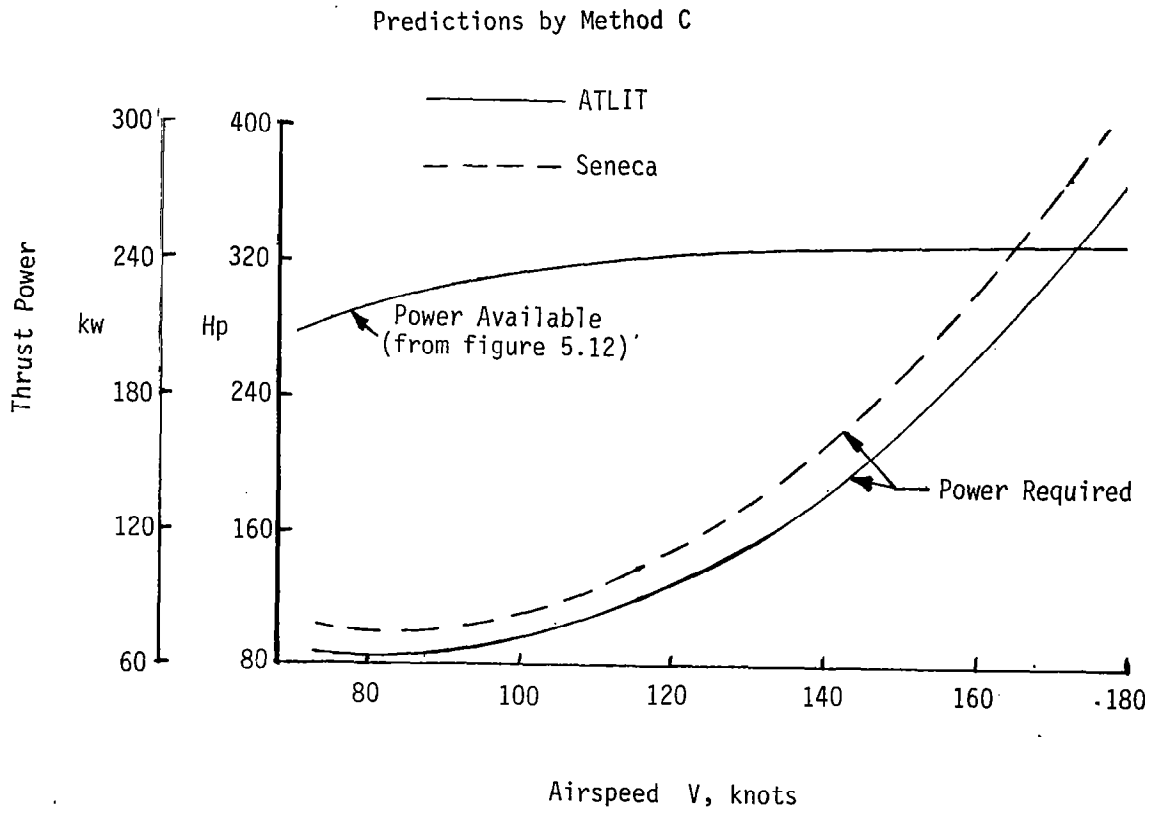

Figure 5.16- Comparison of predicted power required for ATLIT and the standard Seneca.

With the assumptions above, the Seneca and ATLIT performance predictions were computed and are shown in columns (6) and (7) of Table 5.4. Without detailed knowledge of the propulsive efficiencies involved, the primary value of computations such as these is for making comparisons. A comparison of column (6) with column (7) shows predicted increases of 9 knots in top speed and 18 m/min (60 fpm) in best single-engine rate of climb. The expected ATLIT performance would then be determined by adding these increments to the basic Seneca performance figures.

5.4.2 Methods, Data Reduction, and Flight-Test Results*

Speed-Power Relationship

The variation of shaft horsepower with airspeed was obtained by nominally flying the aircraft at constant altitude and airspeed, and recording aircraft data with the onboard measurement system. Data were averaged over a portion of the record and represent from 200 to 400 data points. Measured engine RPM and manifold pressure and free-air temperature were used with the power-altitude charts of reference 39. These charts are for horsepower with the engine leaned for maximum power. Since the flight tests were made at a rich engine mixture setting, a reduction to rich engine power was made using data from reference 40. The resulting value is the brake horsepower of the engine. However, since the horsepower delivered to the propeller is required to establish the ATLIT performance, the power required to drive the engine accessories (alternator, vacuum pump, tachometer, propeller governor and fuel pump) as given in reference 39 was subtracted from the engine brake horsepower.

Figure 5.17 presents the variation of horsepower and velocity corrected to standard weight and sea level conditions for the ATLIT in various test configurations. The basic data points are early measurements with the flaps sealed to prevent airflow through the spoilers at a flap setting of 0^{o}. Subsequently, a region of flow separation on the fuselage and the adjoining wing trailing edge was found to exist. Data obtained during the final phase of flight tests which resolved the flow separation problem are also plotted on figure 5.17. The aircraft had two fuselage and four wing vortex

*The contributions of Mr. Joseph H. Judd (NASA-LaRC) in preparing materials for this chapter are gratefully acknowledged.

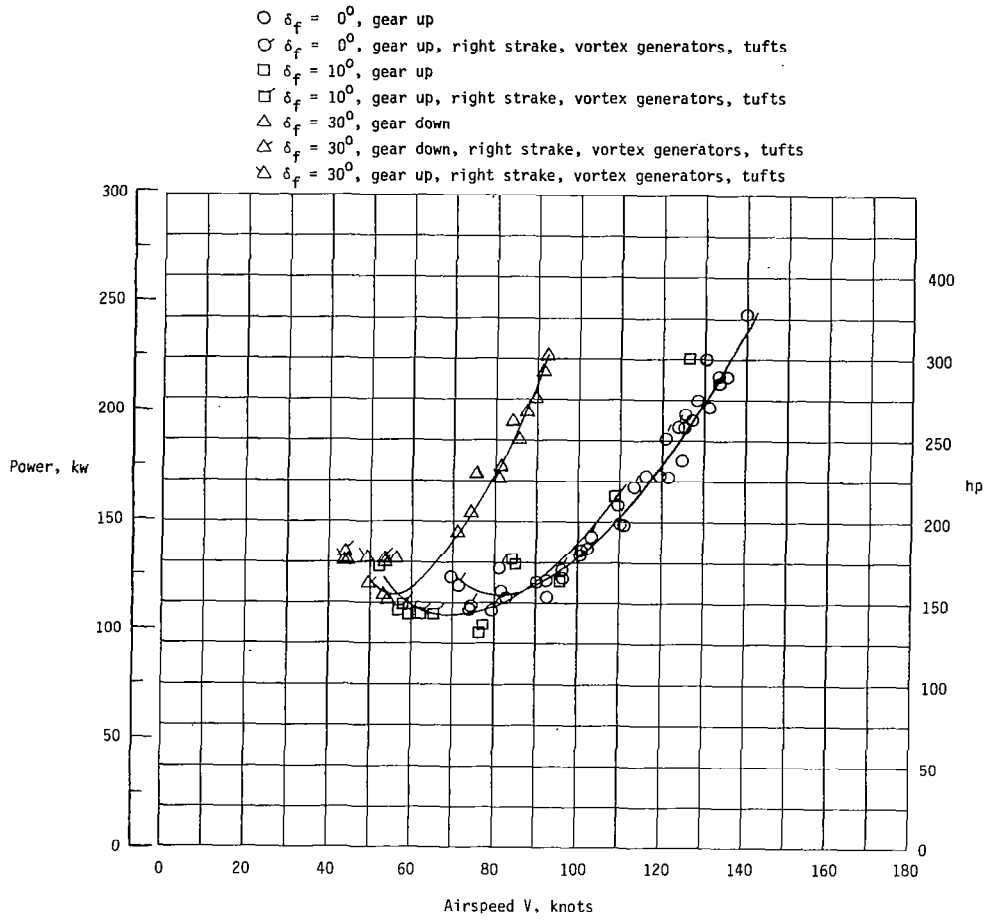

Figure 5.17- Variation of shaft power with airspeed (δ_f = 0°, 10°, 30°).

generators, a leading edge extension (strake) at the right wing/ fuselage intersection (see figure 5.1) and tufts on the fuselage, wing, and nacelles. At higher airspeeds (flaps 0^{o} and gear up), an increase in power required due to these devices is evident. A large portion of this drag increase is caused by the tufts. The data on figure 5.17 shows scatter which is attributable to horsepower variations. The procedure for obtaining horsepower from charts using manifold pressure and RPM is estimated to give values within $\pm$ 2 horsepower which falls within the scatter band. Since most of the flights were made between 1000 and 1600 hours, the more likely cause of the variations is a larger scale atmospheric motion, i.e., data runs were made in slightly rising or sinking air. Although altitudes were sought for data runs that did not have turbulence (as determined by pilot observation of airplane response to external disturbances), large scale atmospheric disturbances (long waves) would not be easily detected.

Aerodynamic Coefficients

The lift coefficients obtained during these runs were computed using average values of measured atmospheric conditions and flight-path angles and a faired value for aircraft weight. The angle of attack and static pressure were corrected for position errors as described in chapter 5.1. The variation of power-on lift coefficient with angle of attack is shown in figure 5.18. The increase in lift coefficient caused by improving wing-fuselage juncture flow is apparent on these figures. Although stall is not shown on these figures, the stall lift coefficient is very little higher than the highest C_L shown.

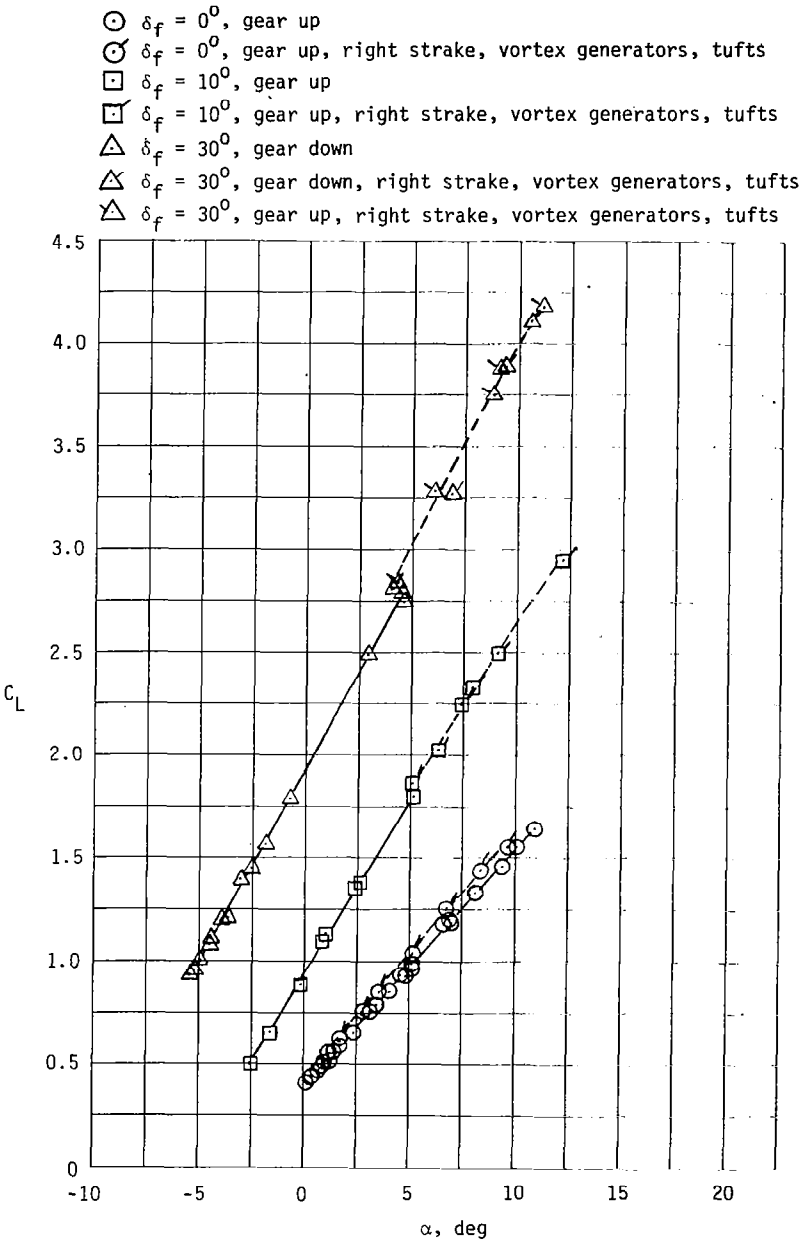

Figure 5.18- ATLIT lift characteristics (power for level flight; $\delta_f = 0^o$, 10^o, 30^o).

The power-on drag of the ATLIT in steady level flight is primarily determined by the force developed by the propeller in the direction of flight. This force is proportional to the propeller shaft horsepower, propeller efficiency, the propeller installation efficiency, and a function of the rotation of the propeller force vector. An estimate of the propeller efficiency was obtained from the Hartzell Corporation, and a computation using the Borst method (ref. 41) was found to agree with this estimate. The flow field of the nacelle affects the efficiency of the propeller. If the propeller is operating in a reduced velocity field -- say in front of a bluff body -- the apparent propeller efficiency is greater than that of the isolated propeller; conversely, if the spinner-nacelle geometrically acts to put the propeller in an increased velocity region, the apparent efficiency is less than that of the propeller. Since the horizontally-opposed engine nacelle combines both factors, an installation efficiency of 96 percent was estimated using data presented in reference 42. Experimental data on propulsive efficiency of a wing-nacelle-propeller installation as a function of angle of attack and propeller location is presented in references 43 and 44. An empirical relationship $(1 - \sin^2 \alpha_{te})$ was found to provide a good correlation for the variation of propulsive efficiency with angle of attack. Physically, this involves rotating the thrust vector so that the propeller slipstream leaves parallel to the mean chord line at the trailing edge and subtracting the drag component of the thrust vector from the propeller thrust. The expression for the drag coefficient then becomes

$$C_D = \frac{(SP)\eta_p\eta_i\left[1 - \sin^2(\alpha + \alpha_{te})\right] \times \text{Const}}{qSV} \qquad (5.18)$$

where SP is shaft power. It is estimated that uncertainties in these estimates influence the drag coefficients to ± 5 percent over the range of test conditions.

The variation of lift coefficient with drag coefficient is shown in figure 5.19. The scatter in the data is primarily due to the scatter in measured brake engine power. Note that the calculated drag coefficient includes the trim drag and some portion of the drag due to power effects.

The variation of C_L^2 with C_D is shown on figure 5.20. The curves are apparently nonlinear. The nonlinearity is attributed to the effect of power. The variation of C_L with C_D due to aerodynamic effects is an exponential function of C_L whereas the variation of the lift due to power will be a trigonometric function. The zero-lift drag coefficient of 0.045 for flaps at 0^o was obtained by extrapolating the data of figure 5.20 to $C_L = 0$. This compares to the estimated value of 0.0358 from table 5.6 at a center of gravity location at 26.5 percent mean aerodynamic chord, whereas the measured values are for an aircraft center of gravity between 15 and 13 percent mean aerodynamic chord. Further, the effect of protuberances was neglected in the estimate. A rough check was made to find the order of magnitude of the protuberance increment using data from reference 45. The estimated equivalent flat plate area of the ATLIT was 0.516 m^2 (5.549 square feet), and the equivalent flat plate area of 22 obvious

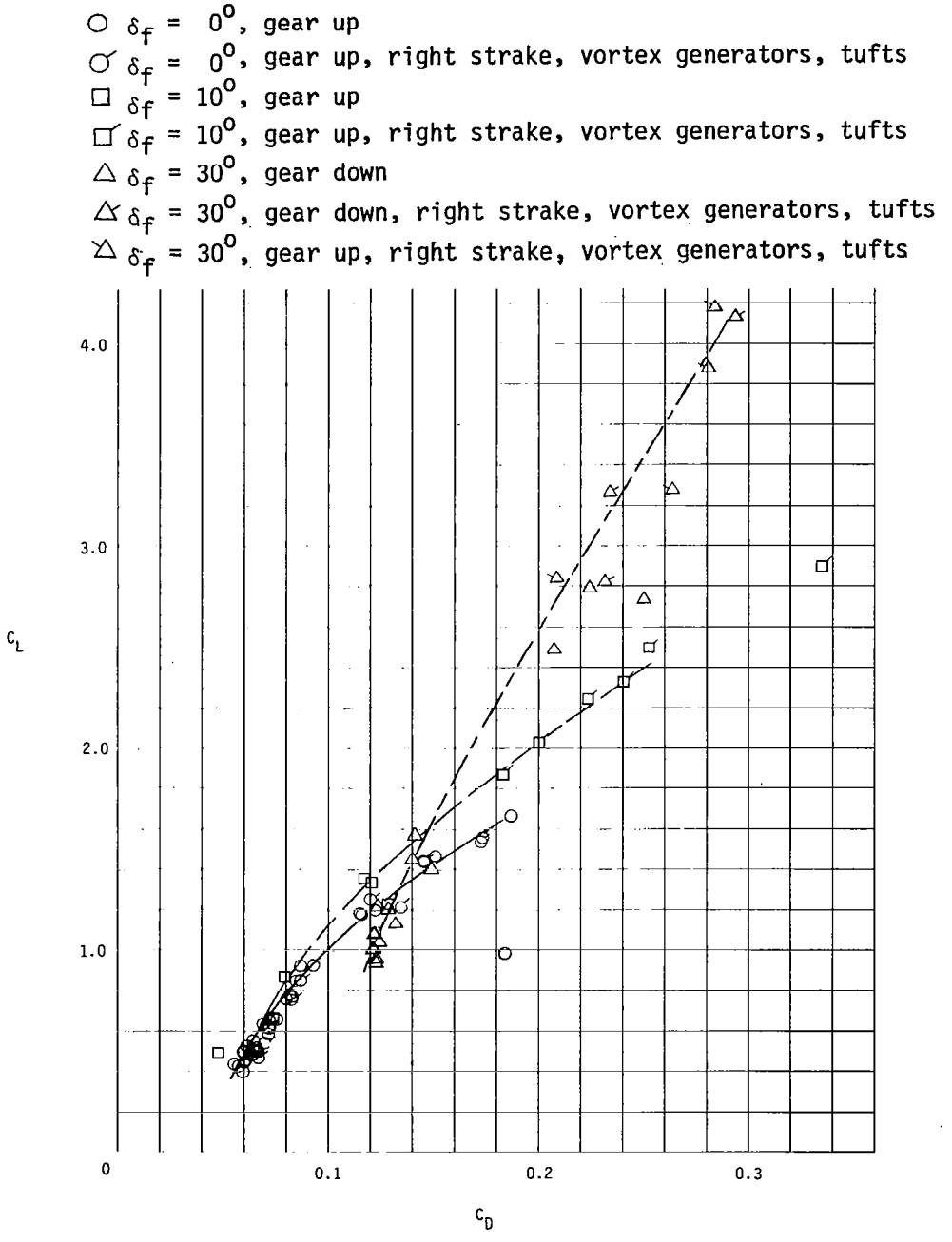

Figure 5.19- Power-on, trimmed drag polars for ATLIT (δ_f = 0°, 10°, 30°).

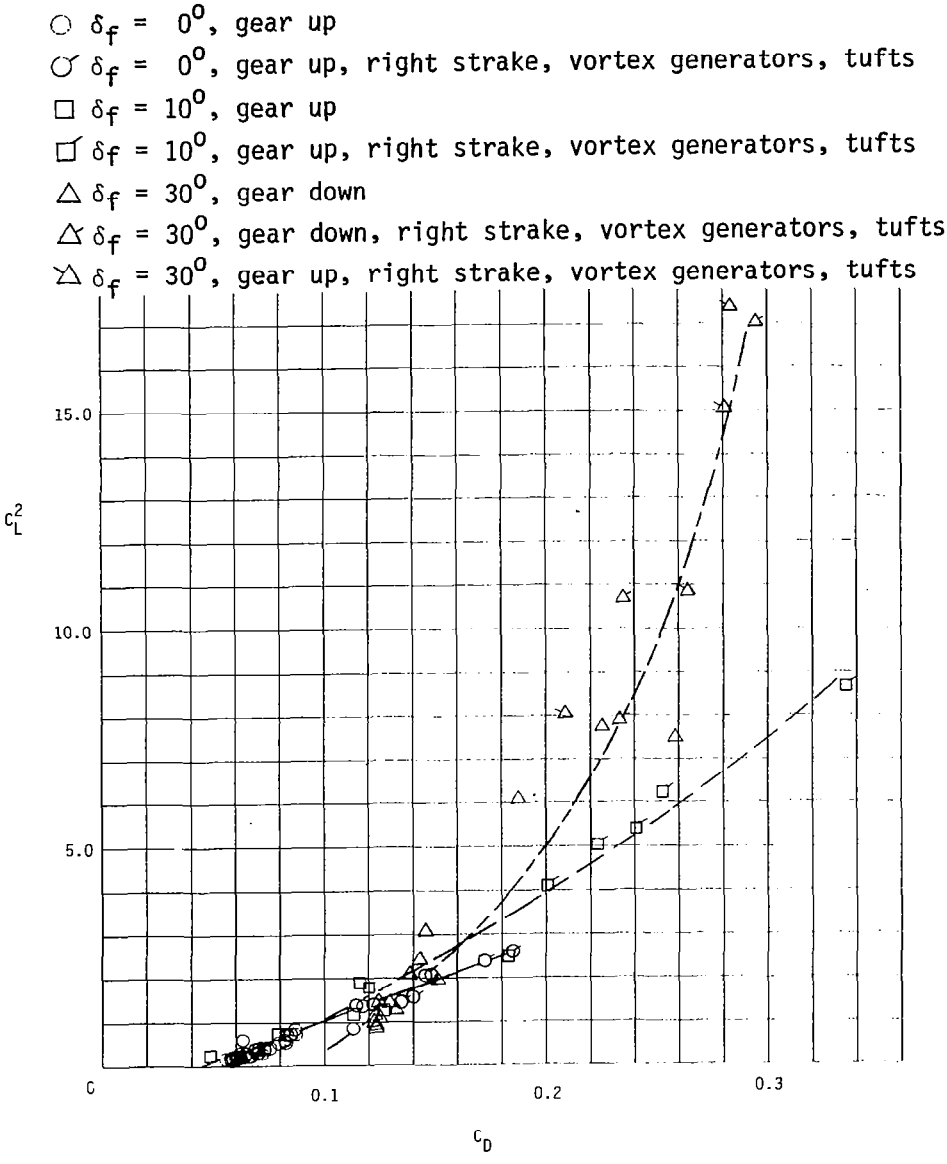

Figure 5.20- Linearized, power-on drag polar for ATLIT, (δ_f = 0°, 10°, 30°).

items was 0.055 m^2 (0.592 square feet) for a total of 0.570 m^2 (6.14 square feet). This compares with the value from measured data of 0.648 m^2 (6.975 square feet). Since power effects were also neglected in the estimate and would bring estimated and measured data closer together, it may be concluded that the method for estimating baseline configuration drag by Method B is acceptable. However, performance measurements based on these values will be optimistic.

The variation of $C_L^{3/2}/C_D$ with C_L is shown in figure 5.21. The measured value of 11.75 for the flaps-up condition compares with estimated values of 12.3 for the Piper Seneca and 12.5 for the worst case ATLIT from table 5.5. Removal of the tufts from the ATLIT is expected to raise this value.

Rate of Climb

Measured climb data are presented in figure 5.22 for single- and multi-engine flight. The multi-engine data are average values at 610 m altitude (2000 ft.) and at an average aircraft weight of 1860 kg (4100 lb.). The aircraft had a single strake on the right wing, vortex generators on the wing and fuselage, and tufts on the fuselage, wings and nacelles. Cowl flaps were closed for the multi-engine climb. The figure shows that changes in rate of climb are quite small for variations of airspeed from that for best rate of climb (approximately 91 knots). Pilot A noted in chapter 5.5.1 that this climb stability is a desirable airplane characteristic. The best rate of climb for the Seneca I is 390 m/min (1280 ft/min) at the test conditions noted above, and is about the same as that measured for the ATLIT.

○ δ_f = 0°, gear up

◔ δ_f = 0°, gear up, right strake, vortex generators, tufts

□ δ_f = 10°, gear up

◪ δ_f = 10°, gear up, right strake, vortex generators, tufts

△ δ_f = 30°, gear down

◭ δ_f = 30°, gear down, right strake, vortex generators, tufts

◬ δ_f = 30°, gear up, right strake, vortex generators, tufts

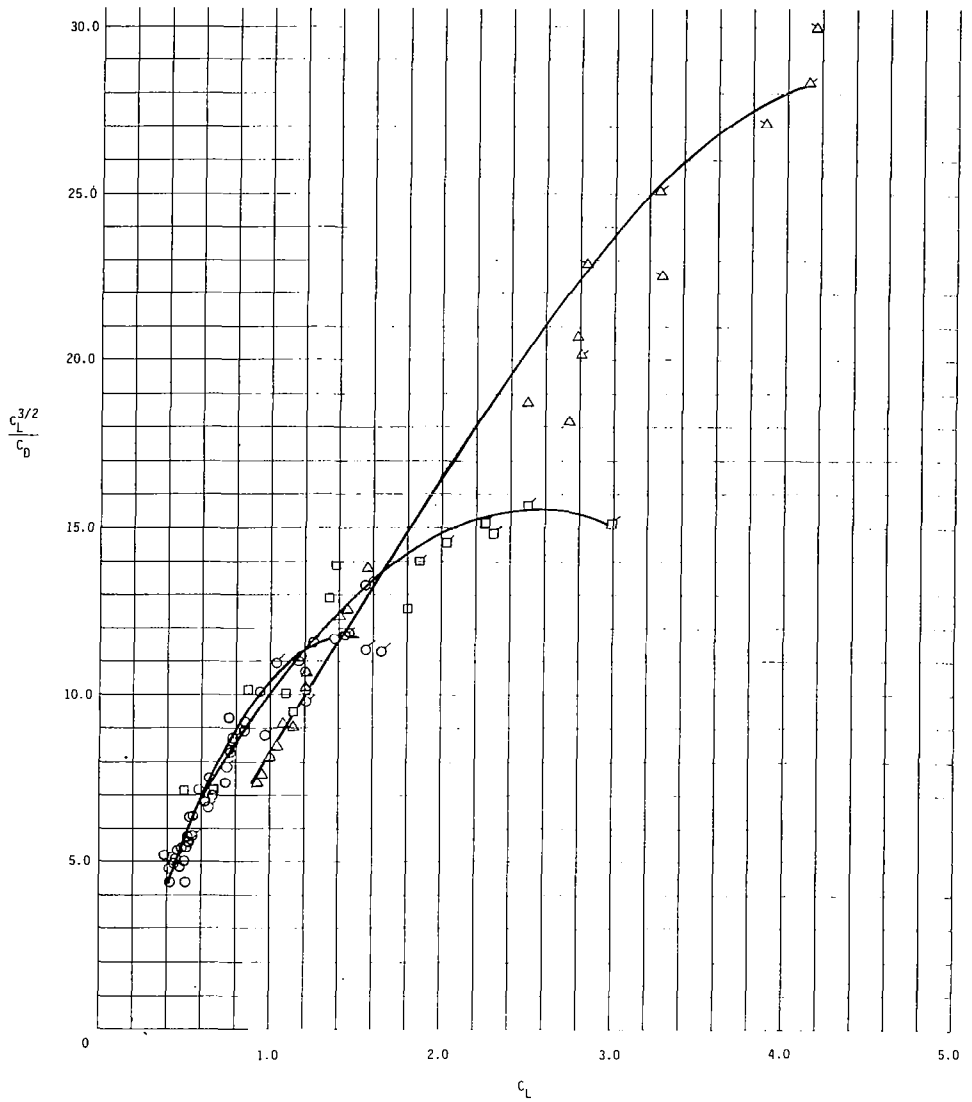

Figure 5.21- Variation of $(C_L^{3/2}/C_D)$ with lift coefficient for ATLIT (δ_f = 0°, 10°, 30°).

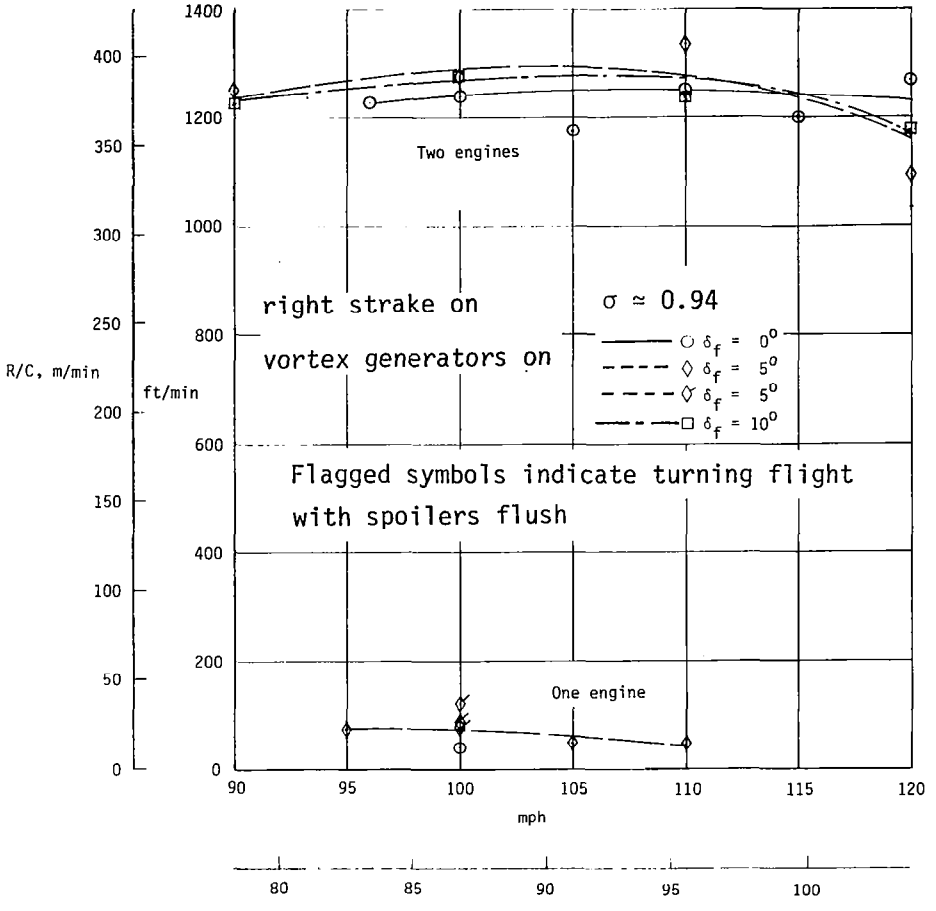

Figure 5.22.- Variation of rate-of-climb with airspeed; single-engine and multi-engine (W = 17.8 N to 18.2 N (4 000 to 4 100 lbs) and $\delta_f = 0^o, 5^o, 10^o$).

Single-engine rate of climb at 610 m altitude (2000 ft) was obtained at an average weight of 1814 kg (4000 lb) with the airplane configuration as described above. The operating engine cowl flaps were open, while the inoperative engine cowl flaps were closed. The ATLIT has no roll trim capability, and straight flight can only be obtained by using spoilers on the side with the operating engine. To find the penalty involved, the spoilers were set approximately neutral, and the airplane was allowed to climb in slowly circling flight. A significant increase in rate of climb occurred at 100 kts airspeed. It is postulated that most of this increase can be retained by use of trim ailerons outboard of the flaps.

5.5 Pilot Descriptions of Stability and Handling Qualities*

Two separate pilot evaluations of ATLIT are presented in this chapter. Both pilots discuss longitudinal and lateral stability and control characteristics throughout the airplane flight envelope.

Care should be exercised by the reader in interpreting the ATLIT pilot ratings for roll-control tasks. The rigging of the spoilers on ATLIT (either down or flush, as described in chapter 3.2.2) strongly influences the lateral control feel characteristics of this airplane. The purpose in rigging the spoilers symmetrically down into the wing was to investigate performance penalties due to spoiler float above the wing. Without exception, the pilots reported that the re-rigging greatly degraded the lateral handling qualities. The performance changes due to re-rigging were negligible. The pilot comments which follow apply to the airplane with the spoilers rigging symmetrically down into the wing. Therefore, the pilot ratings, in some cases, are excessively harsh compared to what they would have been had the airplane been rated with the spoilers rigged statically flush (allowing some float at a negligible performance penalty).

5.5.1 Pilot A Comments on ATLIT Flying Qualities

Cruise Stability

	Cooper-Harper Ratings (see table 5.7)
Spiral	- 4
Longitudinal	- 3

During cruise, it is impossible to fly the ATLIT without constantly controlling the aircraft. Small upsets from rough air cause the pilot

*The contributions of NASA-LaRC research pilots Mr. Robert A. Champine and Mr. Philip W. Brown in preparing the materials in this chapter are gratefully acknowledged.

to make corrections in roll and pitch. The spiral stability is weak and the spoiler friction is very high, about 44 N (10 pounds) wheel force. Since there is no lateral trim control surface, the rudder trim tab must be used. Thus, rolling moment due to sideslip is used to trim laterally. This lateral trimming procedure may be described as follows. The pilot must first look at the wheel or spoilers to be sure they are down flush. Then the rudder is moved to maintain the wings level and the rudder trim tab is used to reduce the rudder forces to zero. The rudder trim tab has a great deal of friction, and along with considerable rudder friction, the trimming task is difficult at best.

TABLE 5.7- HANDLING QUALITIES RATING SCALE

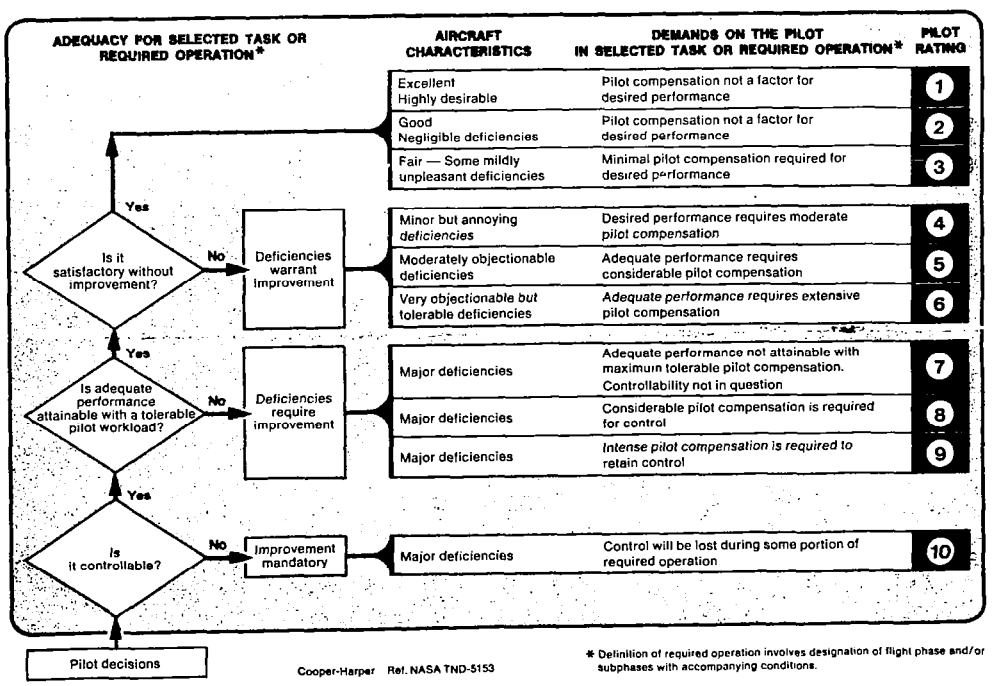

The longitudinal stability in cruise is satisfactory except for a slight friction problem. Altitude control is pretty good in general. The control force is light, the damping is good, and trimming is fairly easy. Also, the phugoid oscillation seems to be of small amplitude and of a fairly long period.

Slow Flight and Stall Characteristics

Cooper-Harper Ratings

Flaps up - 3

Flaps down - 6

Power effects - 2

Flaps Up: Slow Flight and Stall

In general, the ATLIT flys quite well at low speeds, flaps up. The roll control is poor for small (up to 25%) roll control inputs but is satisfactory at higher deflections. There is plenty of pitch control for stalling the wing and also for stall recovery. The rolloff at stall is not too bad, being about 20 degrees of maximum bank. The stall buffet warning is about 5 or 6 mph, which is good.* During the stall, the nose falls through at a modest rate and recovery is quick after lowering the angle of attack and increasing power. Recovery can be effected without losing more than 15 m (50 feet) of altitude. The power-off stalling speed is fairly high, about 70 knots (80 mph); however, if proper operating procedures are adhered to, this presents

*This stall buffet warning disappeared with the addition of the devices for attacking wing-body interference-induced flow separation (i.e., strakes and vortex generators).

no problem. By this it is meant that anytime one wishes to fly at speeds below about 96 knots (110 mph), the flaps should be extended between 5 and 10 degrees to increase the stall margin.

Flaps Down: Slow Flight and Stall

In general, the flaps-down slow-flight characteristics are pretty good. The roll response is good at all speeds, but the roll system friction and force gradient near center are very bad (this is the main reason for poor Cooper-Harper rating). At minimum speeds, particularly with flaps set at 30 or 37½ degrees, the longitudinal stability and damping are very weak. The pitch control is still very responsive. This can lead to some overcontrolling in rough air during landing. During stall recovery, this overcontrolling can also be a problem.

In general, stall characteristics with flaps down are good with little or no rolloff. The spoilers are very effective throughout the stall, and recovery can be made with little loss in altitude. Deep stalls, using full back-pitch control, have not been investigated, and no comment can be made at this time. Stall warning is in the form of airframe shaking; in fact, one can look at the horizontal tail surface and see it shaking up and down about $\pm$ 1.3 cm ($\pm$ 1/2 inch) at the tips. There has been a wing-fuselage separation that buffets the tail and provides about 5 knot warning before the stall. All stall warning seems to be eliminated since the wing-fuselage separation was cleaned up with strakes and vortex generators.

Multi- and Single-Engine Trim with Power Changes

Cooper-Harper Rating

Multi-engine 2
Single-engine 6

Power effects in the ATLIT are very good. The addition of power causes a normal nose-up trim change. The trim system is fully capable of zeroing the forces due to the power-induced trim changes. The control force can be controlled with one hand during a go-round. Since the propellers counter-rotate there is no torque effect.

The single-engine performance is very marginal, and this is the reason for the 6 Cooper rating. At low speeds (below about 96 knots), there is not enough rudder trim authority to trim out rudder forces. At speeds down to 78 knots (90 mph), two feet on one rudder pedal are required. The force is very high. The spoilers are effective in controlling the single-engine forces, but if they are raised more than about 1 cm (3/8 inch), then the additional drag degrades the marginal single-engine climb performance.

Rolling Performance with Spoilers

Maximum Rolling Performance

Cooper-Harper Rating

Flaps up - 3

Flaps down - 2

Lateral Control Feel

Cooper-Harper Rating

Flaps up - 4

Flaps down - 6

The maximum (full wheel deflection) rolling performance with the spoiler control is excellent at all speeds and flap deflections. The rolling velocity is very low when small wheel deflections (up to 25% of total) are used. When 50% of total wheel deflection is used the rolling velocity is more than adequate for most flight conditions. This nonlinearity is mildly unpleasant and is something with which the pilot has to cope. When using small spoiler deflections, there is a small adverse yaw before actual turning flight is started. However, when using more than about 25% deflection proverse yaw results and turning flight starts immediately. These characteristics are very good. These comments apply to all flap conditions.

The lateral control feel forces are poor because of very high friction and a negative centering force gradient up to about 25% deflection. These negative forces, off from center, are greater when the flaps are down. These unacceptable forces need correction, as does the friction level. When the flaps are retracted, the wheel centering forces are nearly zero but the friction is still high.

Crosswind Landings (Sideslip Characteristics)

Cooper-Harper Ratings

Sideslip - 2

Crosswind landings - 6

The sideslip characteristics are good, as the airplane will fly at fairly large sideslip angles. Rudder and spoiler effectiveness are good, and no unusual pitching moments have been noticed.

Crosswind landings are another matter because precise control is required. Usually, crosswind conditions involve gusty and changing directions of the wind. Under these conditions, control of the sideslip angle is difficult and unpleasant. This is due to the nonlinear roll response with small spoiler deflections. Also, the poor force gradient (negative centering) and high friction add to the problem. There is a tendency for overcontrolling due to the low rolling effectiveness at small wheel deflections followed by good roll response at approximately 25-percent deflection of the wheel. Therefore, during gusty wind conditions, the pilot must rapidly move the wheel right and left through ±25 degrees of travel to counter the shifting winds. At best, it can be said that adequate control is available, but a very high skill level is required to make a good crosswind landing during gusty wind conditions.

Instrument Approaches

No ILS-type instrument approaches have been made by this pilot and comment is only conjecture. Control of the aircraft on the ILS approach would be unsatisfactory because of roll-control friction, poor centering forces in roll, lack of trim in roll, and nonlinear roll response. These items have been discussed above.

The reader should note that the poor Cooper ratings for lateral feel characteristics apply to the ATLIT with the spoilers rigged symmetrically down below the wing surface, as described in chapter 3.2.2. This rigging not only worsened the roll response for small wheel deflections (i.e., it takes more wheel deflection to raise the spoiler to a positive deflection),

but the wheel forces also became more wheel decentering. The pilot agrees that with the spoilers rigged in the flush position, the poor Cooper-Harper ratings would improve by about two grades.

5.5.2 Pilot B Comments on ATLIT Flying Qualities

The purpose of this report is to give a qualitative assessment of the ATLIT's handling qualities and to assign Cooper-Harper pilot ratings for a variety of tasks.

The quantitative measures used were taken from panel instruments or instrumentation package "quick-look" records. Though only approximate values, their inclusion is justified to better define the characteristics discussed.

Unless otherwise noted, this report refers to the ATLIT's current configuration of vortex generators, leading edge strakes, taped protuberances, and clay and balsa-filled recesses. The average weight and C.G. are 18.2 N (4100 lb) and 15.5% mac, respectively.

The following configurations and flight conditions were examined:

Configurations or maneuver	Landing gear position	Flap position	V trim IAS, kts	Power
Cruise	Up	0^{o}	139	α = 0
Approach	Up	30^{o}	65	α = 0; idle
Stall	Up	0^{o}	80	α = 0; idle
	Up	10^{o}	58	α = 0; idle
	Up	20^{o}	54	α = 0; idle
	Up	30^{o}	54	α = 0; idle
	Up	37^{o}	54	α = 0; idle
Precision heading, vertical S patterns (cruise)	Up	0^{o}	104	152 m/min (500 fpm) climbs and descents
Landing	Down	30^{o}	65	Idle

CONTROL SYSTEM CHARACTERISTICS

The longitudinal control system utilizes some mass imbalance but no downspring. An anti-servo stabilator tab is used for force tailoring and trimming. The spoiler system utilizes springs to provide a centering tendency. There is no lateral trim system. Rudder force tailoring and trimming are provided by an anti-servo tab.

Friction + breakout forces

	Cruise	Approach
Longitudinal wheel force F_{W_x}	21 N (4.75 lb)	24 N (5.5 lb)
Lateral wheel force F_{W_y}	53 N (12 lb)	36 N (8 lb)

Control Centering

1. Cruise.- The control wheel will quickly return to 30 to 40 percent of the longitudinal-control input necessary for a 1.5 g pulse. Then, in 5 to 8 seconds, the wheel will creep slowly back toward trim another 10 percent of the input amplitude.

Lateral centering is also poor. For wheel deflections of less than 25 to 30 degrees, there is no centering tendency; large deflections will return to this 25- to 30-degree position when the wheel is freed.

2. Approach.- $-\Delta F_{W_x}/\Delta\delta_{STAB}$ appears to be lower here than in the cruise case. Centering is correspondingly worse.

Lateral control centering tendencies are nonexistent. In fact, there is a range of motion on either side of the control wheel centered position, out to $\pm 20^{o}$ of wheel rotation, where $\Delta F_{W_y}/\Delta\delta_s < 0$. The control wheel will not actually decenter when freed, however, because of the high level of friction present in the control system.

Control Raps

Longitudinal control wheel raps resulted in one small amplitude overshoot of the final control position. There was no separately distinguishable aircraft response to this small overshoot.

Control Surface Trimming

The longitudinal electric trim is a little slower than desirable. Manual rudder trim is quite satisfactory. The lack of a lateral-trim system is considered unsatisfactory because of the necessity to deflect the spoilers, sideslip the aircraft, or use differential power to effect lateral trim.

LONGITUDINAL CHARACTERISTICS

Static

Both the wheel position and wheel force versus speed relationships indicate that positive stick-fixed and stick-free longitudinal static stability exist. The force-speed gradient is shallower in the approach

than in the cruise configuration. The high-control system friction results in a wide trim-speed band. Typical figures are given below:

	Cruise	Approach
Trim speed band, IAS	139 - 135 kts	70 - 54 kts

Power effects were noted at 104 KIAS, gear and flaps retracted; to maintain airspeed from a level-flight power setting to a full-throttle climb required F_{W_x} = 27 - 31 N (6 - 7 lb).

Dynamic

	Cruise	Approach
$\zeta_{phugoid}$	0.1	0.35

Short period behavior in cruise was sufficiently high frequency and well damped enough to allow accurate tracking in pitch. The approach-configuration short period was not quite so good; attempts to reset θ in a step-like fashion resulted in a one-half cycle overshoot of the desired value.

Maneuvering

Control wheel position and force versus a_z indicated apparently positive stick fixed and stick free maneuvering stabilities. The influence of mass balance in the control system on wheel forces is unknown.

Sinusoidal stabilator inputs across a wide frequency range showed no tendency to develop pilot-induced oscillations.

LATERAL-DIRECTIONAL CHARACTERISTICS

Static

Dihedral effect is moderately positive in both the cruise and approach configurations. Steady heading sideslips showed the stability derivatives involved to have conventional signs. In the approach configuration, a maximum steady heading sideslip maneuver resulted in the following values:

$\beta = 16.3^{o}$

$\phi \simeq 4^{o}$

$\delta_{wheel} \simeq 30^{o}$

Dynamic

Spiral.- Spoilers and rudder were held fixed while checking this mode and the stabilator was used as necessary to maintain airspeed. Lateral movement of a weight within the cabin upset and then reset the ATLIT's rolling moment equilibrium.

The spiral mode is neutral in cruise. In the approach configuration, time to double amplitude is about 8 seconds.

Dutch Roll.

	Cruise	Approach
$\phi/_{\beta}$	0.75	0.90
$\zeta_{D.R.}$	0.16	0.16

STALL BEHAVIOR

Investigation of stall behavior was limited to cases where $a_z \simeq 1$ and $\dot{V} \leq 1$ kt/sec. During the stall, a definite g break and nose down pitching tendency occurred. Wing dropping tendencies were mild and no tendency to roll in a particular direction existed. With the exception of the stall with stabilator stall, stalling behavior is docile.

Warning

The original configuration (which lacked the leading edge strakes and vortex generators) produced a very vigorous pre-stall buffeting of the stabilator. In the present configuration, however, warning of impending stalls is practically nonexistent. Buffet onset never comes more than 1 to 2 knots before the stall and when present, it is barely perceptible. Typically, a very light buffet occurs simultaneously with the g break itself. In one case, where $\delta_f = 10^0$ and power was set for level flight, some slight lightening of control wheel pull force occurred just prior to the stall.

Control Feel and Effectiveness

The rudder remains very effective throughout the stall. Later control is best achieved through a combination of rudder and spoiler deflection, although in the flaps-up case, the spoilers are nearly ineffective.* The

*It should be noted that the addition of wing-root strakes and vortex generators reduced indicated flaps-up stall speeds by about 9 knots from the stalls described by pilot A. The spoiler effectiveness during these slower stalls is reduced accordingly.

stabilator effectively controls α except when the stabilator stalls during the recovery from a wing stall. This unusual condition is described in more detail shortly.

Control-position force gradients seem to remain approximately the same during stall except for the $\delta_f = 10^0$ case mentioned under the "Warning" discussion above.

Recovery Technique

For the original configuration, recovery from all stalls could be effected by allowing the stabilator to move slightly off the negative stop. Holding the control wheel full aft would result in a moderate porpoising motion.

Recovery technique during the one buffet-onset investigation flight in the present airplane configuration consisted of an expeditious increment of forward wheel movement, followed by an aft repositioning to a point corresponding to a higher than stall trim speed. This technique quickly unstalled the wing and was satisfactory except in the case of stall with stabilator stall.

Power Effects and Stall Speeds

Two conditions, idle power and power for level flight, were explored. Stall warning was lacking in both conditions. Lateral control was roughly the same for both conditions. The stalling speeds were significantly affected by power.

		δ_f				
		0^o	10^o	20^o	30^o	37^o
Approximate stall speeds V_c', knots	Idle power	70	60	57	54	53
	Power for $\dot{\gamma} = 0$	64	56	53	49	47

Stall with Stabilator Stall

This phenomenon has been observed only with a $\delta_f = 37^o$ and power for level flight. Figure 5.23 compares stalls with and without stabilator stalls. Stabilator positioning after the g break is very similar for both stalls. The period necessary to reduce α to the pre-g break value was also the same.

Following the normal stall, flap retraction was begun after it was apparent that recovery from the maneuver was in progress. Although this was only 2 seconds after the g-break, Q had peaked negatively and then reduced in magnitude by 35 percent.

Similarity between the normal and stabilator stall cases ceases 2 seconds after the g break. A sudden force reversal occurs and V'_c, α', a_z and θ continue their divergence. At this point, a decision was made to reduce the negative pitching moment by raising the flaps. A maximum θ of -56^o was attained before the pitch divergence was stopped.

Stabilator stall and the resulting pitch divergence was encountered on one other occasion, this case occurring with the original aircraft configuration (no strakes or vortex generators). Power was set for level flight and $\delta_f = 37^o$. The trim speed, however, was 65 KIAS, a

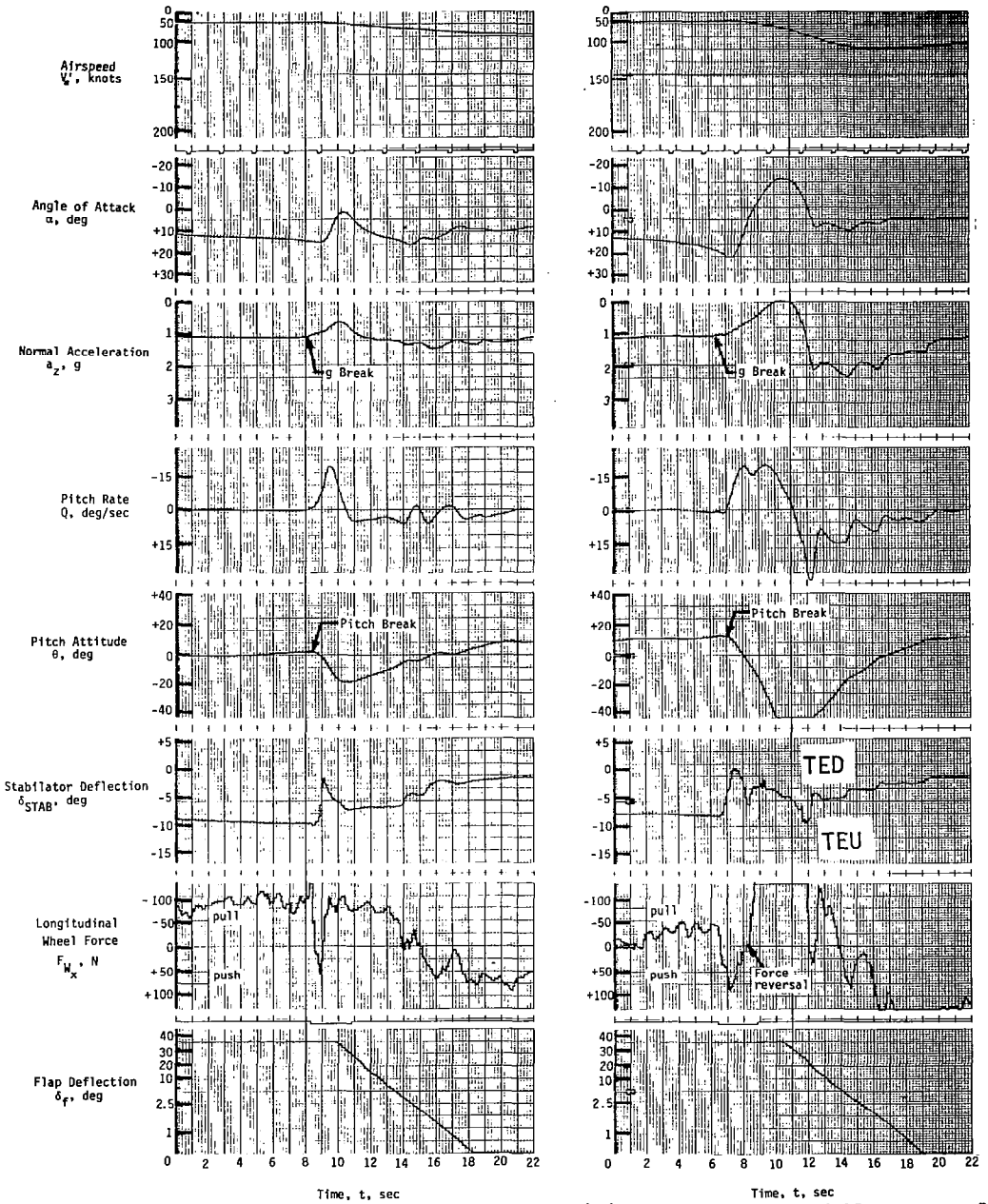

(a) Normal stall throttles idled

(b) Stall with stabilator stall power for level flight

Figure 5.23- ATLIT stall time histories.

value well above the stall speed. As the nose-down portion of a stabilator doublet was initiated, a divergent pitching motion developed; in that instance, recovery was effected by raising the flaps. Unfortunately, no records were taken of that maneuver.

TASKS FOR PILOT RATINGS

Takeoff and Transition to Climb

With a takeoff flap setting of 10 degrees, takeoff trim and a somewhat reduced power setting (to prevent too fast an acceleration through the speed of interest), the nosewheel could be lifted clear of the runway at an IAS = 38 kts. The attitude was then reset, full throttle was applied and liftoff was made at 74 kts. Care had to be used to avoid an overrotation. Directional control was easily maintained. With the gear and flaps retracted, climb power, a moderately heavy push force on the wheel was necessary to maintain 87 knots. The electric stabilator trim was somewhat slow for coping with the large pitching moment changes due to flap retraction and extension. A pilot rating of 2.5 was assigned to this flight phase.

Cruise

Two IFR tasks were evaluated with and without turbulence. The first consisted of precisely holding a heading in level flight. The next was the vertical S pattern depicted in the following figure.

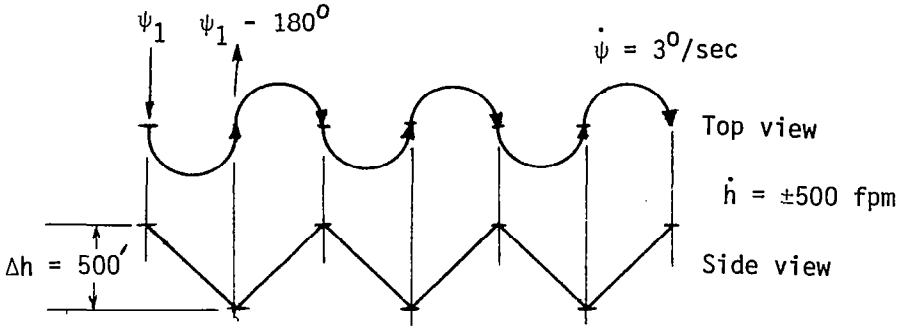

Vertical S Pattern (V = const.)

Without turbulence, precision heading holding was very easy. In rough air, however, excitation of the dutch-roll mode made the task difficult. Because of the high control system breakout and friction forces, it was difficult to reset the controls to trim after correcting for turbulence-induced upsets. Thus, the ATLIT would soon roll off in a direction corresponding to the control surfaces' out-of-trim positions. The net result was a mildly oscillatory rolling and yawing which was not eliminated even with considerable pilot effort. With turbulence, the cruise precision heading hold task was given a pilot rating of 4.5.

The vertical S pattern in turbulence incorporated all of the same difficulties encountered with the heading hold task. Additional difficulty

was introduced by the longitudinal control repositioning necessary as a consequence of power changes. The high control system breakout and friction forces were largely responsible for the assignment of a 5.5 pilot rating for task with turbulence. Without turbulence, there was a slight improvement to a rating of 5.0.

Cruise Turns, Coordinated and Two Control

Coordinated turns and turn reversals were easily accomplished. Rolling performance is indistinguishable from an aileron equppped aircraft. There was no noticeable nonlinear roll response to control-wheel inputs.

Rudder only turns and turn reversals were accomplished in a quick and relatively precise manner. Both spoiler-only and rudder-only turns and turn reversals are satisfactory alternate methods of lateral control. This entire flight phase is assigned a pilot rating of 2.

Formation Flying

High control system friction and breakout forces make the ATLIT very tiring to fly in formation. As a formation lead aircraft, the aircraft's turbulence response coupled with the pilot's corrections for upsets leads to a "wallowing" motion. This phase is given a pilot rating of 6.

Approach

Precision heading holding was again easy except in turbulence. The same type of general aircraft behavior was noted here as in cruise; however, the ratio of rolling to yawing disturbances was higher here than for cruise. Vertical S patterns were more difficult because the

lower longitudinal force gradients coupled with control system friction and breakout forces increased the difficulty of making corrections based on control feel rather than displacement. The previous pilot ratings for the precision heading hold and vertical S pattern tasks are increased numerically by $\Delta = 0.5$.

Nonlinearity of roll response to wheel deflection became noticeable in the approach configuration. On gusty days, tight lateral control of the aircraft was impossible if control wheel deflections were limited to $\leq \pm 45^{o}$. It was not unusual to contact the lateral wheel stops (at a deflection of 90^{o}) when trying to closely control bank angle. The lateral decentering moment "assisted" the pilot in an annoying manner. It should be stressed that the maximum roll rate the pilot can command is satisfactory.

For the approach task in turbulence, the pilot rating was 6.

Approach Turns, Two Control

Spoiler only turns and turn reversals showed generally the same characteristics as in the cruise condition. Rudder only turns from $\phi = 0$ were also similar. But large input, rudder-only turn reversals from some $\phi \neq 0$ were quite peculiar; bank angle built up in the direction of the rudder input but $\dot{\psi}$ built up in the opposite direction. $\dot{\psi}$ did not swing back in the direction of the input until the aircraft rolled through the wings-level position. Roll attitude control, spoiler only, was rated a 3. Rudder only control was given a 6.

Landing

The original ATLIT configuration was landed with the wing-low method in an 18 knot crosswind. The rudder was frequently on the stop for this landing, but, since not much control wheel deflection was necessary to achieve this sideslip, the additional wheel deflection necessary to counter turbulence upsets was available.

A recent steady heading sideslip test indicated that a steady crosswind component of 18 kts could be handled.

The flare maneuver could be easily overcontrolled because of the difficulty of feeling out the inputs thus, corrections had to be made by judging their adequacy initially in terms of displacement rather than force. Friction and breakout masking of a stabilator trim position was very detrimental here.

Once on the ground, directional control via the rudder was very satisfactory, but the spoilers appeared to be very ineffective for directional control (with $\delta = 30^{0}$). A pilot rating of 4 was assigned to the landing phase.

CHAPTER 6

CONCLUSIONS AND RECOMMENDATIONS

6.1 Conclusions

The conclusions for the ATLIT evaluation presented here are based on complete flight-test results of the stalling and the rolling characteristics and partial results for the cruise and climb performance.

1. The stalling speeds and the maximum-lift coefficients were in good agreement with the design estimates and the wind-tunnel predictions. The stalling characteristics are described by the pilots as gentle with very moderate rolloff and adequate lateral control throughout the initial stall departure. The stalling speed with flaps deflected 37 degrees was 51 knots (59 mph) and the corresponding $C_{L_{max,\ A}}$ was 3.03. With flaps up, the airplane stalled at 68 knots (78 mph) for a corresponding $C_{L_{max,\ A}}$ of 1.7. This flaps-up maximum lift and the great effectiveness of the Fowler flap in increasing maximum lift are apparently unequaled for general aviation airplanes of a similar configuration.
2. The spoiler roll-control power met design expectations and was in good agreement with wind-tunnel results. In the current landing configuration ($\delta_f = 30^o$), the maximum helix angles are greater than 0.11. With the flaps deflected, the spoiler roll control on ATLIT exhibits the desirable behavior of increasing helix angles with decreasing airspeeds.

This feature gives the pilot increasing bank-attitude control as the airplane slows down during the landing flare. No adverse yaw was measured during rolls; in fact, a small amount of proverse yaw was noted with large spoiler inputs.

Although the spoilers provided very powerful roll control, this control system did have undesirable control feel characteristics, depending on whether the spoilers were rigged up, flush, or down. These feel characteristics result from the large amount of combined control-system breakout force and friction of about 40 N in combination with the reduced $C_{l_{\delta_s}}$ for small spoiler deflections.

Much has been written (references 37 and 46) recommending against the use of spoilers alone for roll control. Past researchers have endorsed the use of a small trim or feeler aileron, along with roll control spoilers, to provide better feel characteristics, more positive control for small spoiler inputs, as well as to function as a lateral trimming device. In light of the experience with the ATLIT spoiler roll-control system, this recommendation is still a good one. It is a good recommendation not because spoiler systems cannot be designed to adequately serve as the sole means of airplane roll control, but because the use of a trim aileron greatly simplifies the design and implementation of roll spoilers. This situation may change when design data for spoilers are available to the

same extent as for ailerons, thus making the design for a mechanically-actuated, spoiler roll-control system as straightforward as it presently is for an aileron system.

3. In the configuration tested and reported on here, neither cruise nor climb performance of ATLIT met the design expectations. Top speed for ATLIT was 168 knots (193 mph) and maximum rate of climb was approximately equal to that for the standard Seneca. The most reliable predictions for ATLIT performance increases over the standard Seneca indicated about 9 knot (10 mph) increase in top speed to V_{max} = 178 knots (205 mph) and an increase in maximum single-engine rate of climb of about 12 m/min (40 ft/min) from about 58 m/min (190 ft/min) to 70 m/min (230 ft/min). These small predicted performance improvements were not realized because of the poor span efficiency factor ($e \simeq 0.65$) and the high value for zero lift drag ($C_{D_o} \simeq 0.045$). Calculations showed that with proper attention to construction details on the airplane, the predicted cruise and climb performance could be realized.

6.2 Recommendations

Flight testing of ATLIT in its present configuration (strakes and vortex generators on both wings) will continue to the completion of climb performance testing. After that, the following three major phases of testing are planned. The discussion for each phase includes recommendations for topics of pertinent research.

6.2.1 Supercritical Propeller Evaluation

Before the supercritical propellers are installed on ATLIT, baseline data on noise and performance characteristics will be gathered with the standard propellers. Identical tests will then be done with the supercritical propellers on ATLIT.

Both interior and exterior noise measurements will be made. Exterior noise characteristics will be documented by the guidelines of Federal Aviation Regulations (FAR) Part 36 (Noise Standards: Aircraft Type and Airworthiness Certification).

Propeller performance characteristics will be measured by constant altitude, level flight accelerations, and takeoff distance measurements (during these tests, landing distances will also be measured).

6.2.2 Preliminary Plans for ATLIT Full-Scale Wind-Tunnel Tests

ATLIT is scheduled to enter the LaRC full-scale (30- by 60-foot) wind tunnel in the fall of 1976. Several possible areas of research during these tests are listed below. The research items listed include items presented by a poll of U.S. general aviation manufacturers.

The tentative areas of investigation follow:

1. Documentation of baseline aerodynamic and performance characteristics.
2. Drag cleanup. - Several items have been identified as candidates for modification in a drag cleanup program as follows:
   (a) reduce wing trailing edge thickness
   (b) fair flap brackets, spoiler hinges, and other miscellaneous protuberances

(c) construct flush inspection covers to replace 16 presently protruding inspection covers located spanwise on wing lower surface

(d) remove instrumentation noseboom

(e) evaluate improved wheel well fairings

(f) improve the fit and sealing of the cabin door

(g) optimize devices for attachment of the wing-body interference-induced flow separation.

3. Cooling drag studies.
4. Studies of propeller/nacelle interference effects on propulsive efficiency and drag.
5. Studies of trim drag in single-engine climb configurations.
6. Wing-wake surveys for documentation of section profile drag and comparison with 2-D results.
7. Boundary-layer profile measurements for comparison with 2-D data.
8. Spoiler effectiveness and hinge-moment measurements for comparison with 2-D and 3-D scaled data.
9. Static stability derivative measurements.
10. Measurements of high angle-of-attack characteristics.
11. Acoustic (propeller, engine, and airframe) studies.
12. Evaluation of winglets on ATLIT.

Obviously, not all of these areas for research can be studied during the short time ATLIT will be in the tunnel. An order of priorities remains to be determined.

6.2.3 Final Flight Evaluation

ATLIT will return to flight status after the full-scale wind-tunnel tests. Flight data will be gathered to verify the wind-tunnel optimized ATLIT configuration (i.e., to measure, in flight, the effects of any fairing or fillet devices or winglets which may be tested in the tunnel).

Development should continue of the method discussed in appendix A for extracting aerodynamic drag and power parameters from flight data. The major emphasis in the continuing development of this method should be on improved flight-data quality. Additional, independent approaches to such a method should be encouraged.

REFERENCES

1. Crane, Harold L.; McGhee, Robert J.; and Kohlman, David L.: Applications of Advanced Aerodynamic Technology to Light Aircraft. Paper 730318, SAE National Business Aircraft Meeting, Wichita, April 1973.

2. Roskam, Jan; and Kohlman, David L.: An Assessment of Performance, Stability, and Control Improvements for General Aviation Aircraft. Paper 700240, SAE National Business Aircraft Meeting, Wichita, March 1970.

3. Kohlman, David L.: Flight-Test Results for an Advanced Technology Light Airplane Wing. Paper 740368, SAE National Business Aircraft Meeting, Wichita, April 1974.

4. Raisbeck, J. D.: Consideration of Application of Currently Available Transport-Category Aerodynamic Technology in the Optimization of General Aviation Propeller-Driven Twin Design. Paper 720337, SAE National Business Aircraft Meeting, Wichita, March 1972.

5. McGhee, Robert J.; and Beasley, William D.: Low-Speed Aerodynamic Characteristics of a 17-Percent Thick Airfoil Section Designed for General Aviation Applications. NASA TN D-7428, 1973.

6. Stevens, W. A.; Goradio, S. H.; and Braden, J. A.: Mathematical Model for Two-Dimensional Multi-Component Airfoils in Viscous Flow. NASA CR-1843, 1971.

7. Garrett, Robert B.: Experimental Investigation of High-Lift Devices for a Light Aircraft. M.S. Thesis, University of Kansas, 1972.

8. Sapp, Charles W.: Application of Spoilers to Light Airplanes. M.S. Thesis, University of Kansas, 1969.

9. Agler, Rex D.: Experimental Investigation of the Influence of Wing and Spoiler Effectiveness for Light Aircraft. M.S. Thesis, University of Kansas, 1970.

10. Colwell, Robert C.: Improvement of the Performance, Stability, and Control of a Current Light Aircraft. Masters Thesis, University of Kansas, 1970.

11. Kohlman, David L.; Holmes, Bruce J.; and Crane, Harold L.: Preliminary Flight-Test Results of an Advanced Technology Light Twin-Engine Airplane. Paper 750525, presented at the SAE National Business Aircraft Meeting, Wichita, Kansas, April 1975.

12. Holmes, Bruce J.; Kohlman, David L.; and Crane, Harold L.: Preliminary Flight-Test Results of an Advanced Technology Light Twin-Engine Airplane (ATLIT). Paper 760497, presented at the SAE National Business Aircraft Meeting, Wichita, Kansas, April 1976.

13. Roskam, J.; Kohlman, D. L.; and Wentz, W. H.: Spoilers for Roll Control of Light Airplanes. Paper 74-851, AIAA Mechanics and Control of Flight Conference, Anaheim, California, August 1974.

14. Wentz, William H., Jr.; and Seetharam, H. C.: Development of a Fowler Flap System for a High-Performance General Aviation Airfoil. NASA CR-2443, December 1974.

15. Wentz, William H., Jr.; Seetharam, H. C.; and Calhoun, John T.: Wind-Tunnel and Flight Development of Spoilers for General Aviation Aircraft. Paper 750523, SAE National Business Aircraft Meeting, Wichita, Kansas, April 1975.

16. Wentz, William H., Jr.: Effectiveness of Spoilers on the GA(W)-1 Airfoil with a High-Performance Fowler Flap. NASA CR-2583, 1975.

17. Wentz, William H., Jr.; and Volk, C. G., Jr.: Reflection-Plane Tests of Spoilers on an Advanced Technology Wing with a Large Fowler Flap. NASA CR-2696, 1976.

18. Smetana, Frederick O.; and Summey, Delbert C.: Drag-Analysis Methods for Light Aircraft. Paper 750526. SAE National Business Aircraft Meeting, Wichita, Kansas, April 1975.

19. Ellis, David R.; and Tilak, Narayan W.: An In-Flight Simulation of Lateral Control Nonlinearities. NASA CR-2625, November 1975.

20. Paulson, John W., Jr.: Wind-Tunnel Investigation of a Fowler Flap and Spoiler for an Advanced General Aviation Wing. NASA TN D-8236, 1976.

21. Paulson, John W., Jr.: Wind-Tunnel Test of a Conventional Flap and Aileron and a Fowler Flap and Slot-Lip Aileron (Spoiler) for an Advanced Technology General Aviation Wing. Paper 750501, SAE National Business Aircraft Meeting, Wichita, Kansas, 1975.

22. Weick, Fred E.: Aircraft Propeller Design. McGraw Hill, New York, 1930.

23. Roskam, J.: Overview of Trim Drag. Proceedings of the NASA/Industry/ University General Aviation Drag Reduction Workshop, Lawrence, Kansas, July 1975.

24. Fischel, J.; and Ivey, M. F.: Collection of Test Data for Lateral Control with Full-Span Flaps. NACA TN 1404, 1948.

25. Weick, F. E.; and Wenzinger, C. J.: Preliminary Investigation of Rolling Moments Obtained with Spoilers on Both Slotted and Plain Wings. NACA TN 415, 1932.

26. Gracey, W.: Measurement of Static Pressure on Aircraft. NACA TR 1364, 1957.

27. Thompson, Floyd L.: The Measurement of Airspeed of Airplanes. NACA TN 616, 1937.

28. Richardson, Norman R.; and Pearson, Alkin O.: Wind-Tunnel Calibrations of a Combined Pitot-Static Tube, Vane-Type Flow-Direction Transmitter, and Stagnation Temperature Element at Mach Numbers from 0.60 to 2.87. NASA TN D-122, 1959.

29. Sivells, James C.; and Westrick, Gertrude C.: Method for Calculating Lift Distributions for Unswept Wings with Flaps or Ailerons by Use of Nonlinear Section Lift Data. NACA TR 1090, 1952.

30. Smetana, Frederick O.; Summey, Delbert C.; and Johnson, W. D.: Point and Path Performance of Light Aircraft, A Review and Analysis. NASA CR 2272, 1973.

31. Hoak, D. E.; Ellison, D. E.; et. al.: USAF Stability and Control Datcom. Flight Control Division, Air Force Flight Dynamics Laboratory, Wright-Patterson Air Force Base, Ohio 45433, 1972.

32. Engineering Flight-Test Guide for Small Airplanes. Directive Number 8110.7, Federal Aviation Administration, Washington, DC, 1972.

33. Hamlin, Benson: Flight Testing Conventional and Jet-Propelled Airplanes. The MacMillan Company, New York, (1946).

34. Smetana, Frederick O.; Summey, Delbert C.; Smith, Neill S.; and Carden, Ronald K.: Light Aircraft Lift, Drag, and Moment Prediction - A Review and Analysis. NASA CR 2523, 1975.

35. Allen, H. Julian; and Perkins, E. W.: A Study of Effects of Viscosity on Flow Over Slender, Inclined Bodies of Revolution. NACA TR 1048, 1951.

36. Fink, Marvin P.; Shivers, James P.; and Smith, Charles C., Jr.: A Wind-Tunnel Investigation of Static Longitudinal and Lateral Characteristics of a Full-Scale Mockup of a Light Twin-Engine Airplane. NASA TN D-6238, 1971.

37. Wenzinger, Carl J.; and Rogallo, Francis M.: Wind-Tunnel Investigation of Spoiler Deflector, and Slot Lateral-Control Devices on Wings with Full-Span Split and Slotted Flaps. NACA TR 706, 1941.

38. Gilruth, R. R.: Requirements for Satisfactory Flying Qualities of Airplanes. NACA TR 755, 1943.

39. Anon.: Detail Specification for Engine, Aircraft, Model L10-CIE6, 200 Horsepower, direct Drive. Avco Lycoming Specification No. 2416, April 13, 1970.

40. Pfleegor, Cliff: Determination of Installed Horsepower for Lycoming Reciprocating Engines. First Annual General Aviation Technology Fest, November 1975. (Oral presentation only.)

41. Borst, J. V.: A Short Method to Propeller Performance, Curtiss-Wright Corporation, Caldwell, NJ, 1956.

42. Weick, Fred E.: Aircraft Propeller Design. McGraw-Hill Book Company, Inc., 1930.

43. Wood, Donald H.: Tests on Nacelle-Propeller Combinations in Various Positions with Reference to Wings. Part I, ThickWing NACA Cowled Nacelle-Tractor Propeller. NACA Report 415, 1932.

44. Wood, Donald H.: Tests on Nacelle-Propeller Combinations in Various Positions with Reference to Wings. Part II. Thick Wing Various Radial Engine Cowlings-Tractor Propeller. NACA Report 436, 1932.

45. Hoerner, Sighard F.: Aerodynamic Drag. (1951) Published by author.

APPENDIX A

PERFORMANCE PARAMETER EXTRACTION METHOD WITH ERROR ANALYSIS

APPENDIX A

PERFORMANCE PARAMETER EXTRACTION METHOD WITH ERROR ANALYSIS

This appendix is included for the convenience of the reader as a brief description of a method for extracting airplane drag and power information from dynamic, maneuvering flight data. The development of this method and the preparation of the materials for this appendix were done by Dr. Frederick O. Smetana of North Carolina State University. Publication of a full description and the results of flight-test applications of the method is planned in a future NASA contractor report.

MEASURING DRAG AND THRUST IN FLIGHT

The Concept

Most techniques for the determination of aircraft drag in flight rely on the fact that when the aircraft is in unaccelerated flight, the forces along its x-axis, principally the thrust and drag, are in balance. Then, if one knows the propulsive thrust for a particular flight condition, he automatically knows the aircraft drag at that condition. Thus, to apply these techniques one must know that $\dot{V} = 0$ as well as the propulsive thrust as a function of flight speed, altitude, and power setting.

This, unfortunately, is not determined easily. Although engine output can be measured accurately on a test stand as a function of altitude and power setting, and propeller characteristics can be determined in a test cell as a function of rpm and flight velocity, the flow disturbances caused

by putting a cowled engine behind a propeller and mounting the whole on an airplane are not readily determined apriori. Hence, efforts have been made from time to time to measure inflight thrust using such techniques as the torque reaction produced by the engine or the vehicle acceleration at constant altitude produced by varying power levels.

The reader will readily appreciate the difficulties which such techniques entail. In the case of the ATLIT aircraft, instrumentation to measure reaction torques was not available and the longitudinal accelerometer provided in the instrument package was not considered a primary test instrument, at least initially. Further, the establishment of really unaccelerated flight at many different speeds is very consuming of flight-test time. It is for these reasons that an effort was made to develop an alternate technique to measure thrust and drag simultaneously in accelerated flight.

The origin of the concept is quite simple. Recent workers attempting to extract the values of stability derivatives from flight data have all faced the problem of fitting an analytical model containing 13 or more undetermined coefficients to a set of four or five simultaneous time histories. That is, the number of unknowns greatly exceed the number of independent equations one can write to describe the motion. The problem is usually attacked (see ref. A.1, for example) by fitting the equations to the time histories at a number of different times. Theoretically, one need only fit the equation the same number of times as one desires to find coefficient values. In practice, it is fit many, many

times and the values which best satisfy the time history in some statistical sense are chosen. If the initial estimates of the parameter values are reasonably accurate, the procedures usually converge on the correct values. However, since the system is not determinant, convergence is not guaranteed.

The problem in determining both drag and thrust simultaneously in flight is that there is one more unknown than there are equations. Mathematically this means that for any flight condition there are an infinite number of sets of T and D which satisfy the equation. For any T there is only one D, but one can find the corresponding D for any arbitrary choice of T whether it has any physical meaning or not.

Following the fairly successful approach used in stability derivative extraction, it was reasoned that if one would write the equation of motion substituting flight data for different times in the flight, he could create a system of equations equal to the number of unknowns. Formally, the equation of motion of the vehicle along its trajectory in the X-Z terrestrial plane is

$$\frac{\dot{V}}{g} + \sin \gamma = \frac{T - D}{W} \qquad (A.1)$$

In order to apply the technique, we wish to express the thrust and drag in a polynomial expansion of some easily-measured flight variable with the coefficients to be undetermined constants. Now, the thrust is known to depend primarily upon flight speed for a given power setting so that we choose the representation

$$T = \frac{\cos \alpha}{V} \left[P_o + P_1 V + P_2 V^2 \right] \quad . \qquad (A.2)$$

In other words, we assume that the power-speed relationship is a parabola. Given the characteristics of most propellers, P_o and P_1 will be positive and P_2 negative. We insert the $\cos \alpha$ term because we assume that the propeller thrust is always applied along the x-body axis rather than along the flightpath. Drag, on the other hand, is always defined with respect to the flightpath. We can represent the drag by the equation

$$D = 1/2 \, \rho S V^2 \left[C_{D_o} + C_{D_1} \alpha^2 + C_{D_2} \alpha^6 \right] \quad , \qquad (A.3)$$

where α is measured from zero lift and the sixth power for the third term was chosen on the basis of curve fits to some actual data. Note, however, that we may alter the model to represent a particular situation more accurately without affecting the validity of the procedure.

Substituting these relationships into the equation of motion yields

$$\frac{W\dot{V}}{g} + W \sin \gamma = \frac{\cos \alpha}{V} \left[P_o + P_1 V + P_2 V^2 \right] - \frac{1}{2} \rho S V^2 \left[C_{D_o} + C_{D_1} \alpha^2 + C_{D_2} \alpha^6 \right] \quad . \qquad (A.4)$$

This equation has six unknown but constant coefficients. By determining the flight values of γ, W, V, $\dot{V}$, ρ, and α at six different times, we create a system of six linear equations in six unknowns. This can then be solved for the values of P_o, P_1, P_2, C_{D_o}, C_{D_1}, and C_{D_2}.

Difficulties in Concept Execution

Unfortunately, this system of equations is what mathematicians call ill-conditioned; that is, very small changes in any of the measured values (α, W, V, $\dot{V}$, γ, ρ) can cause the coefficient values (P_o, P_1, etc.) to change radically. Further, the solution guarantees to pass through the six selected points only. For any other speed, acceleration, angle of attack, weight, flightpath angle, or altitude, the thrust or drag computed with these six coefficients may be quite wrong. In addition, the coefficient values themselves may be ridiculous (for example, a negative C_{D_1} value) yet the total drag as determined from $C_{D_o} + C_{D_1} \alpha^2 + C_{D_2} \alpha^6$ may be very reasonable.

These problems are to some extent traceable to the adequacy of the analytical model used. A model which does not well represent what actually occurs will, when fit to the data using this procedure, produce nonsense numbers for some of the coefficients, i.e., nonsense numbers in the physical sense but absolutely correct numbers in the mathematical sense. For example, if the speed-power relation should in fact be a constant, then an attempt to fit it with a parabola will usually yield non-zero values for P_1 and P_2. Thus, a successful solution routine must have a provision for examining the results (at least manually) for reasonableness and for changing the analytical model if the results are not reasonable.

There is also a problem concerned with the selection of the six data sets submitted to the solution routine. The reader will recognize that if one selects six points very close together in speed, the data must be extremely accurate because all significance can be lost in taking the differences between adjacent numbers as one does in solving a system of six equations.

The maneuver selected to generate these data was a pullup-pushover. Beginning at the highest speed in a configuration of interest, a pullup is initiated and the airplane is decelerated to the minimum speed for the test. At that point, a pushover is done, allowing the airplane to accelerate back to maximum speed.

Amelioration of Solution Difficulties

One means of selecting the six points submitted to the solution routine so that it will yield reasonable results is to select those points where the velocities are given by

$$V_1 = V_{min} \text{ for the maneuver}$$

$$V_2 = V_{max} \text{ for the maneuver}$$

$$V_3 = V_1 \left[\frac{V_2}{V_1}\right]^{1/5}$$

$$V_4 = V_3 \left[\frac{V_2}{V_1}\right]^{1/5} \qquad \text{(A.5)}$$

$$V_5 = V_4 \left[\frac{V_2}{V_1}\right]^{1/5}$$

$$V_6 = V_5 \left[\frac{V_2}{V_1}\right]^{1/5}$$

This procedure spaces the points over all the available data giving emphasis to the portion of the drag curve when changes with speed are most rapid. When applied to theoretically-generated data, the original coefficients can be recovered to within 1 percent.

For a variety of reasons, flight measurements will never be as accurate or as noise free as theoretically-generated data. One then asks the question, "How can I use the remainder of the data (the sets of α, ρ, γ, V, $\dot{V}$, W beyond the six sets mentioned above) taken during a 30-second maneuver to improve the accuracy of the coefficient extraction procedure?" The classical answer is fit the assumed form of the curve (equation A.4) to the data by a least-squares technique. What this does is to determine those values of the coefficients (P_o, P_1, P_2, C_{D_o}, C_{D_1}, C_{D_2}) which make the sum of the squares of the distance from the curve to each of the data points as minimum.

Data Filtering

All records of the flight of actual aircraft will contain spurious contributions to the data signals arising from electrical noise, instrument errors, structural vibrations, and atmospheric turbulence.

Since the model we have chosen to represent the aircraft does not include such effects, it is desirable to remove them, in so far as possible, before submitting the data to the coefficient extraction routine. Not doing so may cause the extraction routine to produce physically meaningless results.

All filtering schemes proceed from the idea that continuous data signals are composites, each signal made up of sine waves of all frequencies. Each of these sine waves in the composite has a definite amplitude and phase relationship to the other sine waves making up the signal. By suppressing those frequencies which, on the basis of analysis or experience, cannot arise from the aircraft behavior of interest, one can remove most of the spurious contributions to the signal. Traditionally, filtering was done on continuous signals using frequency-sensitive passive networks. In the present case, however, the flight data were received in digital form so that the filtering was accomplished mathematically using a computer.*

Since this procedure permits one to describe a signal time history in terms of its harmonic content, it is therefore possible to reduce the amplitudes of or eliminate certain constituent frequencies from the set before regenerating the signal; in essence, filtering out the unwanted

---

*The data are, nevertheless, just digitized samples of continuous functions. For this reason, we have chosen to employ mathematical techniques more appropriate to such functions than the more commonly-used digital filtering techniques which seem more appropriate to the analysis of data which are inherently trains of impulses.

contributions to any desired degree, without any disruption of the phase relationships among the remaining contributions. This represents a level of filter performance far above that possible with passive elements in analog circuits.

Corrections to Measured Accelerations

The scheme to extract drag and thrust simultaneously from flight data has been found to require accurate indications of the acceleration along the vehicle's flightpath in order to yield acceptable results. Usually it is not possible to locate the measuring instrument (accelerometer) precisely at the vehicle's center of gravity, so it is necessary to correct the instrument's indication for this fact and then to relate the acceleration along the vehicle's x-body axis to the longitudinal acceleration along the flightpath.

Accelerometers are generally masses constrained to move along the axis of a tube and centered by springs at either end. The position of the mass relative to the center of a tube is proportional to the acceleration and is measured electrically. When the aircraft accelerates along the flightpath, the mass moves aft of the center of the tube. Now, the same effect is produced when the accelerometer is tilted nose up even though there is no acceleration. Thus, it is necessary to subtract a term $n_z \sin \theta$ from the accelerometer indication to account for this effect.

If the accelerometer is located x feet in front of the CG, its mass is caused to move forward as a result of the angular rotation of

Then solving for $\dot{V}$, one has

$$\dot{V} = \frac{a_{x_{ind}} - n_{\dot{z}} \sin\theta + x\,q^2 - z\,\dot{q}}{\cos\alpha} + V(\dot{\alpha} + q)\tan\alpha \quad . \tag{A.12}$$

The value given by (A.12) should now be the same as that obtained by differentiating the variation of true airspeed with time.

Corrections to Airspeed Indications

Of course one does not measure true airspeed directly. An airspeed sensor measures only a pressure difference. This difference is affected by the sensitivity of the pitot and static pressure sources to angle of attack, the disturbance to the free-stream pressure at the static-pressure source resulting from the presence of the aircraft, the compressibility of the air, and the difference in pneumatic lags of the pitot and static-pressure lines. The pneumatic lag also introduces a time delay in the airspeed indication. Since the airspeed indicator is calibrated for standard sea-level conditions, any variation in atmospheric temperature will affect the true airspeed at a given pressure difference.

The theory of the pitot-static tube assumes that the air is brought to rest at the pitot pressure source adiabatically and that the static source senses the pressure in the free stream (i.e., away from the airplane). With these assumptions, it is easy to show that the true flow velocity is related to the measured pressures by

$$V = \sqrt{\frac{2\gamma\,RT}{(\gamma-1)}\left\{\left[\frac{q_c}{P} + 1\right]^{\frac{\gamma-1}{\gamma}} - 1\right\}} \quad , \tag{A.13}$$

the aircraft by an amount $x \cdot q^2$. One must therefore add this term to the accelerometer indication. Similarly, if the accelerometer axis is located z feet below the x-body axis, then the accelerometer mass is displaced rearward by an amount proportional to $z \cdot \dot{q}$.

The linear acceleration along the x-body axis in terms of the accelerometer indication location, and angular velocity is therefore

$$a_x = a_{x_{ind}} - n_z \sin \theta + x \cdot q^2 - z \cdot \dot{q} \quad . \tag{A.6}$$

We desire the acceleration not along the x-body axis but rather along the flightpath. We know that for motion in the x-z terrestrial plane

$$a_x = \dot{u} + q \cdot w \tag{A.7}$$

and

$$u = V \cos \alpha \tag{A.8}$$

$$w = -V \sin \alpha \tag{A.9}$$

where V is the velocity of the aircraft along its flightpath and u and w are components of this velocity along the principal axes of the aircraft. In terms of (A.8) and (A.9)

$$\begin{aligned} a_x &= \dot{V} \cos \alpha - V \dot{\alpha} \sin \alpha - q V \sin \alpha \\ &= \dot{V} \cos \alpha - V (\dot{\alpha} + q) \sin \alpha \quad . \end{aligned} \tag{A.10}$$

Equating (A.6) and (A.10) yields

$$a_{x_{ind}} - n_z \sin \theta + q^2 - z \dot{q} = \dot{V} \cos \alpha - V (\dot{\alpha} + q) \sin \alpha \quad . \tag{A.11}$$

where P is the altitude pressure, q_c is the difference between the pitot and static pressures, T is the local free-stream absolute temperature, R is the gas constant for air and γ is the ratio of specific heats of air (1.4 for diatomic gases at normal temperatures). The P indication for use in this equation comes from the static-pressure source of the pitot-static tube and the T indication from a temperature measuring device. Since one cannot measure the local free-stream temperature readily while the vehicle is in motion, temperature sensing devices most often measure the stagnation temperature, T_s, which is related to the free-stream temperature by

$$T = \frac{T_s}{\left[\frac{q_c}{P} + 1\right]^{\frac{\gamma-1}{\gamma}}} \tag{A.14}$$

In terms of the stagnation temperature, the true airspeed is given by

$$V = \sqrt{\frac{2\gamma RT_s}{(\gamma-1)} \left\{1 - \left[\frac{q_c}{P} + 1\right]^{\frac{1-\gamma}{\gamma}}\right\}} \tag{A.15}$$

Unfortunately, it is usually not possible to locate the static-pressure source on an airplane in a region where the static pressure is the same as the free-stream value. Hence, the static-pressure indication is in error by an amount ΔP. This "position error" so called is felt in both the altitude and q_c indications. If we call P' the measured altitude pressure and q_c the measured pressure difference, then because

$$q_c' + P' = q_c + P = P_s \ , \tag{A.16}$$

and

$$P = P' - \Delta P \quad , \tag{A.17}$$

one can write

$$\frac{q_c + P}{P} = \frac{q_c' + P'}{P' - \Delta P} = \frac{1 + \frac{P'}{q_c'}}{\frac{P'}{q_c'} - \frac{\Delta P}{q_c'}} \quad , \tag{A.18}$$

in terms of the measured values and the static-source position error which is usually determined by flight calibration and is expressed in terms of $\frac{\Delta P}{q_c'}$ as a function of q_c' or indicated airspeed. With this effect included the expression for true airspeed becomes

$$V = \sqrt{\frac{2\gamma RT_s}{(\gamma-1)} \left\{ 1 - \left[\frac{1 + \frac{P'}{q_c'}}{\frac{P'}{q_c'} - \frac{\Delta P}{q_c'}} \right]^{\frac{1-\gamma}{\gamma}} \right\}} \quad . \tag{A.19}$$

Fortunately, modern pitot-static tubes are relatively insensitive to changes in angle of attack so that the q_c' and P' indications do not depend on the tube's inclination to the airstream over the useful range of aircraft angles of attack. The position error, however, does depend upon angle of attack and aircraft configurations. At steady speed and constant weight the position error can be related, as it commonly is, to q_c' or indicated airspeed, but during maneuvers it may be necessary to employ a correlation with angle of attack instead. Whether this is necessary may be determined by calibration. If it is, one must then determine true airspeed and true angle of attack iteratively.

The compressibility correction mentioned earlier is already included in (A.19). Conventional low-speed airspeed indicators, it may be noted, are simply mechanizations of the equation

$$V_i = \frac{2q_c}{\rho_o} \quad , \tag{A.20}$$

where ρ_o is the mass density of the air at standard sea-level conditions. If the airspeed indicator calibration includes compressibility effects, equation (A.13) with standard sea-level pressure and temperature is mechanized.

Effect of Pneumatic Lag on Dynamic Airspeed Indications

If pneumatic signals transmitted through the pitot and static lines travel at different speeds then the q_c' and P' values will be in error. In most aircraft with pressure sensors located in cabin area, the pneumatic lines are long enough that their response characteristics can be considered analogies to those of resistance-capacitance electrical circuits. The "resistance" is proportional to length/(diameter)^4 while the "capacitance" is proportional to system volume. Since the static system includes more instruments than the pitot system and, frequently, larger volumes, the static-line diameter must be larger than the pitot or a restriction must be placed in the pitot line in order to keep the response times equal. Even if the line responses are equal, V' will lag the correct value by a time which is proportional to $\dot{h}$ and $\dot{V}$. Corrections for these lag effects will be necessary if the time constants of the pneumatic lines in ATLIT exceed about 0.1 seconds.

The lag corrections are applied as follows:

let

P_2 = the instrument indication

P_1 = correct pressure .

Assume Poiseuille-type flow where the mass flow is proportional to the pressure difference to the first power: $\dot{M} \sim \Delta P$. The rate of change of pressure in a volume connected by long tubing to the atmosphere is, for isothermal conditions, simply

$$\dot{P}_2 = \frac{1}{\tau} (P_1 - P_2) \tag{A.21}$$

where τ is an experimentally determined time constant. In the case where P_1 is changed instantaneously and held at the new value, one may write

$$\frac{dP_2}{(P_1 - P_2)} = \frac{dt}{\tau} \tag{A.22}$$

or

$$-\ln (P_1 - P_2) = t/\tau + C$$

$$P_1 - P_2 = ce^{-t/\tau} \tag{A.23}$$

when $t = 0$, $P_2 = P_{2_o}$

when $t \to \infty$, $P_2 \to P_1$ (A.24)

thus

$$P_2 = P_{2_o} \; e^{-t/\tau} + P_1 \; (1 - e^{-t/\tau}) \quad . \tag{A.25}$$

This says that by differentiating P_2 (t) to obtain $\dot{P}_2$ at any time we can find P_1 by taking P_2 and adding $\tau\dot{P}_2$ (t).

If we now call

P_s the static pressure

P_t the stagnation pressure

τ_1 the time constant in the static system, seconds

τ_2 the time constant in the stagnation system, seconds

then the lag-free value of q_c' is given by

$$q_c' = P_t - P_s = P_{t_m} + \tau_2 \dot{P}_{t_m} - P_{s_m} - \tau_1 \dot{P}_{s_m}$$

$$= q_c'_m + \tau_2 \dot{P}_{t_m} - \tau, \dot{P}_{s_m} \tag{A.26}$$

and the lag-free value of P_s is given by

$$P_s = P_{s_m} + \tau_1 \dot{P}_{s_m} \tag{A.27}$$

where the subscript m indicates the recorded value. Where $\tau_1 = \tau_2$, (A.26) can be written

$$q_c' = q_c'_m + \tau\dot{q}_c'_m \quad . \tag{A.28}$$

This value of $\dot{q}_c$, corrected for lag, is then applied in equation (A.19).

Correction of Angle of Attack Indications

In addition to factors such as transducer linearity, gain, and bias, the angle-of-attack indication is affected by the presence of the carrying aircraft and by its rotation. It will be recognized that for an angle-of-attack vane located x feet ahead of the c.g. an incremental angle

$$\Delta\alpha = \tan^{-1} \frac{xq}{V} \quad , \tag{A.29}$$

must be subtracted to the transducer indication to account for vehicle rotation. In addition, there is usually a relationship of the type

$$\alpha_{true} = C_1 \ \alpha_{indicated} + C_2 \quad , \tag{A.30}$$

between the angle of attack measured in the neighborhood of the aircraft and the true (i.e., at infinity) angle of attack. The values of C_1 and C_2 depend upon the location of the vane relative to the aircraft and the geometry of the aircraft. They are therefore almost always found from flight calibration tests, since the flow field about a complex shape such as a complete aircraft is almost impossible to determine analytically. Assuming that these coefficients are known, one may write the expression for true angle of attack as

$$\alpha_{true} = C_1 \left\{ \alpha_{indicated} - \tan^{-1} \left[\frac{xq}{V} \right] \right\} + C_2 \quad . \tag{A.31}$$

Note that the value of V used in (A.31) should be that obtained from (A.19). One may then smooth $\alpha_{true}(t)$ and compute the derivative, $\dot{\alpha}(t)$, by the Fourier analysis procedure.

Determination of $\rho(t)$

Equation (A.4) requires as an input $\rho(t)$. This is readily determined from

$$\rho = \frac{(P' - \Delta P)}{RT_s} \left[\frac{1 + \frac{P'}{q_c'}}{\frac{P'}{q_c} - \frac{\Delta P}{q_c'}} \right]^{\frac{\gamma-1}{\gamma}} \qquad (A.32)$$

If the altitude pressure transducer is calibrated in feet, then the appropriate pressure versus altitude function must be employed to convert the indications to pressure values.

Conditioning of Other Data Inputs to the Drag and Power Extraction Method

In addition to the velocity, angle of attack, and atmospheric density, $W(t)$ and θ are required as inputs. Fortunately, for the maneuvers of interest W changes so little that it can be taken to be constant or, at most, varying linearly during a maneuver. Usually θ requires no corrections beyond the instrument calibration if the erection mechanism is disabled during the maneuver. Since the indication is sampled and since there may be electrical, airframe, and turbulence-induced noise, smoothing may still be necessary. This is also true for the pitch-rate indication, q, which is used in the C_L computation and the α and a_x corrections.

More General Power and Drag Models

In a normally aspirated engine, the manifold pressure and, hence, the power output for a given throttle setting will usually vary directly

with the atmospheric density. Thus, if the maneuver to provide data for the power and drag extraction process involves a change in altitude, there will be a change in power at a given speed corresponding to the change in ρ even if the pilot does not change his throttle setting or rpm. To account for this, we need to multiply the expression for power by Bairstow's equation (ref. A.2)

$$\frac{\rho_{ref}/\rho_o - 0.165}{\rho/\rho_o - 0.165} \tag{A.33}$$

where ρ_o is the standard sea-level value of ρ and ρ_{ref} is the value of ρ at the beginning of the maneuver.

The parabolic form of the speed-power relation used in equation (A.4) is obviously satisfactory over small differences in speed and should represent the thrust horsepower of fixed-pitch propellers reasonably well over most of the aircraft's speed envelope. The higher efficiency levels provided by a constant speed propeller at the lower speeds, however, makes it necessary to employ a higher order polynomial or other function having additional degrees of freedom (coefficients) to represent the thrust horsepower adequately over a wide speed range. Variants of one such function were chosen for further study:

$$P = P_1 + \frac{P_2}{V^{1/2}} + P_3V + P_4V^2 + P_5V^3 \tag{A.34}$$

These variants include

$$P = P_1 \tag{A.35}$$

$$P = P_1 + P_3 V \tag{A.36}$$

$$P = P_1 + \frac{P_2}{V^{1/2}} \tag{A.37}$$

$$P = P_1 + P_3 V + P_4 V^2 \tag{A.38}$$

$$P = P_1 + \frac{P_2}{V^{1/2}} + P_3 V \tag{A.39}$$

$$P = P_1 + \frac{P_2}{V^{1/2}} + P_3 V + P_4 V^2 \tag{A.40}$$

$$P = P_1 + P_3 V + P_4 V^2 + P_5 V^3 \tag{A.41}$$

One will note also that the drag expression is really satisfactory only if α is measured from zero lift. Since the angle reference for flight data is quite arbitrary, it is difficult to establish the angle for zero lift apriori. To accommodate an arbitrary reference, i.e., to replace α by α_o in equation (A.3), requires that the representation for C_D contain all powers of α through 6. We choose, however, to investigate only variants of the following form:

$$C_D = C_{D_o} + C_{D_1} \alpha + C_{D_2} \alpha^2 + C_{D_3} \alpha^3 + C_{D_4} \alpha^6 \tag{A.42}$$

These variants are

$$C_D = C_{D_o} + C_{D_2} \alpha^2 \tag{A.43}$$

$$C_D = C_{D_o} + C_{D_2} \alpha^2 + C_{D_4} \alpha^6 \quad . \tag{A.44}$$

The three drag expressions and the eight power expressions give us a total of 24 analytical models with which we can attempt to fit experimental data. It will probably be necessary to employ all of the models or at least this number of models until experience with data for a particular aircraft permits one to discard these models which do not apply.

One may also ask why should one also employ a model which is simply a reduced form of a more general model? The answer lies in the extreme sensitivity of the coefficient solutions to small errors in the data. Generally, the more general models are more sensitive to these errors so that under these circumstances a simpler form may yield reasonable results, whereas the more general form may yield nonsense numbers. It should be recalled that since any power, if accompanied by a suitable drag, will solve the equation of motion, these physically absurd numbers are legitimate mathematical solutions. How then does one determine whether the solutions obtained are reasonable?

The first means of assessing the reasonableness of the solution set is to use them along with the experimental data in the proper form of equation (A.4) to compute an error term, S.

$$S = \sum_{i=1}^{N} \left[\frac{W_i \dot{V}_i}{g} = W_i \sin(\theta_1 - \alpha_i) P_0 - \cos \alpha_i P_1 - V_i \cos \alpha_i P_2 + \frac{\rho_i S V_i^2}{2} C_{D_0} + \frac{\rho_i S V_i^2}{2} \alpha_i^2 C_{D_1} + \frac{\rho_i S V_i^2}{2} \alpha_i^6 C_{D_2} \right]^2 , \quad (A.45)$$

For 300 data points, a value of $S < 10^{-13}$ generally indicates coefficient values within 1 percent or so of the correct values. (For the exact coefficient values, $S < 10^{-21}$.) Coefficient values in error by 5 percent, for example, may still be of interest but with errors of this size it may become difficult to identify the best model and coefficient set merely by checking to see which model gives the smallest value of S. S_{min} will now be on the order of 10^{-6} for 300 points, but the coefficient set for S_{min} may give absurd powers and drags. For this reason, it is desirable to add a second constraint which an acceptable model and coefficient set must satisfy: The horsepower for any speed must be positive and less than Y (Y = 400 for ATLIT); C_D must be positive and less than Z (Z = 0.12 for ATLIT) for any α. One frequently finds that with noisy data very few of the 24 coefficient sets satisfy this second constraint.

Effect of Data Errors on Coefficient Extractions

We have noted above that by operating on exact data, it is possible for the coefficient extraction procedure to recover the values of the coefficients in the power and drag polynomials to six significant figures. We have also noted that this procedure is quite sensitive to data inaccuracies. In order to place some quantitative bound on this sensitivity, the exact input data were artificially degraded and resubmitted to the coefficient extraction procedure to determine how the coefficient values were altered. Two types of degradation were employed: random noise and constant bias. For the random noise, a random number generator was employed at each 0.1 seconds of each trace and the output scaled so as to be 1 percent of the maximum value of the function, e.g., 1 percent of the maximum value of $V(t)$ during the maneuver. These scaled noise values were then added to the exact function values to obtain the degraded data. For this experiment, all data which would normally be measured in flight were degraded. This was too noisy. No coefficient set would satisfy the reasonableness criterion.

In an experiment, the data traces were degraded individually by a constant bias error. Reproduced as figures A.1 through A.10 are the recovered speed-power and drag-alpha characteristics for various bias errors compared with the undegraded characteristics used to generate the data traces. Generally, the characteristics for the largest bias error which can yield reasonable results are shown along with the characteristics for smaller bias errors so that the reader may assess the linearity of the change in characteristics with the change in bias

error. Note that weight and altitude bias errors of the magnitude shown are not particularly serious. As might be expected, bias errors in airspeed affect the power determination primarily and have little influence on drag. The same is true with regard to bias errors in $\dot{V}$. Bias errors in θ and α, however, are extremely destructive. Even a 0.7^{o} error in θ results in about a 10-percent error in C_{D_o} while a -1.9^{o} error in θ results in an error of about 37 percent in C_{D_o}. The case for a bias error of $+1.9^{o}$ failed (e.g., gave a power exceeding the limit of 400 hp). An angle-of-attack bias error of as little as 0.1^{o} is noticeable in the final result, while an α bias error of 1.6^{o} results in drag and power errors in the neighborhood of 30-40 percent. In addition, the shapes of the curves are altered drastically.

These results demonstrate the extreme sensitivity of the coefficient extraction procedure to typical noise and instrument errors encountered in flight-test work. This is true even after the data have been filtered to remove the noise components which occur at frequencies above the usual aircraft responses to control deflections. Thus, to obtain accurate drag and power data using this procedure some means must be employed to reduce the noise components in the data at what might be termed signal frequencies.

Reduction of Noise at Signal Frequencies

The filtering technique discussed previously has been shown to be highly effective at suppressing noise components in the data at frequencies above the principal components of the aircraft response. At

frequencies below this cutoff value it is impossible to separate the noise from the signal without resort to additional information! The only additional information universally available are the relationships among the measured variables and the power and drag as functions of time, i.e., the equations of motion and their auxiliary equations:

$$\dot{V} = \frac{gP\cos\alpha}{WV} - \frac{g}{W}\frac{SV^2}{2} C_D(\alpha)\,\rho(h) - g\sin\gamma \tag{A.46}$$

$$\dot{\gamma} = \frac{g}{W}\frac{SV}{2} C_L(\alpha)\,\rho(h) - \frac{g}{V}\cos\gamma + \frac{gP\sin\alpha}{WV^2} \tag{A.47}$$

$$\dot{W} = -cP \tag{A.48}$$

$$\dot{h} = V\sin\gamma \tag{A.49}$$

$$\dot{X} = V\cos\gamma \tag{A.50}$$

$$\rho(h) = \rho_o\,(1 - 6.86 \times 10^{-6}\, h)^{4.26} \tag{A.51}$$

$$C_L(\alpha) = C_{L_\alpha}\,\alpha + C_{L_{(\alpha=o)}} \tag{A.52}$$

$$C_D(\alpha) = C_{D_o} + k\;C_L(\alpha)^{\,2} + k_1\;C_L(\alpha)^{\,k_2} \tag{A.53}$$

$$P \leq P_{max}\,(h, V) \tag{A.54}$$

This system of equations can be solved simultaneously to yield the variable values as functions of time provided any two of these (α, θ, V, h, W, P) are known apriori. C_{D_o}, k, k_1, k_2, $C_{L_{\alpha=o}}$, and C_{L_α} must also be assumed known in order to carry out this procedure. Then, given values for these constants and W(t) and h (t), one can solve the system a self-consistent set of $\alpha(t)$, $\theta(t)$, V(t), and P(t). Since these time

histories are related in a consistent fashion through the equations of motion and since noise will likely affect each time history differently, it is then possible to identify the noise present in each time history at signal frequencies by comparing the solutions to the measured data. Once the noise is identified, one can take steps to reduce or remove it.

Unfortunately, one does not have apriori a very accurate indication of C_{D_o}, k, k_1, k_2, C_{L_α}, and $C_{L_{\alpha=o}}$ so that one's knowledge of these coefficient values will improve in the process. Convergence to the correct values cannot be guaranteed.

Lift Computation

Once the power into the airstream has been determined, it becomes a relatively straightforward task to determine the lift time history. We note that the equation of motion of the vehicle in the direction normal to flightpath in the terrestrial x-z plane is

$$L - W\cos\gamma + T\sin\alpha = V\dot{\gamma}\frac{W}{g} \tag{A.55}$$

from which we may easily obtain

$$C_L = \frac{2W}{\rho S V^2}\left[\frac{V}{g}(\dot{\theta} - \dot{\alpha}) - \frac{P\sin\alpha}{WV} + \cos(\theta - \alpha)\right] . \tag{A.56}$$

Presumbably, W, ρ, V, $\dot{\theta}$, θ, and α are measured directly as functions of time during flight while $\dot{\alpha}$ is obtained by differentiating $\alpha(t)$. A value for P is also a result of the process which extracts $C_D(\alpha)$. This P may be stated as a function of V alone (as in equation (A.4)) or as a more general function, say in terms of V and ρ. In either case

substitution of this value in the foregoing equation then yields $C_L(t)$. By correlating $C_L(t)$ with $\alpha(t)$ it is possible to develop $C_L(\alpha)$ as well as C_L/C_D as a function of α.

APPENDIX A

REFERENCES

A.1 Taylor, Lawrence, W.: A System Identification Using a Modified Newton-Raphson Method -- A Fortran Program. NASA TN D-6734, 1972.

A.2 Oswald, W. Bailey: General Formulas and Charts for the Calculation of Airplane Performance. NACA TR-408, 1932.

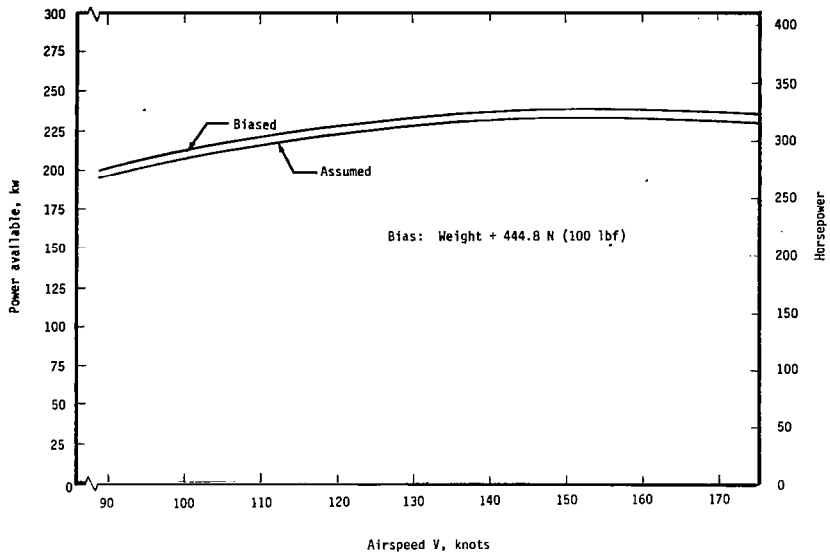

(a) Extracted power coefficient

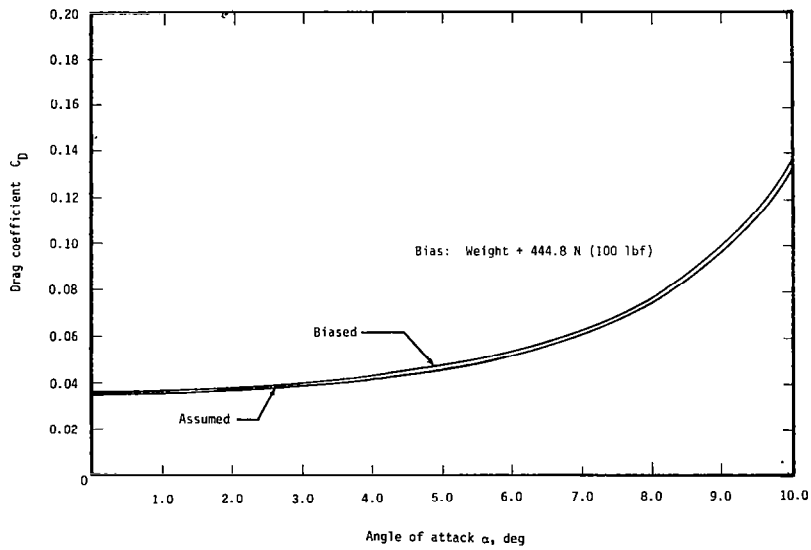

(b) Extracted drag coefficient

Figure A.1- The effect of weight biasing.

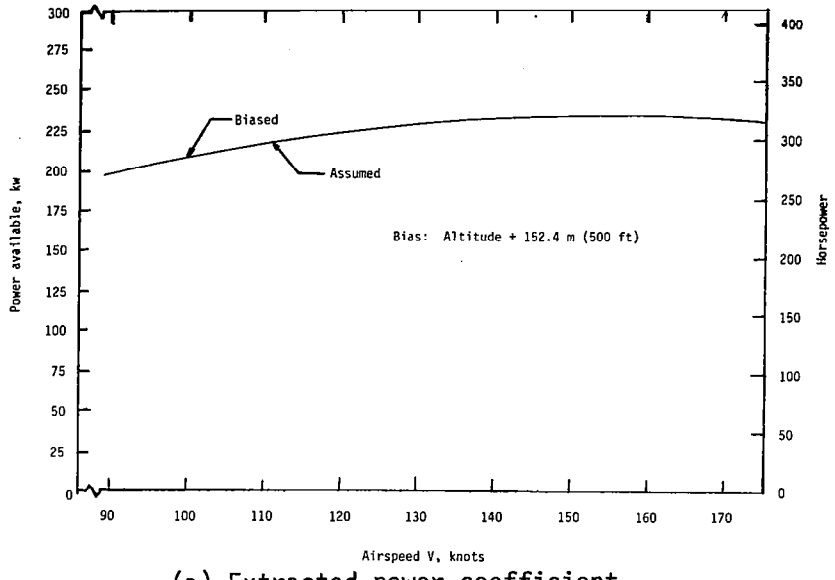

(a) Extracted power coefficient

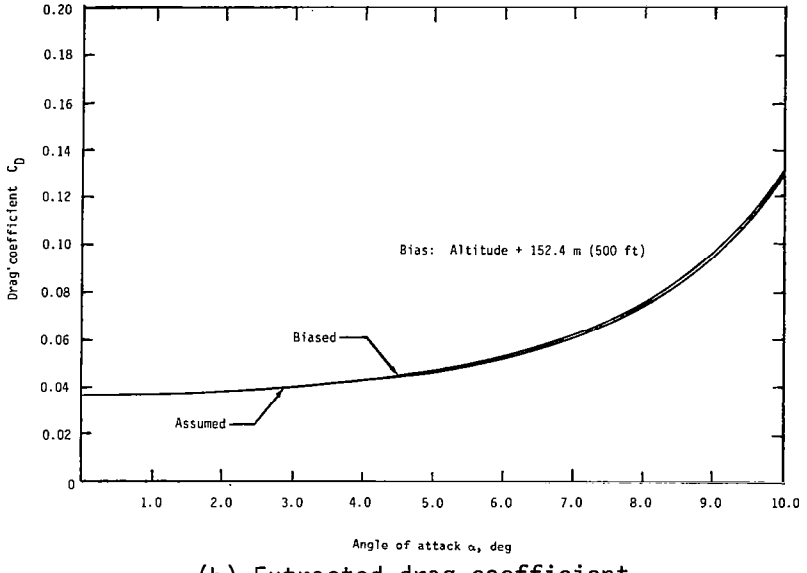

(b) Extracted drag coefficient

Figure A.2- The effect of altitude biasing.

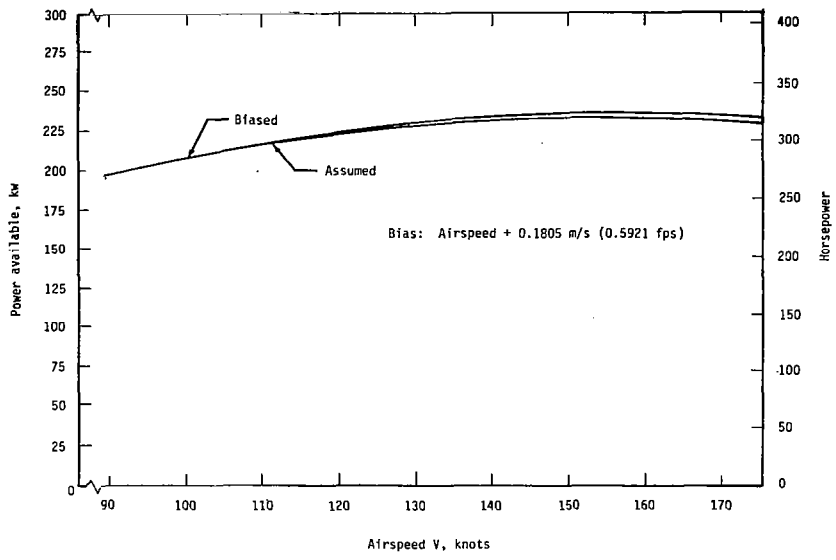

(a) Extracted power coefficient

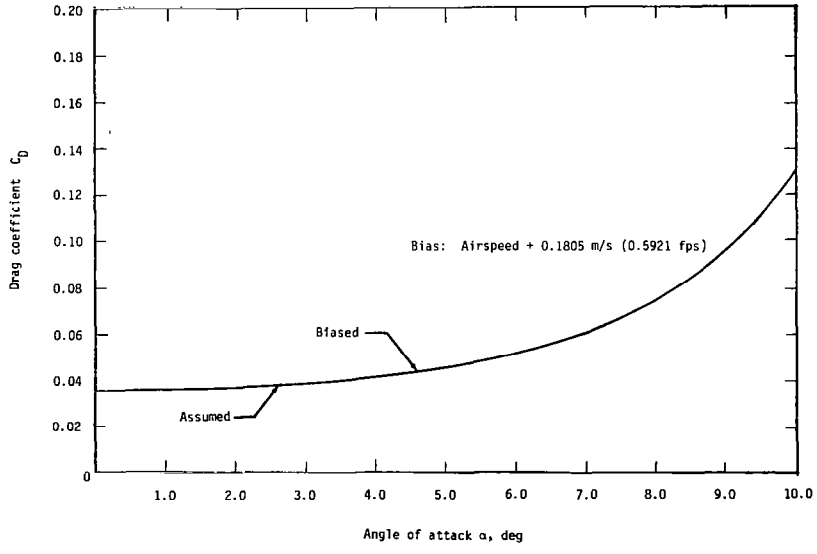

(b) Extracted drag coefficient

Figure A.3- The effect of airspeed biasing

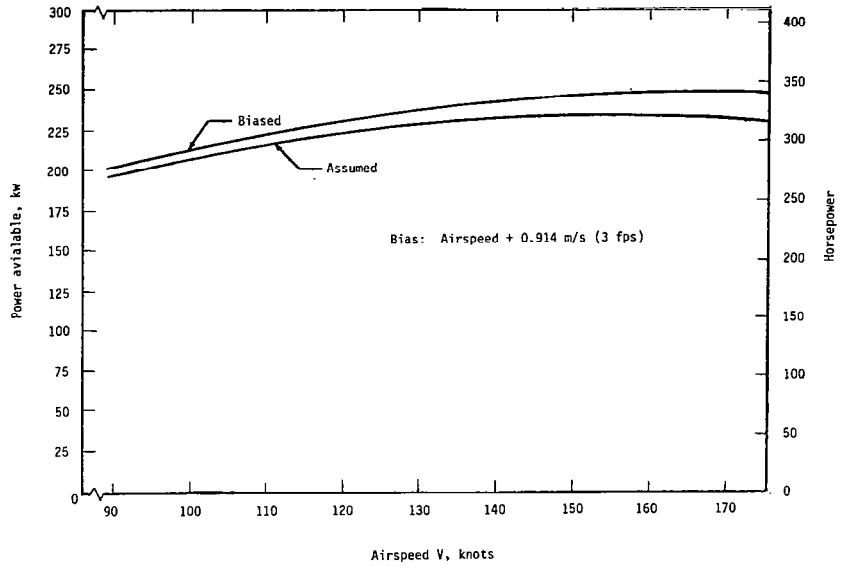

(a) Extracted power coefficient

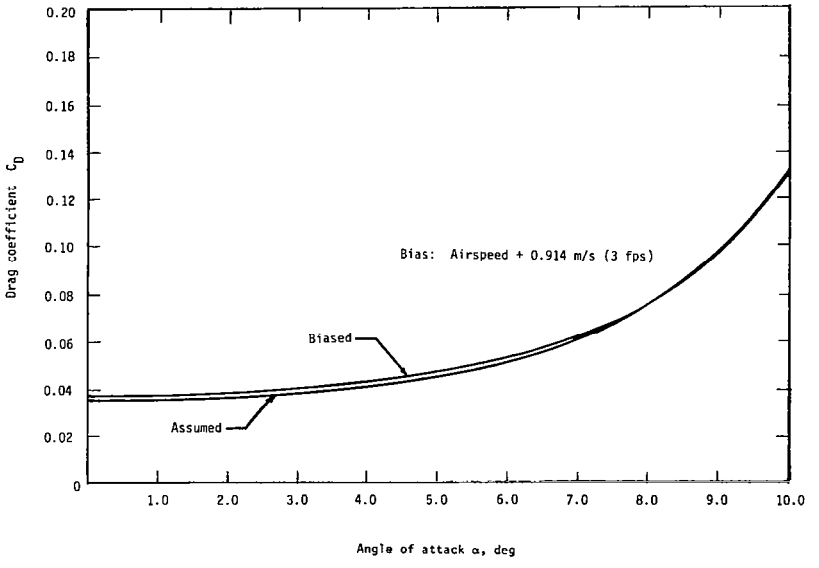

(b) Extracted drag coefficient

Figure A.4- The effect of airspeed biasing

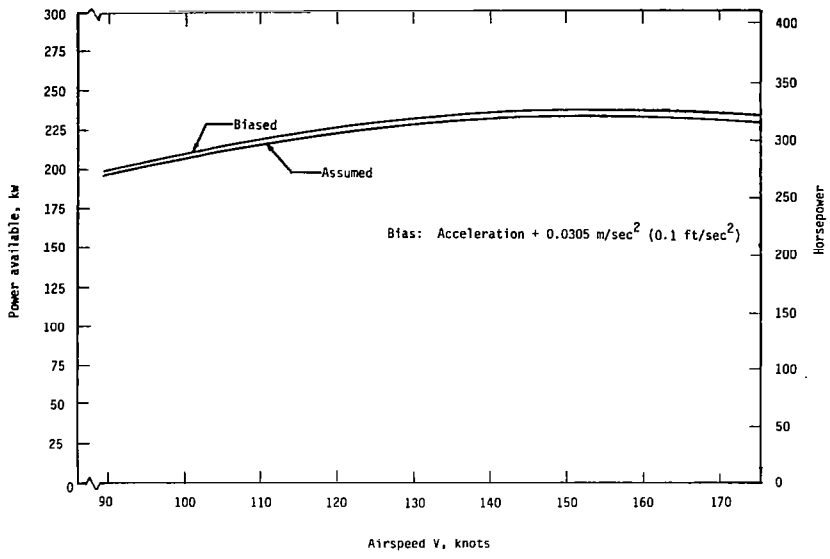

(a) Extracted power coefficient

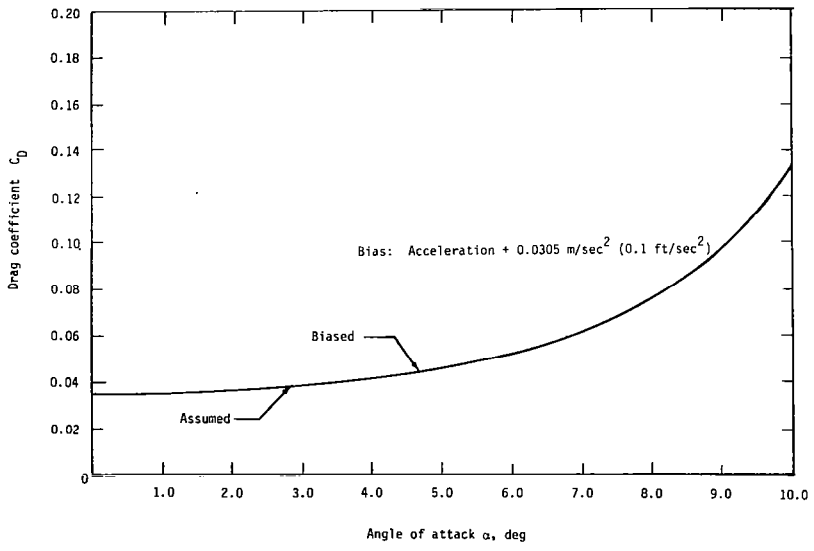

(b) Extracted drag coefficient

Figure A.5- The effect of acceleration biasing

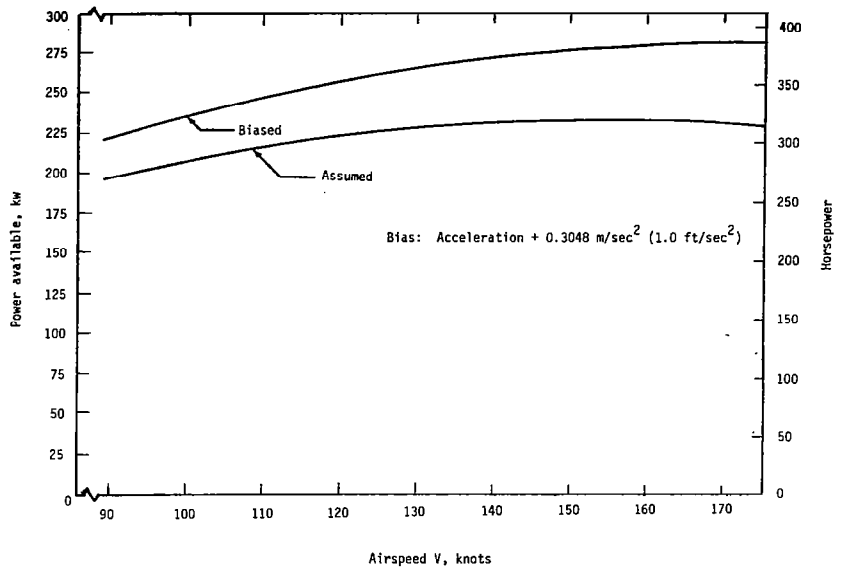

(a) Extracted power coefficient

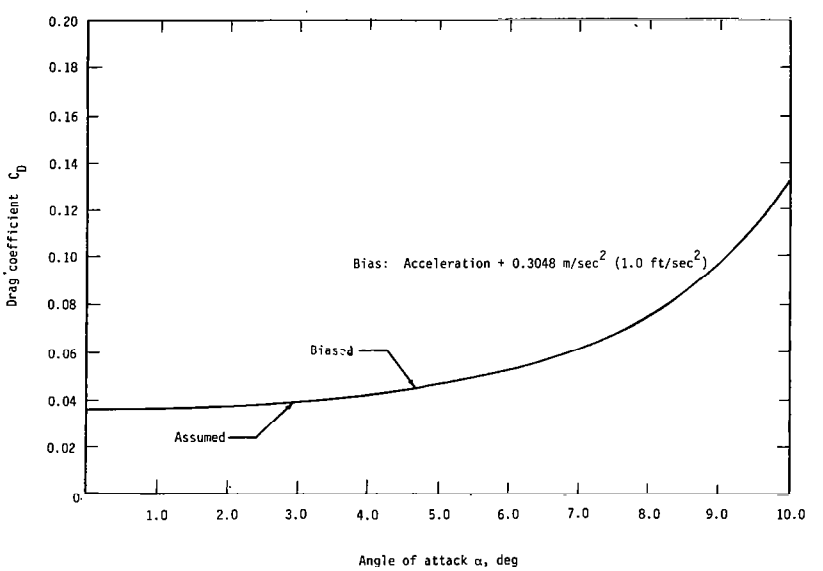

(b) Extracted drag coefficient

Figure A.6- The effect of acceleration biasing

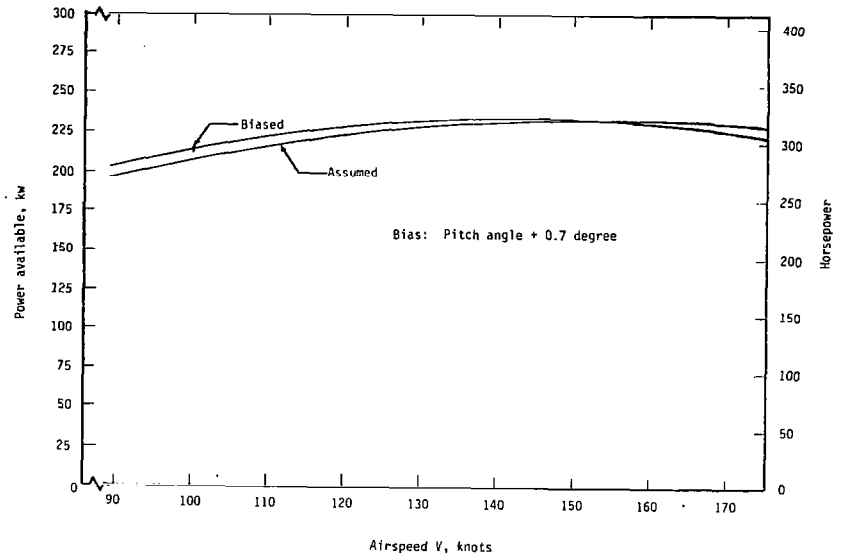

(a) Extracted power coefficient

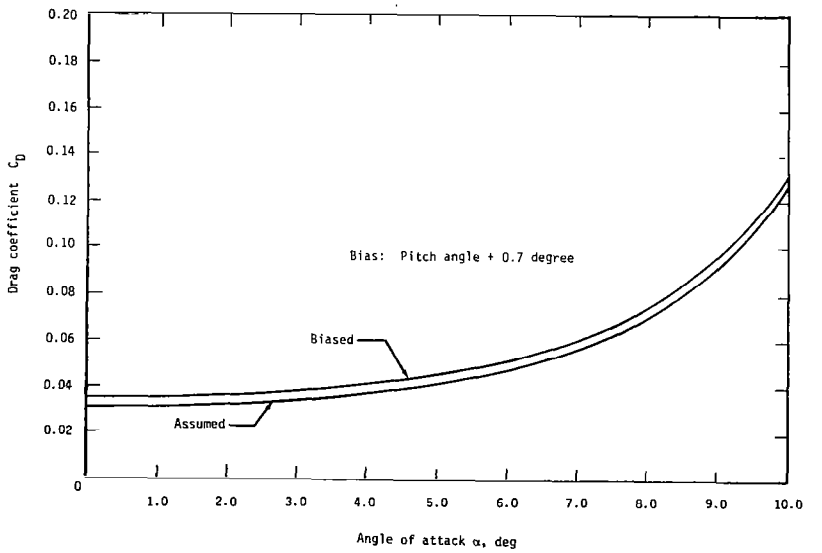

(b) Extracted drag coefficient

Figure A.7- The effect of pitch angle biasing

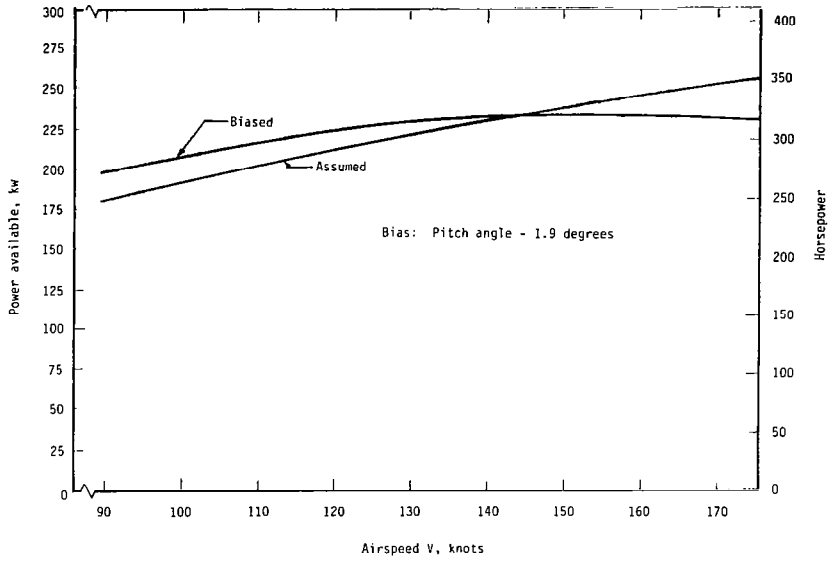

(a) Extracted power coefficient

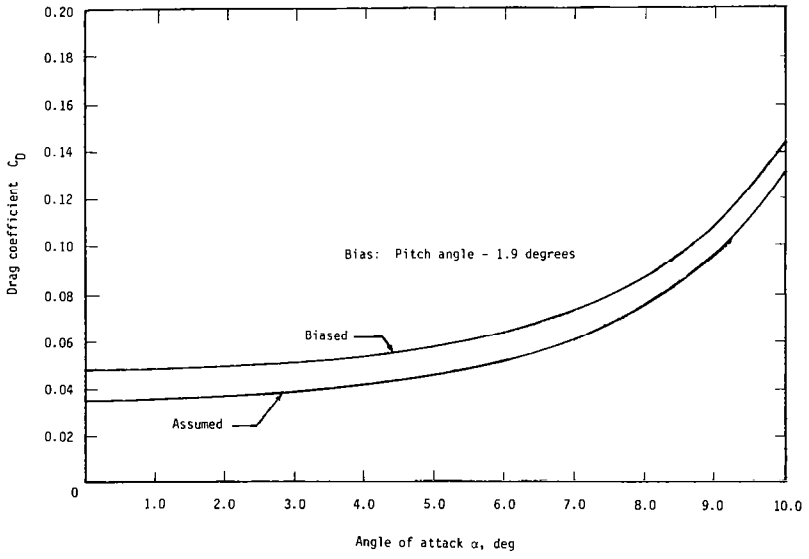

(b) Extracted drag coefficient

Figure A.8- The effect of pitch angle biasing

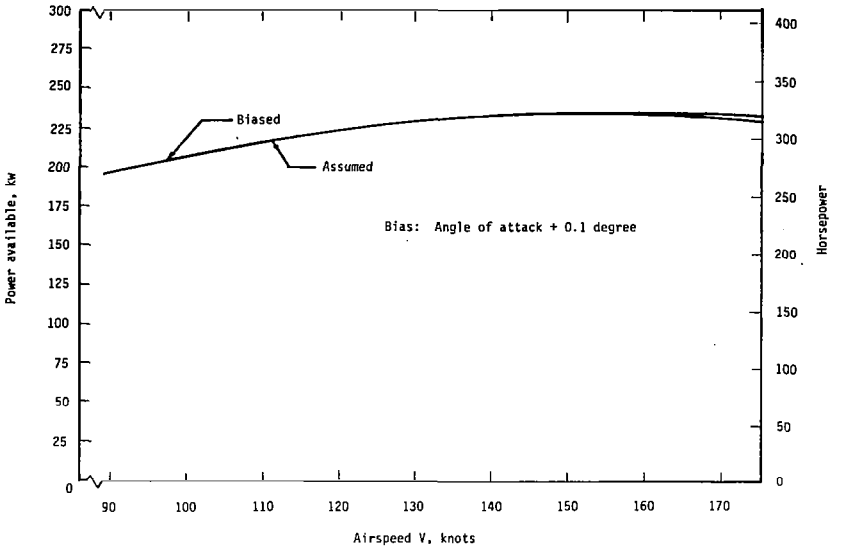

(a) Extracted power coefficient

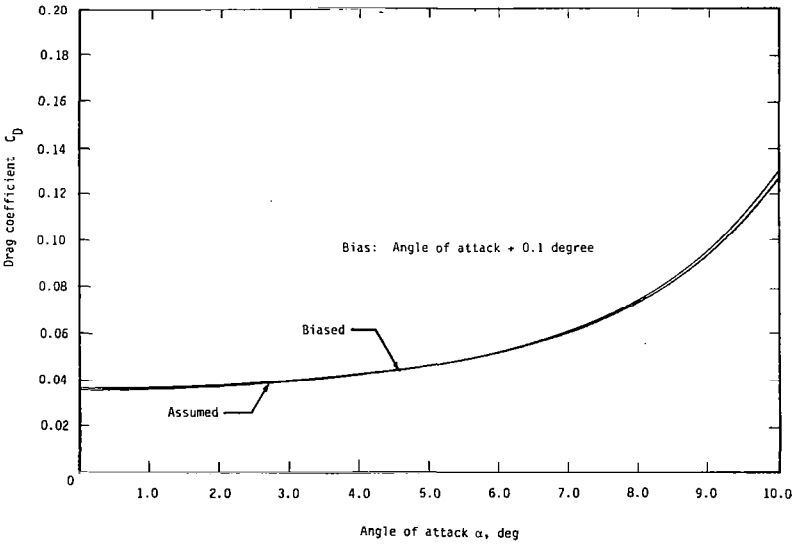

(b) Extracted drag coefficient

Figure A.9- The effect of angle of attack biasing

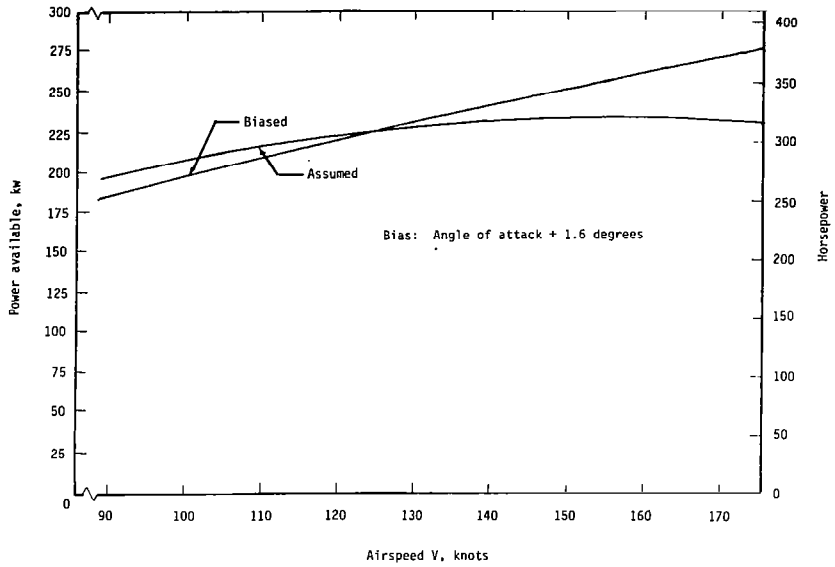

(a) Extracted power coefficient

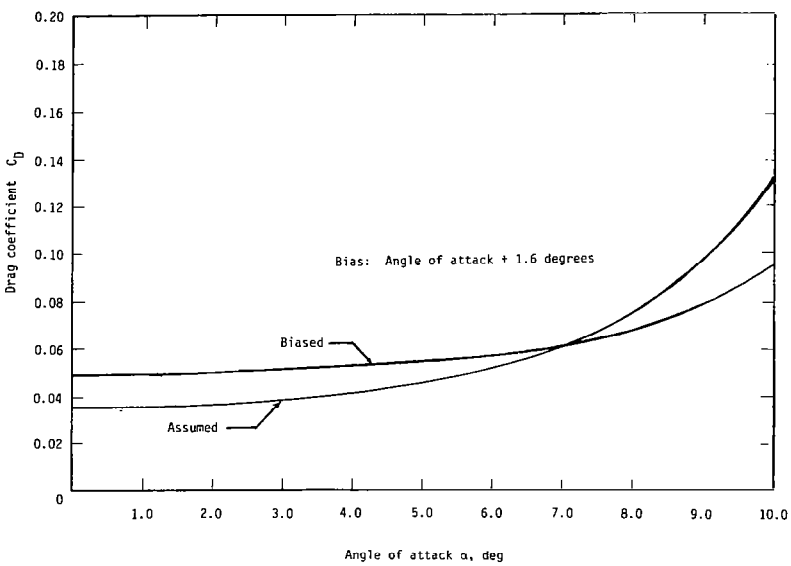

(b) Extracted drag coefficient

Figure A.10- The effect of angle of attack biasing.

APPENDIX B

POSITION-ERROR CALIBRATIONS FOR STATIC PRESSURE AND ANGLE OF ATTACK

APPENDIX B

POSITION-ERROR CALIBRATIONS FOR STATIC PRESSURE AND ANGLE OF ATTACK

The purpose of this appendix is to present instrumentation, methods, data reduction, results, and conclusions on position-error calibrations for static pressure and angle-of-attack measurements. It should be noted that the pressure calibrations are performed only for static pressure; that is, it is assumed that total pressure is measured accurately.

STATIC-PRESSURE POSITION-ERROR CALIBRATION

Instrumentation and Equipment

In addition to the onboard instrumentation described in Chapter 4.2, the static-pressure calibrations required the following additional equipment.

Trailing Anemometer Installation.- The installation of the trailing anemometer on ATLIT is shown in figure B.1. The self-contained system consists of: (1) an anemometer airspeed sensor which is trailed from the aircraft by a cable in the undisturbed airflow, (2) a mechanism to deploy and retract the cable which supports the sensor, (3) the operator's control box, and (4) a 27 volt d.c. power supply to drive the deployment mechanism. Details on the installation and operation of this device are found in reference B.1. Details on the design and construction of the device are presently unpublished.

Based on wind-tunnel calibrations, the anemometer airspeed sensor is accurate to within ±0.5 kt of true airspeed. With data system accuracies, this degrades to ±1.kts. The computed location (reference B.2) of the device below and behind the aircraft is shown in figure B.3. These locations are based on an extension of 30.48m (100 ft - 2½ wingspans) of cable. Also, based on calculations of reference B.2, the anemometer locations shown in figure B.2 will result in an airplane-induced error in measured airspeed less than 0.23 percent. This airplane-induced error converts to an airspeed-position error of less than 0.3 kt (0.35 mph) at 130 kts (150 mph).

Tower Flyby Equipment.- The tower flybys were performed at NASA Wallops Flight Center. The only airplane equipment required for the method was a C-band transponder beacon compatible with the AN/FPQ-6 radar at Wallops. The AN/FPQ-6 radar facility was used to produce a time history of the aircraft location during the test runs. The angular precision of this radar is ±0.05 mils (RMS) (from unpublished data). The tower involved in the flyby maneuvers is located 3287.6 m (10,786 ft) from the radar antenna (see figure B.3). At that range, the angular precision gives altitude within ±0.2m (±0.5 ft). The effect of this amount of altitude error on the airspeed calibration parameter, $\Delta p/q'_c$, is shown in figure B.4. An altitude error of ±0.2m (±0.5 ft) results in a maximum airspeed error of ±0.4 kts (at 50 KCAS). This error diminishes with increasing airspeed.

A 76.1m (250 ft) meteorological tower was used for the flybys. The tower was equipped with barometric, wind, humidity, and temperature

recording devices at the 45.7, 61.0, and 76.2 m levels (150, 200, and 250 feet, respectively). Tower barometric pressure measurements were accurate to ±16.76 Pa (±0.35 psf), and tower temperature measurements were accurate to $\pm 0.6^{0}$ C ($\pm 1^{0}$ F). The effects of the temperature errors on the meteorological tower are insignificant.

Table B.1 presents a summary of the accuracies involved in determining velocity by either the trailing anemometer or the tower flyby method. Sample velocity errors have been computed at the velocity limits for each method to illustrate the approximate magnitudes of overall accuracies. The errors indicated for flight-measured variables are derived from the instrumentation accuracies listed in Chapter 4.3. The table shows that with the trailing anemometer method airspeed can be calibrated within ±1.4 knots (one standard deviation) at the low-speed end, and within ±0.9 knots (one standard deviation) near the upper speed limit for this device. Accuracies for the tower-flyby method range from ±2.6 knots (one standard deviation) at 90 knots, to ±1.3 knots (one standard deviation) at about 170 knots.

This analysis of accuracies makes it evident that the trailing anemometer, not considering its airspeed limitations, is more accurate than the tower-flyby technique. Also, the tower flyby requires much greater accuracy for flight-measured static pressure. A 1500m (5000 ft) altimeter was used on ATLIT for this purpose; therefore, the accuracy in flight-measured p is better for the tower flyby than for the trailing anemometer where a 0 to 102.4 kPa (15 psia) pressure transducer was used.

A large error can be tolerated in flight-measured p with the trailing anemometer method, but not with the tower-flyby method.

Experimental Methods and Flight-Test Programs

Static Pressure Calibration with the Trailing Anemometer.- Two calibration techniques were used with the trailing anemometer device. First, steady-state data were gathered in the conventional manner, during unaccelerated level flight. Second, quasi-steady-state data were gathered during slow decelerations (a_x less than one knot per second) in level flight. The deceleration is accomplished by gradually reducing power starting with power required for the maximum speed in the configuration of interest and bleeding power off until the stall occurs. The power-off data were gathered by idling the throttles at the maximum speed of interest in a configuration and decelerating to the stall.

With either the static or the continuous deceleration method (steady state or quasi-steady state, respectively), the calibration theory is the same. At each speed of interest during a test run, the true airspeed from the trailing anemometer can be compared to the true airspeed as computed from the onboard measurements of dynamic pressure, static pressure, and temperature. The difference in velocities is the position error. This position error will be presented as static-pressure error.

No demanding pilot techniques are required for either the static or dynamic trailing anemometer methods. During the continuous calibration maneuver, a simple form of quality control is accomplished by timing the maneuver from beginning to end to determine that the average flightpath deceleration is less than one knot per second. This assures the effects of pitot-static-system pneumatic lag and time-dependent aerodynamics can be ignored. It is also necessary that the throttle(s) be smoothly

retarded with as little "jockeying" as possible. Jerky motions during retarding of the throttles can result in fore and aft swinging of the trailing anemometer, making data reduction difficult.

Static Pressure Calibration by Tower Flyby.- The procedure for static-pressure system calibration by tower flyby consists of flying the airplane at the same geometric altitude as a fixed-barometric pressure recording device. The static-pressure error is determined by comparing the static pressured measured onboard the airplane to the pressure measured with the fixed-barometric pressure recording device on the tower.

The test-pilot technique for the tower flyby consists of passing the tower at constant power setting while striving to maintain constant altitude. During these constant-power, constant-altitude flybys, airspeed is allowed to vary. Of the two, airspeed and altitude, it can be shown that accurate determination of altitude at the tower passage is critical to the overall accuracy of this method.

Flight-Test Programs

The methods used for the calibration of the static pressure measuring system on the ATLIT were determined by the equipment readily available for the task. The use of two overlapping methods, trailing anemometer and tower flyby was necessitated by the limitations of each. In general, the trailing anemometer covered the low-speed end of the flight envelope and the tower-flyby method covered the high-speed end.

The tests were conducted in smooth air. Table B.2 presents the configuration/airspeed combinations for which calibration tests were performed.

Test Conditions for the Trailing Anemometer.- Calibration tests with the trailing anemometer are limited to a maximum speed of 165 knots (190 mph). This is the speed at which cable instability is predicted for the anemometer device used. An additional limiting consideration is the maximum cable trail-back angle which is considered safe for the airplane on which the device is installed. The trail-back angle for the installation on ATLIT was computed at 135 knots to be about 5 degrees (from horizontal, at the aircraft), which allowed for safe clearance between the cable and the airplane empennage.

Tests were run to determine the effects of landing gear position, flap deflection, and power on static-pressure position error. The testing was done at a pressure altitude of about 305m (1000 ft). The airplane weight during these tests varied from 17570 N (3950 lb) to 17348 N (3900 lb) at a CG of about 16-percent mac. If position-error data are plotted against angle of attack, neither weight nor CG location will have a significant effect on the static-pressure error at the noseboom. However, since position error as a function of airspeed (V_C') is more readily interpreted, the present data appear plotted in this manner with V_C' corrected to gross weight (4200 lb).

Test Conditions for the Tower Flybys.- Calibration of static-pressure error by the tower-flyby technique is limited by safety considerations to speeds above a certain minimum. A safe margin above stall speed is required because of the close proximity of the airplane to the ground during the passes by the meteorological tower. For ATLIT, this meant tower flybys could be done at speeds as low as 85 knots, or a speed margin of about

25 percent above stall speed (flaps 0^{o}). In addition, for speeds below 85 knots (flaps 0^{o}), it becomes difficult to maintain the required level, constant-altitude flight past the tower.

All tower-flyby tests were conducted with flaps up. The airplane weight during these tests varied from 17615 N (3960 lb) to 17259 N (3880 lb) at a CG of about 14-percent mac.

DATA REDUCTION

Trailing Anemometer Data Reduction

Data reduction methods are the same for both the static and the dynamic trailing anemometer techniques.

The static-pressure error is defined as

$$\Delta p = p' - p \tag{B.1}$$

where p' is measured onboard the aircraft and p is the ambient static pressure. For the speed range of the present tests, incompressible flow can be assumed

$$q_c = q = 1/2\ \rho\ V^2 \tag{B.2}$$

where

$$\rho = \frac{p' - \Delta p}{RT} \quad . \tag{B.3}$$

Also

$$q_c = p_t - p = q'_c + \Delta p \quad . \tag{B.4}$$

Equating (2) and (4), and simplifying yields an equation for static-pressure (position) error

$$\Delta p = \frac{\frac{p'V^2}{RT} - q'_c}{1 + \frac{V^2}{2RT}} \qquad (B.5)$$

This derivation appears in detail in reference B.1. In equation (B.5), V is measured with the trailing anemometer and p' and q'_c are measured with the noseboom. Temperature, T, is corrected for adiabatic temperature rise based on measured temperature, T_t

$$T = T_t \frac{\gamma - 1}{1 + \frac{\gamma - 1}{2} \varepsilon M^2} \qquad (B.6)$$

where $\varepsilon = 1.0$ for the ATLIT temperature probe.

In order to handle high sample rate data (10 samples per second) from the continuous calibration maneuvers, the data reduction method was programed for a high-speed digital computer. The program expedites averaging and smoothing the data over selected time intervals of the test run. The resulting data may be either manually faired or numerically curve fitted. Data presented in the figures of this appandix have been manually faired.

Tower Flyby Data Reduction

In the tower-flyby test runs, the difference between the height of the airplane and the height of the barographic device in the tower averaged about 4m (about 13 ft). Therefore, a standard lapse-rate

correction is applied to the tower-reduced static pressure by a form of the hydrostatic equation

$$\Delta p_c = p_1 \left(e^{\frac{-\Delta z}{RT_1}} - 1\right) \quad . \tag{B.7}$$

The actual lapse rate for this correction may be computed based on data from different sensors on the tower.

Then

$$p = p_1 + \Delta p_c \quad . \tag{B.8}$$

The true static pressure, p, is thus determined at the airplane geometric altitude by the standard lapse rate. Pressure, p_1, and emperature, T_1, are measured on the meteorological tower using values from the barograph which is closest to the airplane at tower passage. The difference in geometric altitude between the aircraft and the barograph closest to the aircraft is Δz

$$\Delta z = z_a - z_b \quad . \tag{B.9}$$

Once the atmospheric-static pressure (p) at the airplane geometric height has been determined, the static-pressure error is the difference between p and the static pressure measured with the airplane noseboom (p') at the time of tower passage

$$\Delta p = p' - p \quad . \tag{B.10}$$

RESULTS AND DISCUSSION

A comparison is presented in figure B.5 of static and continuous trailing anemometer data and tower-flyby data (flaps up). It is shown that data gathered by these techniques fall within the same region of

experimental scatter. The bars on the trailing anemometer static-run points indicate the extremes in calculated results due to instrumentation errors.

At cruise speed for ATLIT ($\alpha \simeq 0$), $\frac{\Delta p}{q'_c} \simeq 0.015$. Data (3) predict that a boom ($\frac{X}{D} = 1.0$) on a conical body of revolution (nose shape) yields $\frac{\Delta p}{q_c} = 0.01$, and on a parabolic body of revolution, yields $\frac{\Delta p}{q_c} = 0.04$ (both at M = 0.21, $\alpha = 0$ with no lifting wing body only). This agreement between predicted and flight-test values of $\frac{\Delta p}{q'_c}$ is explained by the shape of the ATLIT fuselage nose resembling some combination of the parabolic and conical nose shapes tested in reference B.3. No data exist which allow accurate prediction of $\frac{\Delta p}{q'_c}$ for a given airplane configuration with varying α, M, and δ_f. The shape of the ATLIT airspeed-calibration curve agrees with trends for noseboom installation in reference B.3.

Figure B.6 presents the effects on flaps-up airspeed calibration of power on and off and landing gear up and down. It was found that the gear effects were minimal; therefore, all data are presented gear up.

Figure B.7 presents the effects of increasing flap deflections on airspeed-calibration curves. It is noted that the shape of the curve is largely unaffected by flap position, but the location of the curve shifts with changing flap deflection. The effect of power-on position error is greater with flaps deflected 30 degrees than with flaps up.

In general, the reduction in position error $\frac{\Delta p}{q'_c}$ achieved by mounted pressure sources on a boom is smaller in magnitude than the accuracy with which these position errors may be calibrated. Thus, the error in a calibrated boom-mounted pressure source is no less than the error in a calibrated pressure source mounted closer to the aircraft.

CONCLUSIONS CONCERNING AIRSPEED CALIBRATION

1. Use of the trailing anemometer device during a continuous calibration maneuver (gradual deceleration from maximum to minimum airspeed in a given configuration) produces the same results as data gathered during conventional steady-state (static) runs. The advantage of the continuous maneuver is a reduction by a factor of about 10 in the flight time required to do an airspeed calibration.
2. Airspeed calibration data from the tower-flyby method agree with data from the trailing anemometer methods.
3. The effect of landing gear position on airspeed calibration is negligible for ATLIT.
4. The effect of power-on airspeed calibration is significant for ATLIT. The effect of power-on position error is greater with flaps down than with flaps up.
5. The value in the use of a "long" instrumentation boom is questionable. Conventional practice dictates the use of standard lengths of nose or wing booms for pressure and airflow direction measurements. Typically, the boom length is prescribed as 1.5 body diameters (in the case of a nose boom) or 1.0 chord lengths (in the case of

a wing boom) in order to minimize position errors in pressure and airflow direction measurements. It can be argued that, if an installation is to be calibrated, the prescribed boom lengths can be shortened considerably. It can be shown that the calibration methods used have greater accuracy than the accuracy achieved in uncalibrated measurements from sensors on booms of the above lengths. For installations which are to remain uncalibrated, the above boom lengths would be appropriate, yielding pressure- and flow-direction measurements with minimal position errors.

ANGLE OF ATTACK POSITION-ERROR CALIBRATION

Calibration flights were performed to determine angle-of-attack position errors due to the airplane influence field. The test methods, data reduction, and results are discussed below.

No additional instrumentation was required other than that described in Chapter 4.3.

The calibration method used consists of equating indicated angle of attack (α') to pitch attitude angle (Θ) in straight and level flight conditions ($\alpha = 0$). True angle of attack (α) is defined for the present tests as the angle between the airplane longitudinal axis and the freestream velocity, or $\alpha = \Theta$.

An effective means of smoothing the scatter in the flight measured α and Θ is achieved by plotting C_L against both α and α'. Since the shape of these curves can be confidently faired through the

flight data (see figures B.8 and B.9), the angle-of-attack calibration curves are readily determined by plotting α vs. α' at constant C_L's (see figure B.10).

Calibrations were made for flap settings of 0^o, 10^o, and 30^o. Tests were run with airplane-weight variations from 17300 N (3900 lb) to 18700 N (4200 lb). Center-of-gravity (CG) locations during the tests ranged from 12-percent mac to 15-percent mac. The varying CG locations result in different distributions of lift between the main wing and the horizontal tail; therefore, a given value of C_L could be generated by different angles of attack. The resulting effect on the flow field at the angle-of-attack vane is small and has been neglected.

Results show a linear calibration correction between α' and α in the linear range of the C_L vs α curves. The slope of the flaps-up calibration curve (figure B.10) is 0.867. The figure also shows the effect of flap deflection on the angle-of-attack position-error calibration.

The accuracy to which angle of attack may be calibrated by this method is limited to the accuracy of the vertical gyro. The gyro accuracy in the present tests is $\pm 0.7^o$.

APPENDIX B - REFERENCES

B.1 Fisher, Bruce D.; Stough, H. Paul; and Kershner, David D.: Trailing Anemometer for Low-Airspeed Calibration. SAE Paper No. 760461, presented at the National Business Aircraft Meeting, Wichita, April 1976.

B.2 Glauert, H.: Heavy Flexible Cable for Towing a Heavy Body Below an Aeroplane. Aeronautical Research Committee Reports and Memoranda No. 1592, London, 1934.

B.3 Gracey, William: Measurement of Static Pressure on Aircraft. NACA TR 1364 (supercedes NACA TN-4184), 1957.

B.4 Thompson, Floyd L.: The Measurement of Airspeed of Airplanes. NACA TN-616, 1937.

TABLE B.1.- SUMMARY OF STATIC PRESSURE POSITION-ERROR CALIBRATION METHOD ACCURACIES

Method	Source of Error	Sample errors Δ V knots @50 knots	Sample errors Δ V knots @140 knots
Trailing Anemometer	Anemometer Accuracy (Data System Noise and Wind-Tunnel Calibration)	±1.1	±1.1
	Induced Velocity (Fig. B.2)	±0.1	±0.1
	Flight-Measured Static Pressure (±43.2 psfa)	±0.5	±1.4
	Flight-Measured Dynamic Pressure (±1.0 psfd)	±2.9	±0.9
	Flight-Measured Temperature ($\pm 1.0^{o}$ F)	≃0	≃0
	Root Mean Square Accuracy (one standard deviation)	±1.4 kts	±0.9 kts
		@90 knots	@170 knots
Tower Flyby	Radar Angular Precision of ±0.2m (Fig. B.4)	±0.4	≃0
	Tower-Measured Static Pressure (±0.35 psfa)	±0.6	±0.3
	Tower-Measured Temperature	≃0	≃0
	Flight-Measured Static Pressure (±3.5 psfa)	±5.6	±3.0
	Flight-Measured Dynamic Pressure (±1.0 psfd)	±1.6	±0.9
	Flight-Measured Temperature ($\pm 1^{o}$ F)	≃0	≃0
	Root Mean Square Accuracy (one standard deviation)	±2.6 kts	±1.3 kts

FLAPS	GEAR	POWER	V'_c, AIRSPEED	METHOD
0^o	Up	Bleed Off	130 kts to stall	Trailing Anemometer - continuous run
0^o	Down	Bleed Off	130 kts to stall	Trailing Anemometer - continuous run
0^o	Up	Off	130 kts to stall	Trailing Anemometer - continuous run
0^o	Up	For Level Flight	75 kts	Trailing Anemometer - static run
0^o	Up	For Level Flight	90 kts	Trailing Anemometer - static run
0^o	Up	For Level Flight	110 kts	Trailing Anemometer - static run
10^o	Up	Bleed Off	110 kts to stall	Trailing Anemometer - continuous run
20^o	Up	Bleed Off	110 kts to stall	Trailing Anemometer - continuous run
30^o	Up	Bleed Off	110 kts to stall	Trailing Anemometer - continuous run
30^o	Up	Approach	110 kts to stall	Trailing Anemometer - continuous run
40^o	Up	Bleed Off	110 kts to stall	Trailing Anemometer - continuous run
0^o	Up	For Level Flight	87 kts	Tower flyby
0^o	Up	For Level Flight	105 kts	Tower flyby
0^o	Up	For Level Flight	130 kts	Tower flyby

TABLE B.2- CONFIGURATION/AIRSPEED COMBINATIONS FOR ATLIT STATIC PRESSURE-SYSTEM CALIBRATION TESTS.

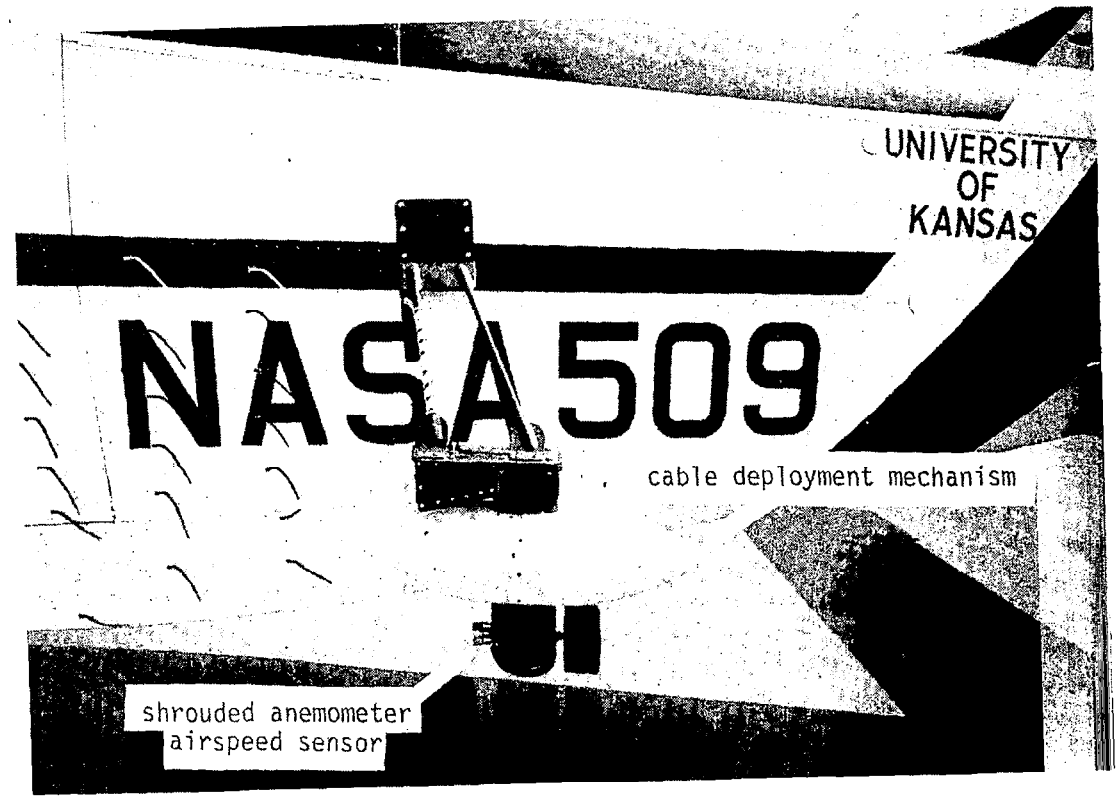

Figure B.1.- ATLIT trailing anemometer installation detail.

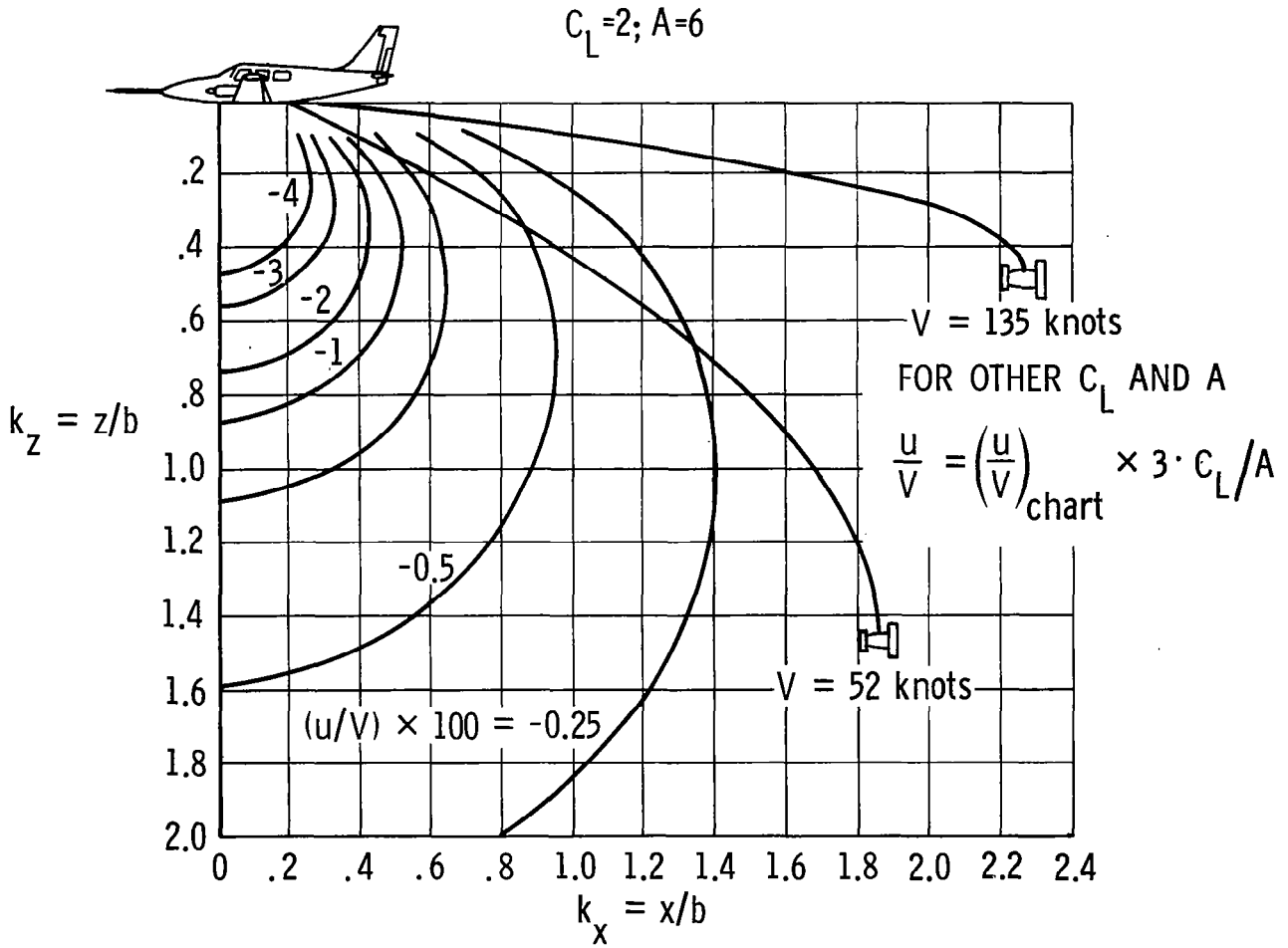

Figure B.2.- Induced velocity contours (from reference B.4) and trailing anemometer locations.

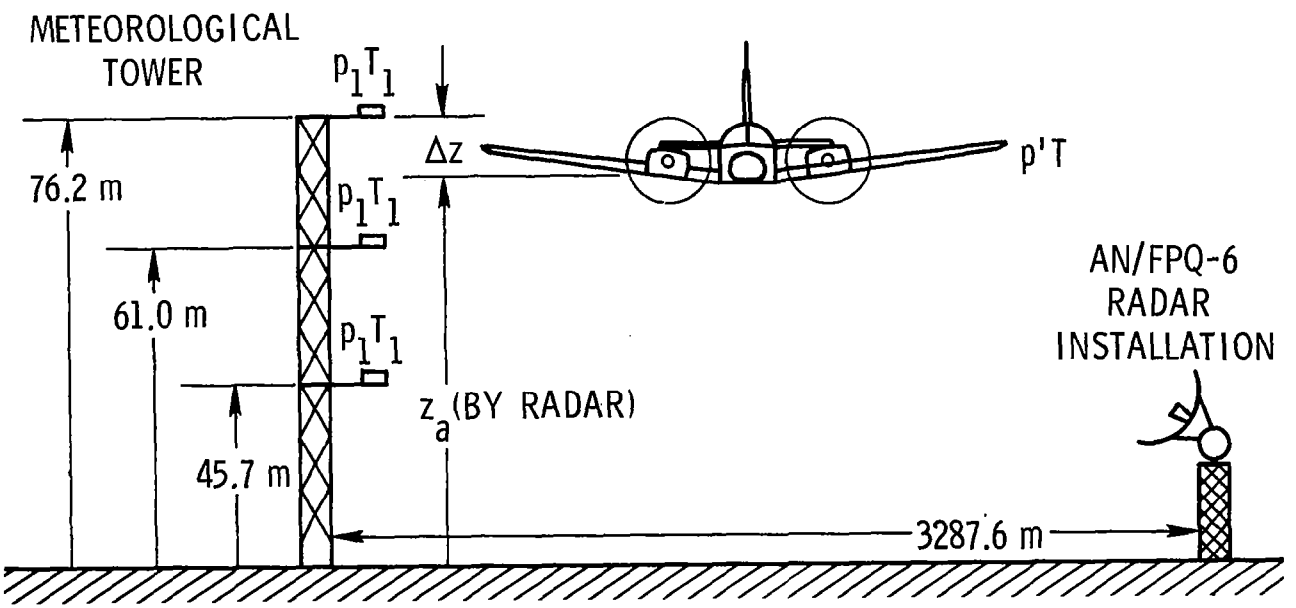

Figure B.3.- Wallops tower flyby airspeed calibration dimensions.

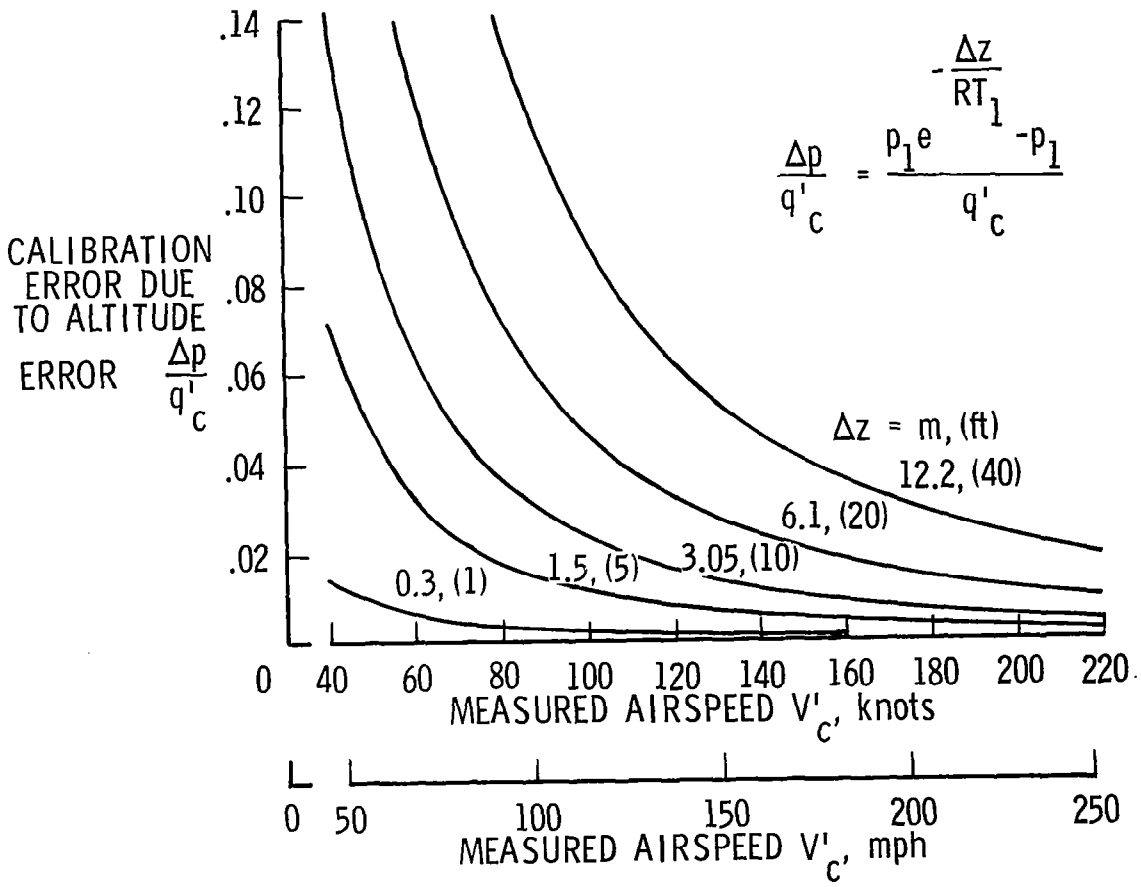

Figure B.4.- Effect of altitude error on tower flyby airspeed calibration.

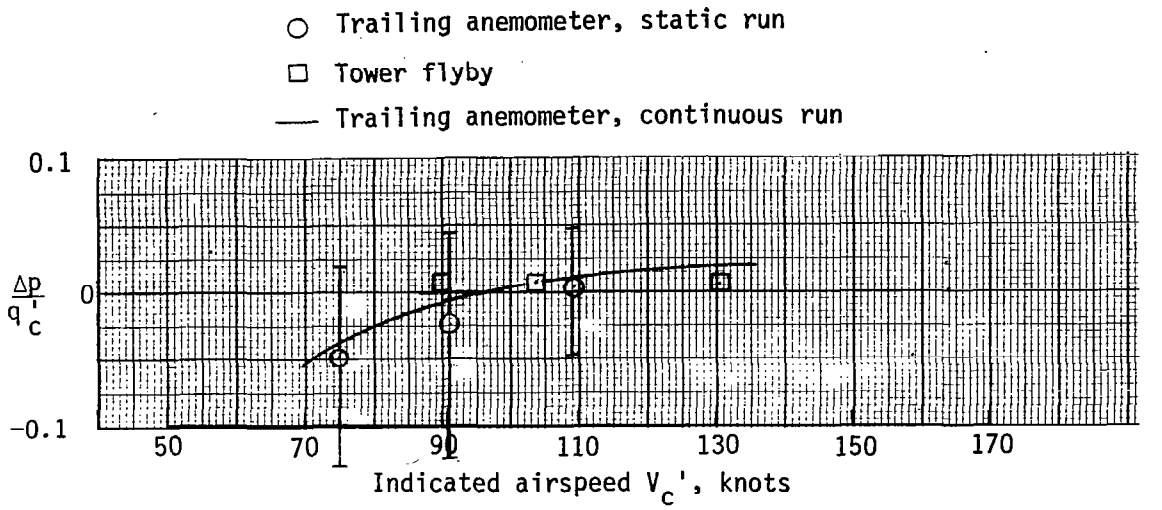

Comparison of Tower Flyby and Trailing Anemometer(Static and Continuous Runs)
Static Pressure Position Error Calibrations(δ_f=0°)

FIGURE B.5

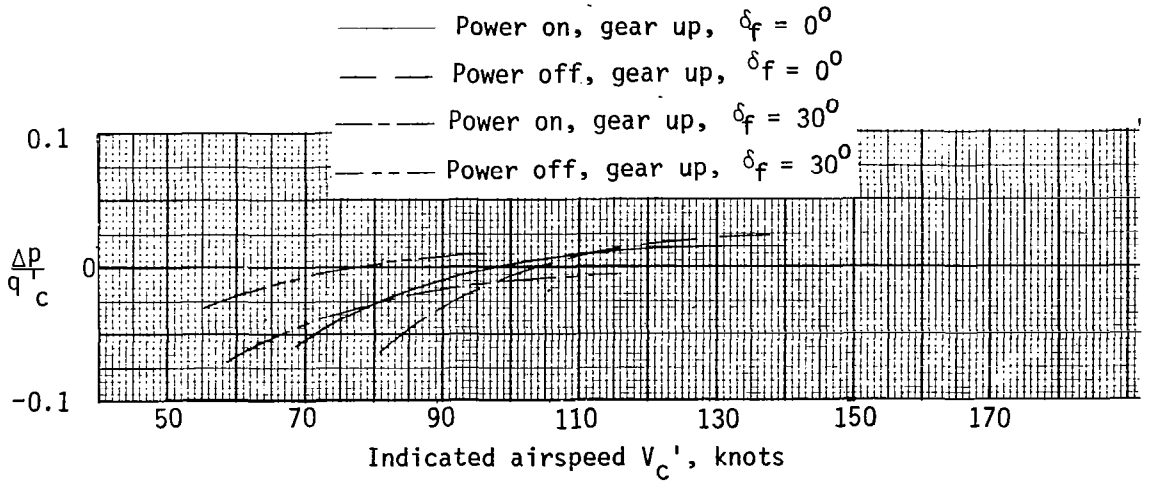

Effect of Power on Static Pressure Position Error Calibrations
(Trailing Anemometer Continuous Runs)

FIGURE B.6

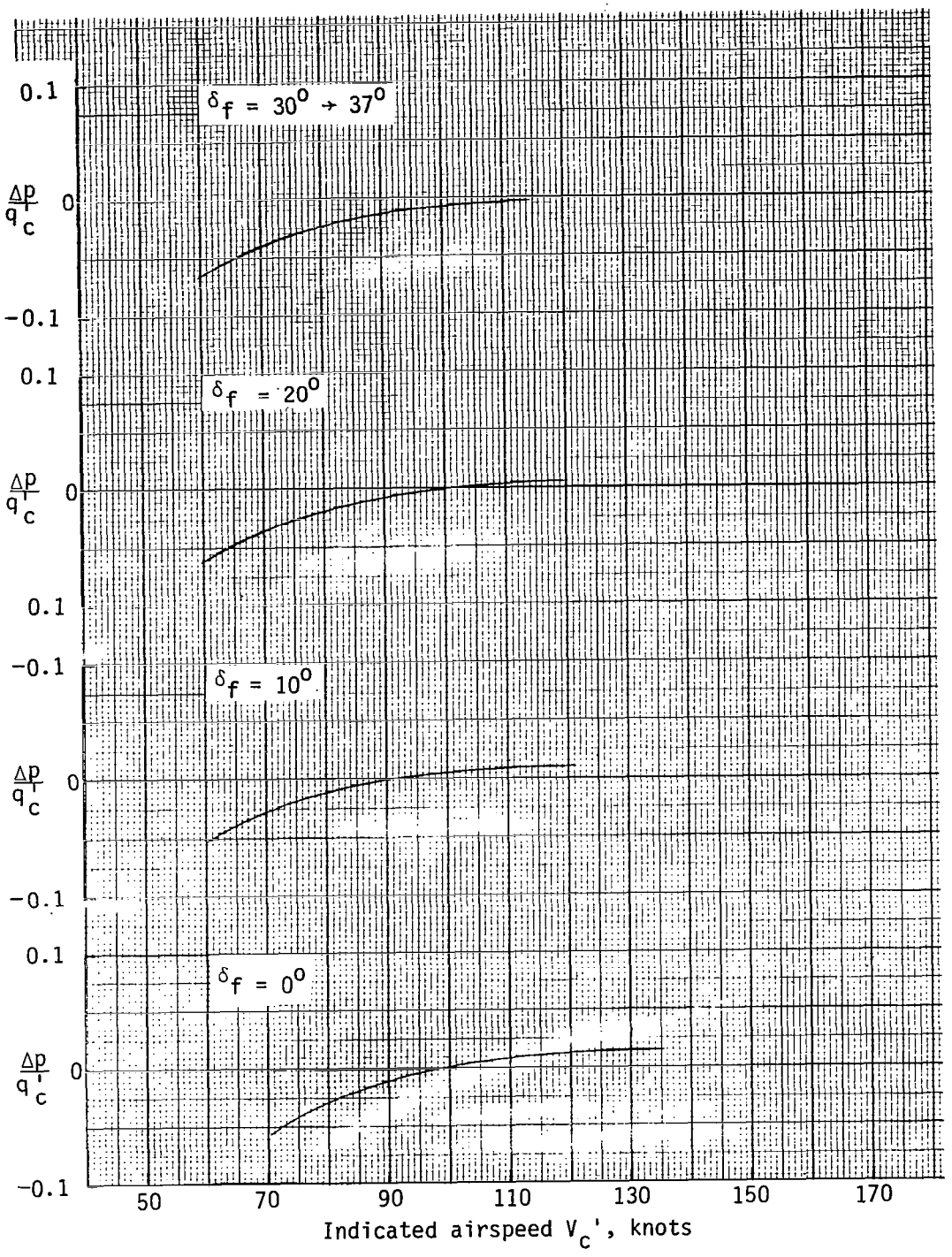

Effect of Flap Deflection on Static Pressure Position Error Calibration
(Trailing Anemometer Continuous Runs) Power on

FIGURE B.7

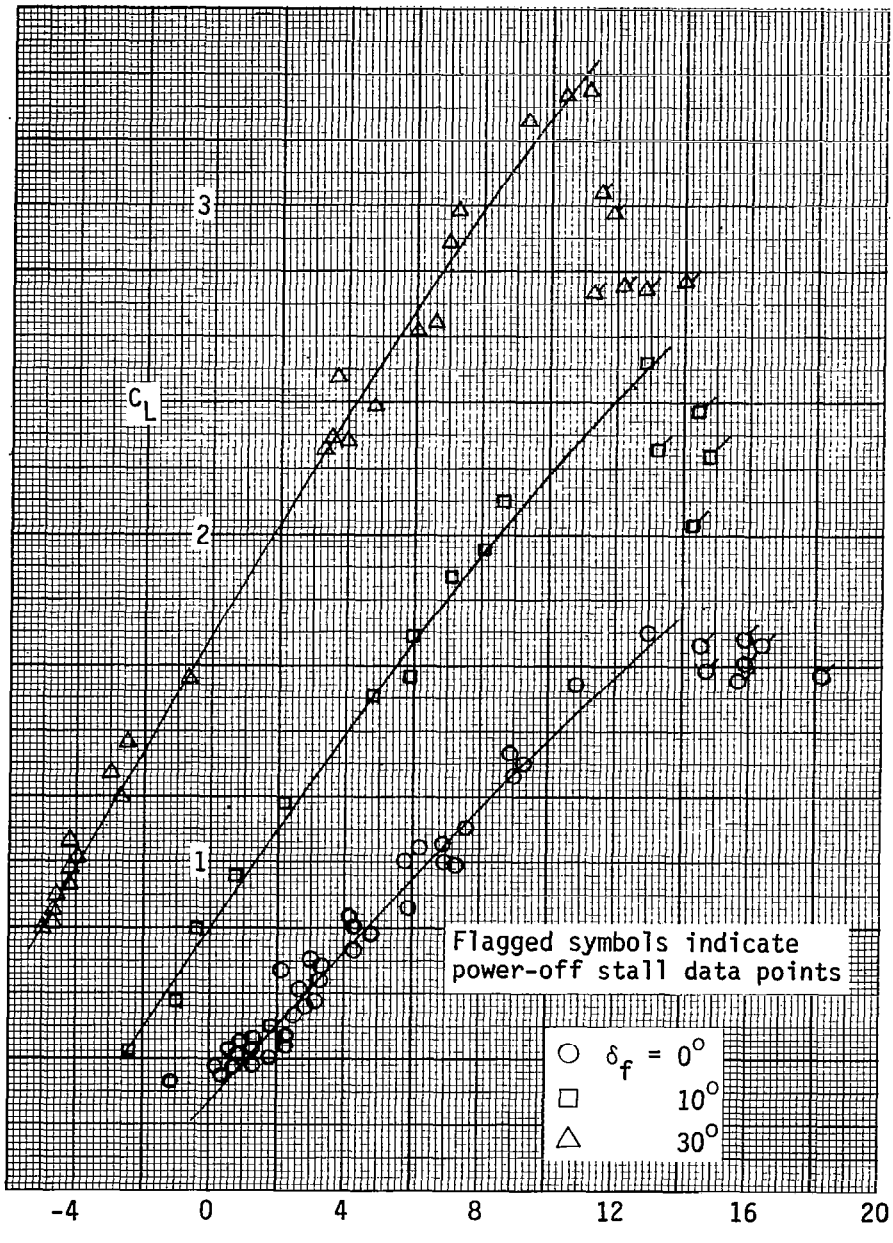

Figure B. 8.- Flight-test lift data for true (geometric) angles of attack (δ_f = 0° (spoiler leak path sealed), 10°, 30°). CG ≃ 15% mac

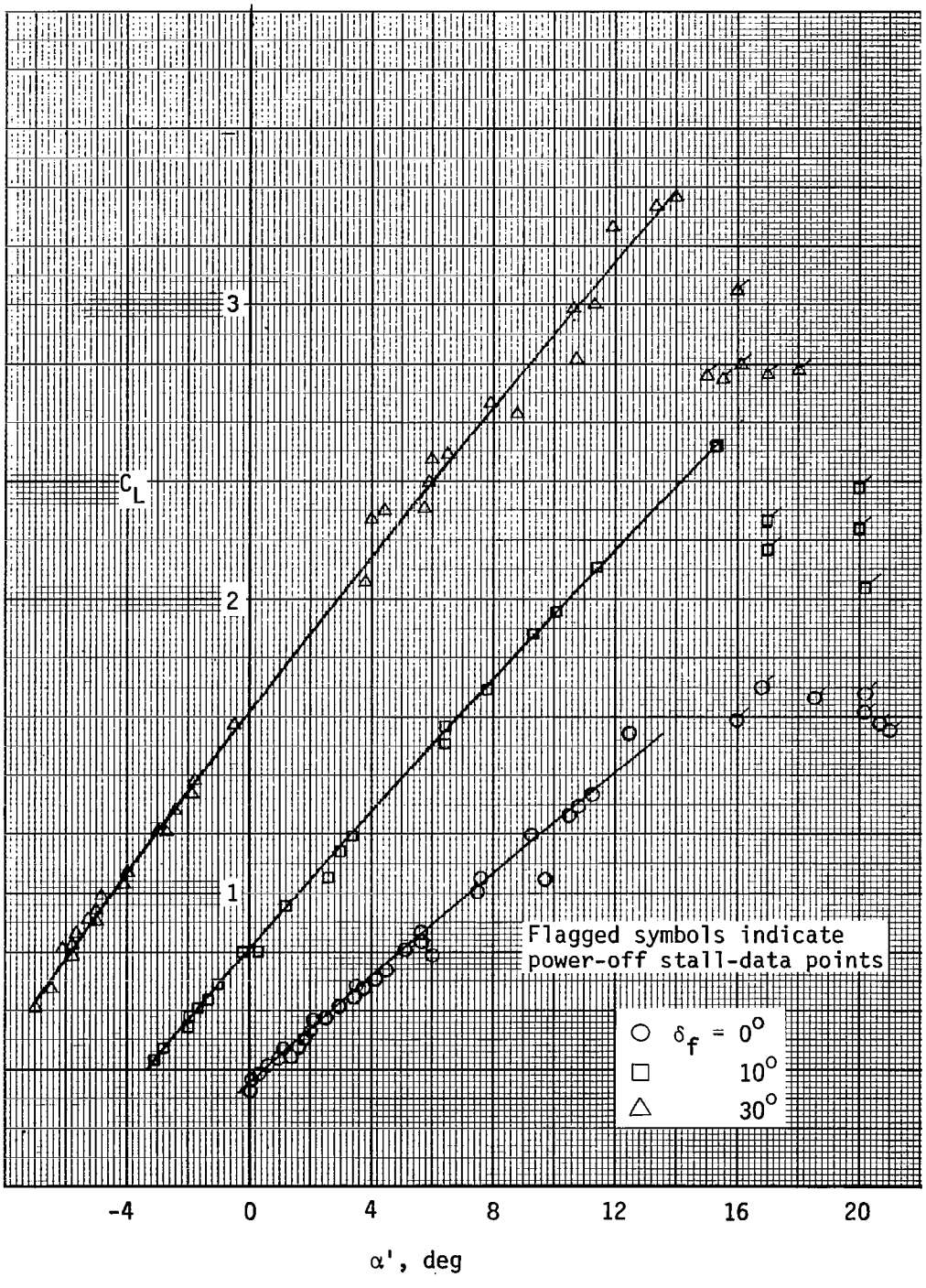

Figure B.9.- Flight-test lift data for indicated angles-of-attack.
(δ_f = 0° (spoiler leak path sealed) 10°, 30°) CG ≈ 15%mac

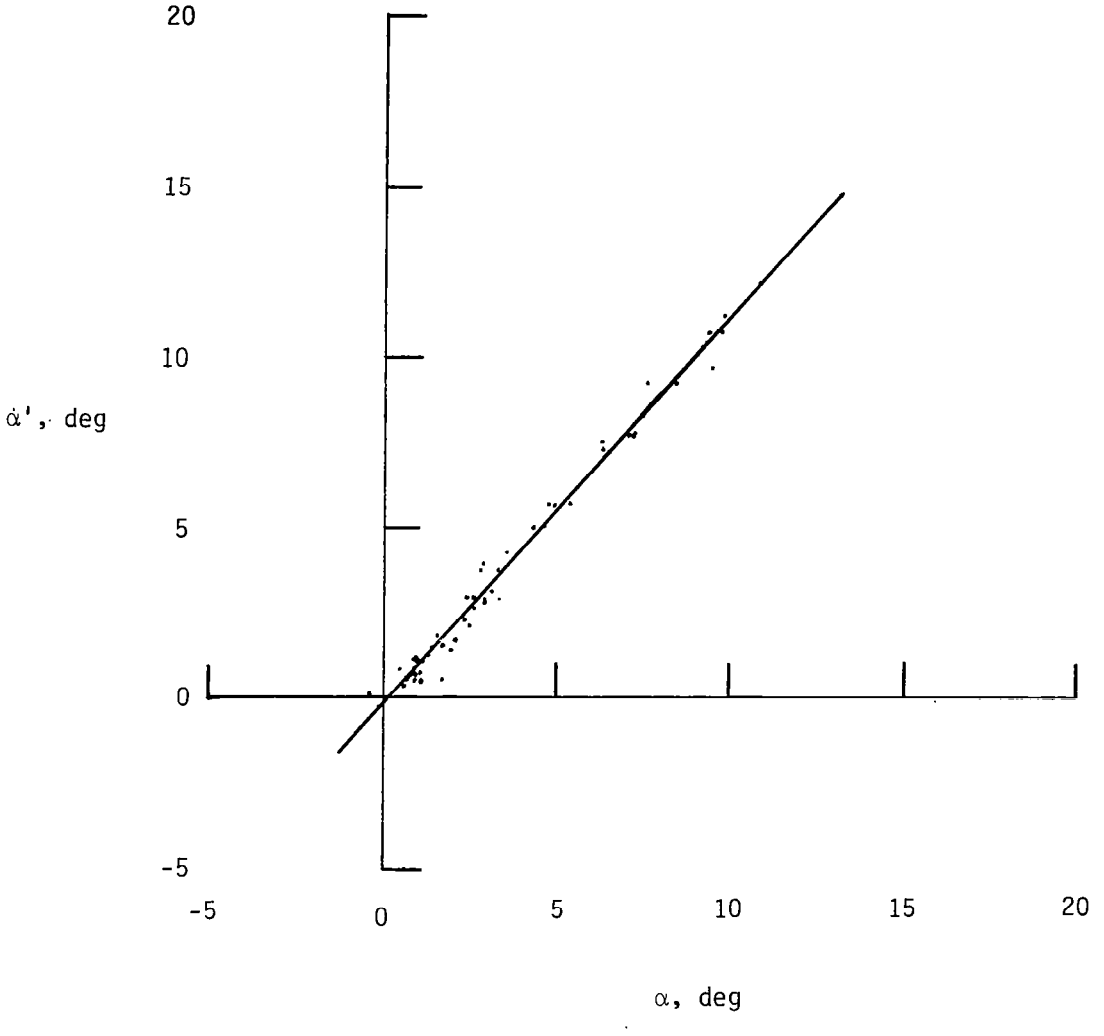

(a) Flaps up

Figure B.10- Angle-of-attack position-error calibrations

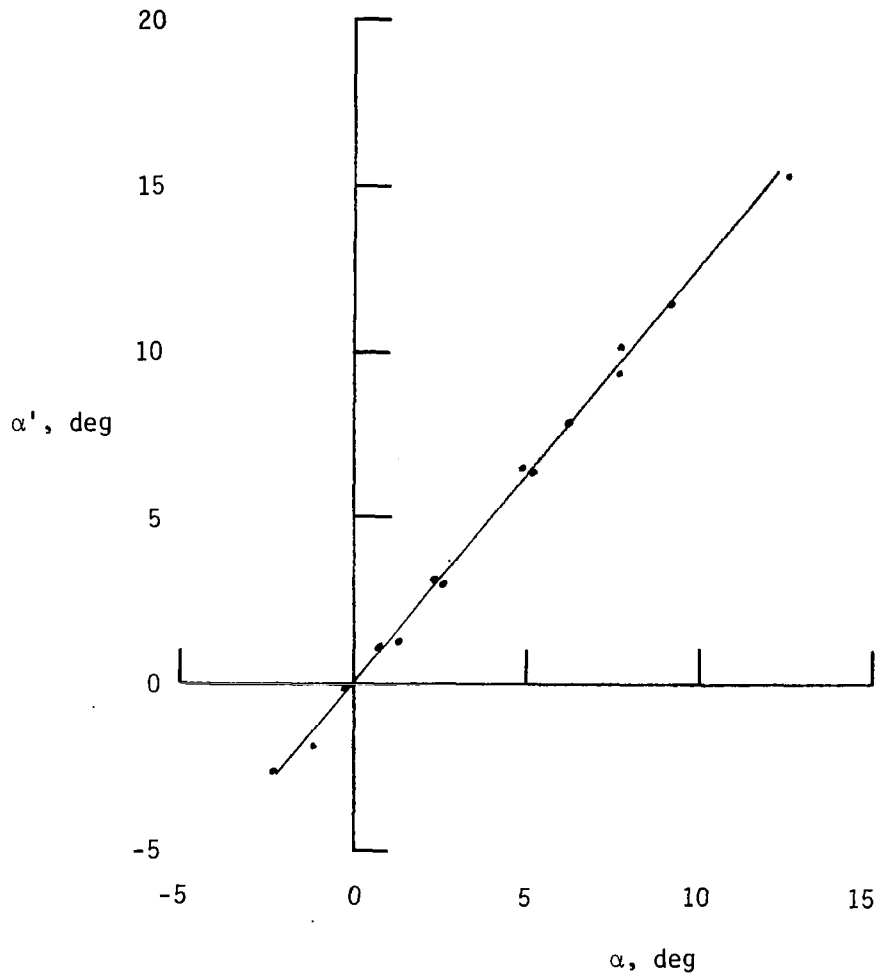

(b) Flaps 10^{o}

Figure B.10- continued

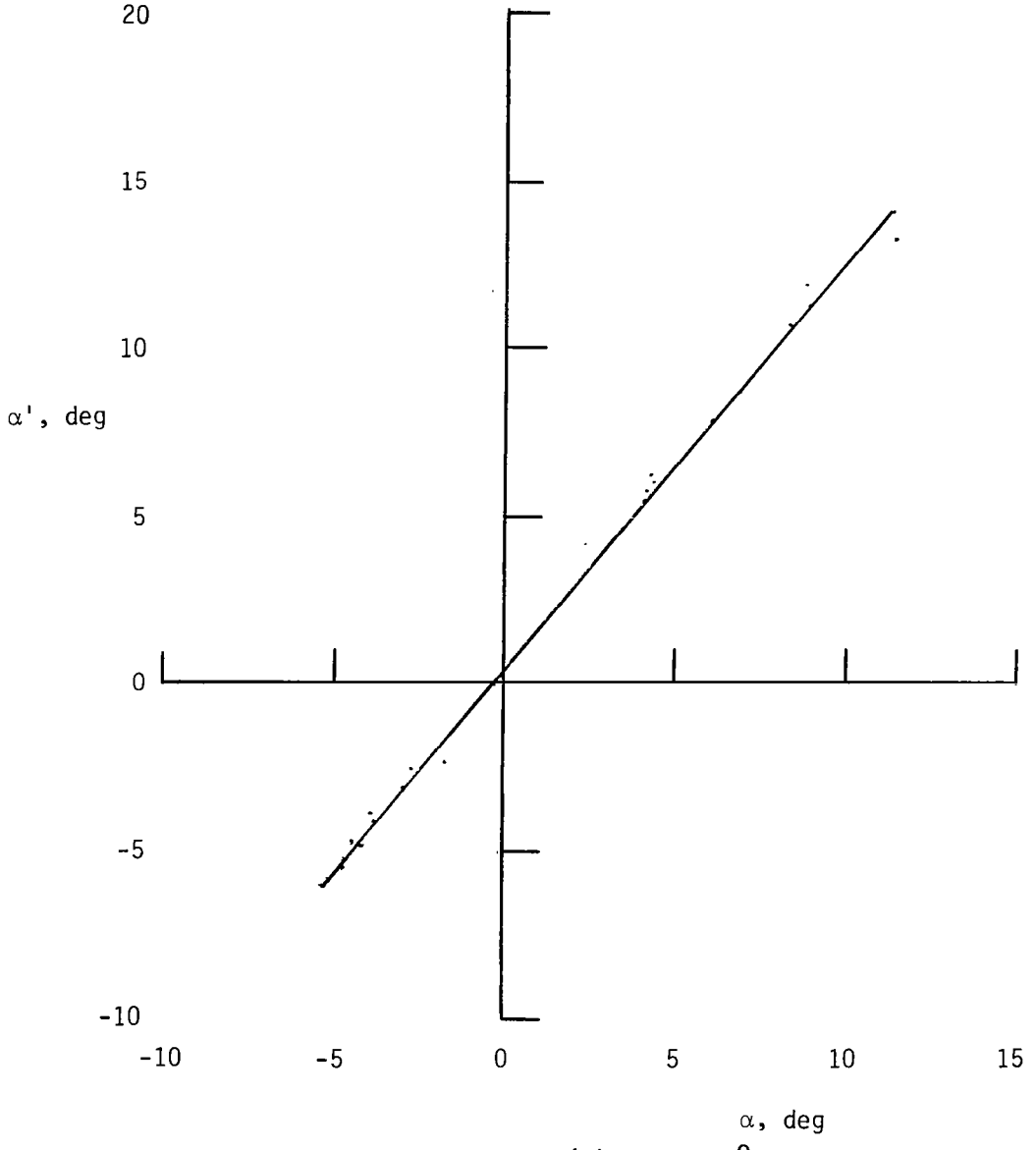

(c) Flaps 30^{o}

Figure B.10- Concluded.

APPENDIX C

PREDICTION OF ROLL DAMPING DERIVATIVES

APPENDIX C

PREDICTION OF ROLL DAMPING DERIVATIVES

The purpose of this appendix is to present the method, data, and results for analytical predictions of ATLIT roll damping derivatives, C_{l_p}, for several combinations of lift coefficient and flap deflection. The bulk of the computational work for this appendix was performed by Mr. Bradley J. Vincent and his contributions are gratefully acknowledged.

Method of Analysis.- The method used to predict roll damping derivatives is from reference C.1. The method is incorporated in a computer program described in reference C.2. This method does not provide for airplane configurations with wing-mounted engine nacelles or with flaps deflected. The methods by which these cases were handled are described below.

Effect of Engine Nacelles.- A sample calculation of the contribution of the engine nacelle to the total airplane roll damping will show the effect to be small.

The rolling moment coefficient of the nacelle alone is computed for the conditions and assumptions presented in figure C.1.

Computing the increment of rolling moment coefficient contributed by the nacelle yields:

$$\Delta C_{l,\,n} = \frac{L_n \cdot d}{q_c\, S_W\, b} = -C_{L_{\alpha,\,n}}\, \alpha_n\, \frac{S_n}{S_W}\, \frac{d}{b}$$

$$\Delta C_{l,\,n} = -0.00018$$

Nondimensionalizing, with respect to airplane, pb/2V yields the nacelle contribution to the airplane roll damping derivative:

$$\Delta C_{l,\,n} = \frac{\Delta C_l}{\left(\frac{pb}{2V}\right)}$$

$$\Delta C_{l_{p,\,n}} = -0.0034$$

This value amounts to less than 1 percent of the estimated total airplane roll damping at low-lift coefficients (flaps up) and is neglected in the final analysis of C_{l_p}.

Effect of Flap Deflections.- To estimate C_{l_p} with flaps down, the geometry of the wing was recomputed at each flap deflection (see table C.1). Thus, the assumption is made that roll damping with flaps down may be estimated by considering the flap deflection simply as a change in the wing area, aspect ratio, and taper ratio.

The sources for additional inputs to the program are explained as follows:

α The computer program requires true (geometric) angles of attack. First, C_L is computed for the condition of interest. Then, α is obtained from the flight-test C_L vs α curves of Appendix B and Chapter 5.

C_{l_α} The program requires two-dimensional lift curve slopes. These are based on wind-tunnel test data (reference C.3) for the GA(W)-1 airfoil with the Fowler flap. These values for C_{l_α} are summarized in figure C.2.

C_{D_o} The airplane zero-lift drag coefficient was estimated based on preliminary flight-test results. Based on wind-tunnel reflection plane-test data for the ATLIT wing (reference C.4), increments were added to account for increases in zero lift drag at increased flap deflections The estimated values for C_{D_o} follow:

δ_f	C_{D_o}
0^o	0.040
10^o	0.050
20^o	0.083
30^o	0.136
40^o	0.181

The final estimates of airplane roll damping derivatives appear in figure C.2. The estimates are presented for varying lift coefficients with flap settings of $\delta_f = 0^o$, 10^o, and 30^o. The trends shown in the figure for decreasing roll damping with increasing C_L are expected due to decreasing lift curve slopes at higher angles of attack (higher C_L). The large increase in flaps-down roll damping is expected due to both increases in C_{l_α} and changes in the wing planform with the flaps deflected.

APPENDIX C

REFERENCES

C.1 Hoak, D. E.; Ellison, D. E., et al: USAF Stability and Control Datcom. Flight Control Division, Air Force Flight Dynamics Laboratory, Wright Patterson Air Force Base, Ohio, 45433, 1972.

C.2 Smetana, F. O.; Summey, D. C.; and Johnson, W. D.: Flight Testing Techniques for the Evaluation of Light Aircraft Stability Derivatives, a Review and Analysis. NASA CR 2016, 1972.

C.3 Wentz, W. H., Jr.; and Seetharam, H. C.: Development of a Fowler Flap System for a High-Performance General Aviation Airfoil. NASA CR 2443, 1974.

C.4 Wentz, W. H., Jr.; and Volk, C. G., Jr.: Reflection-Plane Tests of Spoilers on an Advanced Technology Wing with a Large Fowler Flap. NASA CR 2696, 1976.

TABLE C.1.- WING GEOMETRY WITH FLAPS DEFLECTED

Flap Deflection	S, m^2 (ft^2)	A	λ
$\delta_f = 0^o$	14.4 (155.0)	10.32	0.5
$\delta_f = 10^o$	16.7 (179.6)	8.91	0.5
$\delta_f = 20^o$	17.1 (183.9)	8.70	0.5
$\delta_f = 30^o$	17.3 (186.1)	8.60	0.5
$\delta_f = 37^o$	17.0 (183.2)	8.73	0.5

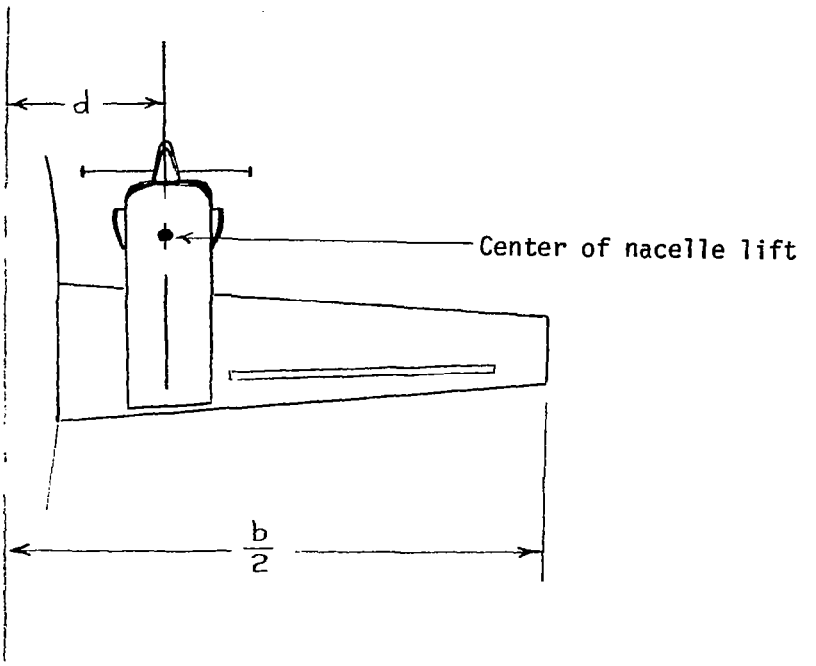

V = 174 knots (200 mph)

p = 1.0 rad/sec

d = 1.85m (6.08 ft)

b = 12.2m (40 ft)

$C_{L_{\alpha,n}}$ = 0.86 rad^{-1}

$\alpha_n = \frac{d.p}{V}$

S_n = 1.23m^2 (13.27 ft^2)

S_w = 14.4m^2 (155 ft^2)

Figure C.1.- Conditions and assumptions for estimating engine nacelle contribution to airplane roll damping derivative.

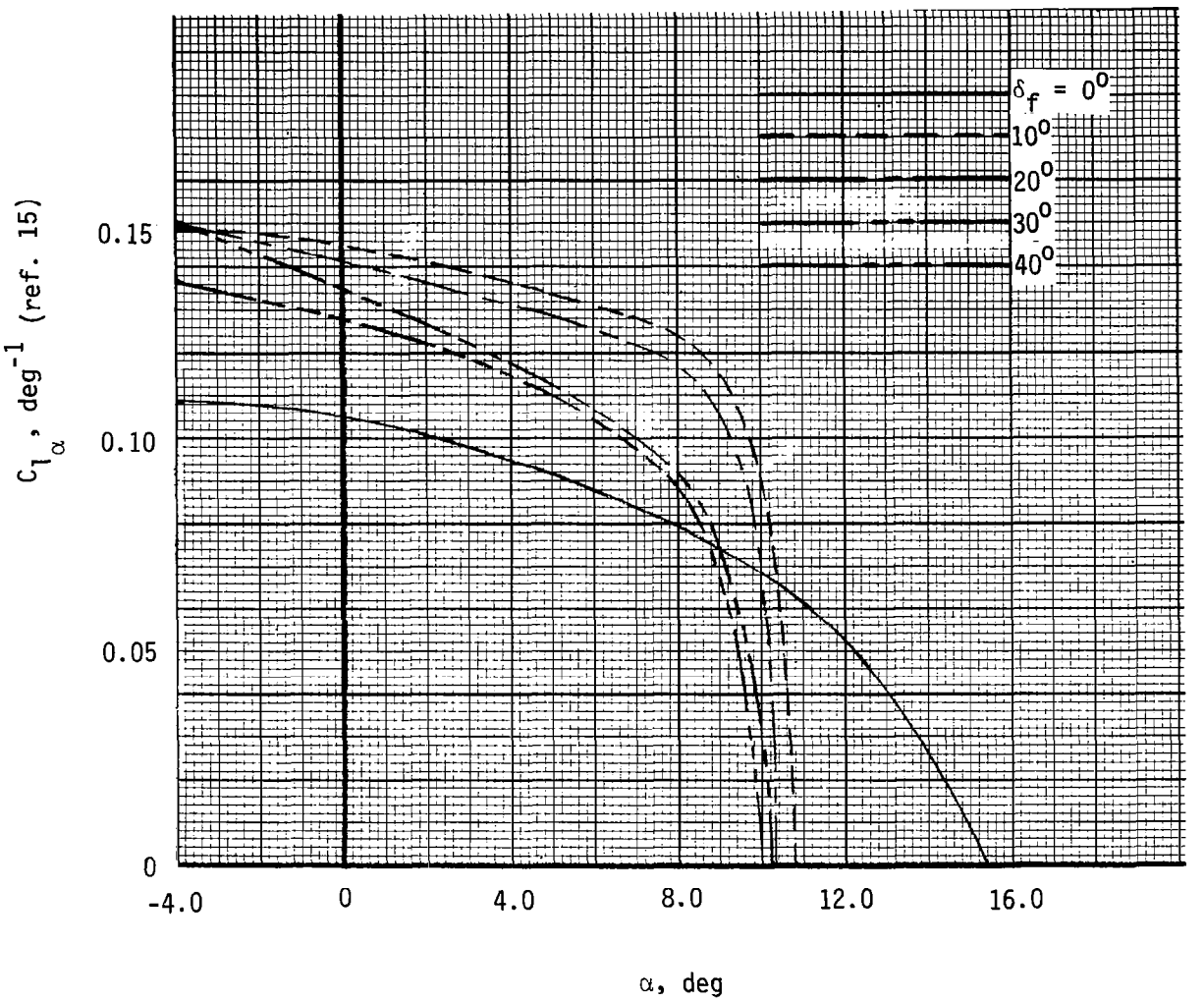

Figure C.2.- Variation of two-dimensional lift curve slope with angle of attack (δ_f = 0°, 10°, 20°, 30°, 40°).

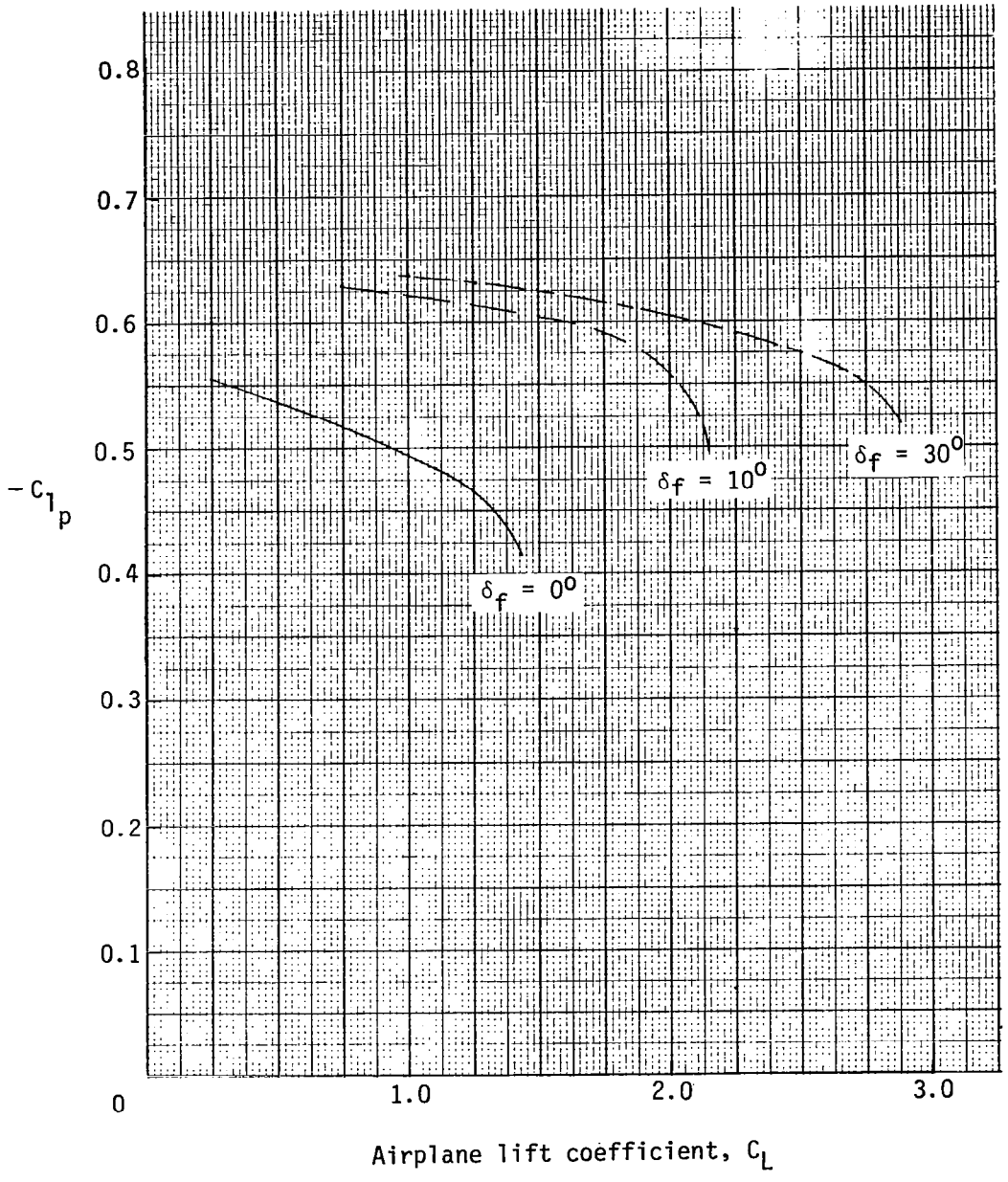

Figure C.3.- Predicted airplane roll damping derivatives ($\delta_f = 0^0, 10^0, 30^0$)